MATHEMATICAL MODELLING AND IN-PROCESS MONITORING TECHNIQUES FOR CUTTING TOOLS

By

Samy El-Sayed Oraby

B. Sc. Eng., M. Sc. Eng., Suez-Canal University, Port-Said, Egypt

Thesis Submitted to the University of Sheffield for the Degree of Doctor of Philosophy in the Faculty of Engineering

The University of Sheffield

Department of Mechanical and Process Engineering

Mappin Street, Sheffield S1 3JD, England

October, 1989

ACKNOWLEDGMENT

The author is highly indebted to **Professor D. R. Hayhurst** for his guidance, supervision, and encouragement throughout the period of this research.

He would like to thank the **Egyptian Government** and **Suez-Canal University, Egypt**, for financial support. **Dr. S. Billing** from the **Control Department**, the **University of Sheffield**, kindly provided helpful discussions and advice throughout the different stages of this project. **Messrs M. Hudson, J. Goodliffe**, and others in the machine shop of the **Mechanical Engineering Department** provided much practical assistance. The academic and secretarial staff in the same department, and also in the **University Computing Services**, were most co-operative. Many thanks also to **Sandvik**, and to **British Steel** in **Rotherham**, for providing the tool and the workpiece materials.

Sincere thanks are due to **Mrs. P. A. Hayhurst** and **Ms. J. Sexton** for helping his family during some difficult times during their stay in Sheffield, and **Mr. & Mrs. M. E. Field** who gave great help and encouragement during the past year for which he is most grateful.

The author wishes to express special thanks to his wife **Amal** for her patience and encouragement, and to his children, **Mohammed and Mona**, who had to return to Egypt without him in January of this year.

SAMY ORABY

MATHEMATICAL MODELLING AND IN-PROCESS MONITORING
TECHNIQUES FOR CUTTING TOOLS
SAMY E. ORABY

SUMMARY

The need is expressed for mathematical models which describe the cutting tool-workpiece interaction and for accurate on-line monitoring of tool-state. These are essential requirements for the achievement of unmanned and computerized machining processes.

Techniques are used to design the experiments which substantially reduce the number of tests while providing all the essential information for statistical analysis and for the development of mathematical models. The testing conditions are chosen to reasonably conform with the practical requirements. Multi-coated carbide tool inserts [Sandvik GC435] are used to cut an alloy steel [EN 19] under normal cutting conditions and for a wide range of operating parameters. An accurate and sensitive three-component dynamometer was designed, manufactured and used to measure the tool forces through a BBC microcomputer. Continuous records of the tool vibration have been collected in two different co-ordinate directions simultaneously together with measurements of tool wear and cutting forces.

Linear and non-linear regression techniques are used to develop mathematical models for the experimentally measured responses: cutting forces, tool vibration, and tool wear. Special attention is devoted to the identification of the most appropriate models. Each model being capable of representing the tool state throughout its working lifetime.

Tool life wear-based models are developed to relate the expected tool lifetime to the operating parameters: speed, feed, and depth of cut. A robust regression analysis technique, used in conjunction with iteratively re-weighting least-squares, has been

found to improve the accuracy of the models, and to stabilize its computed residuals through the elimination of the effect of influential observations having high experimental error. Response surface methodology **RSM** has been used to signify the non-linear nature of tool life response.

The force variation has been shown to correlate strongly with the wear progress so that it can be used for accurate in-process determination of tool wear and for monitoring tool state. It has been shown that the variation in the ratio between force components correlates with wear and is independent of the effect of other machining parameters; this enables the approach to be used for a wider range of materials and more extensive operational domain.

Study of the power spectral analysis of the tool vibration indicates that among the tool's vibration modes, the first fundamental natural frequency of vibration in the feed direction exhibits a consistent correlation with wear-progress. The Vibration amplitude decreases with the increase of the wear level until it reaches a limit after which it tends to reverse its characteristic. The time at which the characteristic changes is found to closely correspond with the practical end of the tool lifetime. Based on this fact, an in-process approach is investigated to determine the tool life on-line. Also, a model has been developed for tool wear estimation based on a combination of vibration and force; and, very good agreement has been obtained with the experimental data.

The validity of the models; their feasibility; and, their industrial significance are confirmed for adaptive control **AC** systems, and for machinability data base systems **MDBS.**

Contents

Chapter 1

INTRODUCTION AND PURPOSE

1.1 Foreword

In the past century, a large amount of research work has been carried out in the field of metal cutting. However, it is difficult to find total agreement amongst researchers about all aspects of machining operations. There are many descriptive theories which evaluate some of the aspects involved in the metal cutting process such as wear mechanism, metal deformation during cutting, chip formation, cutting force on the tool, and machining stability but, in most cases, the general conclusions are inconsistent and contradictory. Moreover, the developed theories have rarely been successfully implemented in practice so that most of the manufacturing judgements depend, to a great extent, upon personal skills and experience. In machine shops, the optimum cutting conditions are usually determined through a trial and error method by expert tool engineers who utilize a combination of personal experience, qualitative knowledge, and metal cutting theories.

The main object of any machining operation is to deform a certain workpiece to economically achieve final prespecified configuration with acceptable surface quality and dimensional accuracy. The achievement of such objectives depends upon the overall efficiency and performance of all the elements involved in the process: the machine tool, the workpiece, the cutting tool, and the machine operator. Therefore, metal cutting is usually accompanied by different and unrelated topics such as tribology, chemical, physical, and even physiological processes. Each variable affecting the process is itself derived from a number of other variables, and each of these interacts with the others to produce a combined effect on the process.

Since it is very difficult to relate all these unlimited factors satisfactorily, all descriptive investigations have concentrated on one or more of the principal processes in isolation. This may produce an accurate descriptive theory but in a practical situation its effect is often diluted or masked by other unaccountable factors. Predictive theories were, therefore, introduced as an alternative way to accomplish optimization of the manufacturing process. However, to meet the urgent demand for a fully auto-

mated machining process, an expert system which combines both the descriptive and predictive theories is essential.

1.2 Research Topics in Metal Cutting

Each of the machining elements mentioned above has attracted many investigators. As far as research in the development of machine tool technology is concerned, the object has been to construct a machine which is stiff enough to withstand cutting forces and to produce little distortion, and which works economically to give the shortest production time by employing high speeds, feeds, and power. Also, attention has been paid to other aspects such as stability, rigidity, flexibility, and accuracy.

Although the workpiece material is not a controllable parameter during the machining process in the same sense as the tool or the machine, attempts have been made to improve its metallurgical properties (machinability) to reduce cutting forces, to reduce tool wear and wear rates, or to improve surface quality while maintaining the other characteristics of strength [1 – 8].

The cutting tool itself is one of the most important factors which directly affect the machining process. Many investigations in the field of tool technology have resulted in methods of prolonging the period during which the tool cuts efficiently. This is a very important parameter, especially when production optimization is required. This is not only because of the cost of the tool but, because of the undesirable consequences when it unexpectedly fails. This not only affects the quality of the workpiece and the safety of the machine tool, but leads to total disorder when it is being used in unmanned manufacturing techniques, such as Flexible Machining *FMS* and Adaptive Control *AC* systems.

The aim of achieving optimized machining has attracted a vast amount of research work. Even though there are different definitions of the term "Optimization",

it can generally be defined as the optimal selection of operating conditions to satisfy an economic objective within the operational constraints. For full implementation of machining optimization, four main elements should be available. They are:

1. A reliable and sensitive technique for in-process detection of the state of the cutting tool in real-time cutting.
2. Mathematical representation of the functional relationships between cutting variables, system outputs (responses), objective functions, and system constraints.
3. Operational strategies and algorithms with a suitable micro- or mini-computer to act as an organizer between the above elements.
4. A stiff and accurate machine tools with the capacity of high speeds, feeds, and power.

Empirical relationships of the machining variables were first proposed to obtain information about the machining process, as it was impossible to obtain these by using the descriptive theories [9]. An empirical equation usually consists of parameters, each of which represents one or more of the machining variables and conditions: tool geometry and its material properties; workpiece material and its chemical and mechanical properties; machine tool and its characteristics; lubricant; etc. The resulting experimental equation is used either to estimate the system parameters or to obtain approximate information for similar operations. *Taylor's* work on the tool life of high-speed-steel *HSS*, as affected by cutting speed and cutting temperature [10], was the first reported attempt to formulate some of the parameters involved in the turning operations. However, the approach of using empirical equations has some drawbacks, such as the difficulty in updating the equation and the inaccuracy when applied to different conditions from those for which it was intended. Moreover, an empirical equation usually requires plenty of time, materials, and experience before it takes an acceptable practical form.

Mathematical formulation of a specific process can lead to the achievement of

fully automated manufacturing systems. With mathematical models it is possible to obtain a considerable amount of information about a system with a minimum of effort and money invested in the investigation. A mathematical model can also be used to describe and predict in advance the different outputs of the system under consideration.

The current revolution in computer technology has made a considerable contribution to metal cutting technology, especially in the case of metal removal by conventional methods of turning, milling, drilling, etc. The result has been very powerful machine tools equipped with extremely advanced electronic and computational facilities. In 1952, the first numerical milling machine was introduced which started a new era in the search to achieve full automation of the machining process. The logical extension of numerical control machine tools *NC* was computerized numerical control machine tools *CNC,* in which a mini- or micro-computer was included as an integral part of the controller. Some other advances, such as direct numerical control machine tools *DNC,* and industrial robots, were developed simultaneously with *CNC* systems. A fully automatic factory which employed a Flexible Manufacturing System and computer aided design *CAD* followed the advent of *CNC. FMS* includes manufacturing cells, each one containing a robot serving several *CNC* or *DNC* machines, with an automatic material-handling system interfaced with a central computer. This group of machine tools combines the rigidity, accuracy, and flexibility which are required in the production optimization.

The complex stochastic nature of tool wear and failure represents one of the great unsolved obstacles for achieving the target of production optimization. Also, the proper selection of the operating conditions and the tool life criteria still lag far behind the advanced technology of machine tools and, the need still arises for more intelligent techniques. The need for such techniques has become even more necessary since the introduction of the smart technique of adaptive control AC of machine tools. The main idea in AC is the improvement of the production rate, or the reduction of machining costs, by calculating and setting of optimal operating parameters during the machining. This calculation is based upon measurements of process variables in real

time and is followed by a subsequent on-line adjustment of the operating parameters subject to machining constraints in order to optimize the performance of the overall system. Although it is still in its early stages, AC technique offers a real hope of a solution to the machining optimization. In some research work [11], AC is claimed to hold the potential of 20 to 40 percent reduction in machining time.

1.3 Purpose

Manipulation of the problem of metal cutting using the conventional one-variable-at-a-time approach is no longer appropriate for today's requirement. Also, the strategy of studying one aspect in isolation from the whole operation seems to be ineffective in tackling the problem of production optimization. An investigation is considered which takes the whole operating history of different outputs simultaneously in order to find a region of cutting conditions at which desired levels of tool wear, tool forces, tool vibration, and rate of metal removal may be achieved under system constraints. Generally, the purpose of this study has been to investigate the state of the tool in turning operations as affected by process variables and conditions, bearing in mind today's requirements of automated manufacture and machining optimization. It appears that an understanding of the turning operations will provide a good insight into the general problem of metal cutting. This study included the following concepts:

- The development of mathematical models which quantitatively relate the system outputs either to each other or to machining variables. The experiments were statistically organized so that they covered a wide range of operating conditions using tool and workpiece materials which are commonly used in advanced turning operations. Also, it was intended that the models developed would deal with the different phases of both tool and system outputs at different stages of tool life. Special attention was devoted to the possible utilization of the developed models in the optimization procedures and adaptive control systems. Also, it

was anticipated that the models, in their original forms, might contribute to building a machinability data base system for use both with computerized, and with conventional turning systems.

- The investigation of new techniques for in-process monitoring of the tool state was one of the objects of this study. The possible correlation is investigated between the different forms of tool failure; the variation in cutting forces; and, the tool vibration.

1.4 Thesis Outline

- **Chapter 2** provides a general survey of the relevant literature. This includes different investigations and viewpoints about tool wear mechanisms, development of tool materials, determination of tool life, and techniques of the on-line and in-process sensing of tool wear and failure.

- **Chapter 3** explains the experimental design and set-up which have been used in the testing procedures of the project. This includes the design and manufacture of a three-component force dynamometer and the measuring techniques for both cutting variables and outputs. Also, data processing procedures are described.

- **Chapter 4** develops the general modelling strategy used to develop the approach to mathematical modelling. Procedures are explained to select the appropriate functional form of models; to fit the postulated model to the experimental data; and, to examine the significance and adequacy of the resulting model. These aspects were investigated considering tool life model as a case study.

- **Chapter 5** develops mathematical models of tool wear and cutting force, together with their technical and statistical evaluation. Mathematical models are developed to characterize tool wear within different phases of tool's working life. A new approach of tool life modelling is introduced using advanced modelling techniques.

Mathematical models are developed for the different cutting force components and their ratios. The possible correlation is investigated between the different force components and the various wear elements on the clearance face. An in-process approach of detecting tool wear, fracture, and failure is investigated using the possible correlation between the force variation during cutting and the tool state.

- **Chapter 6** is a self-contained report concerning the tool state during cutting when assessed from a dynamical point of view. The possibility is investigated of using tool vibration for in-process sensing; for estimation of tool wear; and, for failure assessment. Mathematical models are developed to formulate tool wear-vibration behaviour; to investigate the effect of cutting variables on tool vibration; and, to study the possible use of a combination of vibration-force signals to monitor the tool state in real time cutting.

- **Chapter 7** explains how the developed mathematical models and in-process techniques can be implemented to establish fully computerized machining systems. Adaptive control software for different production objectives has been suggested together with the relevant optimization algorithms. Also, the building of a computerized machinability data base system based on mathematical models of the turning operations is discussed.

- **Chapter 8** introduces a general discussion and recommendations for possible research extension.

- **Chapter 9** summarizes the general conclusions and concluding remarks.

Figures and plots are found at the end of each corresponding section.

Chapter 2

TOOL WEAR MECHANISMS AND TOOL LIFE IN TURNING OPERATIONS

2.1 Foreword

Even though there are references to many publications throughout this thesis, it is convenient to collect together in this chapter the reports of previous investigations into some of the aspects which are relevant to the scope of this project.

The wear and life of the cutting tool are so important from an economical point of view that many efforts have been made to identify the quantities which affect the wear behaviour during cutting operations. Major reasons for the importance of the term of tool life are:

1. The fundamental necessity to predict when to remove the cutting tool from operation to avoid the bad consequences of tool breakage, and deterioration of surface quality.
2. The tool life determination allows the selection of the optimal cutting conditions required in all economic optimization studies of cutting processes.
3. The tool life has often been used as a very good index of machinability and for categorizing the tool and workpiece materials.
4. All the outputs from metal cutting (responses) are related, by one means or another, to the mechanism in which the tool deteriorates, and therefore, no clear identification of the process is obtained without prior information about the tool wear and tool life.

Tool life is usually defined as the cutting time that can be obtained before reaching a point after which the tool should be scrapped. This is usually determined by specifying a certain level of wear scar on the cutting edge and this level is generally selected to achieve some production functions such as maintaining a certain level of surface finish and dimensional accuracy of the machined part; maintaining the magnitude of the resulting cutting forces well within the capacity of the machining system; or, achieving a certain economic optimization objective.

Many of studies have been carried out to investigate tool wear and tool life and, these can be split into three main categories:

1. The nature of tool wear mechanism [12,13].
2. The inherent nature of tool life data [14 – 17].
3. The development of alternative techniques and mathematical formulation of tool life [18 – 22].

Each of these aspects is now reviewed in some detail.

2.2 Tool Wear and Tool Life

2.2.1 Tool Wear Mechanisms

A characteristics of the wear which leads to tool failure is that it never takes place on one part of the tool surface only. It is the result of various wear mechanisms operating at various planes close to the cutting edge. During turning operations, *Fig. 2.1.a,* the tool is in intimate contact with the workpiece and as a result of their relative motions some of the workpiece material is removed. This severe contact, on different planes at the junction, causes many forms of tool wear to occur individually or in combination. These wear forms are as shown in *Fig. 2.1.b,* and can be classified as:
1) rake face or crater formation which is usually experienced with roughing operation; and 2) flank wear or clearance face wear which is usually experienced with either roughing or finishing cut. While these two forms are inevitable in any machining operation, and can be regarded as the gradual type of tool wear, there are other forms of tool failure such as: 3) tool failure by fracture of the cutting edge; 4) failure by loss of hardness of part of the tool being operated at excessive temperature as when turning at very high speeds; or, 5) formation of cracks, usually at right angles and next to the cutting edge on the rake face or on the flank of the tool. These latter forms of tool failure usually

result from the incorrect design of one or more of the machining elements. These types $(3-5)$ may be defined as the random type of tool wear. However, wear and friction at one site may subsequently accelerate wear at another site, which in turn has some effect on wear development elsewhere, and that usually results in complex mechanisms of tool wear.

The first attempt to clarify the problem was made by *Taylor* [10] when he classified tool wear as two types: a primary type, which results in heat being produced by pressure of the chip without a softening effect on the surface of the tool; and, a secondary wear type, with softening of the tool, where heat plays the principal part in the wear of the tool.

Shaw [23] classified tool wear types according to the system developed by:

1. Adhesive wear which occurs when the mating surfaces come close enough together to form strong bonds. If such bonds are stronger than the local strength of the material, a particle may transfer from one surface to the other.

2. Abrasive wear which involves the loss of material by the formation of chips, as in abrasive machining. For such a type to be initiated it is necessary that one material be harder, or have harder constituents, than the other member of the sliding pair; or, that hard particles be formed by chemical reaction of the wear debris.

3. Diffusion wear which results when surface temperatures become very high and surface velocities are very low, allowing the solid state to play a role in the wear process.

Shaw [23] stated that all of these might generally be present in combination, the predominant wear mechanism depending upon cutting conditions. He added that in addition to the above sources of tool failure, micro chipping, gross fracture, and plastic deformation might also pertain.

In addition, *Shaw and Smith* [24] explained that the formation and subsequent break-

ing of welds between the cutting tool and the chip may result in accelerated wear. They explained that the welds were of two types, namely: pressure, and temperature welds. Pressure welds occur at a low cutting speed, and at a temperature below the recrystallization temperature of workpiece material. Temperature welds occurs at high cutting speeds, and at a temperature above the recrystallization temperature of the work material. Pressure welds cause the formation of a built-up-edge, which is hard and is largely responsible for flank wear since it fractures and abrade the tool [24]. When temperature welds occur, the surface of the cutting tool and chip separate without the formation of a built-up-edge, but small particles of the cutting tool are removed. *Shaw and Smith* [24] indicated that all of the welds were of the pressure type at low cutting speed. However, as the cutting speed were increased, the generated temperatures rose and all failures were of the temperature weld type. With increased cutting speeds, the time required for plastic flow was insufficient and weld formation decreased. *Takeyama and Murta* [25] studied the effect of cutting temperature on the wear rate and found that it was constant, regardless of the cutting temperature, up to a critical limit. *Bhattacharya and Ham* [12], *Boothroyd et al* [26], and *Chao and Trigger* [27] agreed with *Takeyama and Murta* [25] that the interface temperature for gradual wear on flank face increased proportionally with the growth of the wear level. However, they added, there was a critical temperature above which the tool-workpiece interaction was temperature sensitive and rapid loss of tool hardness occurred, *Fig. 2.2.* This critical point was found to be dependent on the material of both tool and workpiece together with cutting conditions. Above this critical point for a given workpiece-tool combination, the two materials interfused and welded together and that a high wear rate took place. *Ber* [28] studied the effect of thermal conductivity of the tool insert on the tool wear and found that a low coefficient of thermal conductivity of the cemented carbide resisted heat transfer from the cutting zone to the insert and thus no rapid loss of the tool hardness was occured.

The obvious solution to improve the tool performance is either to use light values of cutting conditions or to develop new and tough tool materials with high wear-

resistance capability. Since the former is economically undesirable, the latter has always been the target for those working in this field.

2.2.2 Development of Tool Materials

To realize the enormous accomplishment in the field of tool technology, *Colding* [ ] has presented data as shown in *Fig. 2.3.* Since 1900, the time required to rough turn a low alloy steel shaft of 100 mm diameter and 500 mm length has been reduced from approximately 105 minutes to one minute due to the continuous development of new cutting tool materials.

Carbon steel was first used as a tool material. However, due to its limited capability to cut at high speeds and to achieve high metal removal rates, high speed steel *HSS* tool material was invented as a result of a study by *Taylor* [10]. This can cut at a speed which are two or three times higher than carbon steel. The alloy component tungsten gave the steel a greatly increased hot-resistance and, therefore, higher cutting speeds could be selected.

Cast cobalt-based alloys [2% *carbon*, 50% *cobalt*, 30% *chrome*, *and* 16% *tugsten*] were also used as tool materials. The high content of chromium and tungsten carbide resulted in a material of superior resistance to wear. Although higher cutting speeds could be selected in this case, the high cost of this alloy restricted their use for only the most specialised production applications.

Cemented carbides (consisting of cobalt and tungsten carbides) were found to be very satisfactory for machining cast iron. A major step in the development of cemented carbides was the introduction of titanium carbides TiC and tantalum carbides TaC into the tool material. Tools made from TiC or TaC bonded with Ni or Co experienced much less cratering wear than tugsten carbides WC alloyed with Co when used for cutting steels. The effectiveness of TiC in resisting cratering results from the increased resistance to oxidation; and, the decreased adhesion between carbides and steels [31]. Accordingly, wear resulting from the process of welding and tear away is reduced.

There are two types of sintered tungsten carbides [23] : a) *ISO K-type* is used for machining gray cast iron; non-ferrous metals; and, abrasive non-metals such as fibre glass and graphite. *b) ISO P-type* is for machining ferrous metals. The cast iron type consists of WC crystals with normally 3 to 12% cobalt as a binder, while the steel-cutting grade of carbide has some of the WC substituted by TiC, TaC, or niobium carbides NbC, all of which render greater crater resistance with different degrees of loss of strength, abrasive wear, impact, and corrosion (oxidation) resistance.
The introduction of ceramics allows the tool to be used at higher speeds when machining non-ferrous metals and cast iron. Ceramic cutting tools demonstrated extremely high resistance to wear and deformation at high temperatures.

The continuous attempts to create tools with reasonable toughness and good wear resistance led to the use of hard coatings on the surface of cutting tools. The idea was that a thin layer of hard constituents would improve wear resistance without affecting the toughness of the tool. Among the promising hard constituents, titanium carbide TiC was first chosen owing to its high chemical stability; and, to its suitability as a constituent in conventional cemented carbide steel cutting grades [3*f*]. The earliest research on coated tools which led to a U.S. Patent was carried out by *W. Ruppert* in 1960. However, the commercial use of coated tools did not start until 1969 when the *Sandvik* patent for TiC coated tools was filed. Since then, a very large number of coated inserts have appeared on the market. Today, the Chemical Vapor Deposition *CVD,* which was first described in *1970,* is one of the most successful methods of applying coatings to cutting tools [28 – 35]. Among the materials used for coating layers are titanium carbides TiC, titanium nitride TiN, aluminium oxide Al_2O_3, and hafnium nitride HfN. The use of multiple-layer coatings - such as TiN over TiC, and Al_2O_3 over TiC - has also become popular. As claimed by most investigators, coated tools have the advantage of prolonging the tool life. This stems from their superior combination of wear and breakage resistance. The main reason for the popularity of coated cutting tools is the significant increase in cutting speed that can be obtained with no loss of tool life. As claimed by *Shabaik* [30], coated cemented carbide tools

showed considerable reduction of flank wear and crater wear as compared to uncoated tools. *Ekemer* [31] stated that not only the cutting forces but also the edge temperature were lowered through using coated tools. This decreased plastic deformation and the growth of thermal and mechanical fatigue cracks. Titanium carbide increased the crater as well as the flank wear resistance through its chemical stability at elevated temperatures and not through its hardness at room temperature.
Wood [36] stated that coated carbide cutting tools were preferred whenever reliability was required. They offered a safer and more certain solution to some of the toughest and most dangerous engineering applications, as in non-metal cutting and mining operations.

In his study on the weae characteristics of TiC coated carbide tools, Ham [37] indicated that the wear caused by diffusion (or reaction) of either carbon or cobalt from the tool into the iron-containing chip was decreased because the coating acted as a barrier. *Schintlmeister et al* [38] stated that the coating layer reduced the coefficient of friction between the cutting tool and workpiece and, therefore, it performed better at lower cutting temperatures than uncoated inserts under similar cutting conditions. *Chubb and Billingham* [39] examined the wear of TiC-coated inserts and reported that the initial flank wear was abrasive but once breakthrough of the coating occured, wear was accelerated since there were both diffusion and abrasive wear. Surface irregularities caused by the thermal cracks or by the welding of chip-iron fragments to the tool were also shown to enhance the rate of crater formation since they acted as chipbreakers.
Gates and Peters [34] explained that Al_2O_3/TiC coatings on cemented carbide tools combined the resistance to oxidation and abrasive wear at both low and high cutting speeds.In a unique and comprehensive investigation of wear mechanisms of coated car-

bides tools, *Hale and Graham* [40] reported that for a given tool life of ten minutes, a cutting speed increase of 50% was obtained for TiC tools while it was 90% when Al_2O_3 was used. Also, it was noticed that crater wear resistance was directly proportional to coating thickness and strongly dependent upon coating composition. The inherent crater wear resistance of Al_2O_3 coatings was more than twice that of TiC or TiN coatings. Crater wear rates increased significantly when the crater depth exceeded the coating thickness, but even when the coating was penetrated, the coating at the edge of the crater retarded crater growth at a rate dependent upon coating thickness. The use of coating appeared to improve crater wear resistance by providing a chemical diffusion reaction barrier at the chip contact zone. Flank wear resistance was insensitive to coating thickness beyond a minimum value of about five to nine microns, and the flank wear rate did not increase when the coating was penetrated. The critical region for flank wear appeared to be a narrow zone at the bottom of the flank wear scar. The coating only needed to cover this zone to improve flank wear resistance. Coating thus improved flank wear resistance by providing a contact bearing surface between the cutting edge and the workpiece which worn slowly by a combination of mechanical and chemical reaction degradation. As cutting speed increased, the chemical wear increasingly dominated. Thus, more abrasion-resistant coatings, such as TiC, worked better at lower speeds, while more chemically stable coatings, such as Al_2O_3, resisted wear better at high speeds.

Colding [29] summarized the reasons for the effectiveness of the TiC coating during the whole life of the tool as follows:

1. The chip is supported on the periphery of the crater which contains the hard and thin TiC coating. The mechanical loading on the crater surface may therefore be relatively smaller than in the case of pure cemented carbide.

2. The rear end of the crater acts as a very good chipbreaker due to the hard TiC edge.

3. The TiC coating is successfully pressed down into the matrix during the formation

of the crater, the latter thus containing TiC in spite of the fact that the thin TiC film is broken through after only 10 to 20 seconds of cutting.

4. The TiC coated carbide forms oxide layers with the work material. During the crater formation these oxides are formed close to the tip of the tool and are transported by the chip into the crater zone.

However, *Shanshal and Dugdale* [35] indicated that titanium nitride coatings applied to tool tips of cemented carbides and *HSS* were effective in delaying certain types of wear but less effective in delaying others, hence the increase in tool life brought about by coating was dependent on the cutting conditions imposed. For both *HSS* and carbide tool tips, the extension of life gained by coating diminished under severe cutting conditions of high feeds and speeds. Additional life was gained largely while the coating remained intact, and the residual life after the coating had worn through was short. Also, they indicated that coatings increased tool life, but only under conditions of abrasive wear.

Even though coated cemented carbide tools have made a considerable contribution to solving most machining problems, there are still some cases that require absolutely safe machining and a very high quality of surface finish.
Synthetic diamond was introduced in 1974. This was brazed onto a steel tool shank as in tungsten carbide tool manufacture. The new tool material, polycrystalline diamond *PCD*, and another tool material, cubic boron nitride *CBN*, are today very interesting because of their low rates of wear at high cutting speeds [41 – 44]. *PCD* consists of very fine diamond grains hot pressed at extremely high pressure. They are used for fine machining cuts on very abrasive non-metallic materials such as graphite and glass reinforced plastics. They are also useful for fine cutting of aluminium and copper alloys and other non-ferrous metals and alloys. *PCD* tools are virtually destroyed by ferrous metals.
CBN has proved effective for machining nickel base alloys and hard cast iron.

Sialon is a tool material developed by *Lucas Ltd.* in the *U.K.* [45]. It basically consists of silicon nitride and aluminium oxide and may also contain titanium carbide. Sialon competes with *CBN* in machining nickel base and high temperature alloys and has also been successful in high speed machining of cast iron. According to *Kalish* [42], Sialon provides better tool life than aluminium oxide coated carbide or hot pressed composite ceramic at heavy chip loads and at speeds above 300 m/min. At lower speeds, aluminium oxide coated carbide will perform better; and for lighter chip loads at high speeds, ceramic will be the material of choice. Sialon is not suitable for machining steel.

Fig. 2.4 [46] diagrammatically shows the application areas and range of cutting variables for different tool materials which are now available on the market. It can be seen that coated carbide tools take a prominent place, especially in machining steel and ferrous materials using moderate to high feeds and speeds. According to *Kalish* [42], coated tools (*HSS* and carbides) account for over 80% of machining applications. *CNC* machines are being loaded up with approximately 80% coated inserts. The other 20% is divided among ceramics or cermets and titanium carbide base and uncoated tugsten carbide base materials.

2.2.3 Wear Time Relationship

As explained earlier, the tool is subject to different forms of failure during cutting. These forms have been categorized as gradual and random types. The former is inevitable in any machining operation while the latter is due to unexpected disturbances. If wear level is plotted against cutting time (or volume of metal cut), a curve of the shape shown in *Fig. 2.5* is obtained. Initially the slope is high in region *(A)*, but soon reduces to a constant value for a relatively long period of time. Eventually the curve again turns upward and the tool fails fairly rapidly. *Shaw* [23] studied the wear-time trend in the light of theory of friction. Wear rate is high at the beginning because the applied load is finite but the contact area between tool and workpiece is zero. After the apparent contact area reaches a critical value, but with the stress still less than the

uniaxial flow stress of the tool material, the wear rate is decreased as shown in region *(B), Fig. 2.5.* Once the apparent contact area has reached a critical value at which the mechanical stress is larger than the uniaxial flow stress, thermal softening of the tool material occurs in region *(C).*

The region of initial wear has been long ignored on the ground that initial wear lasts for only a few seconds of the cutting time and therefore has an unimportant role on the subsequent performance of the tool. The idea was accepted that the initial wear W_o could be approximated as the intercept of the straight line in region *(B)* at zero cutting time as shown in *Fig. 2.5.* However, failing to understand what is happening in the first few moments of cut may affect the evaluation of the tool performance during the rest of the tool's lifetime.

Ber and Kalder [33] indicated that without a prior comprehensive knowledge of the actual value of initial wear, at least a 20% uncertainty in evaluating wear level and tool life would result. They indicated that in this period, which usually lasts from one to two minutes of cutting time, the wear behaved in the form of an exponential curve. They added that the wear in this period was in the form of tool chipping which increased when the tool was very acute. The first engagement between the tool and work material has the nature of a discontinuous machining which leads in the case of sharp tools to the initiation of a chipping mechanism. This mechanism was found to last for only a few seconds and created a naturally protected cutting edge. This uncontrollable mechanism caused the scatter nature in region *(B)* of wear-time curve.

According to *Chandrupatta* [47], the levels of initial wear are fixed for all speeds. With a higher speed, less time is required for this level to be attained. *Taylor* [48] agreed that the wear-time curve would settle down from the initial region to a straight line more rapidly for higher speeds. However, *Taylor's* results showed some deviation from the assumption that the levels of initial wear were the same for different speeds. *Mills* [49] reported that with a new tool, the time consumed in region *(A)* was dependent on cutting conditions but, typically, for a given workpiece material, the amount of primary wear was approximately constant, although the time to produce it decreased as the cutting speed increased.

Groover [50] indicated that the amount of wear in the initial region was dependent on cutting conditions and workpiece hardness. However, other investigations [51] showed that this zero point never matched the curve origin; and, did not even seem to be located at any fixed point for a set of tests. Most investigations have dealt with the middle part (region *(B))* of the wear-time curve.

According to *Ber and Kalder* [32], the second region covers the total period of effective cutting time in which the wear propagation is linearly related to the cutting time. This part of the curve usually provides the most important information about the performance of the tested tool. *Taylor* [48] assumes that the wear rate in region *(B)* is proportional to the area of wear scar and, therefore, the total amount of wear W at any time t takes the form $W = mt + W_o$, where m is the slope of the straight line in region *(B)*. In this region, wear rate is almost independent of the cutting temperature. This independency continues until the tool reaches its third phase of high rate temperature sensitive zone [12,25 – 27].

In most studies the tool was prevented from cutting in region *C*. In this region, wear behaves differently when different groups of tool-workpiece materials are machined [32]. In some cases the wear rate increases gradually in an increasing exponential manner until a total tool failure stops the machining process. In other cases, which are typical for coated tools, the wear grows rapidly at an extremely high rate [32]. This wear propagation ends very soon with a total failure of the cutting edge.

The effect of feed and depth of cut on the tool wear has been investigated by a few investigators. *Taraman* [52]indicated that for a given speed, longer tool life could be obtained by using heavy cuts and moderate feeds for a specific amount of metal removal. According to *French et al* [53], tool life decreases as feed and/or depth of cut increase.

2.2.4 Tool Life Determination

Tool life describes the useful cutting time for certain cutting conditions. The second region of the tool-wear curve, in which the wear is almost linear or, in practice may be treated as such, is always used for easy prediction and estimation of the tool life. The tool life for a given cutting speed is considered as the time taken to reach a prespecified level of tool wear. As shown in *Fig. 2.6,* tool life increases with the decrease of the cutting speed. Longest life T_A in curve A is obtained with lowest speed while highest cutting speed in curve D results in the shortest lifetime of T_D minutes.
The first approach to determine tool life for a given speed was made by *Taylor* [10] when he produced his famous equation $TV^n = C$, where T is the tool life in minutes, V is the cutting speed, and n and C are constants depending on test conditions and materials. As is explained later, this equation suffers from many drawbacks when it is applied to some tool and workpiece materials other than those used by *Taylor* in about 1900. Moreover, much time and materials are required to develop this equation for certain tool-workpiece combination. Some investigations, however, tried to reduce the cost, or to increase the accuracy of tool life assessment through using different techniques. All these attempts tried to measure the rate of loss of tool material during machining. This included the use of radioisotopes as radioactive tracers [54 – 60], the use of the electron probe analyzer [57], the use of the chemical analysis of the tool particles carried by chip [58], or even weighting the tool before and after cutting. However, the conventional approach of terminating tool life at a certain level of wear, using a previously established wear-time curve still the most practical criterion for tool life determination [59].

Today, the problem of tool life determination is a critical aspect of the manufacturing environment because of the introduction of new hard and tough tool materials and after the introduction of most powerful tooling and machining systems. The laboratory technique of evaluating and assessing tool life is no longer the best option for today's requirements for the four following reasons:

1. <u>The scatter and variation in tool wear and tool life.</u>

One of the bugbears of metal cutting analysis is the variation or uncertainty in determining tool life. Wear mechanisms are not yet fully understood. Scatter in wear rate distribution is a common problem in machining and this affects the accurate estimation of the tool life. This scatter is caused by many factors such as non-uniform structures of work and tool materials, vibration of tool-work system, experimental errors, etc [60]. *Hsü* [61] found that the wear rate was not constant either from one tip to another of the same composition, or from one layer of the work material to the next. The wear resistance of one tip, *Hsü* explained, can differ by as much as 20% from that of another tip. Also, he added, the workpiece wears the tool faster at smaller diameters due to the fact that impurities, or inclusions, in most steel bars are not uniformally distributed, but vary in their concentration with the diameter.

2. <u>The lack of practical criteria to assess tool life.</u>

A cutting tool may fail by a process of softening due to plastic deformation or by brittle fracture due to mechanical loads or shocks or by a process of gradual wear. Total failure of the tool is the most economical and practical criterion when considering roughing cut where tolerance and finish are not very important while the maximization of the metal removal rate is the main target. This case is represented by points *P's* in *Fig. 2.6.* The difference between using this criterion point and the one using fixed wear level is significant. The problem is how these points can be reached without going further to the zone of tool total failure. Also, tool fracture or chipping can readily occur during machining under some uncontrollable conditions. A tool may fail by edge fracture or chipping while it is well within its supposedly life range. Chipping of the cutting edge and breakage of the tool wedge are of a random nature and still very little understood. Furthermore, even with gradual wear as a tool life criterion, it is still difficult to determine which element of the tool wear type is significant and can be used as a criterion for a certain production objective. There are a number of wear types

on the clearance face of the tool that can be regarded as candidates for a wear measurement. However, they all are different from standpoint of variability and reliability of the measures. It was shown by *DeVor et al* [17] that the maximum depth of wear at tool nose was not only the least variable under replicated tests over a wide range of cutting conditions but appeared consistently and systematically and was simple to measure. According to *BS* 5623 [59], the criteria most commonly used for sintered carbide tools are either the average width of the flank land of 0.3 *mm* if it is considered to be regularly worn or, the maximum width of flank land of 0.6 *mm* if the flank wear is not regularly worn.

The notch wear, *Fig. 2.1.b,* is a special type of flank wear at the spot where the major cutting edge intersects the work surface. According to *BS* 5623 [59], this seldom makes the change of tool necessary but in special cases where the notch wear is predominant over the other tool-wear phenomenon, the length of the wear notch may be used as criterion measure for tool wear.

Many investigations [35,52, 62] employed the average value of the three measures on nose, flank, and notch in their studies. However, this has the major disadvantage of uncertainty when a wear measure dominates at a certain location while still being low at the others. This does not reflect the accurate state of tool wear. Specification of a fixed limit of tool wear level at any of these locations as a failure criterion, is not wise, since cutting outputs such as forces, temperature, surface finish, etc. are not equally affected by different wear levels at the clearance face of the tool. All these contradictory assessment make the selection of the criterion wear level a matter of personal opinion and a universal criterion is still being looked for.

3. The use of variable cutting for the same cutting tool.

In many situations it is necessary to change one or more of the cutting variables- speed, feed and depth of cut- during the same operation or to use the same tool in successive cutting operations under different cutting variables. In this case, the tool wears in a complex manner and the traditional wear-time curve no longer

represents the machining operations [47,63–66].

4. Constraints domain of operability.

   The operability region for machining operations in which tool life is studied is highly non-symmetrical and irregularly shaped [67]. The operability region in the N space of controllable cutting conditions is bound by various economic and operational constraints such as minimum power, minimum metal removal rate, minimum tool force, or surface finish specifications. These constraints are generally non-linear equations and vary for different cutting processes and part requirements.

In conclusion, although the seemingly straightforward task of accurately predicting the useful life of a cutting tool has been examined by many researchers, it still remains an extremely troublesome problem. Improvement in modern manufacturing technology have led to great advances in the ability to produce products through automated systems to the extent that computers now directly control machining operations and even packing. Current research into fully automated production includes complete computer control from design to production *CAD/CAM*. This stage should include very precise information on when tools should be removed from use if economically optimized production is to be maintained. This requires more reliable ways to assess the useful lifetime of the tool. Among alternatives yet to be studied on-line tool wear monitoring seems to hold the best prospect of success. If it is combined with an integrated strategy of machining optimization, this may lead to a significant contribution to the purpose of optimization, and to unmanned, machining operations.

2.2.5 In-process and On-line Monitoring of Tool Wear and Fracture

The techniques for on-line tool wear sensing are always divided into direct and indirect methods. Direct tool wear sensing implies the measurement of actual progress of the physical wear on the tool edge while cutting is being done. As explained earlier, this

technique has gained little practical success, therefore, all efforts have been directed toward the approach of indirect on-line tool wear sensing. Indirect methods of wear sensing measure certain process variables and then relate them to the degree of wear. The basic concept is to observe and measure the deviation from the normal conditions when the tool is healthy.

Measurements of motor power, torque, or current of the main driving motor or the feed drive motor by using electronic equipment have been reported by many investigators [68 – 70]. It is claimed that changes in the levels of these outputs can be used to detect or estimate the level of tool wear. However, according to *Martin et al* [71], there is little evidence that power consumption is related accurately to the progress of tool wear. According to *Lister and Barrow* [72], the two basic limitations of such techniques are that firstly, torque (and power) increments due to tool wear alone are likely to be small and so difficult to detect, and secondly the increment may not be easily separable from those due to other events during machining.

Cutting temperature may give a good indication of wear and wear rate during cutting. Three different approaches were followed to measure cutting temperature. Thermochemical reaction techniques utilize thermo-sensitive paints which change colour with temperature; electromagnetic radiation utilizes total radiation pyrometers [73]; and thermo-EMF techniques rely upon tool/work thermocouples [73]. However, these techniques have been restricted to research purposes due to the inherent problems of calibration and of wiring-up. Moreover, these techniques are suitable only to control temperature, which achieve a constant wear rate, while other forms of tool failure are not detectable.

Among techniques which have recently gained a wide acceptance in detecting tool wear is the study of the dynamic behaviour of the cutting tool. The vibration signature of the machining process, including both the relatively low vibration of the tooling system and the high frequency acoustic emission *(AE)* signals from the chip formation process, have been investigated as potential sources for in-process monitoring of the

tool state during cutting. This subject is dealt with broadly in **Chapter 6.** Sensing of the acoustic emission signal from the cutting process gives a good diagnosis, especially in detecting the modes of tool failure. The *AE* is the elastic stress wave generated as a result of the rapid release of strain energy within a solid material in association with the deformation, fracture and phase change of material [74 – 76].

One of the most reliable and sensitive techniques to detect tool wear and breakage during cutting is the use of the cutting force components. According to *Kinnander* [77], the cutting force is the parameter which seems most likely to provide a solution to monitor flank wear and crater and, therefore, it is the most appropriate criterion to determine the exact time to replace the tool. *Moriwaki* [78] reported that most tool failure sensors in the practical use or under investigation were based on some kinds of cutting force measurement.
In a study on about 180 turning centres in the *FMS* system equipped with a motor current monitoring system, *Navak and Ossbahr* [69] reported that the direct force measurement applied, as an extra monitoring method, improved both response time and sensitivity.

Bhattacharya and Ham [12] indicated that cutting forces increased almost linearly because of the increase in normal force on the flank with growth of flank wear, *Fig. 2.7.* When wear develops on the tool flank, forces increase by values depending on the extent of wear scar. As shown in *Fig. 2.7.a & b,* the additional force due to wear are: the normal force N in the horizontal plane XZ; and, the frictional force F in the vertical plane Y. The force diagram for a worn tool is as shown in *Fig. 2.7.b* where the total force are $F_{xz} + N$ and $F_y + F$ for the horizontal and the vertical plane respectively. For given conditions and tool-work material pair, the rate of increase of the horizontal component relative to the developed flank wear $\{\frac{dN}{dFW}\}$ is constant, *Fig. 2.7.c,* but, they explained, this proportionality ends once the wear enters its temperature sensitive zone at later stages of the tool life.

Although it is agreed by many investigators that cutting force is a reliable and

sensitive way to detect or estimate tool wear, disagreement still exists over which force component (or ratio) is the most sensitive. It seems that the degree by which each component is affected by wear depends on many factors, such as tool geometry, variation in work hardness; and, the level of the developed wear.

Uehara [79] proposed a method based on an experimental observation that the shape of a curve, showing the relationship between feed force F_x and the feed per revolution, was sensitive to the extent of both flank and crater wear. *Colwell* [80] monitored the tool wear through measuring both F_x and F_y components. A phase shift which was noticed between these two components was sensitive to tool wear. In subsequent work [81], *Colwell* used the ratio $[F_y/F_x]$ as well as cutting temperature to monitor tool wear. *Taraman et al* [82] reported that only the vertical force F_y was sensitive to tool wear while the other two components were not suitable for in-process monitoring of tool wear. *Wolf and Magadanz* [83] reported that for a 0.7 *mm* flank wear, a difference in the vertical force F_y of 10% was obtained whilst the feed force F_x increased by approximately 150%.

Micheltti et al [84] concluded that variations in cutting force with time were too small to monitor tool wear but could possibly be used to detect tool failure.

Köning [85] studied the possibility of using the variation of the cutting forces to monitor tool wear in an adaptive control system. He indicated that the correlation between the increase of the cutting forces and the tool wear made it possible to furnish information on the current state of tool wear.

Mackinnon et al [86] developed a method of wear estimation for carbide tools using a function of the cutting forces. To minimize (or eliminate) the effects of several of the variables on the cutting forces, he used the ratios of several force components such as $[F_x/F_y]$, $[F_z/F_y,]$ and $\{\frac{\sqrt{F_x^2+F_z^2}}{F_y}\}$.

Generally, tool forces give promise of finding a technique that will solve the problem of in-process detection of tool wear and breakage.

The next chapter includes the experimental design of the instrumentation which were used to collect the experimental data used in the analysis.

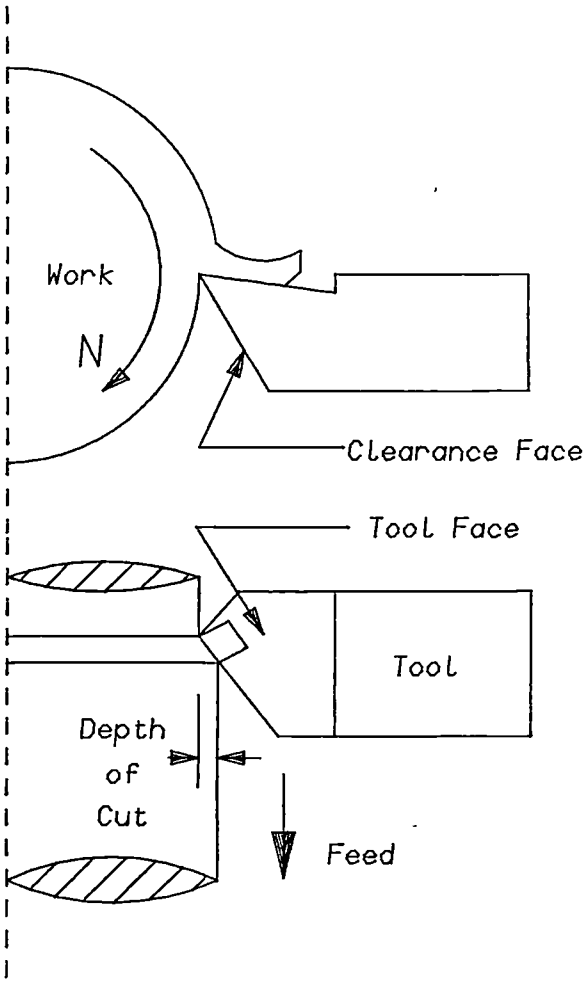

a) Turning Operation

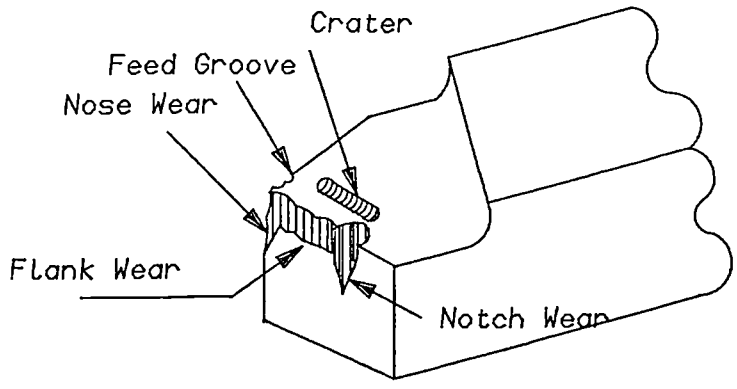

b) Sites of Tool Wear

Fig. 2.1 Tool Wear in the Turning Operations

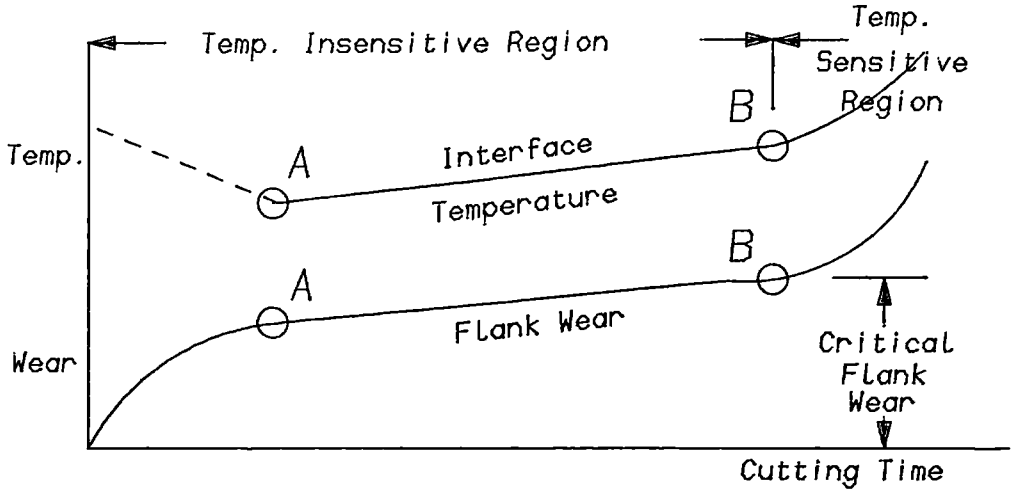

Fig. 2.2 Relationship Between Flank Wear and Interface Temperature [12]

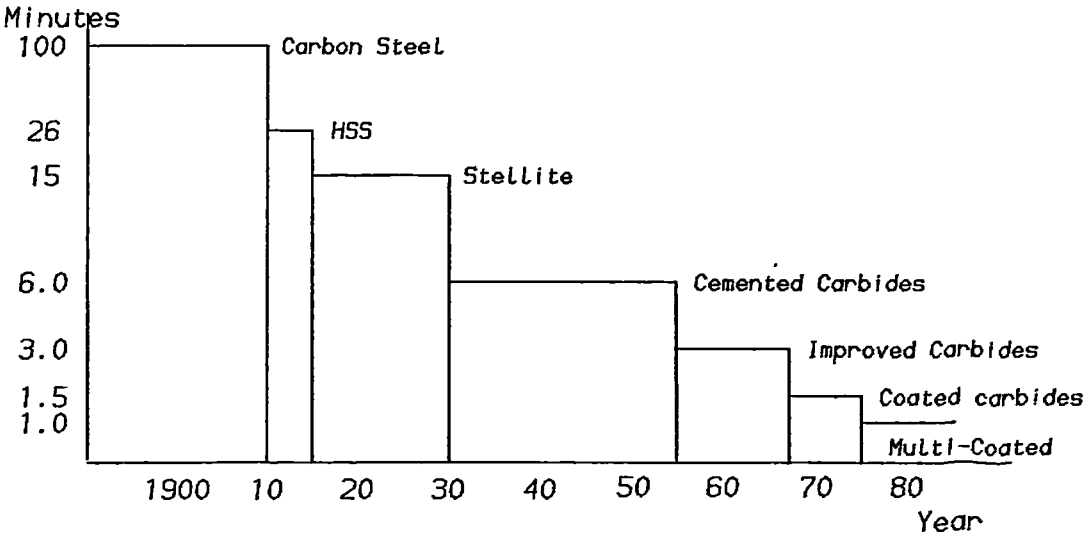

Fig. 2.3 Improvement in Cutting Time During the Past Century[29]

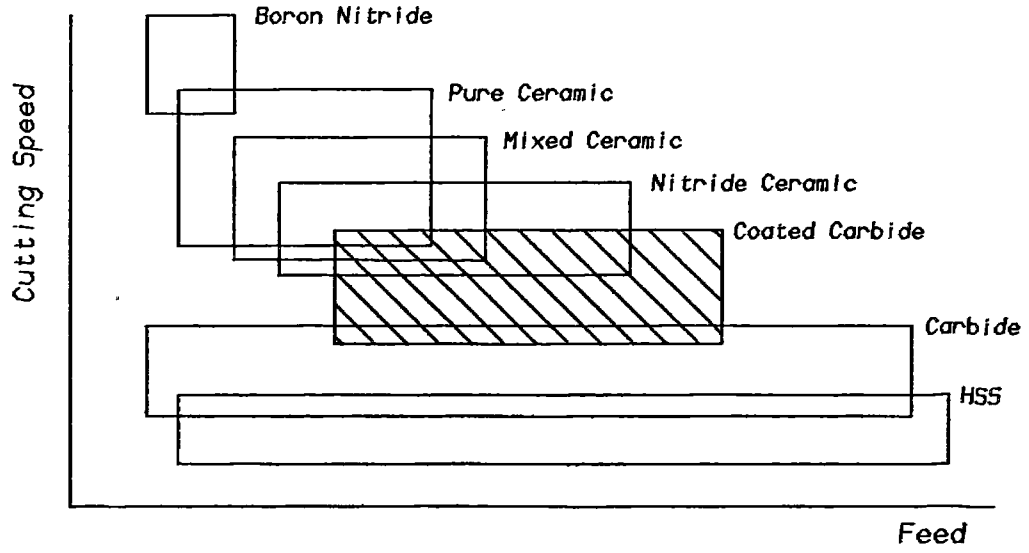

Fig. 2.4 Ranges of Feeds and Speeds for Different Tool Compositions[46]

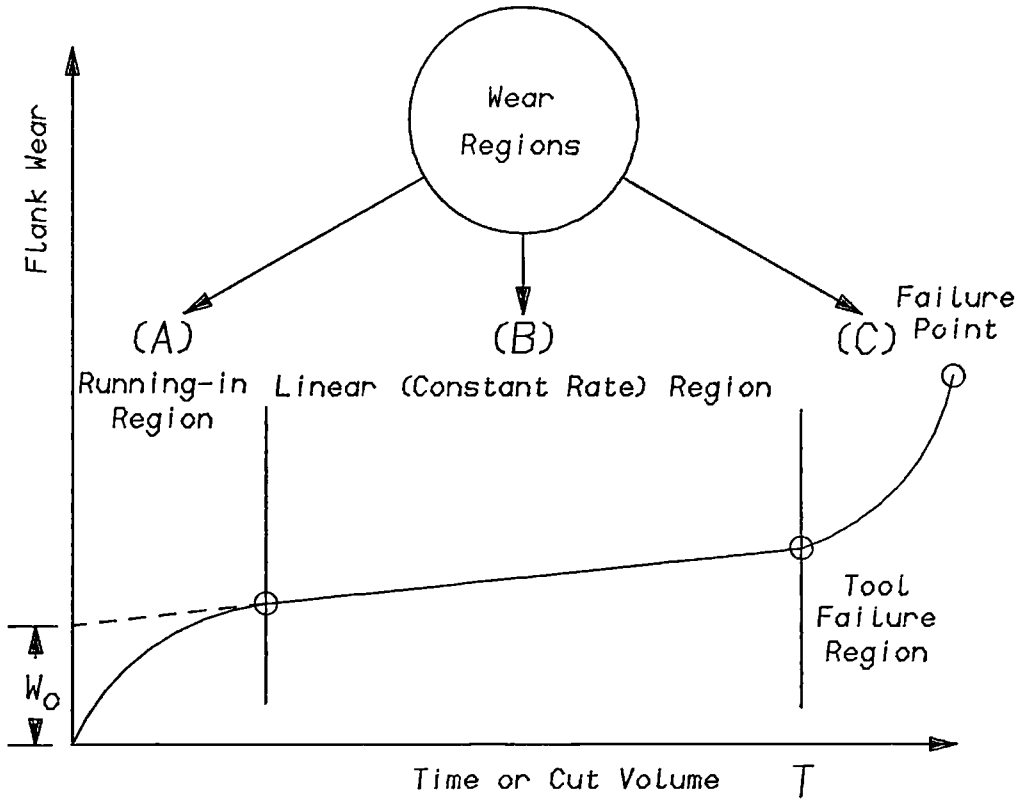

Fig. 2.5 Wear-Time Relationship in Metal Cutting

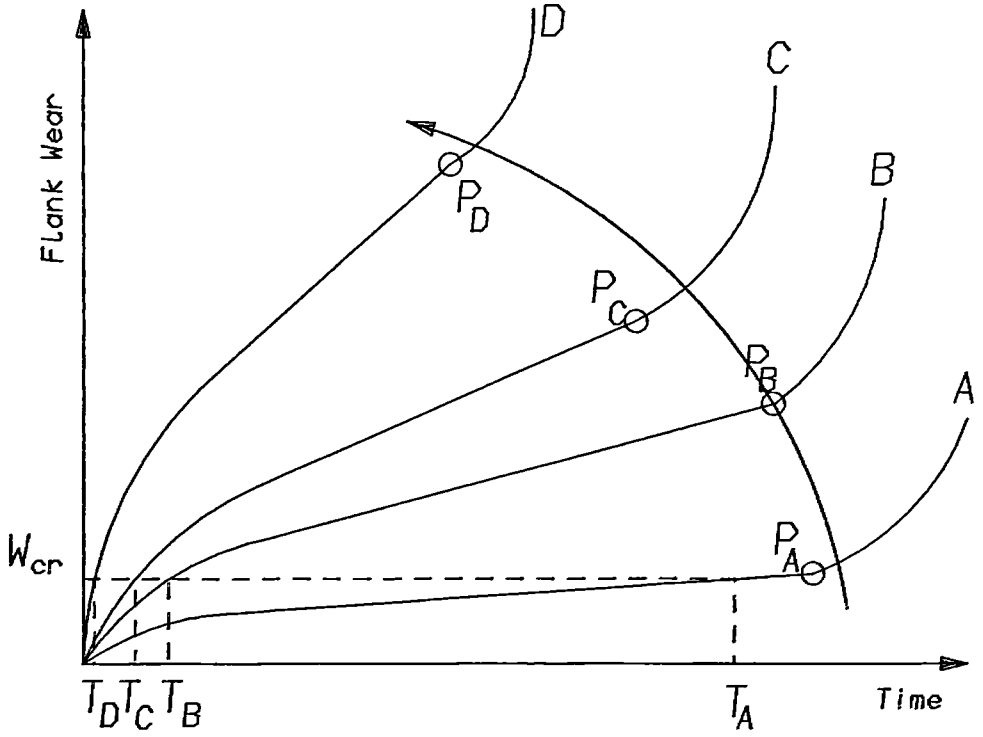

Fig. 2.6 Effect of Cutting Speed on Wear Behaviour

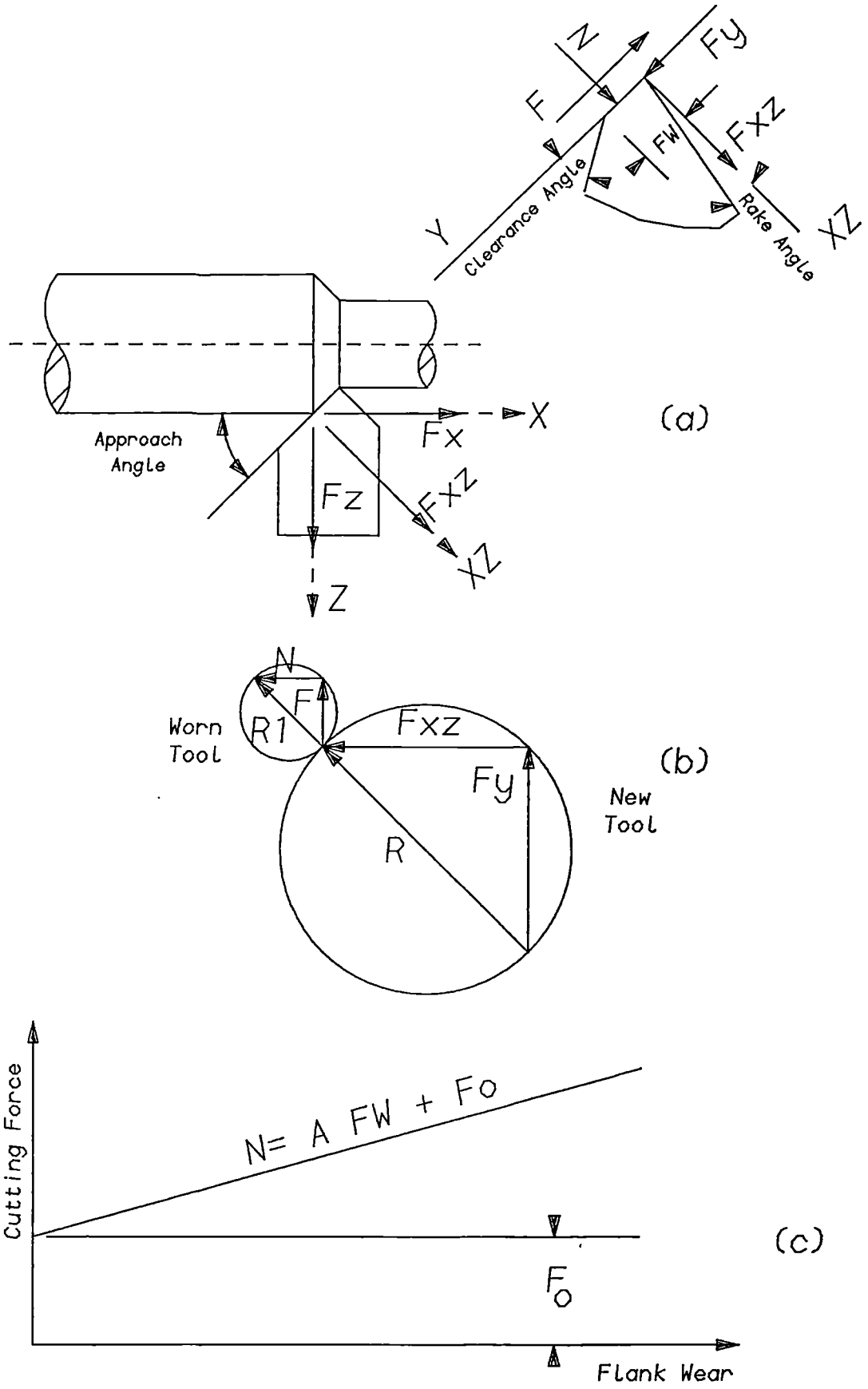

Fig. 2.7 Relationships of Flank Wear and Cutting Force Systems on Worn Tool and Dependence of Normal Force on Flank-Wear-Land on Growth of Flank Wear [12].

Chapter 3

EXPERIMENTAL DESIGN AND SET-UP

3.1 Design and Manufacture of a Three-Component Dynamometer

3.1.1 General Introduction and Foreword

In order to establish a quantitative basis for the analysis of metal cutting operations, certain observations must be made before, during, and after a cut. Due to the complications involved in machining operations, the number of reliable observations is inevitably rather limited. One of the most important measurements of this type is the determination of cutting force components. Cutting force is important for many reasons: *i*) its strong correlations with the inevitable tool wear during cutting; *ii*) because it is a useful source of information for rational design of machine tools and cutting tools; and, *iii*) because it is needed in judging and adjusting machining stability. Moreover, the control and optimization of the cutting process, especially since the introduction of adaptive control in recent years, depends, to a large extent, on the on-line cutting force measurement. This adds to the importance of developing reliable and accurate cutting force transducers.

The on-line measurement of cutting force in turning operations is made using dynamometric tools or dynamometric toolholders. Generally the most basic requirements in dynamometer design are rigidity, sensitivity, and accuracy. Also, a dynamometer performance is often assessed by the range of its frequency response and by its level of cross-sensitivity. To be as practical as possible, the apparatus should be compact and simple enough to be safely accommodated within the cutting zone without interrupting the production flow.

In this section, a new apparatus for measuring tool forces will be considered. A three-component, tool-shank, non-central circular-hole, strain-gauge dynamometer has been investigated, designed, manufactured, and calibrated. The analysis and distribution of stress in the circular-hole technique are explained. Optimum and most sensitive

positions for gauges have been investigated. Dynamic, static, and thermal calibration tests have been conducted. Mathematical models have been developed to characterize and formulate the dynamometer performance.

3.1.2 Mechanical Design Considerations

One of the main objects of this project is to use cutting force to estimate or predict the state of the cutting tool. During cutting, the tool is deformed in different ways, such as gradual wear, and random wear of chipping and fracture. These disturbances can be accurately identified only when all the cutting force components in all the three mutual co-ordinate directions, *Fig. 3.1,* are accurately measured. Measuring only one or two components is not the best way since, in most cases, many components are required to investigate the tool state.

Even though many types of dynamometers have been designed to meet some of the performance requirements, some problems, such as apparatus sensitivity and accuracy have never been solved. Also, most such models have some additional deficiencies such as low capacity, complicated design, large size, and difficulty in adopting to different cutting situations.

In a turning operation, cutting force components are often measured using either the octagonal-ring dynamometer type *[87 & 88],* or the tool-shank type *[54,89-91].* In addition to its large size, the conventional octagonal-ring prototype is capable, in most cases, of measuring only up to two force components. The tool-shank type is always characterized by its inaccuracy and insensitivity in measuring only one or two force components.

In the current design, *Fig. 3.2,* performance requirements such as high sensitivity, high rigidity, high accuracy, simplicity, and compactness have been attained. The way these have been achieved is discussed in detail in the rest of this section.

In order to estimate the capacity of the current dynamometer to be safely and efficiently used within the range of force levels expected during experimental procedures, it was necessary to use some of the general empirical equations developed by other investigators. *Shaw [23]* has proposed that the vertical force component F_y can be computed as :

$$F_y = \mu \left(1 - \frac{\alpha}{100}\right) \left(\frac{0.25}{t}\right)^{0.2} (F \times d) \qquad (N) \qquad (3.1)$$

where;

μ is the workpiece specific cutting energy (N/mm^2);

α is the tool side rake angle $(deg.)$;

t is the undeformed chip thickness (mm);

d is the depth of cut (mm); and,

F is the cutting feed $(mm/rev.)$.

Shaw states that the cutting force component in the feed direction F_x is not easily computed but for a first approximation it may be assumed to be one half of F_y. However, he adds, such a method of estimating cutting force is only approximate and is useful only in the absence of an actual experimental way of assessment. Application of Eq. *3.1* for conditions similar to those encountered in this project, a maximum value of vertical force F_y of 5120 N results. However, maximum capacity of 8000 N is thought to be necessary to take account of the force increase, especially at a late stage of tool life when wear level is rather high.

It can be seen from *Fig. 3.3* that the space to be occupied by the device is limited by take the size of the machine tool-post. Moreover, the dynamometer dimensions are adjusted to enable the existing clamping T-slots of the tool-post to be re-used in holding the dynamometer without any modification of the lathe structure. As seen in *Fig. 3.2,* the dynamometer consists of two main parts: the base; and, the body. The dynamometer base, *Fig. 3.4,* utilises a block of cast iron to replace the original tool-post. The base height is adjusted so that, when it is assembled with the dynamometer

body, the tool-tip vertical level is equivalent to the machine spindle height, h in *Fig. 3.3.* While the lower part is used in clamping the base to the lathe saddle, *Fig. 3.4,* the upper part is well ground to ensure smooth and firm clamping with the the dynamometer body. The top clamping area is restricted to the circumference of the base to ensure free straining of the dynamometer. The resulting engraved space (A, *Fig. 3.4*) is used to accommodate the wiring of the electrical circuits and to pass it through to the external interfaces. A clamping free area is left between the clamping positions a and $a1$, and the transducer sensing elements so that the clamping force does not affect the dynamometer performance.

In order not to affect the strain values recorded by the sensing elements of the dynamometer, a symmetrical and even tightening conditions were carefully applied amongst the clamping bolts. As shown in *Fig. 3.2,* a rectangular steel block was clamped on the top of the dynamometer body to ensure similar tightening conditions. In addition to its basic object, this block is used to hold the vibration accelerometers, as will be explained later in this chapter.

A special metal sheet guard is produced to protect strain-gauge circuits and wiring system from chips and accumulated dirt. This guard is designed to cover all the dynamometer body and base except for the tool-holder part. Enough clearance is left between the dynamometer body and the guard wall to ensure free straining of the dynamometer. The guard is clamped to the base in order not to make any real contact with the dynamometer body. Finally, special pass-ways for wiring terminals are prepared at the rear of the guard.

Fig. 3.5, indicate the basic elements of the dynamometer body. The dynamometer material is a direct hardening alloy steel grade [817.M40 *no.*24] (En24). Its chemical compositions and mechanical properties, as supplied by the manufacturer, are as follows:

a) Chemical Compositions

C	Ni	Si	Mn	P	S	Cr	Mo
0.4	1.5	0.2	0.6	0.038	0.04	1.2	0.31

b) Mechanical Properties

- Tensile Strength 1150 N/mm^2.
- Yield Stress 940 N/mm^2.
- Young's Modulus 2.157×10^5 N/mm^2.
- Elongation 11%.
- Hardness 360 HB.

As shown in *Fig. 3.5,* the dynamometer body consists of three main zones: the front zone A which is the tool-insert holder; the middle zone B which is the transducer house; and, the back area C which is used to clamp the dynamometer body to the base. The front part, the tool-insert holder, is designed to accommodate the standard *SPUN* 12 03 12 indexable cutting tool insert to take the same geometry as of the *SANDVIK* standard toolholder *CSTPR* 20 20 *K*12, *Fig. 3.6.* As indicated in *Fig. 3.7,* the geometry of the tool-insert holder is adjusted so that the true cutting application point O passes through the centroid of the dynamometer body. The tool-tip point is not the true force application point since the cutting process is executed on the tool-workpiece contact length rather than only on the tool tip. Since a maximum depth of cut of 4 mm will be used in this study, a distance of 1.2 mm exists between the true application point and the tool tip. Similarly, the height of the true application point is set so that when the tool-insert is assembled with its shim, chip-breaker, and the clamp, the force line action will pass through the centroid of the dynamometer body. This minimizes the interaction, or cross-sensitivity, among the various force components through eliminating the causes of their mutual moment components. As shown in *Fig. 3.7,* if the point of force application is considered as the tool-tip, a cross-sensitivity will result in terms of two moment components: M_x which is due to F_x; and, M_z which

is due to F_z. For a light force component of 100 N, a total moment of 240 Nmm would exist in the horizontal plane alone. The problem would be made worse if such a situation was accompanied by a similar deviation in the vertical plane. The problem of accurately locating the true point of force application has long been a subjective matter. *Sun et al [91]* stated that the relative position of the point of application of the cutting force with respect to the transducer was a problem of much concern and had never been satisfactorily solved. *Levi [89]* stated that the effect of the deviation between the application point and the reference point (dynamometer centroid), in terms of moments, was so important that it must be considered if an accurate measurement is to be obtained. Since this could not be solved mechanically within the design stages, *Levi* developed mathematical equations to take account of such additional components. *Shanshal [92]* also faced the same problem of high cross-sensitivity which forced him to modify his design several times.

The configuration of the toolholder is machined so that the generated cutting forces are faithfully transferred to the sensing elements. Sharp corners, where stress concentration is most likely to occur, are avoided, and a gradual and stepped increase in the cross-sectional area from tool-holder to greater size of transducer house, has been achieved. Another important element of the dynamometer body is the transducer house which contains the sensing elements, part B in *Fig. 3.5.* This consists of two zones: the first acts as sensing elements for each of X and Y force components, and the second, which is shoulder shaped and situated at the back of the dynamometer body, acts as sensing elements for the Z force component.

Tani et. al. [93] have developed various types of circular hole dynamometers. They used the finite element method FEM to obtain information about the characteristics of the circular hole for different shapes of structures and loading conditions. Results indicated that the circular hole provided higher stiffness, but lower sensitivity than that obtained from parallel beam square hole dynamometer, which they developed at previous stages. However, the use of a circular hole reduced interaction and, it was easier to manufacture. In addition, strain output of a circular hole dynamometer was found to be many times as large as that of an octagonal type. The dynamometer design

to be used in this thesis is based on the research of Tani et al [93]. As pointed out by them, the shape of the circular hole dynamometer, Fig. 3.8, is governed by the following dimensions:

1. diameter of the hole D;
2. width of the dynamometer b;
3. the minimum section t;
4. the distance from the fixed end to the centre of the hole l1; and,
5. the distance from the loading point to the centre of the hole l2.

In the FEM study carried out by Tani et. al., the effect was investigated of a variation of the dynamometer shape upon the following parameters:

1. Output strain ϵ.
2. Stiffness (load per unit displacement) κ.
3. Angle of inclination at the loading point θ.

Tani found that the performance of a circular hole dynamometer is determined by the shape factor which can be defined as:

$$ShapeFactor = \frac{D}{D + 2t}. \tag{3.2}$$

The results of Tani's study may be summarized as follows. The output strain ϵ increased by decreasing of the wall thickness at the minimum section t for a given hole diameter. A reduction in the wall thickness caused a decrease in stiffness κ, while the inclination angle θ at the loading point increased. For a given plate thickness (2t+D), an increase in the hole diameter caused an increase in both output strain ϵ and inclination angle θ, while stiffness was reduced. For a given plate thickness, an increase in the dynamometer width b was found to increase stiffness κ, while both output strain and inclination angle

were non-linearly decreased. It has been found that for a constant shape factor, Eq. 3.2, the output strain suddenly increased when the distance from the fixed point to the hole centre l1 approached the hole radius. Beyond this value, the output strain was not greatly changed. Nevertheless, the dynamometer stiffness was greatly affected by increasing l1. Similar characteristic, but with lower rate of change, were obtained when the effect of the distance from the loading point to the hole centre l2 was investigated. A minimum cross-sensitivity of the dynamometer was detected when the longitudinal load, shown in Fig. 3.8, was applied to the centre of the plate thickness (centroid of the dynamometer). Also, FEM results showed that there was no interaction when the ratio of lower to upper thickness in the minimum section was unity. Also, it has been shown that the cross-sensitivity was affected by the dimensional error in terms of change of the plate thickness in the longitudinal direction; or of the axis inclination.

Tani et. al. [93] used these characteristics to develop various types of *circular hole* dynamometers as shown in Fig. 3.9. In the paper [93] they stated that the configuration of two non-central circular holes connected by a slit, as shown in Fig. 3.9.b,, has the same characteristics. If, however, a larger output is desirable, a design like that in Fig. 3.9.c, or Fig. 3.9.d, was recommended. However, the latter would increase the overhang, especially when another hole is required for the other coordinate direction, and this is not desirable in the case of metal cutting dynamometers. As shown in Fig. 3.10, to increase the dynamometer sensitivity, for a given plate thickness, the central hole should be increased from d1 to d2, and consequently, the wall thickness at the minimum section is reduced from t1 to t. As shown in the figure, by using a non-central circular, the dynamometer sensitivity is maintained and, at the same time, higher stiffness is resulted in terms of reducing the overhang from L1 to L.

The Finite Element Analysis of the situation by Tani et. al. [93] has been used to predict the shape of the current design. Both the width and depth of the dynamometer have been determined by the best position of the point of force application in conjuction with the configuration of the standard toolholder. According to Tani's finite element analysis for a given plate thickness (depth), the best shape factor to maintain both

stiffness and sensitivity of the dynamometer, is given by:

$$0.4 \leq \frac{d}{2t+d} \leq 0.6. \tag{3.3}$$

These inequalities are useful to determine the hole size for a given plate thickness, and have been used to estimate the initial hole size. Using this relation, in conjunction with the dynamometer dimensions in Fig. 3.7, leads to the evaluation of the most practical values of hole diameters, which are : (8.56 - 12.8 mm); (7.6 - 11.4 mm); and, (4 - 6 mm) for the load in X; Y; and Z directions, defined in Fig. 3.1, respectively. However, to determine the minimum wall thickness, for a given hole size, it is necessary to make use of the following inequality determined by Tani [93] from finite element analyses:

$$\frac{d}{2t+d} \leq 0.7. \tag{3.4}$$

The FEM results indicated that, beyond this value, the dynamometer stiffness and strain per unit displacement decreased. Using the limit value of 0.7, Eq. 3.4 becomes:

$$\frac{d}{2t+d} = 0.7, \tag{3.5}$$

therefore, the least thickness t_{min} can be determined as:

$$t_{min} = \frac{0.3\ d_{min}}{1.4}. \tag{3.6}$$

Thus, in the range of hole diameters predicted above, *tmin* takes the values of 1.83, 1.63, and 0.86 for holes receiving loads in X, Y, and Z directions respectively. These dimensions were used as initial values for prototype design manufactured in aluminium. The Final Design has been arrived at following experimental development described below.

3.1.3 An Aluminium Trial Model

For the dynamometer to produce its highest output, the wall thickness under strain should be investigated and an aluminium model was used to fully investigate the design and to elucidate some of its characteristics such as accuracy; stiffness; and, sensitivity.

According to the Finite Elements Method *FEM* by *Tani [93]*, the stress-distribution around the hole boundary, as a result of the applied load, is as shown in *Fig. 3.11.* While a maximum strain exists at distance of 0.10 of the hole diameter towards the hole centre, only 90% of the maximum output exists at the hole boundary. Therefore, great care must be taken to determine the positions at which the gauge gives its highest and most accurate output and, at the same time, to maintain the stability of the bridge through ensuring identical conditions of the employed gauge in the same circuit. However, one of the unclear aspects was the dynamometer sensitivity as affected by the relative hole diameter-wall thickness dimensions and this is investigated in this section.

The aluminium model was designed, manufactured and calibrated with fundamental configurations as indicated in *Fig. 3.5.* A non-central circular-hole was produced for each of X and Y directions while a central one was for the Z direction. A single self-temperature-compensation micro-measurement strain gauge type ($EA-13-045AL-350$), as recommended for aluminium, was bonded to each direction at positions a, b, and c for X, Y, and Z directions respectively, *Fig. 3.12.*
The model was a *NP8* in aluminium with a chemical compositions, as provided by the manufacturer, of [0.1 Cu, 0.45 M, 0.4 Si, 0.4 Fe, 0.75 Mn, 0.2 Zn, 0.25 Cr, 0.15 Ti, and the remainder Al]. The tensile strength was 277 N/mm^2, therefore, for a given load, the model was expected to produce about four times as much output as given by the steel dynamometer. A Denison tension-compression testing machine was used in calibrating the various directions in turn. For each direction, a gradual load was applied in 200 N steps up to 2800 N. The output was recorded by connecting the circuits terminals to a Vishay strain-indicator. After reaching the objective maximum, the load was gradually released in the same order and the corresponding readings were recorded. *Fig. 3.13* shows the calibration curves for the various components with good linearity and no-hysteresis is detected among most of the load range. However, due to the huge capacity of the Denison testing machine, it was difficult sometimes to control the machine to obtain low loads. This was one of the reasons why the calibration procedures for the real dynamometer were carried out using different arrangements, as

will be explained later. Output levels showed that the sensing elements for Y direction were the most sensitive, about 1.6 times as much of that for X direction , and twice as sensitive as that for Z direction. Such results are essential since the wall thickness for Y direction is thinner than that for X direction and its overhang is longer.

A separate procedure to determine the most sensitive hole position for Z direction, indicated that the least output was when the hole was at the middle of the shoulder. This supported the previous choice of such holes at the shoulder just outside the overhang end, *Fig. 3.5.* However, the output level was very low for all directions and further mechanical modifications were required. Therefore, the hole diameters were enlarged and the wall thickness was reduced, and another study was carried out to check its feasibility. The sensing elements for Y direction was taken as an example. The gauge position relative to the hole centre was kept fixed, while the hole diameter, and consequently the wall thickness, was changed in three steps expressed by cases 2, 3, and 4 in *Fig. 3.14.* For each case in turn, calibration procedures were done using the arrangements previously described.

The outputs for each case, along with the original output for case 1, are shown in *Fig. 3.15.* Results indicate that, despite the reduction in the wall thicknesses for cases 2 and 3, the output decreased, while it significantly increased in case 4. This increase in case 4 was due to the new relative gauge-hole position rather than the wall thickness reduction for two reasons. First, for cases 2 and 3, the output was decreased despite the reduction in the wall thickness; the second reason may be explained by the *FEM* by *Tani [93]. Tani's* results indicated that when the ratio $\left\{\frac{d}{2t+d}\right\}$ was increased by 2.75 times, a 50% increase in the output was obtained. Considering cases 1 and 4, an average output increase of 34% was obtained by increasing the ratio by only 10%. Therefore, almost all the improvement was due to the new relative gauge-hole border position and not to the mechanical modifications of reducing the wall thickness. Higher level of output would be obtained if the gauge centre was at a distance of $\left\{\frac{1}{10}d\right\}$ so as to take the geometry indicated in case 5 in *Fig. 3.14.* Also, output would be improved if the wall thickness was reduced without increasing the hole diameter through shifting the hole centre. This would not affect the overhang length since the non-central

circular-hole technique would be used.

3.1.4 Final Configuration and Dynamic Calibration

The information which emerged from the aluminium trial study, such as output level, and optimum gauge position, was used to determine the relative hole-thickness ratios for the actual steel dynamometer. As shown in *Fig. 3.16,* the hole-thickness ratio was increased from 0.5, for the aluminium model, to 0.65 for each of Y and Z directions while a ratio of 0.7 was found to be necessary for X direction. This higher ratio for X direction was needed because in practice the feeding force component F_x is always less than one half of Y component, and therefore, its bridge should be more sensitive.
For each direction, a temporary single gauge was used to study the static and the dynamic characteristics of the dynamometer in its final mechanical form. The relative gauge-hole positions were set to meet the point of maximum output level, *Fig. 3.16.* This stage of tests includes : (i) examining the improvement in output level due to the new modification, and (ii) determining the dynamometer frequency response.

Firstly, the output level was examined using the same calibration arrangement as that used in calibrating the aluminium model. For each direction, the output, in microstrains $\mu\epsilon$, was recorded by a Vishay strain-indicator. Output levels in *Fig. 3.17* reveal a significant improvement which is about four times as much as that from the aluminium model. As intended, the X channel was the most sensitive, followed by the Y channel, and finally the Z channel was the least sensitive one.

The second aspect to be studied at that stage was the dynamometer frequency response. The object of this study was to obtain the fundamental natural frequencies and the dynamic characteristics of the dynamometer, so as to enable the determination of the range of its working frequencies.
The natural frequency of the dynamometer usually determines its general dynamic stiffness. Machine tools operate with some vibration, and in certain circumstances,

these vibration may have large amplitudes. In order that the recorded force is not influenced by any vibrating motion of the dynamometer, its frequency must be large, at least four times as large *[23]* compared to the frequency of the exciting vibration.

Due to the complication of the dynamometer configuration, in particular the existence of the circular holes in the three different coordinate directions, along with its end clamping conditions, its shape modes cannot be simply described using a lumped parameter system. To describe, for instance, the motion of any point within the dynamometer body it is therefore not enough to describe the instantaneous vibration amplitude as a function of time only. It must also be described as a function of spatial coordinates. Also, lateral, transitional, compressional, and torsional vibration might simultaneously occur when the structure is subjected to excitation in practical situation. For such conditions, a complex analysis, in terms of higher order differential equations, is required to simulate all possible vibration modes. In most situations, however, this strategy will not be fruitful since the direction in space of each excitation source may vary instantaneously and randomly. Therefore, a better and more realistic way to obtain the frequency response of the dynamometer is by exciting the system and, by observing its response. This was achieved by means of exciting the dynamometer in each direction, and recording the corresponding output over a wide range of frequencies.

Fig. 3.18 shows a block diagram for the frequency response test while *Fig. 3.19* shows a view of the arrangement and instrumentation used. The dynamometer was rigidly clamped to its base, and then to one of the tables of a die-sinker engraving machine, which has three-axis movements. The dynamic characteristics of each direction were obtained by applying a sinusoidal excitation force of approximately constant amplitude using an electro-magnetic excitor at a wide range of frequencies. The electro-magnetic excitor was clamped to one of the die-sinker machine tables. A sinusoidal signal was generated using a signal generator, and then fed to the excitor through a power amplifier. For each direction, the exciting force was applied at the centre of the corresponding cross-section area to avoid higher dynamic transverse sensitivity. The excitor head was

designed to ensure that the force acted precisely on the desired position. The magnitude of the excitation force, and the distance between the dynamometer surface and the excitor head were kept fixed throughout the test stages. The frequency of this force was gradually increased from 200 Hz to about 8000 Hz and the corresponding acceleration values were recorded through bolting a vibration accelerometer parallel to the line action of the exciting force. Then, the accelerometer output was fed to a 3-Channel vibration pick-up pre-amplifier which was adjusted to give a constant calibration factor of 0.1 volts per 10 m/sec^2 of the dynamometer acceleration. Finally, the output was displayed on and stored in a 2-Channel oscilloscope.

Fig. 3.20 represents the frequency response curves of the different co-ordinate directions of the dynamometer, along with the dynamic cross-sensitivity among the different mutual direction. This was obtained by simultaneously recording the output from all directions when the excitation force was applied in each direction in turn. It can be seen that when resonance occurs in any direction, all the directions are activated generating a symphonious motion. However, in most cases, the transverse sensitivity is not as strong as the main component. For each direction, the frequency at which the peak amplitude has occured (resonance ω_r) is considered as the first fundamental natural frequency. The curves show that the fundamental resonant frequency in each of the co-ordinate directions are 1360, 750, and 3000 Hz for X, Y, and Z directions respectively. These frequency levels were considered high enough to prevent any interference to steady-state force measurement due to the dynamometer oscillations.

Precautions should be taken during interpretation of the results of such tests, one should be aware of many aspects and, in the following a discussion is presented of those factors which might influence the test results. First, the die-sinker machine on which both the dynamometer, its base, and the exciter were mounted, did not have the same stiffness and damping characteristics as the lathe used in metal cutting tests. The die-sinker machine may therefore impose its own characteristics on the dynamic response of the the dynamometer [94 & 95]. Andrew [96], however, indicated that the dynamic difference, in terms of inertia force due to motion of the dynamometer's head, could

be accounted for by mounting an accelerometer directly on the dynamometer head and thus monitoring the inertia force correction for any condition of the underlying structure.

Second, the dynamometer base was clamped to an angle plate, which in turn was clamped to the far left of one of the die-sinker's tables as shown in Fig. 3.19. In such a position, the dynamometer and its base might be subjected to an angular oscillation during excitation. This might explain why in Fig. 3.20.c the dynamometer seems to have a principal direction not coincident with the axis on which the exciting force was applied (direction Z in Fig. 3.1). Also the mass of the connector to the exciter, along with the mass of the accelerometers, may add to the dynamometer moving mass and affect the dynamical response.

Third, the characteristics of the electromagnetic exciter may be changed within the range of frequency employed in the test. The electrodynamic exciter requires a constant magnetic field to produce a constant force level. In the test, a certain amount of power from the vibration exciter was fed to the dynamometer body at a slowly changing frequency. Due to the fact that the back-EMF is changing as a function of many factors, among them the exciting frequency [97], a constant force is not ensured throughout the range of frequencies studied. In order to maintain the constancy of the exciting force, a closed-loop compensatory mechanism is required to keep the supplied current constant. The lack of achievement of constant force using conditions over the frequency range prevents the quantitative assessment of the results.

As is evident from the above discussion, it may be said that the results obtained are of qualitative significance only and approximate to the dynamometer true dynamic characteristics. However, to confirm the above dynamometer frequencies, the dynamometer was set into vibration by a hammer blow while mounted on the die-sinker table, Fig. 3.19, and oscilloscope records of the output were obtained, *Fig. 3.21.* For each of the co-ordinate directions, the number of oscillations per unit time was counted to represent the damped natural frequency ω_{nd}, or the time taken until the structure

reached a standstill state. For X, Y, and Z directions, the values of such damped natural frequencies were found to be 1648,850, and 3046 Hz respectively.

The relationships between a structural natural frequency ω_n, resonant frequency ω_r and a damped natural frequency ω_{nd}, in the case of light (viscous) damping, are given by:

$$\omega_r = \omega_n\sqrt{1-2c^2}; \quad and$$
$$\omega_{nd} = \omega_n\sqrt{1-c^2}, \tag{3.7}$$

where c is the damping ratio. For solid structures where the damping is small, being of hysteretic type caused by internal friction [98], the values of the three frequencies ω_r, ω_n, $\&\omega_{nd}$ are almost equal. When the set of equations (3.7) is used to determine the values of system damping, unrealistic values resulted, which contradict what would be expected from the free vibration traces shown in Fig. 3.21. This is because the large difference in the corresponding values of resonant ω_r and damped ω_{nd} frequencies measured. As discussed before, the connector of the exciter and the three accelerometers were added to the dynamometer mass during the resonant test, while for the damped natural frequency test only one accelerometer was clamped to the intended direction, without the connector attached.

However, the dynamometer damping may be better estimated by observing the rate of decay of oscillations of the free vibration signatures shown in Fig. 3.21. For viscously damped harmonic motion, the successive amplitudes of a motion have a logarithmic relationship with one-another expressed by the term "logarithmic decrement", which is defined as the natural logarithm of the ratio of any two successive amplitudes. For more accurate estimation, however, decrement δ may be computed over N cycles from the relationship [98]:

$$\delta = \frac{1}{N} \ln\left[\frac{X1}{X_{N+1}}\right] = \frac{2\pi c}{\sqrt{1-c^2}}. \tag{3.8}$$

According to Eq. (3.8), in conjunction with Fig. 3.21, the damping ratio, c, for X, Y, and Z directions were found to be 0.00737, 0.00996, and 0.00668 respectively.

Computations were carried out so that to eliminate the effect of disturbances in the first few cycles by considering an exponential envelope tangential to peaks of the signature.

3.1.5 Dynamometer Electrical Design

3.1.5.1 Strain-Gauges Circuits Design

The theory of strain gauges is based on the fact that the resistance of a conductor changes when the material of the conductor is subjected to strain. Such variation in the resistance is due to two factors: the specimen deformation; and, the change in the resistivity. The filament resistance R increases by ΔR when the filament is stretched. Generally, a linear relationship between the strain and the resistance is in form: $\left\{\frac{\Delta R}{R} = K\frac{\Delta L}{L} = K\epsilon\right\}$, where K is called the K-factor and represents the proportionality constant, and ϵ is the strain. Thus the K-factor gives the relation between the specific change in resistance and the specific change in the length ϵ of the filament. The value of the K-factor is generally in the range 2 to 4 depending on the material used for the filament.

Stress investigation with a strain-gauge is usually carried out in the elastic range where *Hook's* law applies, i.e, where ϵ is about 0.001. Considering a K-factor of 2, then the maximum resistance variation ΔR is about 2×10^{-3} or 0.2% with a strain of order of 1×10^{-6} $\mu\epsilon$. It will thus be clear that the resistance variation is very low and, therefore, it is very important to locate accurately the point of maximum deformation. Also, a proper selection of the very sensitive measuring instrument is required. Such mea-

surements of the very low output of a strain-gauge are usually made by means of the Wheatstone bridge, *Fig. 3.22.* No output is obtained if the four resistors satisfy the conditions $\left\{\frac{R1}{R4} = \frac{R2}{R3}\right\}$ or $V_C = V_D$. If, for instance, the resistor R1 has been replaced by a strain gauge to consisting of a single active arm bridge, the condition of $V_C = V_D$ no longer exists when the gauge is stretched producing voltage difference at points C and D. If, at the same time, R4, or R3, is an active arm with a gauge in place of the resistor, the output will be duplicated when the gauge in position of R4 is negatively stretched, or when the one in position of R3 is positively stretched. Generally, the Wheatstone bridge output V_{out} can be expressed as:

$$V_{out} = \frac{N}{4} \quad V_{in} \quad K \quad \epsilon \tag{3.9}$$

where;

N	is the number of the active arms in the bridge;
V_{in}	is the excitation voltage to the bridge;
K	is the gauge factor; and,
ϵ	is the gauge longitudinal strain.

As indicated in *Fig. 3.23.a,* the hole wall under applied load is deformed in such a way that a maximum positive strain exists at one end of the hole boundary while a maximum negative one exists at another end. This operation is reversed at the opposite hole so that, if gauges arrangement is set as shown in *Fig. 3.23.b* to consisting of a full active arms bridge, *Fig.3.23.c,* the bridge output become eight times as much as if a single arm bridge is used.

Alongside the significant improvement in the apparatus sensitivity achieved by this arrangement, the bridge is fully compensated for any change in resistance due to temperature rise. Also, the use of two gauges per arm instead of one enables the excitation voltage to be doubled without overheating the gauges. These two aspects will be discussed in detail shortly.

While this circuit design is suitable for the sensing elements of each of X and Y directions, the case is slightly different for Z direction. As previously mentioned, the sensing

elements of Z direction are affected by two force components, F_z and F_x, *Fig. 3.24*. While the F_z produces a direct effect of simple bending *sb*, the F_x produces an indirect effect of double bending *db*. The total effect of both direct and indirect causes on the sensing elements of Z direction are shown in *Fig. 3.24.d*. Gauges positions are chosen, *Fig. 3.24 (b & c)*, so that the effect of the double bending tension *tdb* in gauge *no.* 2 will cancel the effect of the compression *cdb* in gauge *no.*3, and the same will occur for gauges *nos.* 1 and 4. This results in a four active arms bridge by which the only direct effect of F_z is detected, *Fig. 3.24.d*.

The employed strain-gauge was of self-temperature-compensation type ($EA-06-045AL-350$), which is recommended for steel specimens, and has the following characteristics:

- Gauge Factor (K) 2.01 $\pm$ 1.0%.
- Effective Gauge Length 1.14 *mm*.
- Gauge Resistance 350 $\pm$ 0.15% Ω.
- Transverse Sensitivity +0.6%.

3.1.5.2 Selection of the Optimum Excitation Voltage

As indicated in Eq. (3.9), the output voltage from the bridge depends upon the strain level, gauge factor, and bridge supply voltage. However, the maximum safe excitation voltage to a bridge is determined by the desired stability. The voltage applied to a bridge creates a power loss in each arm, all of which must be dissipated in form of heat. This causes the sensing grid to operate at a higher temperature than the substrate to which it is bonded. When the temperature rise is excessive, gauge performance is affected in terms of loss temperature-compensation, hysteresis, and creep effects. This always causes zero-shifting of the bridge. If a stable zero setting is required over a long time, the limit of maximum excitation voltage should be carefully selected.
The factors of primary importance in determining the optimum excitation voltage for

any strain applications are: grid area; resistance; and, heat-sink properties of the mounting surface. According to *[99]*, the power dissipated in gauge grid Pg takes the form:

$$Pg = \frac{(V_{in})^2}{4R} \qquad (watts) \tag{3.10}$$

and the power density in grid is :

$$P'g = \frac{Pg}{Ag} \qquad \left(kW/m^2\right) \tag{3.11}$$

in which Ag is the active grid area *(active gauge length* $\times$ *grid width)*. Thus, the excitation voltage takes the form:

$$V_{in} = 2\sqrt{R \;\; P'g \;\; Ag} \qquad (volts) \tag{3.12}$$

When each arm consists of two gauges in series, this relation becomes:

$$V_{in} = 8\sqrt{R \;\; P'g \;\; Ag} \qquad (volts) \tag{3.13}$$

Since the bridge output V_{out} depends on the excitation voltage V_{in}, the bridge output is further improved by factor of 4.

According to *[99]*, for a thick steel mounting surface working under dynamic conditions (short-time exposure), a grid power density $P'g$ may be between 7.8 and 31 kW/m^2. Substitution of these values, along with the gauge area and its resistance value R, in Eq. *(3.13)*, the recommended excitation voltage is found to be between 5.47 and 10.62 volts. For convenience, an excitation voltage of 10 volts was selected for use in this study.

To examine the effect of this level of excitation voltage on the temperature rise on the dynamometer surface near the gauges positions, a set of thermocouples was bonded at positions indicated in *Fig. 3.25.* As will be explained later, this apparatus was used to study the effect of cutting temperature on the gauges performance. *Table 3.1* shows the results collected from this set of experiments.

	Top-Left	Bottom-Left	Bottom-Right	Top-Right	Zero Reading		
Time	$°C$	$°C$	$°C$	$°C$	X	Y	Z
01.05 pm	18.0	18.0	18.0	17.9	0.000	0.000	0.000
02.10 pm	18.4	18.4	18.4	18.3	0.000	0.000	0.000
04.05 pm	18.8	18.8	18.8	18.5	0.000	0.000	0.001
11.00 am	17.9	17.9	17.9	17.5	0.002	0.000	0.005

Table 3.1 Temperature Rise due to Excitation Voltage

It can be said that the selected excitation voltage has a negligible effect in both the dynamic case (short-time exposure), and the static case (long-term exposure).

3.1.5.3 Dynamometer Instrumentation

The output from the strain-gauge bridge was amplified by means of a specially designed strain gauge amplifier. The requirements for this amplifier were to include three strain-gauge circuit bridges each with a 10 volts input voltage. Preliminary cutting tests proved its high stability where no drifting was noticed in either short or long term. The gain of the amplifiers was adjusted to give an electrical output of $0.994, 1.01475$, and 0.954 millivolts/N for X, Y, and Z bridges respectively.

The output from the amplifier was fed to a specially designed 3-Channel $12 - bit$ analogue-to-digital converter ADC as shown diagrammatically in *Fig. 3.26.* The requirements for the ADC were to include three separate circuits to receive voltage range from -5 to $+5$ volts with accuracy of 2.44 millivolts/bit. The analogue value for each direction was transferred sequentially with a sampling rate of 1666 samples/sec.

The output of the ADC was received in by BBC microcomputer memory using basic and assembly software programs. Due to the low storage of the $BBC\ RAM$ of the memory of 32 kbytes, a storage extension of 128 kbytes was added, resulting in a sampling rate of 27.8 sample/sec. Such a rate was high enough to allow, in most cases,

at least three readings per workpiece revolution to be recorded. Following machining of each sub-test, which lasted for about two minutes, the stored data in *BBC* memory was transferred to floppy disks for permanent storage. *Fig. 3.27* shows a view of the instrumentation used in this study.

3.1.6 Dynamometer Static Calibration

The static calibration of the dynamometer usually determines the relation between the input, in terms of applied load, and the output, in terms of bridge output. Due to the problems involved with the Denison machine used in calibrating the aluminium model, other procedures were used in calibrating the dynamometer in its final form. To ensure similar conditions to those that would be found in a real machining situation, the calibration procedures were carried out while the dynamometer was mounted on the lathe, *Fig. 3.28.* A hydraulic jack was used to induce the load, in forms of one-way displacement from the jack piston. This load was transferred to the dynamometer body through a pre-calibrated load cell and a carrier bar. The load cell was calibrated to read the output in Newtons. The corresponding microstrains $\mu\epsilon$ was recorded by parallel connecting the output to a Vishay strain-indicator.

To ensure that the load was accurately applied to the true application point, a flat dummy tool-insert was machined and used in the calibration procedures. As indicated in *Fig. 3.29,* this ensures an accurate location where the applied load is perpendicular to the intended surface. It also avoids any slipping which may occur due to the geometry of the true insert. A hardened steel ball was inserted between the load carrier bar and the dummy insert to ensure an accurate location.

The bridge output was fed to the strain-gauge 3-Channel amplifier, and then displayed on three voltage display units. The calibration procedures were carried out for each of the three co-ordinate directions in turn. For the X direction, a supporting bar was clamped by the lathe chuck to hold the cylinder of the hydraulic jack by means of two magnetic V-shape blocks, *Fig. 3.28.a.* The same procedure was used to calibrate the dynamometer when the load was in Z direction by rotating the dynamometer by

90 *deg.* anti-clockwise to make the line of action of the load parallel to the machine centre-line, *Fig. 3.28.c.* When the load was in Y direction, *Fig. 3.28.b,* the jack piston was clamped to the lathe saddle, and the dynamometer body turned upside down with the load applied upward.

For each direction, the load was gradually increased in 100 N steps, and the reading from the corresponding channel, along with the readings from the other two inactive channels, were simultaneously recorded. On reaching the full load of 4000 N, the load was gradually released in 200 N steps, and the equivalent readings were recorded. The static rigidity of each of X and Y directions was determined by measuring the dynamometer deflection at full load using a dial gauge.

The calibration curves for each direction together with cross-sensitivity curves with the other two components are shown in *Fig. 3.30.* These curves indicate the relationship between the load and the output both in volts and microstrains $\mu\epsilon$ for each channel. Excellent linearity was obtained in all directions, and no hysteresis was detected.

A comparison of the level of output with those obtained in different stages of this study is summarized in *Table 3.2.*

	Aluminium Model	Steel with One Gauge		Final Design	
Direction	$\mu\epsilon$	$\mu\epsilon$	% Imp.	$\mu\epsilon$	% Imp.
X	94	170	723	1836	1080
Y	152	149	392	1630	1049
Z	74	120	649	622	552

Table 3.2 Output Improvement in Various Stages of Design

A great improvement in output level has been achieved from the aluminium model to the steel one; this is basically due to the accurate location of the strain gauges at the point of maximum strain. The final improvement in the level of the dynamometer output was due to the final design of the bridge as a full active two-gauge per arm

circuit. For each of X and Y bridges, the improvement is about 1000%, while it is only 500% for Z bridge since only one gauge per arm was used for this circuit. Both the dynamic and the static dynamometer characteristics are summarized in *Table 3.3.*

Characteristics	X	Y	Z
Damped Natural Frequency ω_{nd} (Hz)	1650	850	3046
Resonant Frequency ω_r (Hz)	1360	750	3000
Damping Ratio c	0.00737	0.00996	0.00668
Mechanical Calibration Factor ($\mu\epsilon$/N)	0.3808	0.3410	0.275
Electrical Calibration Factor (mv/N)	0.995	1.0148	0.954
Rigidity (N/mm)	10068	11249	–

Table 3.3 Dynamometer Static and Dynamic Characteristics

3.1.7 Mathematical Modelling of Dynamometer Output

3.1.7.1 Dynamometer Performance and Cross-sensitivity Manipulation Technique

The goal in any multi-channel transducer is that the output of each channel should be affected only by the corresponding influence, and the influence of the remaining effects being nil. In dynamometry and cutting force transducers this goal has never yet been reached even when the most sophisticated techniques have been used. In this work efforts have been directed towards the minimization of the undesired effect of so-called interaction, or cross-sensitivity.

In this section, the possible elimination of the effect of the cross-sensitivity among the different component is examined through mathematical modelling of the dynamometer performance. Mathematical modelling of the dynamometer output allows on-line assessment of the whole operation. For accurate measurement to be obtained, a certain force component is not related to output only from its channel but, to some extent, to

the output from the other channels. While interaction is easily detectable in the static situation when only one channel is active, it is impossible to know what is happening in the real application where all channels are loaded. The only way to distinguish the real output, of a certain channel, from the measured signal is through the analytical pre-determination of the whole system performance, or mathematical modelling of the system characteristics.

The idea is to relate a certain force component not only to its channel but to the simultaneous output of all three channels. This takes the general form:

$$F = a1\ Vx + a2\ Vy + a3\ Vz \tag{3.14}$$

where F is the force component (N); Vx, Vy, and Vz are the output voltage for X, Y, and Z channels respectively; and, $a's$ are the output contribution from each channel. Generally, the entire system can be expressed by the arrangement:

$$[A] = [B][C] \qquad where; \tag{3.15}$$

$$A = \begin{bmatrix} F_x \\ F_y \\ F_z \end{bmatrix};$$

$$B = \begin{bmatrix} a_{xx} & a_{xy} & a_{xz} \\ a_{yx} & a_{yy} & a_{yz} \\ a_{zx} & a_{zy} & a_{zz} \end{bmatrix}; and,$$

$$C = \begin{bmatrix} Vx \\ Vy \\ Vz \end{bmatrix}.$$

A non-linear regression procedure was used to determine the coefficients of each direction in turn using the experimental data of the static calibration procedures. Data were fed to a computer program suitable for the $SPSSX$ statistical package available on the IBM 3083 main-frame computer. This resulted in the best predicted parameters as

follows:

$$B = \begin{bmatrix} 1008.2 & 20.100 & -45.400 \\ 12.570 & 987.46 & -6.4800 \\ -48.00 & 16.690 & 1059.80 \end{bmatrix}.$$

Thus, the different application equations take the forms:

$$\begin{aligned} F_x &= 1008.2\ Vx + 20.100\ Vy - 45.400\ Vz \\ F_y &= 12.570\ Vx + 987.46\ Vy - 6.4800\ Vz \\ F_z &= -48.00\ Vx + 16.690\ Vy + 1059.8\ Vz \end{aligned} \tag{3.16}$$

Table 3.4 summarizes the confidence intervals of the parameters, along with the other statistical characteristics.

	Coefficients Asymptotic 95 % Confidence Interval						Corrected Correlation Factor
	a1		a2		a3		
	Lower	Upper	Lower	Upper	Lower	Upper	R^2
F_x	1007	1009	19.28	20.95	-46.3	-44.5	0.999
F_y	10.93	14.2	985.8	989	-8.20	-4.75	0.999
F_z	-51.4	-44.6	13.3	20.0	1056	1063	0.999

Table 3.4 Statistical Characteristics for Force Models

As shown, the models are statistically perfect.

The percentage of interaction among the different directions can be computed from arrangement (3.16) as follows:

	X	Y	Z
X	–	1.99	4.5
Y	1.27	–	0.66
Z	4.5	1.6	–

(3.17)

It can be seen that the level of the cross-sensitivity is very low, and the set of equations as in (3.16) can faithfully represent the practical cutting operation. The lowest level

of interaction is between Y component and each of X and Z ones, while the highest values are between X and Z components ,and with negative effects.

3.1.7.2 Mathematical Models of Cutting Temperature Compensation

The inevitable heat generated during cutting is usually troublesome for the instrumentation of metal cutting especially those that are required to be in close proximity with the cutting region. Generally, a self-temperature-compensation gauge STC is designed to deal with such situations. An STC gauge has certain metallurgical properties for its alloys which minimize the apparent strain over a wide range of temperatures when it is bonded to test material with thermal expansion coefficient for such it is intended. However, the gauge is always employed in conditions different from those for which it was calibrated. For instance, the set of gauges employed here has been calibrated by the manufacturer at room temperature, using a specific steel material, and with an average gauge factor of 2. For different application conditions, compensation is usually necessary using a special chart that is usually supplied with the product.

However, since full active arms bridges are used in this study, the need for compensation has been discarded, and apparent positive and negative strains cancel each other. However, such a situation is correct only when all gauges in the bridges are subjected to the same temperature.

The preliminary cutting tests indicated that the bridges for each of Y and Z are fully temperature compensated, while the output from X bridge revealed a slight decrease as cutting progressed.

The measurement of temperature during cutting showed a homogenous gradient among all gauges in each of Y and Z bridges, while an uneven temperature gradient was detected among the different gauges of X circuit. A temperature difference up to 10 ^{o}C was detected at the end of two minutes cutting. Therefore, a set of thermocouples was bonded at the positions shown in *Fig. 3.25.* Thermocouples readings showed that the highest temperature rise existed at position 4 (bottom-left), followed by position 3 (bottom-right), then position 2 (top-left), and the least rise was detected at position

1 (top-right). Basically, this is due to the way the cutting temperature is conducted through the dynamometer body. The configuration of the tool-insert holder allows more heat to reach some positions quicker than others. However, the highest temperature at position 4 was always well within the working temperature of the gauges (-195 ^{o}C to 205 ^{o}C). However, the level of temperature rise among the different positions seemed to be dependent upon: cutting time; workpiece diameter; and cutting conditions. Therefore, it was thought that this situation could be mathematically modelled to reveal the thermal characteristics of the system. A total of 360 cases representing different cutting times, cutting conditions, and workpiece sizes was used to build a quantitative relationship between the temperature rise during cutting at position 4, *Fig. 3.25,* and the test conditions.

Using the linear regression technique available in the $SPSSX$ computer package resulted in the following linear model:

$$\Delta T = -25.38 + 0.271\ t + 4.13\ d + 23.01\ F + 0.0044\ V + 0.013\ D \qquad (^{o}C) \quad (3.18)$$

where;

ΔT	is the temperature rise after t minutes cutting (^{o}C);
V, F, and d	are the speed, feed, and depth of cut respectively; and,
D	is the workpiece diameter mm.

The statistical criteria for such a model are as follows:

- Correlation Factor R^2 =0.94.
- Adjusted Correlation Factor = 0.94.
- Standard Error (SE) = 2.6.
- F-Ratio = 1069.

This equation shows that the temperature rise at gauge position 4 is positively affected by: cutting time; cutting conditions; and workpiece diameter.

For the worst conditions of $D = 200\ mm$, $t = 3\ minutes$, $V = 200\ m/min.$, $F = 0.6\ mm/rev.$, and $d = 3mm.$, the maximum temperature rise ΔT is $5°C$. The effects of such a temperature rise upon the output from the bridge is investigated in the next section.

A thermal calibration procedure was conducted to determine the bridge output over a wide range of temperatures. The tool tip was subjected to a heat source (welding nozzle) for different time periods. The final temperature, along with the output from the different bridges, was recorded. Again, no output was observed from either Y or Z bridges, while there was a slight negative output from X bridge. Such output exhibited some non-linearity with the recorded temperature rise. A fifth order polynomial of the form *(3.19)* was found to accurately fit the data.

$$\begin{aligned} Vax &= 3.01 \times 10^{-4} - 2.08 \times 10^{-3}\ \Delta T - 4.48 \times 10^{-4}\ \Delta T^2 \\ &+ 3.43 \times 10^{-5}\ \Delta T^3 - 9.03 \times 10^{-7}\ \Delta T^4 + 8.02 \times 10^{-9}\ \Delta T^5 \quad (volts) \end{aligned} \tag{3.19}$$

where Vax is the apparent output in volts due to temperature rise.

Substitution of the value of maximum temperature rise of 5 $°C$ into relation *(3.19)* results in a maximum apparent voltage of -0.018 volts. For an accurate measurement to be obtained, both *Eqns. (3.18)* and *(3.19)* are included within the data processing software to compensate for such difference. *Fig. 3.31* shows the force signal in X direction before and after compensation for the temperature rise together with the Y and Z force signals. As it can be seen, both Y and Z signals, *Fig. 3.31.c & d*, the domain of the signals is constant over the test duration. For X force signals, *Fig. 3.31.a*, this domain indicates a slight decrease. *Fig. 3.31.b* shows this curve after compensating for the temperature effects using relation *(3.18) and (3.19)* in conjunction with the test conditions.

Generally, the steps, between collecting force signals from experiments and until three values of different force components are obtained, are summarized in *Fig. 3.32.* These force values will be used in the analyses in the following chapters.

3.1.8 Dynamometer: Concluding Remarks

In summary, a very efficient three-component cutting force dynamometer has been designed and manufactured to occupy the size of the original lathe tool-post block. Its features and techniques may be summarized as follows:

- A technique of non-central circular-hole has been used, which has been found to increase the apparatus' sensitivity and rigidity.
- An aluminium model has been designed and manufactured to study the most sensitive positions at which the gauges should be bonded, and to examine the effect of the relative hole-thickness configuration. This has led to a significant improvement in the dynamometer sensitivity, accuracy, and stability.
- Interaction among the components has been reduced to its lowest level. This has been achieved by locating the true cutting application point with great accuracy so that each component is hardly affected by the influence of the other components.
- A set of experimental tests has been carried out to determine the dynamic, static, and thermal characteristics of the dynamometer. The dynamometer has been found to have a fairly high natural frequency so that the true cutting force signals are not affected by the dynamometer oscillations. The static calibration test has indicated a very high standard of system linearity.
- The output level (the dynamometer's sensitivity) has been significantly improved by the accurate selection of the proper hole-thickness ratio, by the accurate location of the point of maximum strains, and by the proper arrangement of the gauge circuits.
- A *BBC* microcomputer has been used in the on-line data collection through a specially designed analogue-to-digital converter and strain-gauge amplifiers with sampling rate high enough to detect even a tiny dynamic force variations.

- A set of software for both on-line and off-line data processing procedures has been written in forms of *SPSSX, BASIC, ASSEMBLY,* and *FORTRAN* languages programs. The processing procedures include the data transformation, and the data averaging and filtering. Also, mathematical models are developed to deal with: the system output and cross-sensitivity; the effect of cutting conditions on the heat generated during cutting; and, the effect of cutting temperature on the apparent output of the strain-gauge.

  These procedures result in a very accurate valuation of the three cutting components used in the analysis in the subsequent chapters.

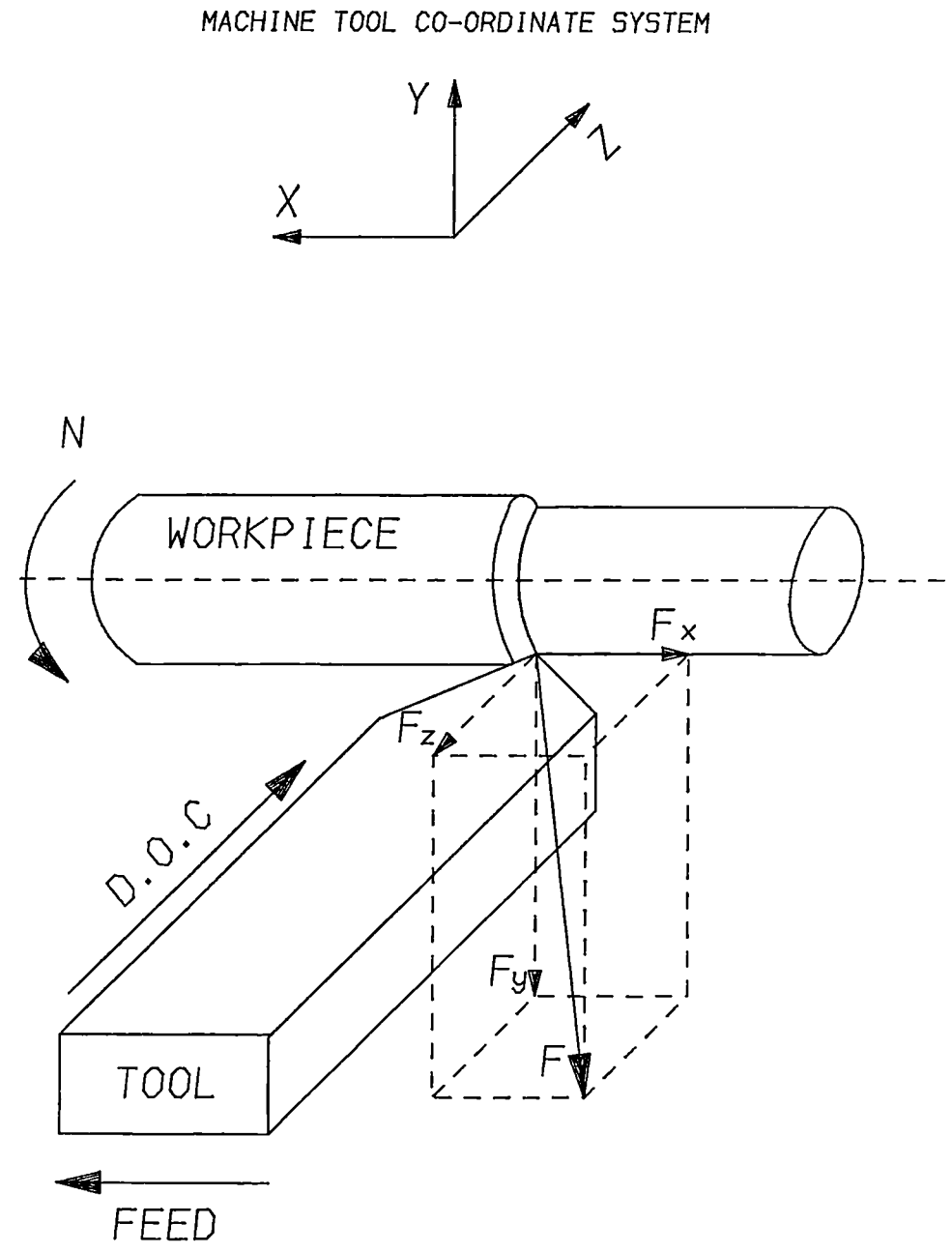

Fig. 3.1 Cutting Force Components for Turning Operation

Fig. 3.2 A General View of the Dynamometer Mounted on the Lathe

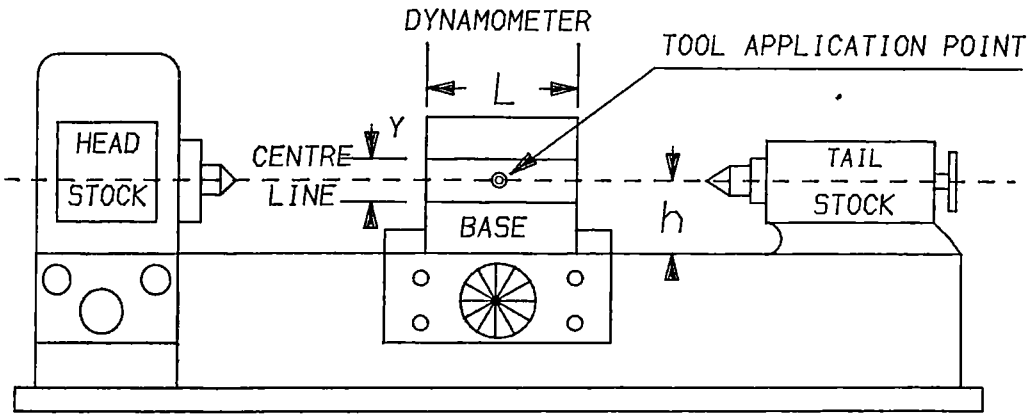

Fig. 3.3 Location of the True Application Point

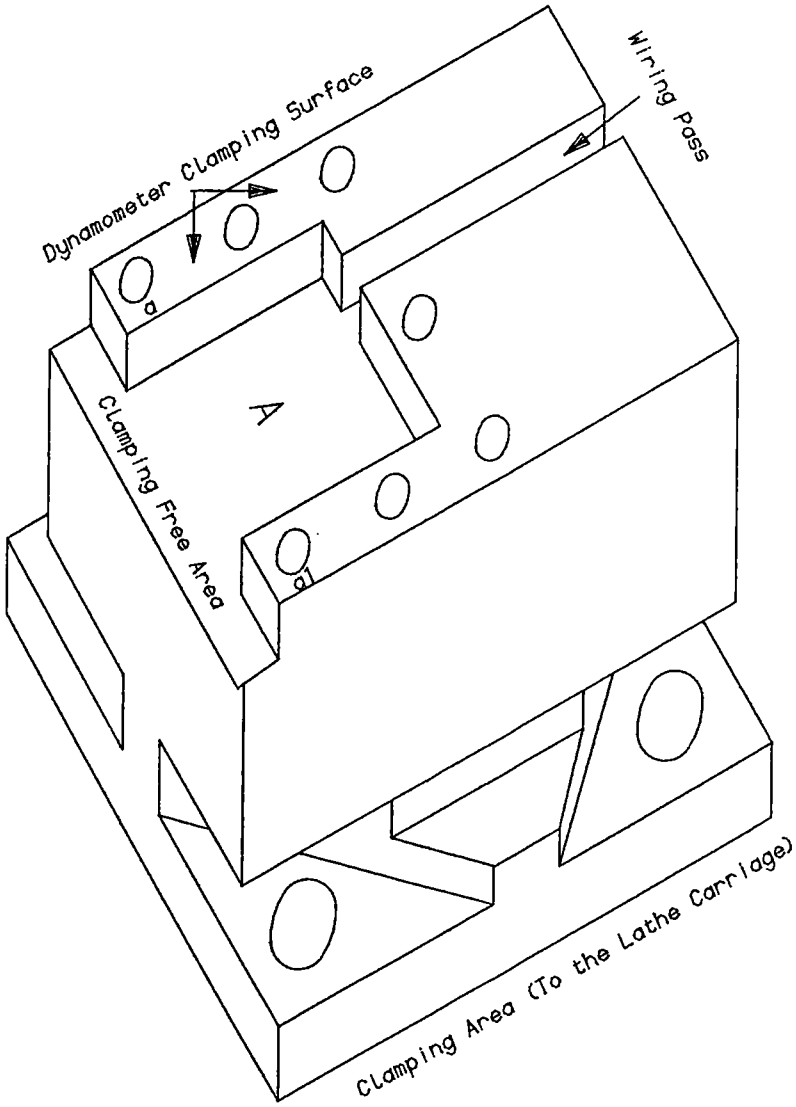

Fig. 3.4 The Dynamometer Base Configuration

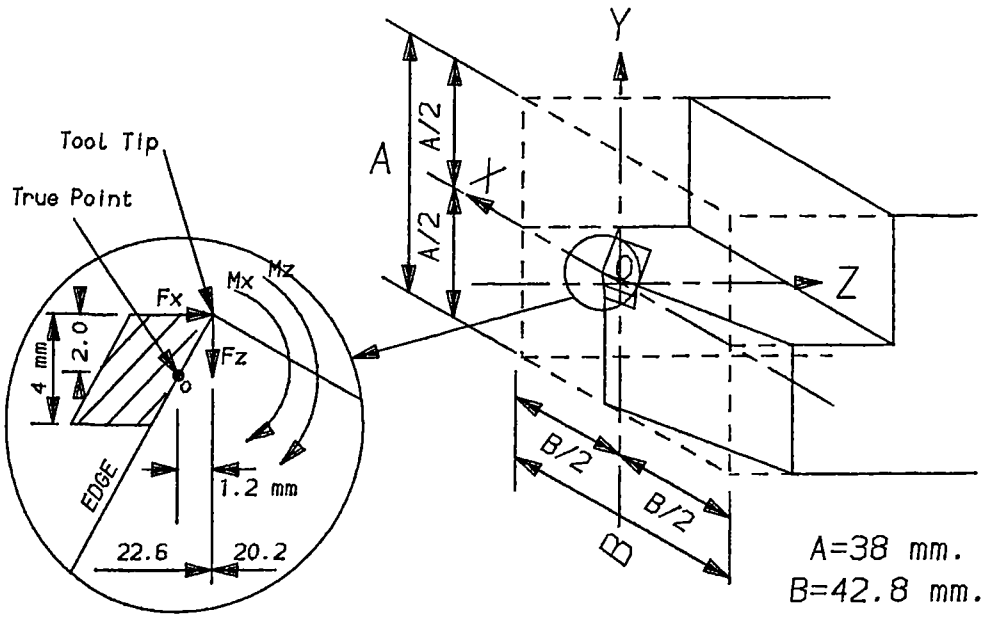

Fig. 3.7 Determination of the True Application Point

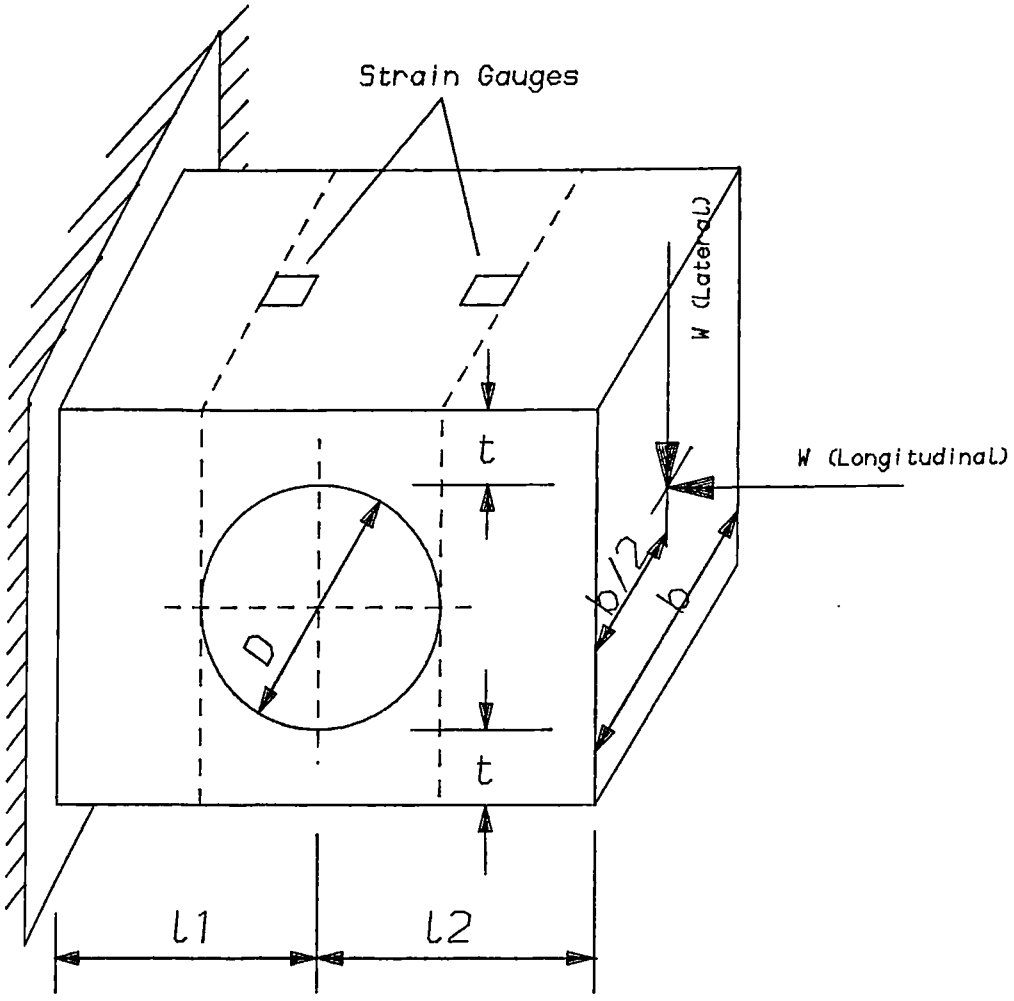

Fig. 3.8 One Component Dynamometer with a Circular Hole [93]

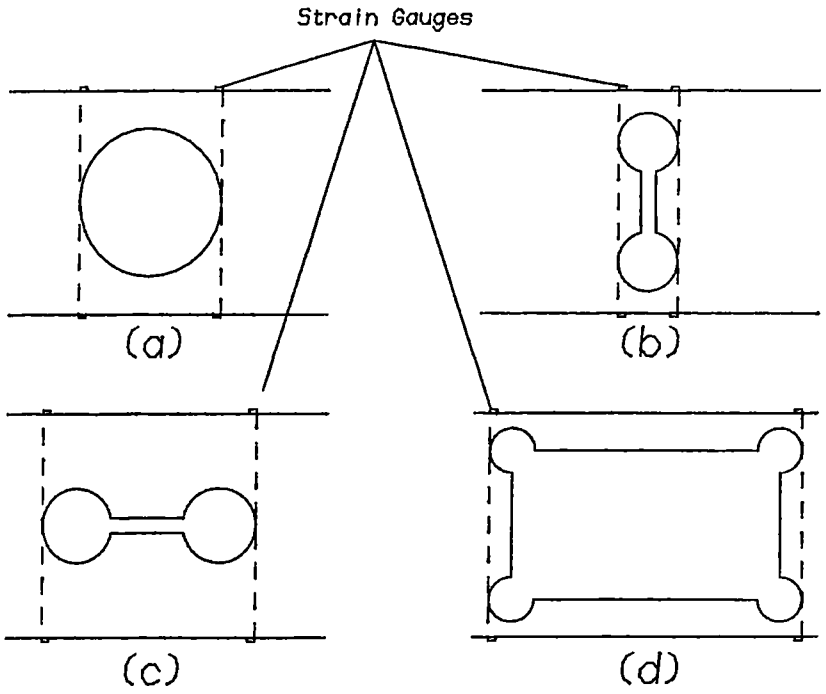

Fig. 3.9 Various Types of One Component Dynamometer with Circular Hole [93]

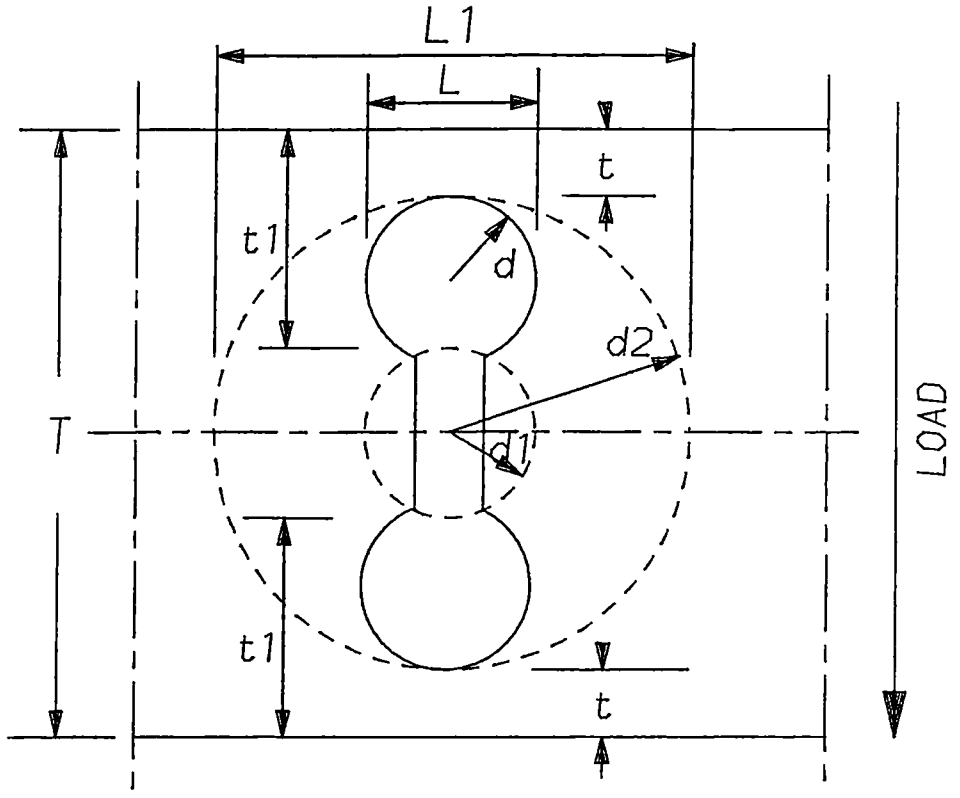

Fig. 3.10 Central and Non-Central Circular Holes

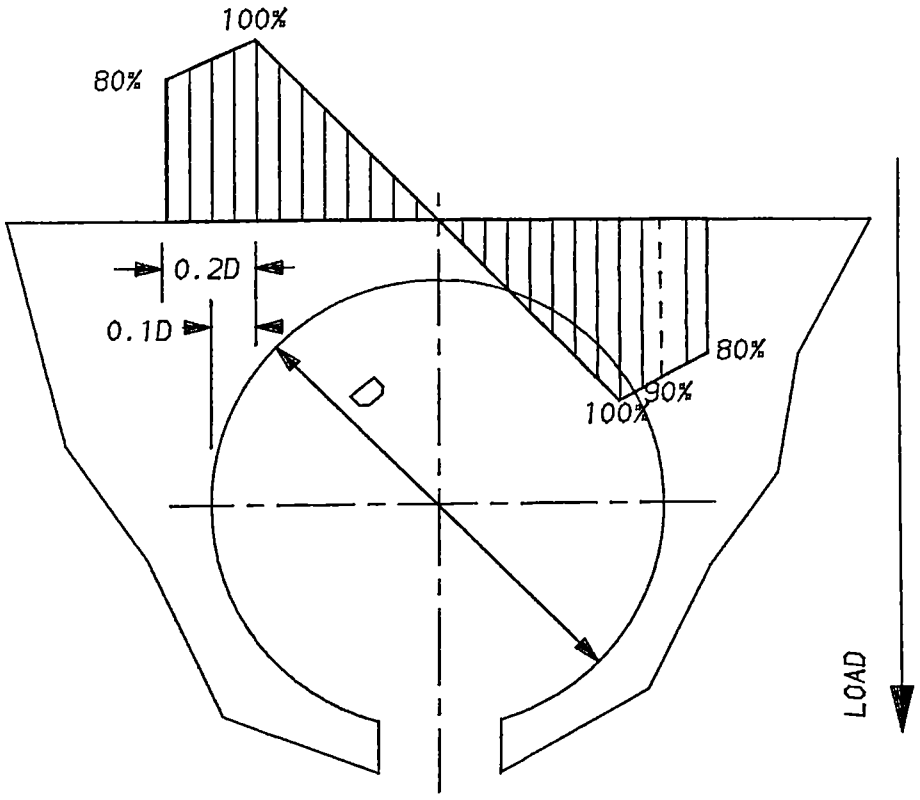

Fig. 3.11 Strain Levels Distribution in Circular Hole [93]

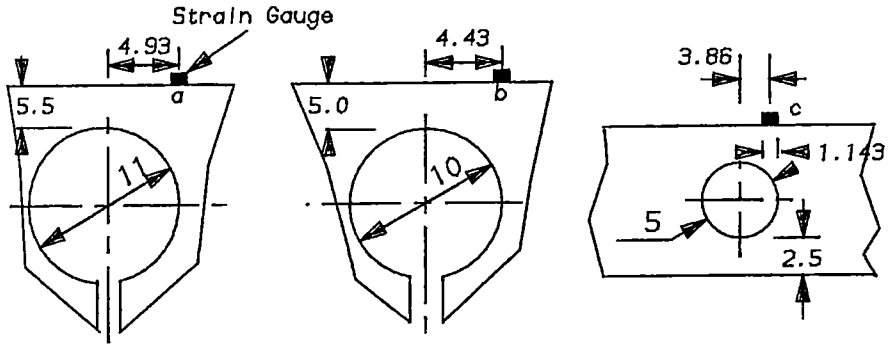

a) X-Direction b) Y-Direction c) Z-Direction

Fig. 3.12 The Relative Gauge-Hole Positions For the Aluminium Model

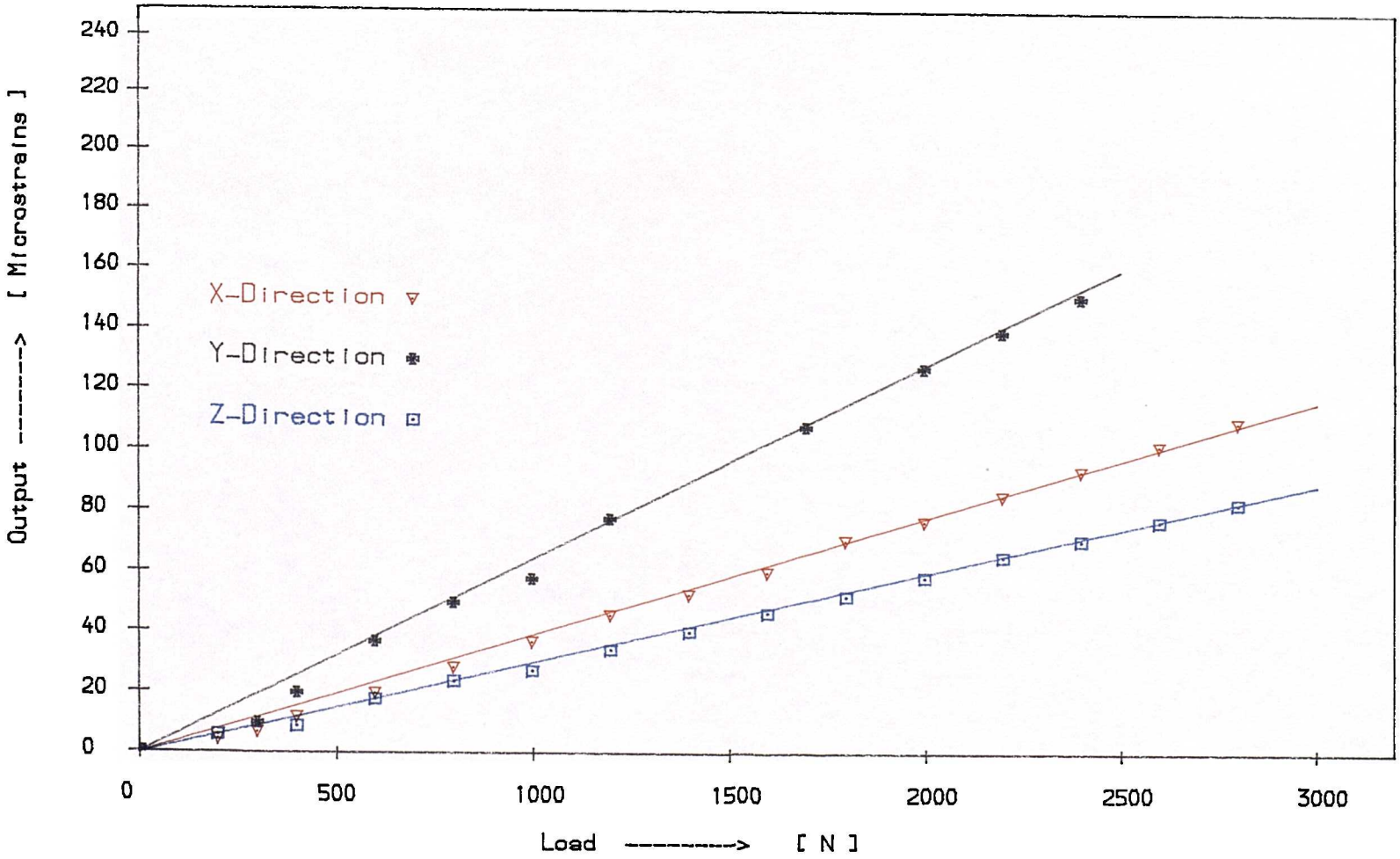

Fig. 3.13 Initial Calibration Curves of thee Aluminium Mode

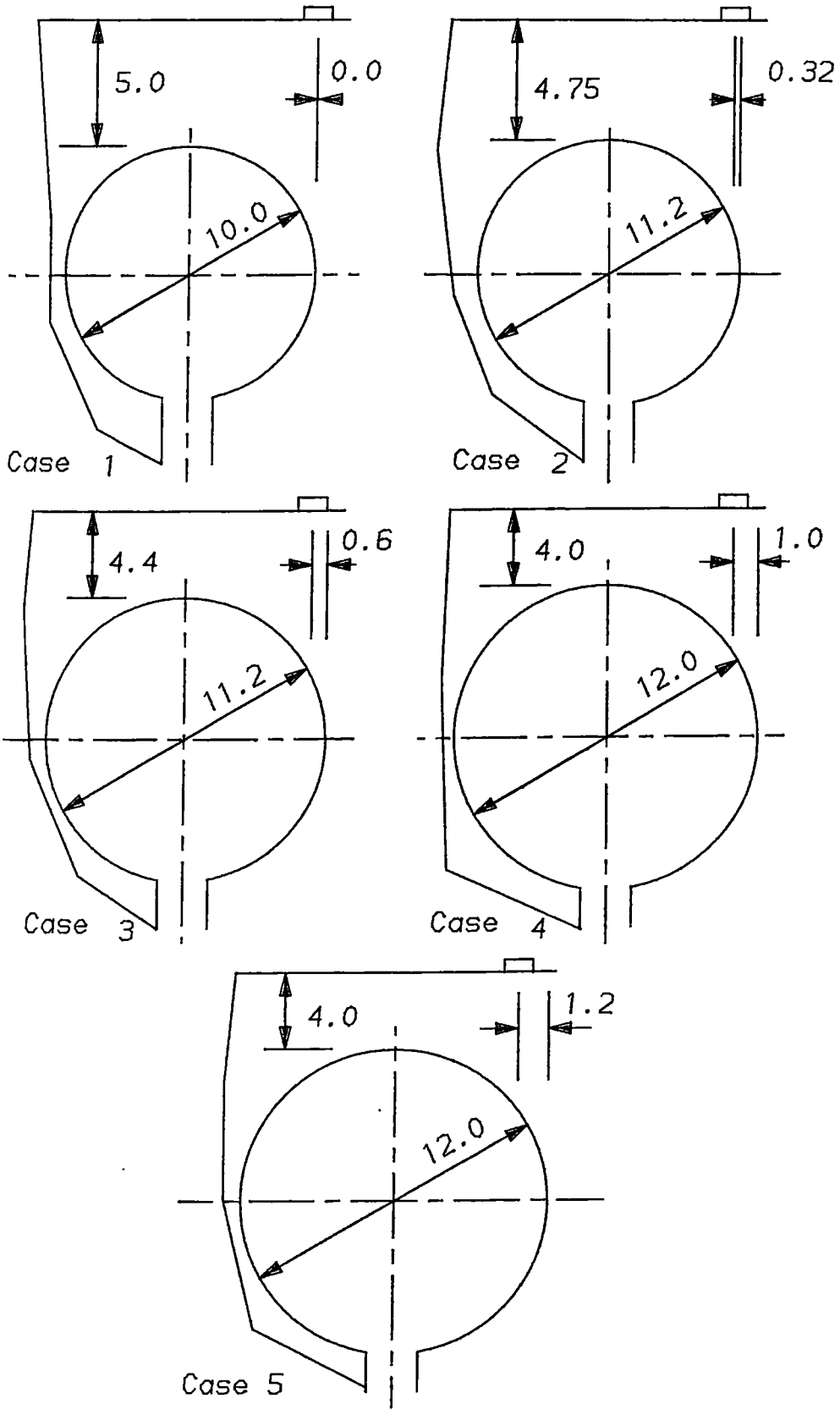

Fig. 3.14 Different Ratios of Wall-Thickness For Y-direction

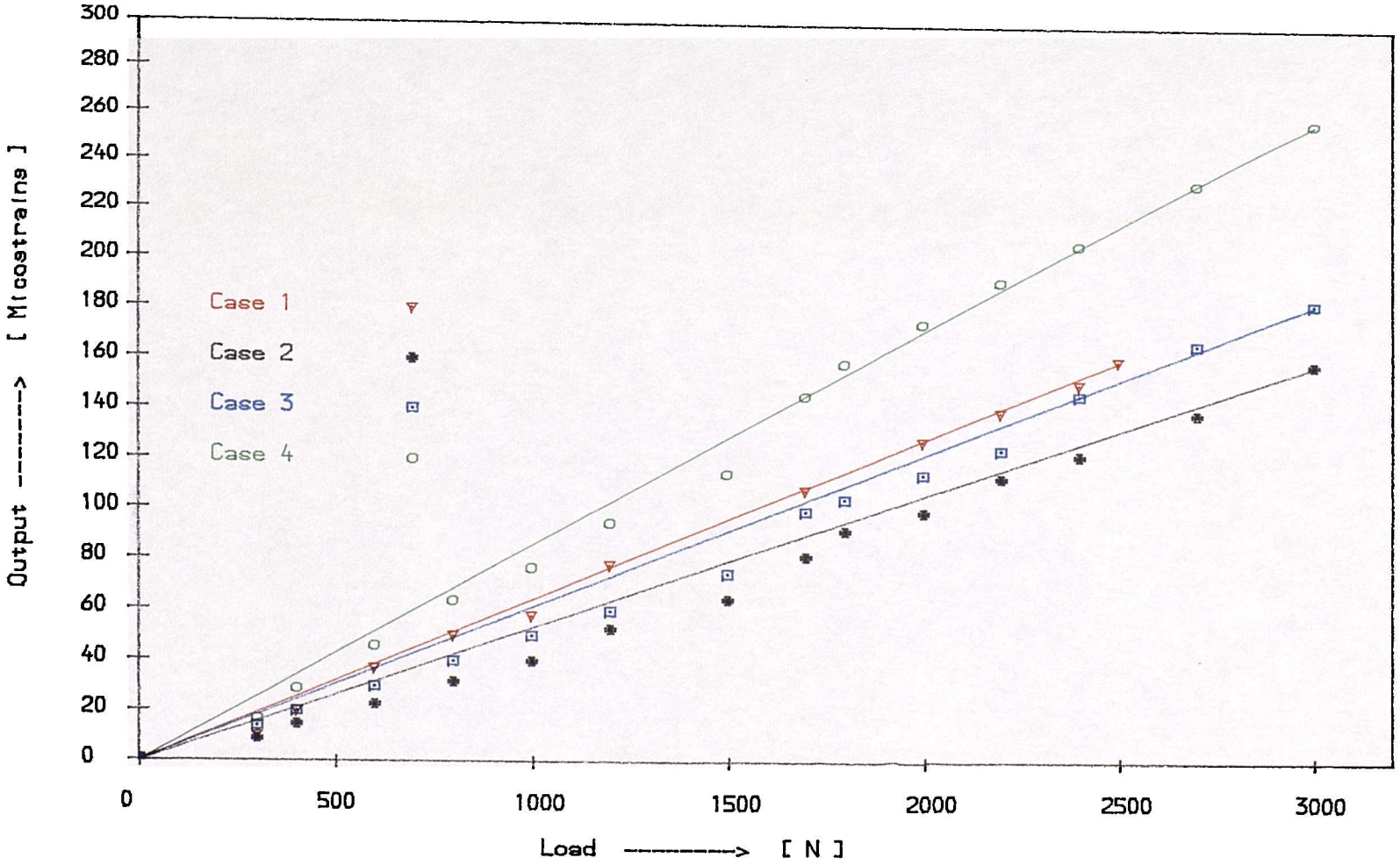

Fig. 3.15 The Effect of Different Wall Thicknesses on the Output of Y-Direction

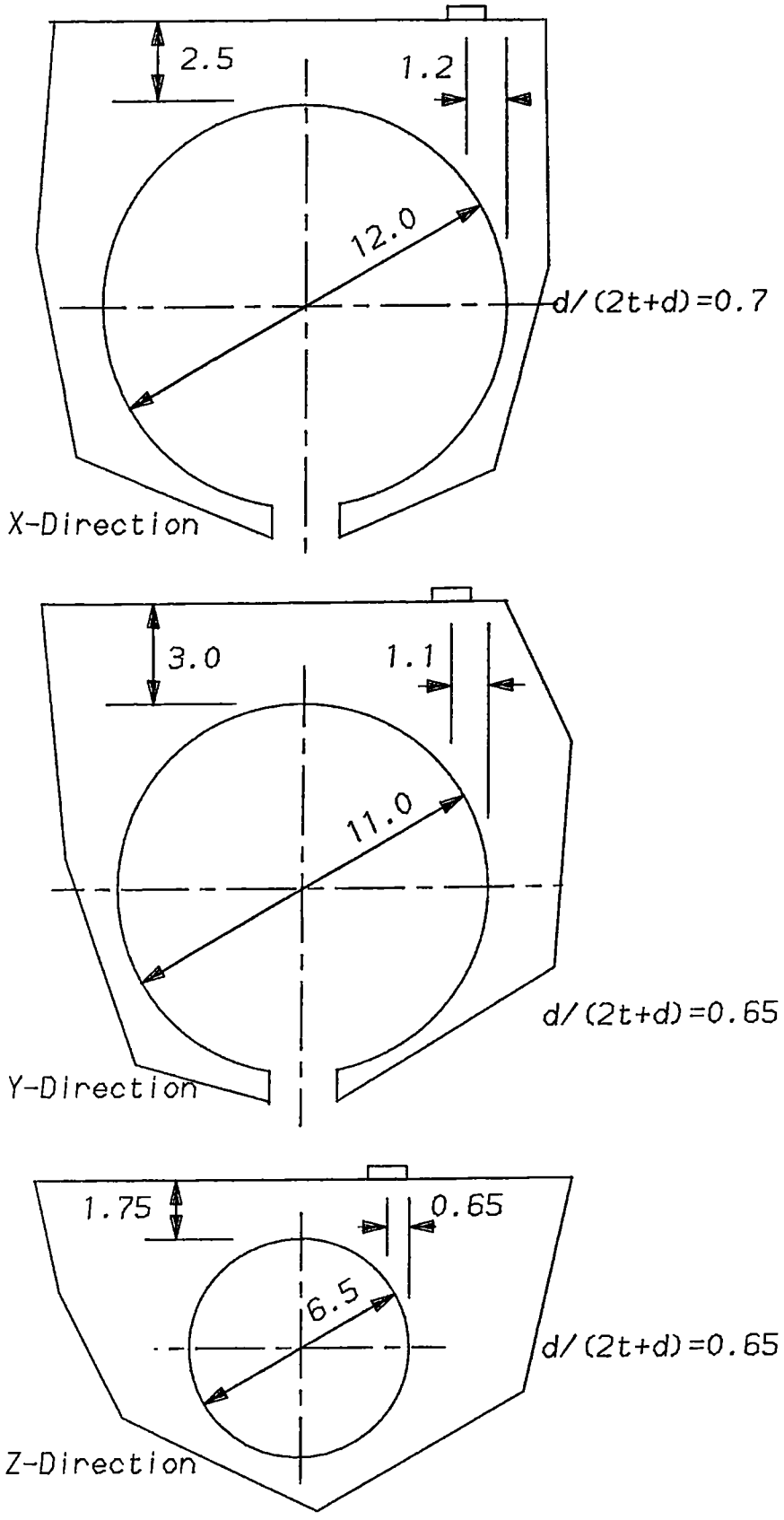

Fig. 3.16 The Relative Hole-Gauge Positions of the Actual Dynamometer

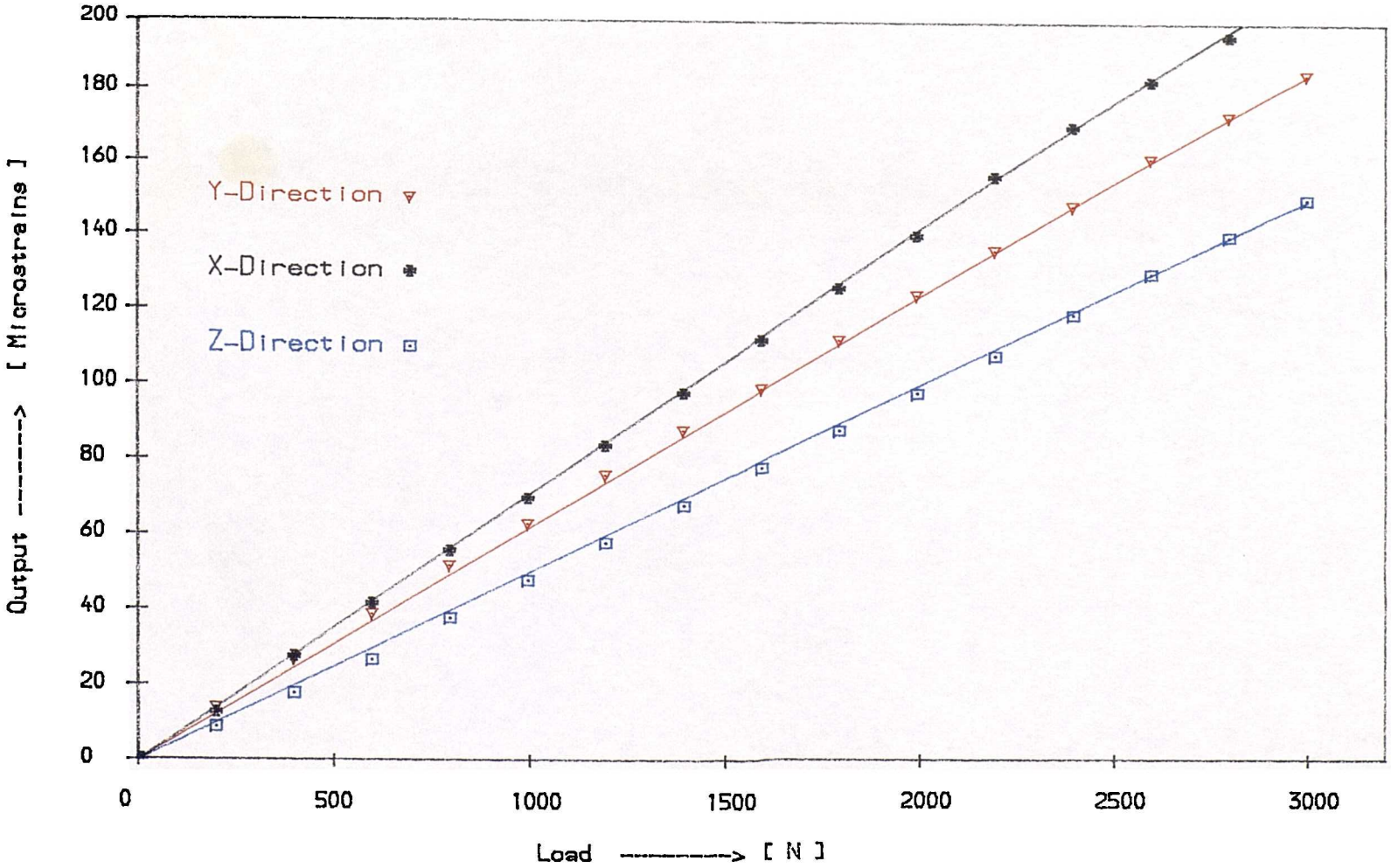

Fig. 3.17 Calibration Curves for Steel Dynamometer Using One Gauge in Each Direction

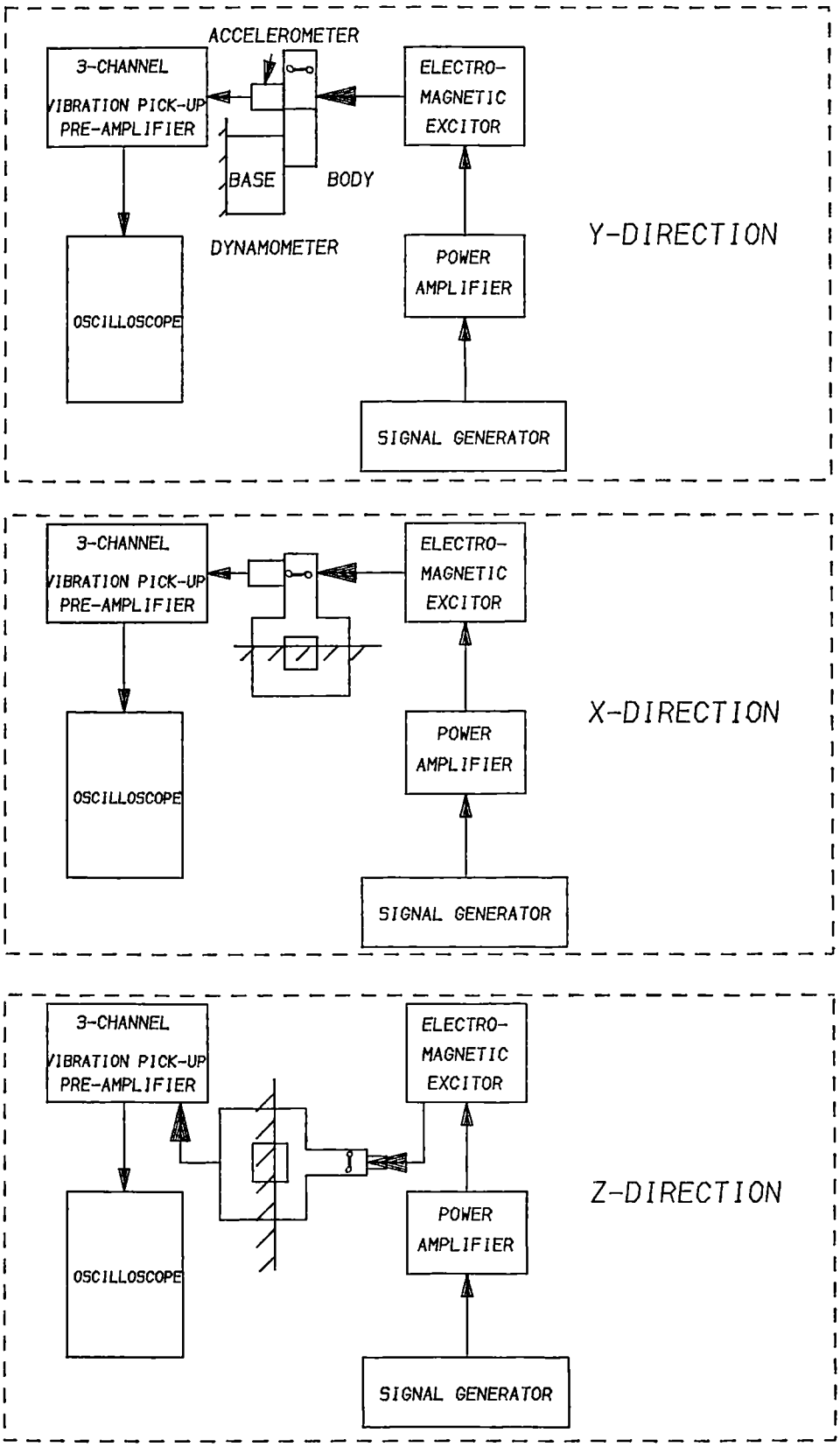

Fig. 3.18 Block Diagram of the Frequency Response Test Procedures

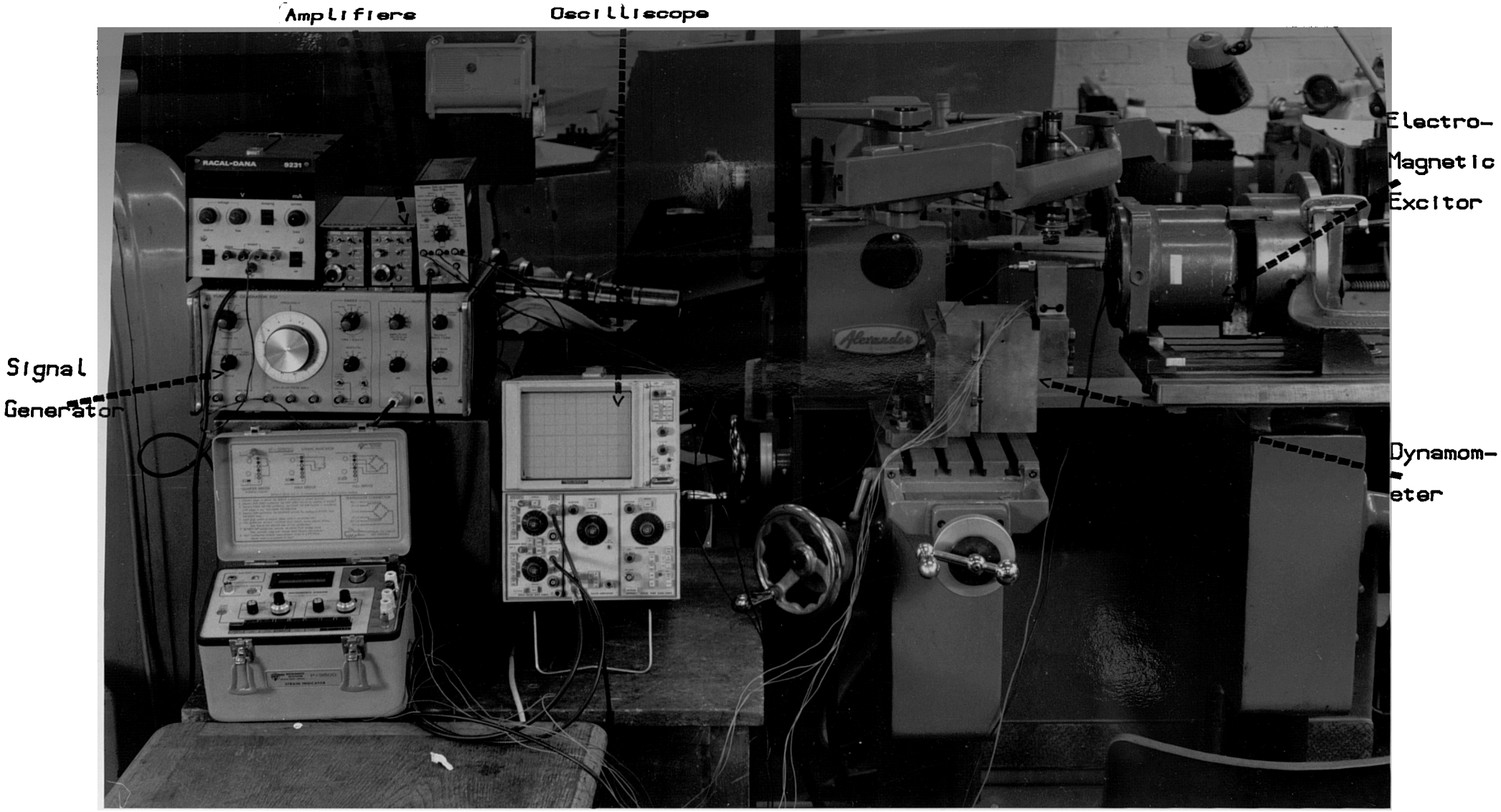

Fig. 3.19 A General View of the Instrumentation Used in the Dynamic Calibration

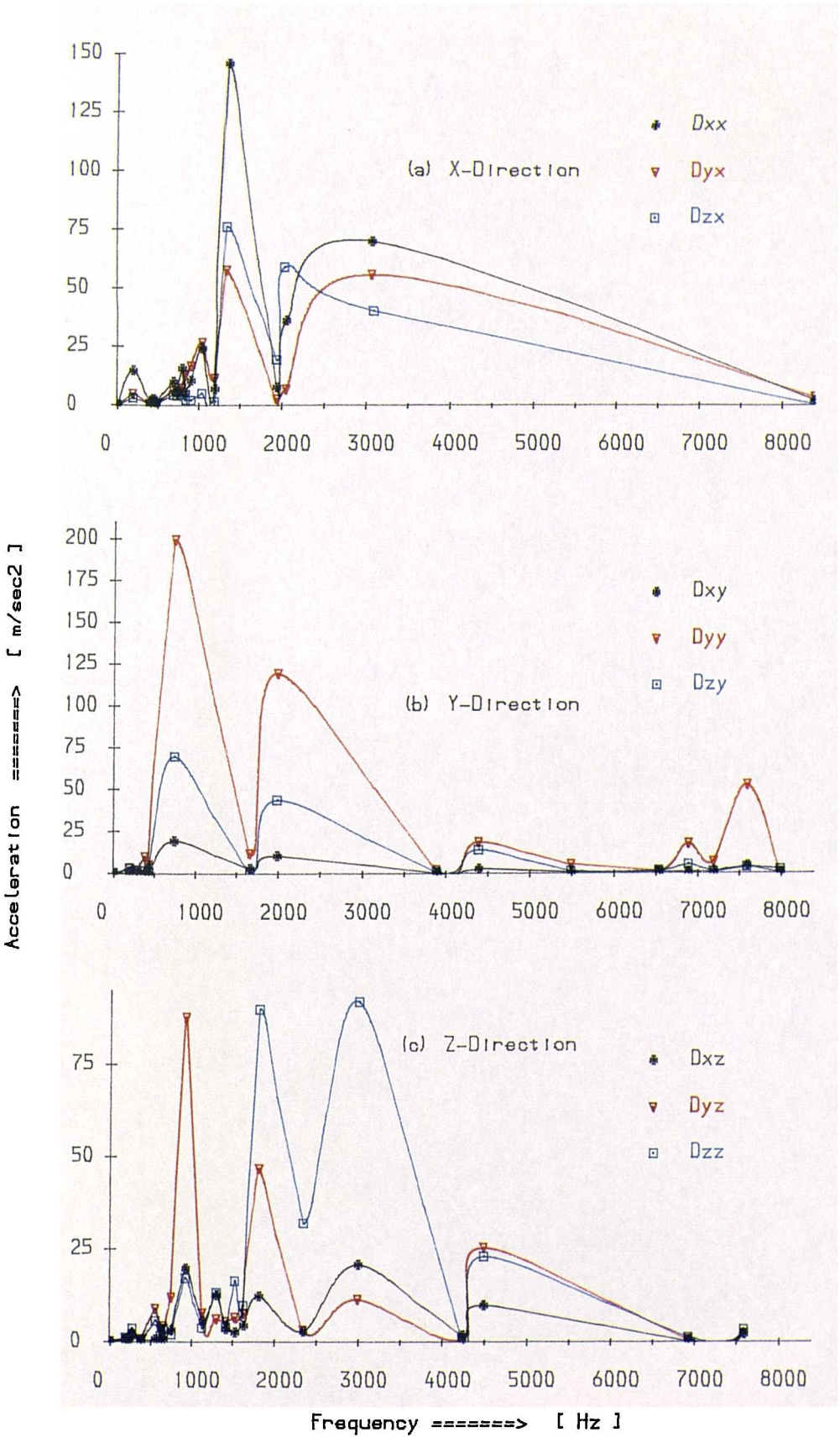

Fig. 3.20 Frequency Response Curves and Dynamic Cross-Sensitivity

0.018 second

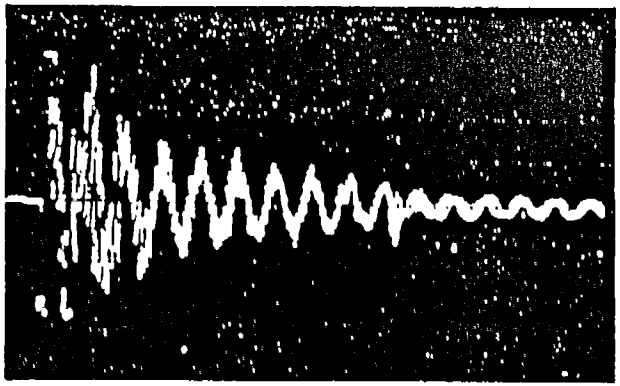

b) Vertical Direction (Y)

0.018 second

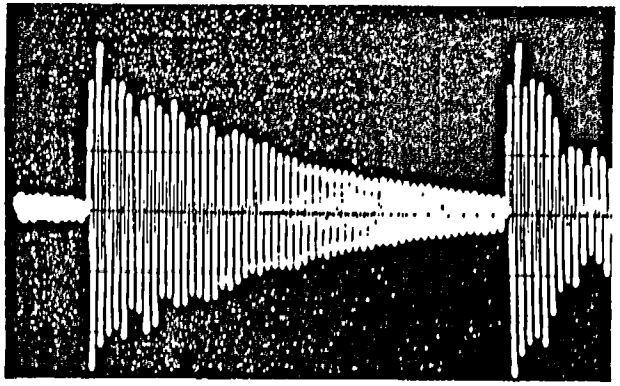

c) Radial Direction (Z)

0.02 second

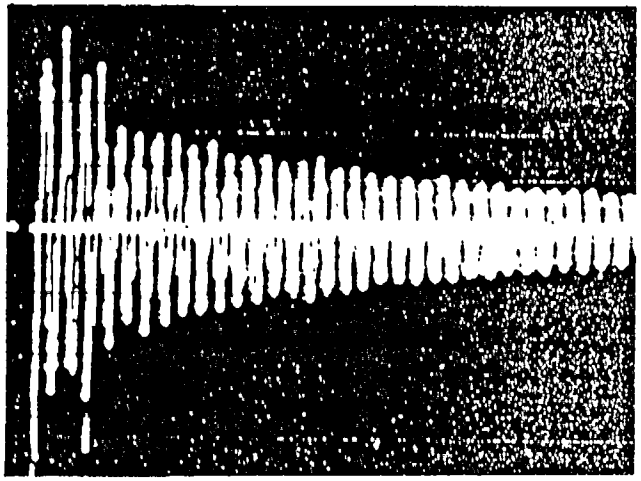

a) Feeding Direction (X)

Fig. 3.21 The Damped Natural Frequencies of The Dynamometer

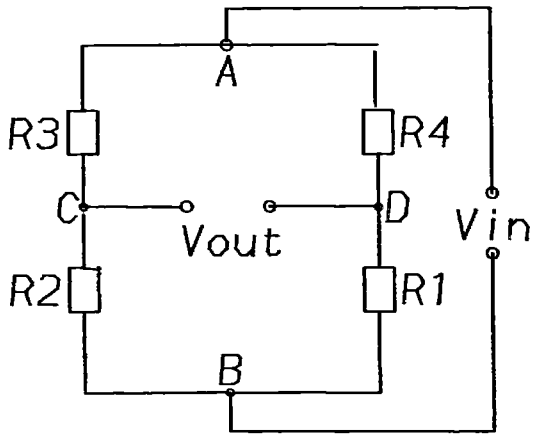

Fig. 3.22 Wheatstone Bridge for Strain-Gauge Applications

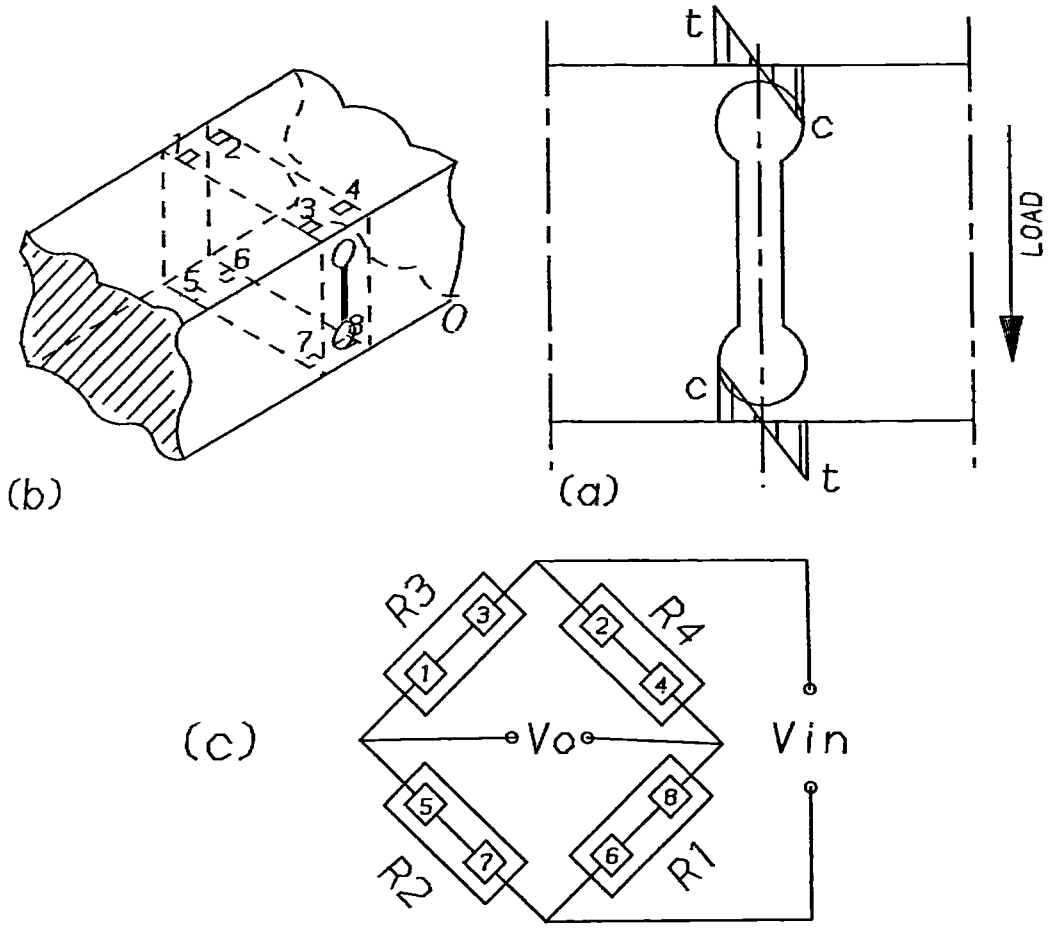

Fig. 3.23 Circuit Design for each of X- and Y-Directions

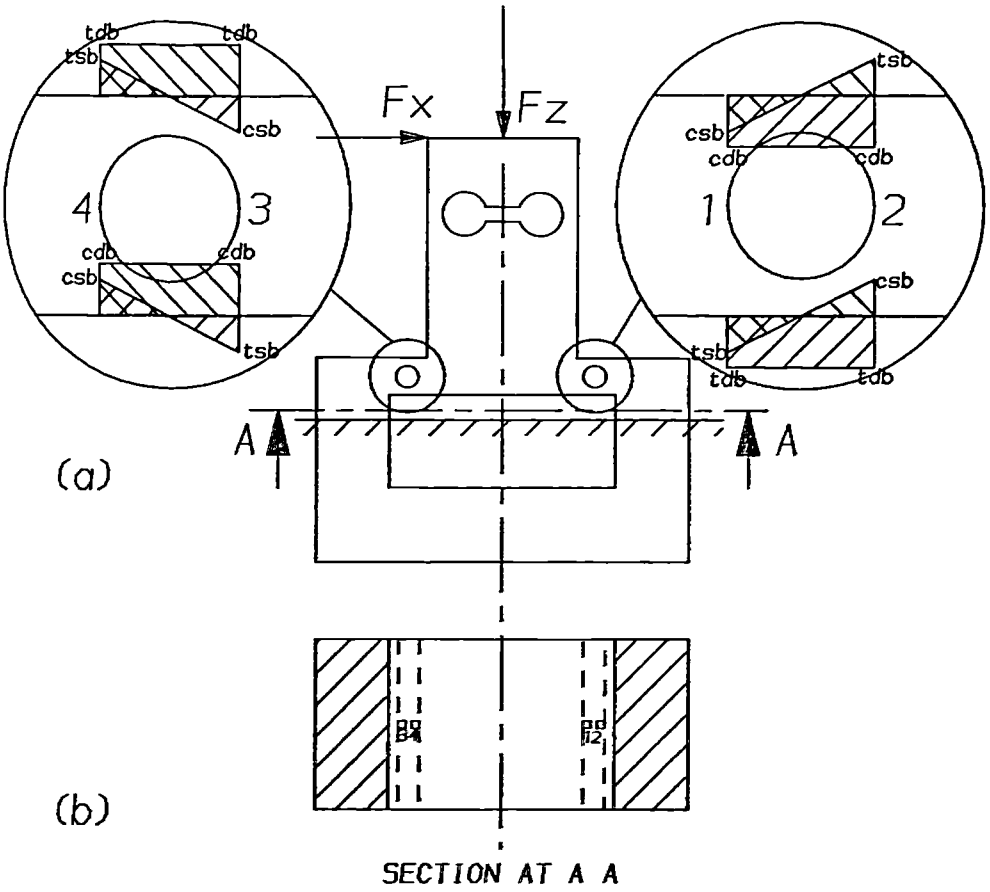

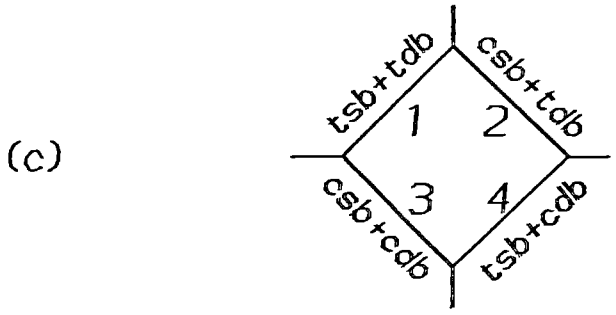

(c)

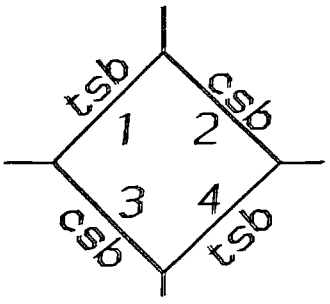

(d)

Fig. 3.24 Mechanical and Electrical Circuit Design for Z-Direction

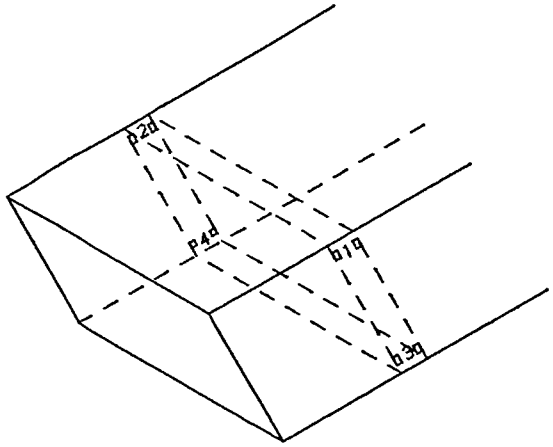

POSITION 1 top-right
POSITION 2 top-left
POSITION 3 bottom-right
POSITION 4 bottom-left

Fig. 3.25 Thermocouples Positions for X-Direction

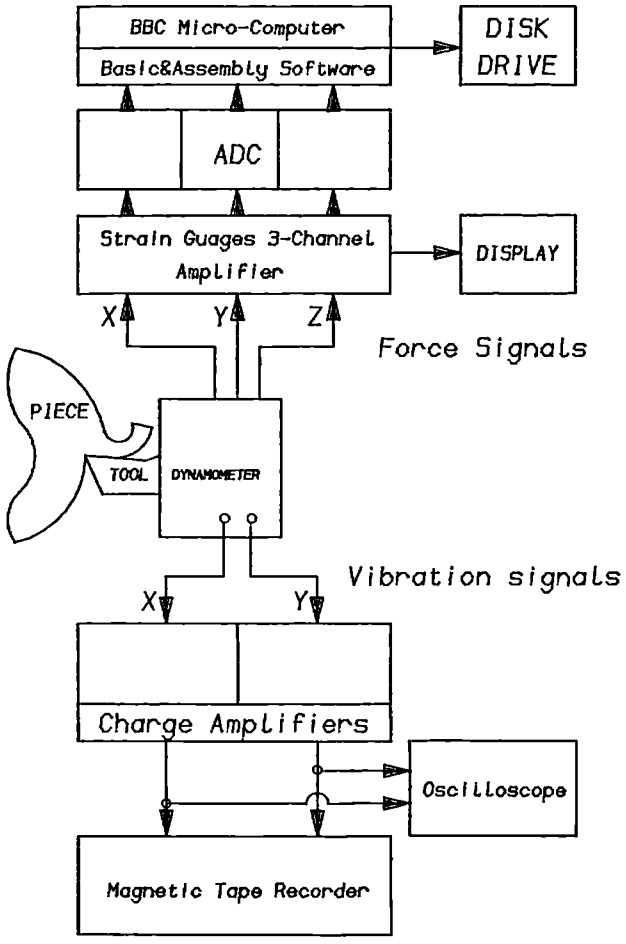

Fig. 3.26 Data Collection and On-Line Processing Procedures

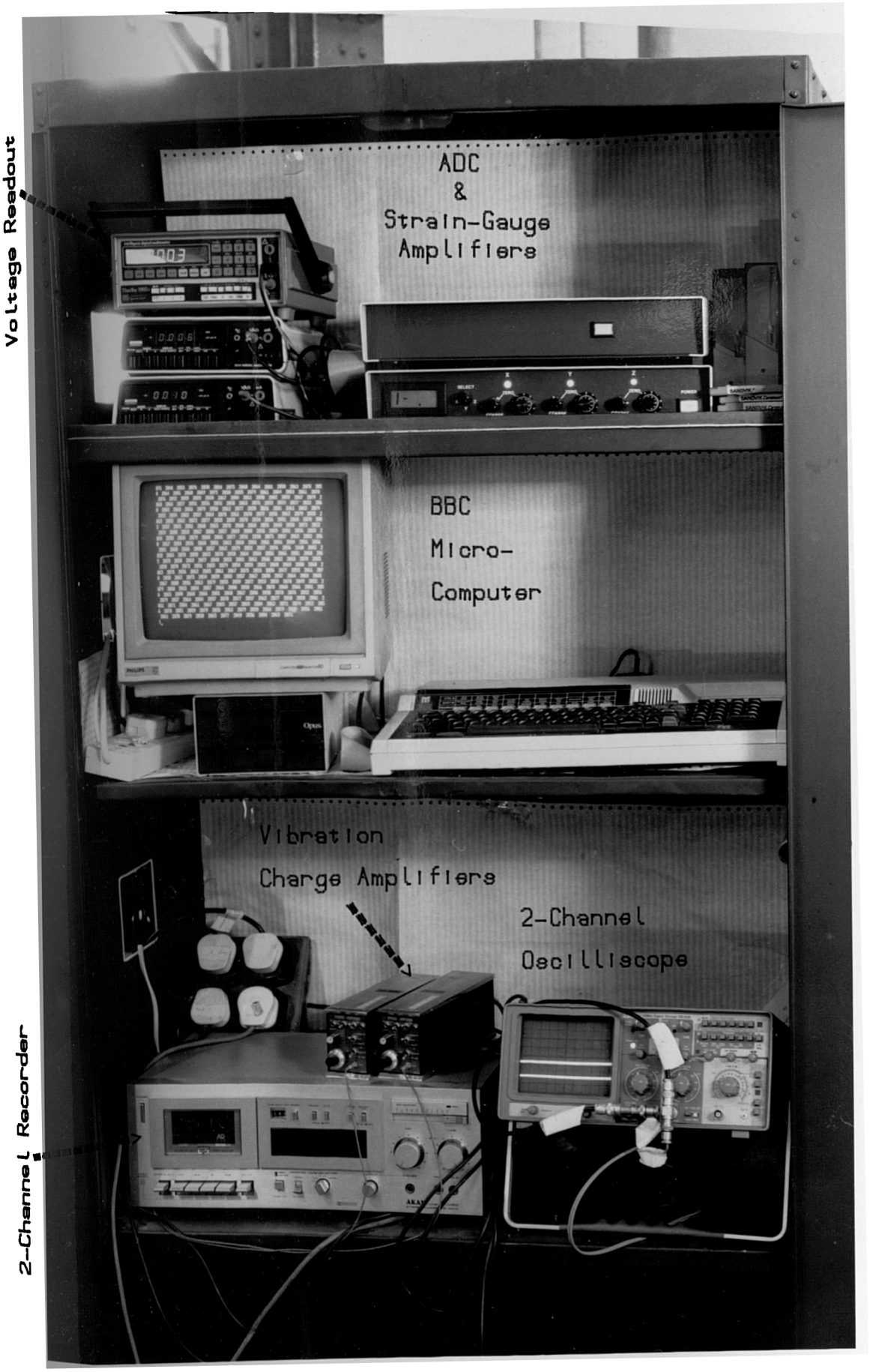

Fig. 3.27 A View of the Instrumentation Used in On-Line Data Processing

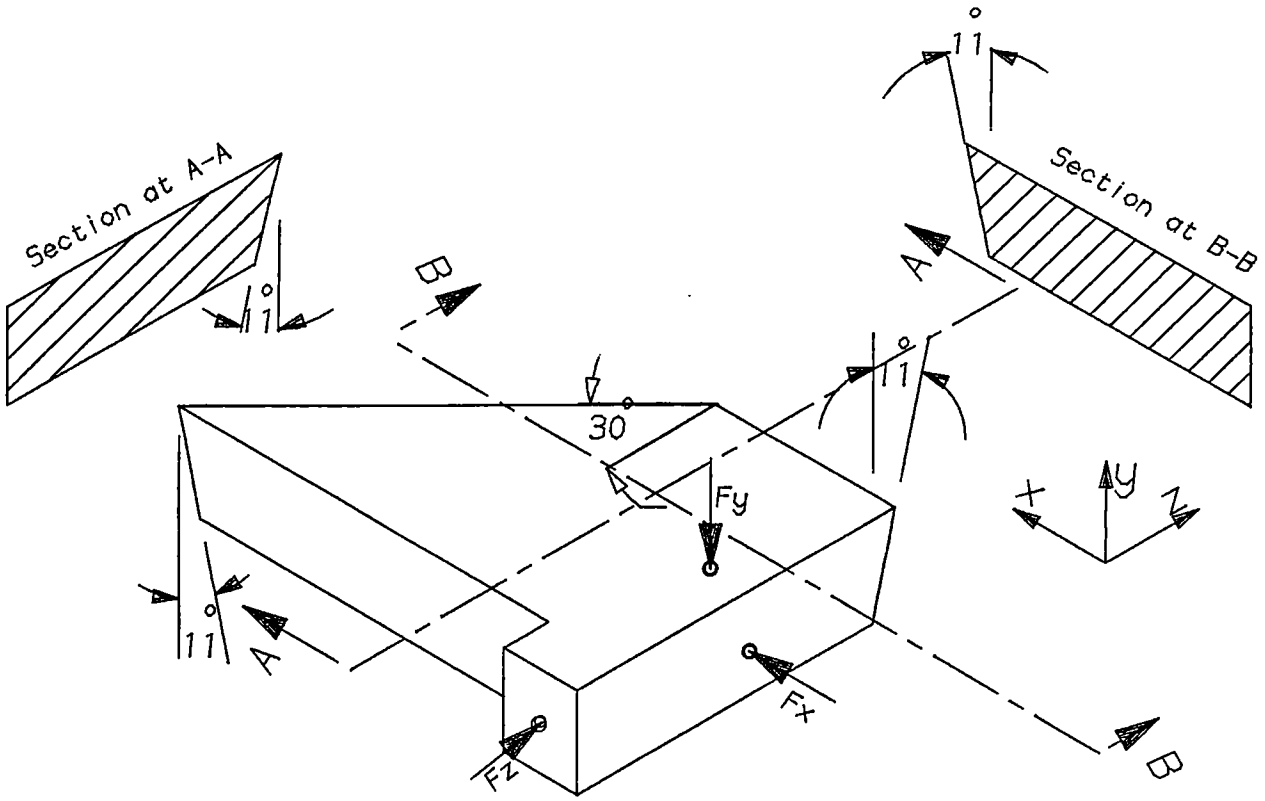

Fig. 3.29 Dummy Tool-Insert for Dynamometer Static Calibration

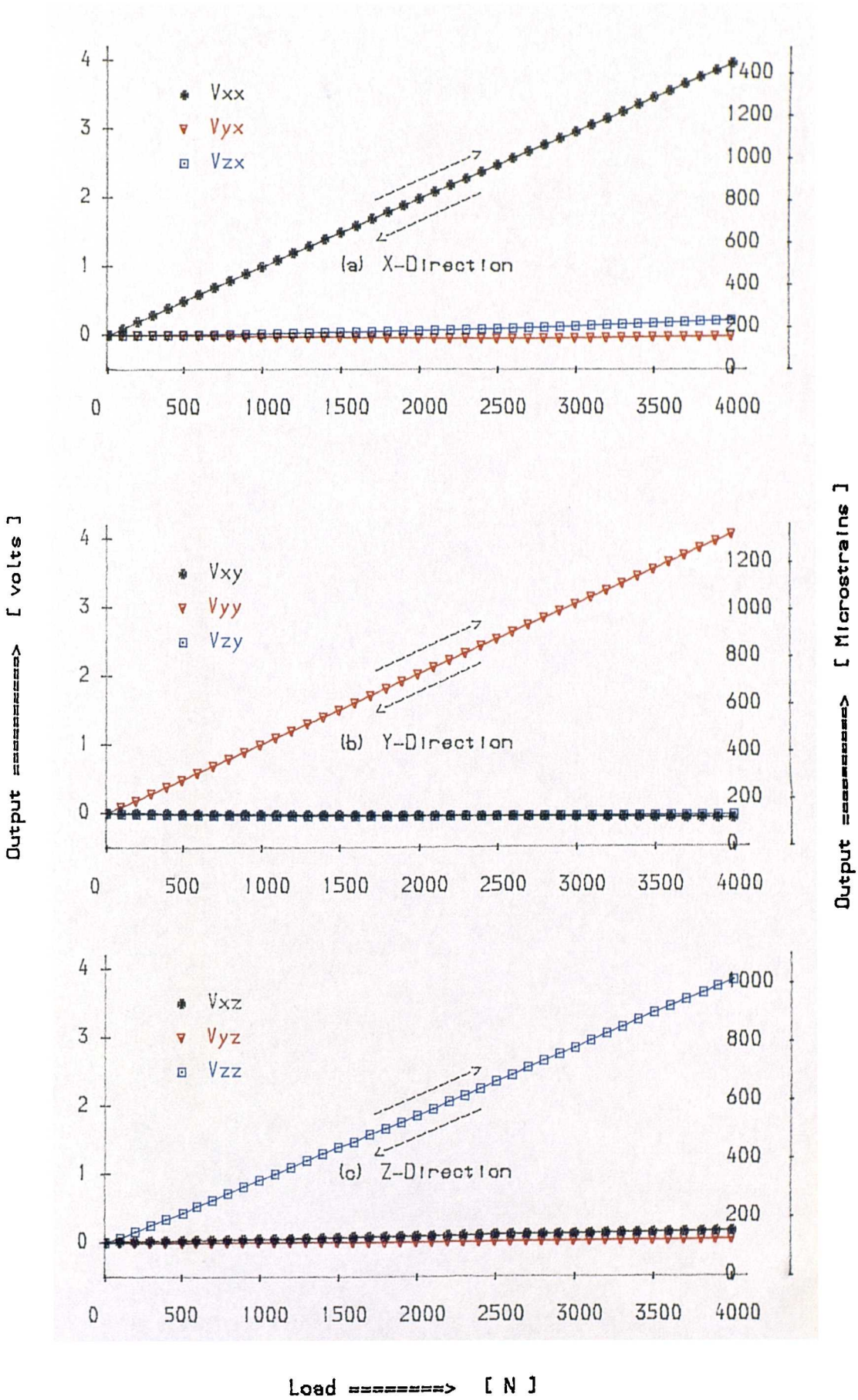

Fig. 3.30 Calibration Curves and Cross-sensitivity of The Dynamometer

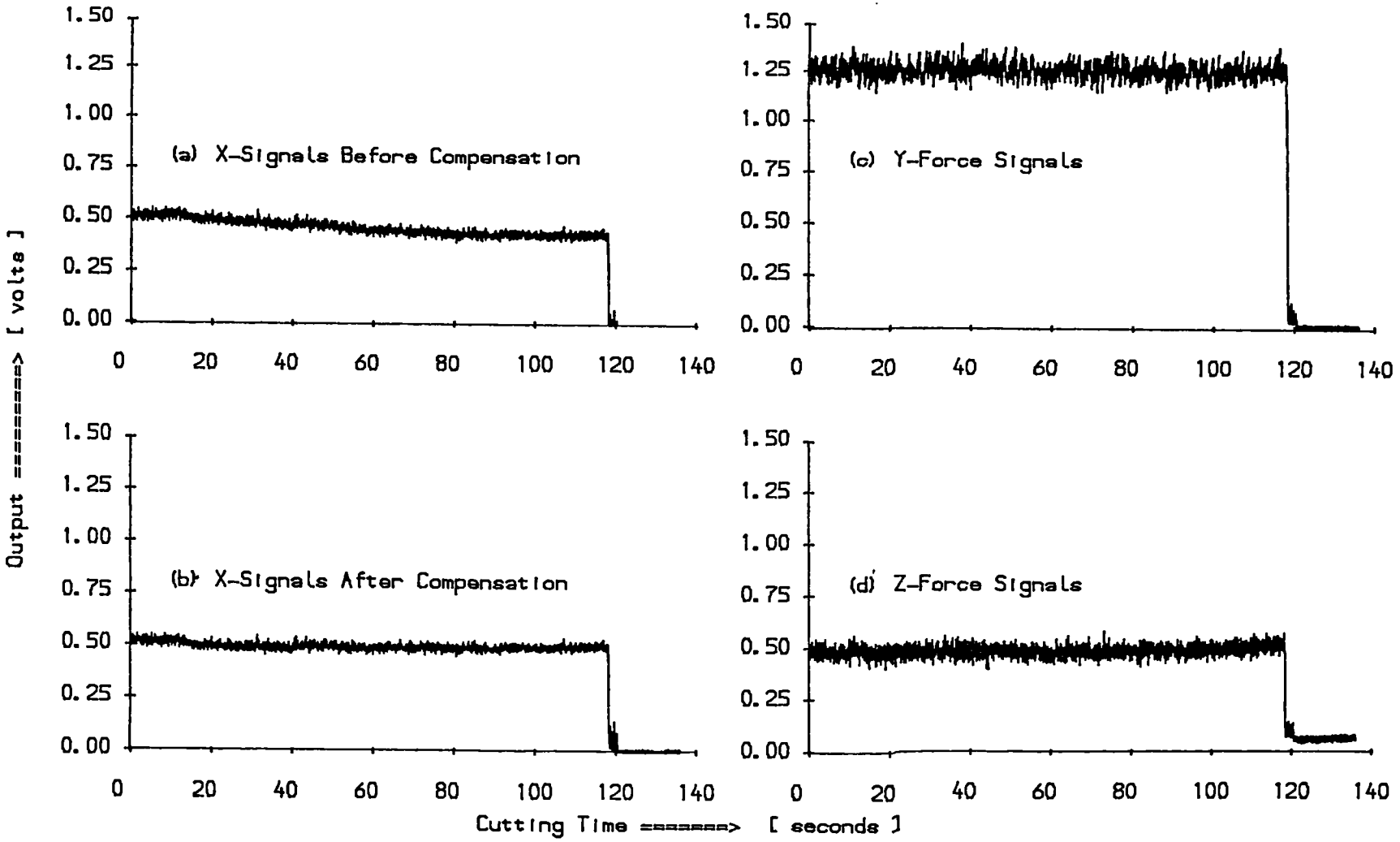

Fig. 3.31 The Dynamometer Cutting Force Signals and Temperature Compensation for The Feed Signals

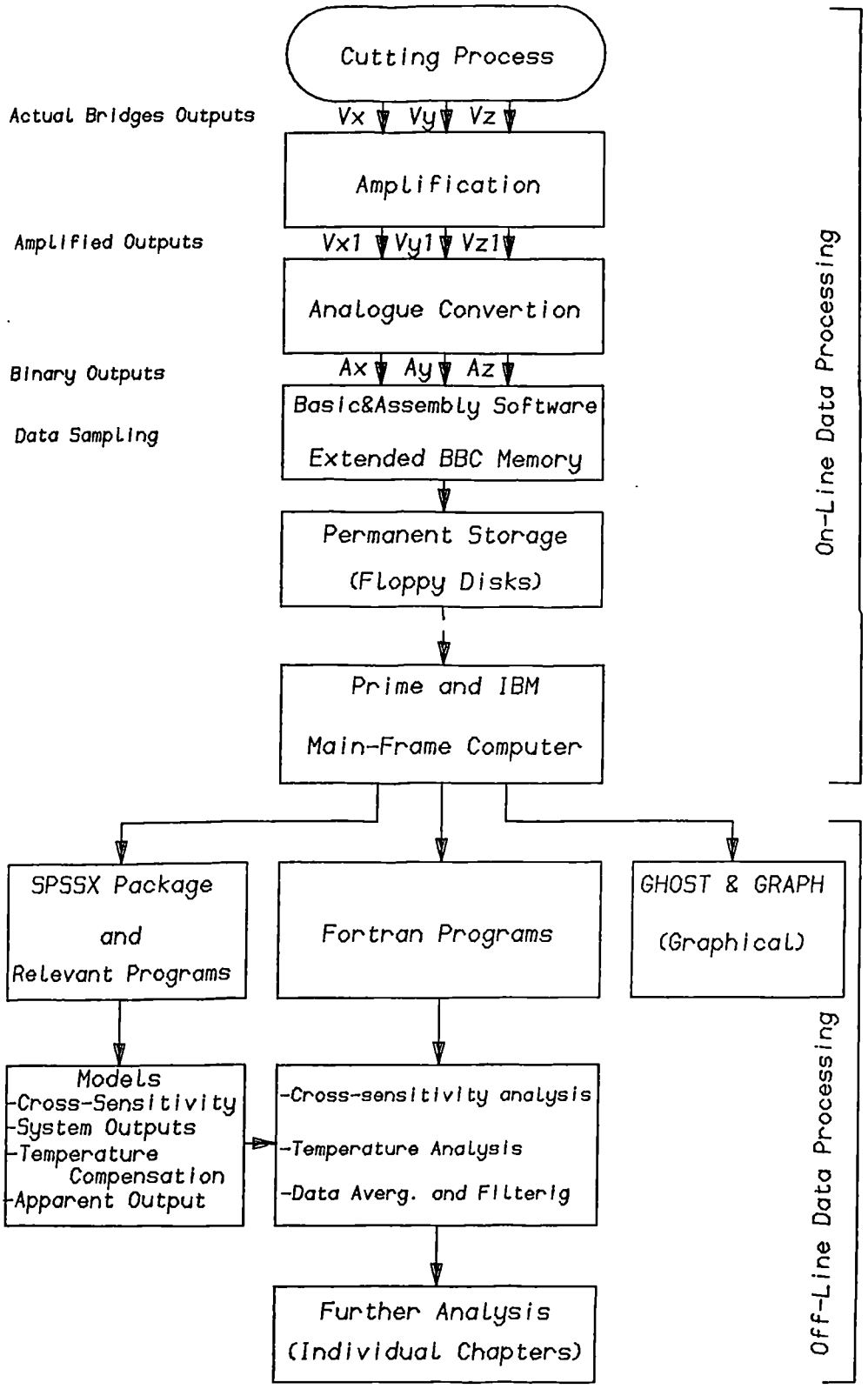

Fig. 3.32 Data Processing Procedures for Force Signals

3.2 Tool Vibration Measurement

Two Kistler piezo-electric type 8005 accelerometers were bolted to the back of the dynamometer body, *Fig. 3.33.* One accelerometer was located vertically to pick up the tool vibration in that direction, and the other in the horizontal direction, parallel to the workpiece axis, to pick up the tool vibration in the feed direction (X). They were located so that their axes met at the dynamometer centre-line. This was to prevent, or minimize, the transverse sensitivity. Location of the accelerometers at the back of the dynamometer body has protected them from the hostile conditions of heat generated and swarf accumulated at the cutting zone. Also, this position has not affected the vibratory characteristics of the toolholder system. Both accelerometers has the following characteristics:

- Measuring Range $(+5000 \text{ to } -5000g), g$ is the acceleration due to gravity.
- Sensitivity $(4.99\ pC/g)$.
- Transverse Sensitivity $(\leq 1\%)$.
- Resonant frequency $(21\ kHz)$.
- Operating Temperature $(-250 \text{ to } 240\ ^oC)$.

Each of the accelerometers was connected to a charge amplifier which was previously calibrated to produce 5 mv/g. However, the charge amplifier gain could be adjusted to give ten times this value when required.

The amplified signals are recorded on *TDK-AD* low-noise high output magnetic tapes using a *GX-M50 AKAI* dual channel tape recorder. The recording rate was set at the recorder speed of 4.76 cm/sec. The range of linearity of the tape recorder was from 25 to 17000 Hz with a higher signal-to-noise ratio. A dual-channel oscilloscope was used for displaying the real-time signal during the actual machining. *Fig. 3.34* shows a block diagram of vibration signals collected using the recording system and both the on-line and off-line signals processing.

Following the recording of experimental data, the recorded signals are off-line analyzed using a dual-channel *NICOLET 660 Fast Fourier Transform (FFT)* analyzer.

Power spectrum in *(RMS)*, which determines the average power of a signal in any specific frequency band, is among the several functions the analyzer can perform. The analyzer can be employed as either a single or dual channel(s). For single mode, a resolution of 800 points is available while in the dual mode only half of this is available for each channel. Therefore, a slight difference in value of the same signal is expected due to the difference of the pass band frequency. Although this difference, in most cases, is negligible, all the quantitative calculations for the function values are assumed to be performed using the dual mode unless it is otherwise stated. The analyzer has the capacity to manipulate signals with frequencies from 1 Hz to $100kHz$. The analyzer has a cathode-ray tube *CRT* on which the spectrum, along with much other relevant information, could be displayed. The analyzer uses the *Fast Fourier Transform* which computes the spectrum more rapidly than the direct approach with discrete functions. For a frequency function $F(k), k = 0,1,2,\ldots,N-1$, to be calculated from the series of time-domain function $F(t)$, a Discrete Fourier Transform (DFT) is used in the form;

$$F(K) = \frac{1}{N}\sum_{N=0}^{N=N-1} F(N)e^{\left(\frac{-2\pi K}{N}\right)}, \qquad K = 0,1,2,\ldots,N-1 \tag{3.20}$$

For each value of N in $F(K)$, N multiplications of the form $F(N)e^{\left(\frac{-2\pi K}{N}\right)}$ are required, and so, the total calculations of the full sequence $F(K)$ requires N^2 multiplications. However, by using the *Fast Fourier Transform (FFT)*, this number of multiplications is reduced to the order of $N\ log_2 N$. The FFT works by partitioning the full sequence $F(K)$, $K = 0,1,2,\ldots,N-1$ into a number of shorter sequences. Instead of calculating the DFT of the original sequence, only the $DFTs$ of the shorter sequences are worked out. The FFT then combines these together in an ingenious way to yield the full DFT of $F(K)$. Details of this procedure may be found in *ref. [100]*. An X-Y plotter was connected in parallels to the analyzer to produce a hard copy of the output. Also, an oscilloscope was used to display the real-time signal.

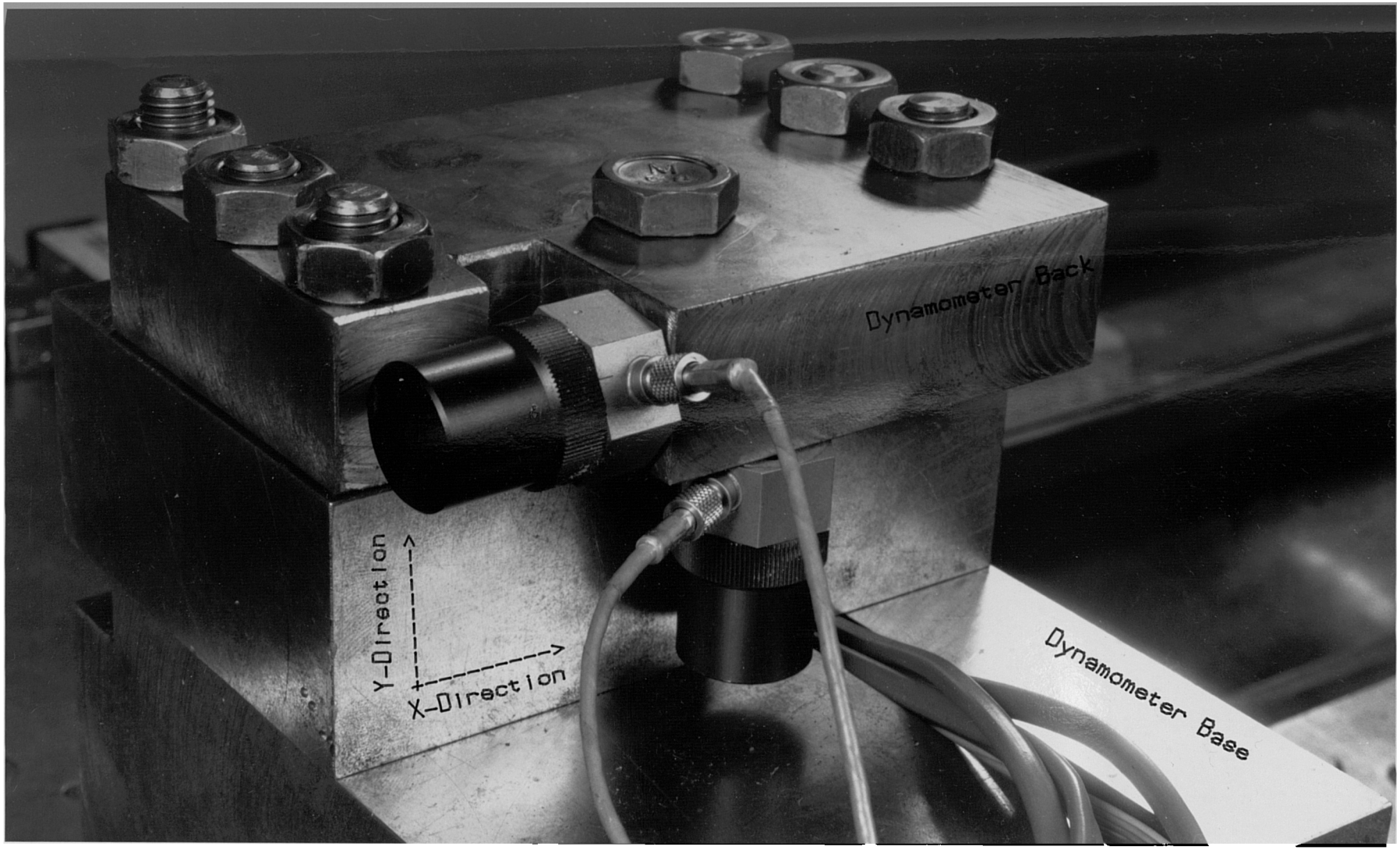

Fig. 3.33 The Vertical and the Horizontal Vibration Accelerometers

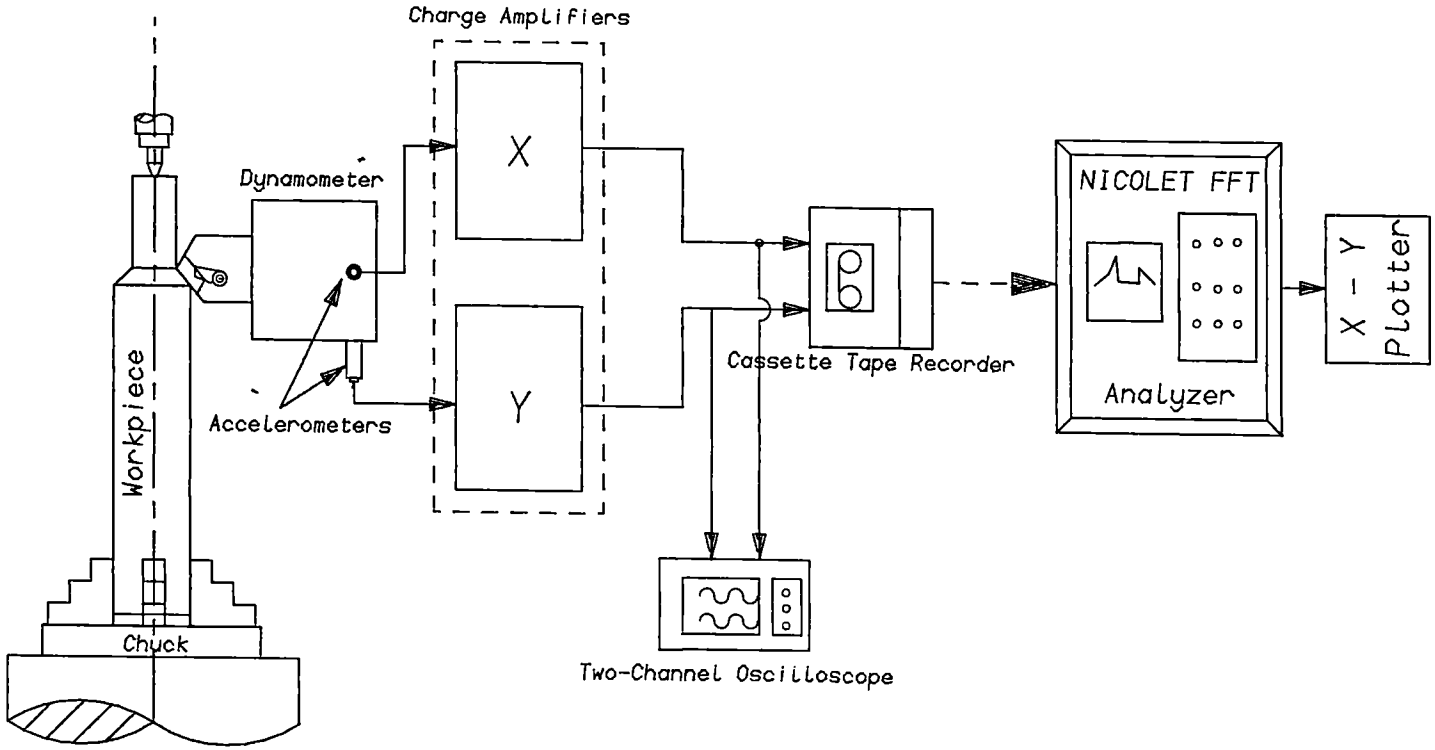

Fig. 3.34 On-line and Off-line Vibration Signals Processing

3.3 Machine Used and Its Relevant Measurements

3.3.1 Machine Characteristics

A new (*Feb* 1983) *Colchester Mascot 1600* centre-lathe, *Fig. 3.35,* was used in the experimental work of this study. Following are the machine's characteristics:

- Height of the Centre over Bed — 215 *mm.*
- Max Distance Between Centres — 1500 *mm.*
- Spindle Diameter — 76 *mm.*
- Motor Power — 7.5 *kW.*
- Speed Range — $20 - 1600$ *r.p.m* in 16 steps.
- Feed Range — $0.06 - 1.0$ *mm/rev.* in 10 steps.

A four-independent direct jaws 405 *mm* diameter chuck was used to hold the workpiece from one end, while a *GMT* live centre (rotating) was used on the tail-stock to guide it from the other end. As explained before, the tool-post is replaced by the dynamometer block, *Fig. 3.35.*

Prior to the experimental work, the motor belts were replaced by a new set, and the machine's accuracy was examined. An engineers precision level was used to check the level accuracy in both longitudinal and transverse directions, and no deviations were found. Also, no deviation was observed when a test was carried out to check the lathe alignment.

3.3.2 Measurement of Cutting Parameters

The parameters which were measured and adjusted during the experiments are: feed; speed; cutting time; depth of cut; and, chip thickness. The feed longitudinal motion, and transverse displacement of depth of cut were measured by means of a digital read-

out, using magnetic transducers. This has been already fitted to most of the machine tools as a part of modernizing plan to improve their accuracy, *Fig. 3.35.*

Since the surface speed is the product of workpiece diameter and spindle speed, a test was done to determine the accuracy of spindle rotation. Using a speed-meter and a tachometer, it was found that the prescribed revolution values were correct only when the machine was full-loaded. Otherwise, a certain increase in rotation speed of up to 6% existed. Therefore, it was necessary to determine the actual value of rotational speed.

A magnetic pick up was held against a sixty teeth gear mounted on the end of the spindle, *Fig. 3.36,* so that when the spindle rotated, electronic pulses corresponding to the number of passed teeth were given. Output was fed to an electronic counter, *Fig. 3.35,* to read the occurrences of pulse per second which were the actual workpiece revolutions.

The cutting time was measured by using an accurate stop-watch, while the chip thickness was measured using an end-ball micrometer.

3.3.3 Workpiece Preparation

The workpiece material used in this study was an alloy steel *En19.* The chemical and mechanical properties are as follows:

a) Chemical Composition (Using Physical-Chemical Section Methods)

C	S	P	Mo	Ni	Si	V
0.37	0.027	0.016	0.23	1.51	0.22	≤ 0.02
	Cr	Mn	Nb	Ti	Al	Cu
	1.10	0.57	≤ 0.02	≤ 0.02	0.03	0.15

b) Mechanical Properties

- Hardness $355HV$.
- Tensile Stress $933\ N/mm^2$.
- Young's Modulus $2.05 \times 10^5 N/mm^2$.
- Shear Stress $610\ N/mm^2$.

Seven 200 mm diameter 600 mm length bars were employed in the various stages of the experimental work. Prior to tests, the two faces of each bar were faced, chamferred, centered, and then loaded between the machine centres. Fine cleaning cuts were made until a smooth high quality surface was obtained. The final value of the workpiece diameter, in conjunction with the reading from the speed counter, was used in computing the surface speed of a specific test. Following the machining of each workpiece layer, a cleaning cut was carried out to obtain the desired diameter.

The workpiece rigidity recommended by *BS 5623 [59]* was maintained by taking account of the value of $\{\frac{1}{10}\}$ workpiece length-diameter ratio, therefore, the minimum workpiece diameter value used in this study was 60 mm.

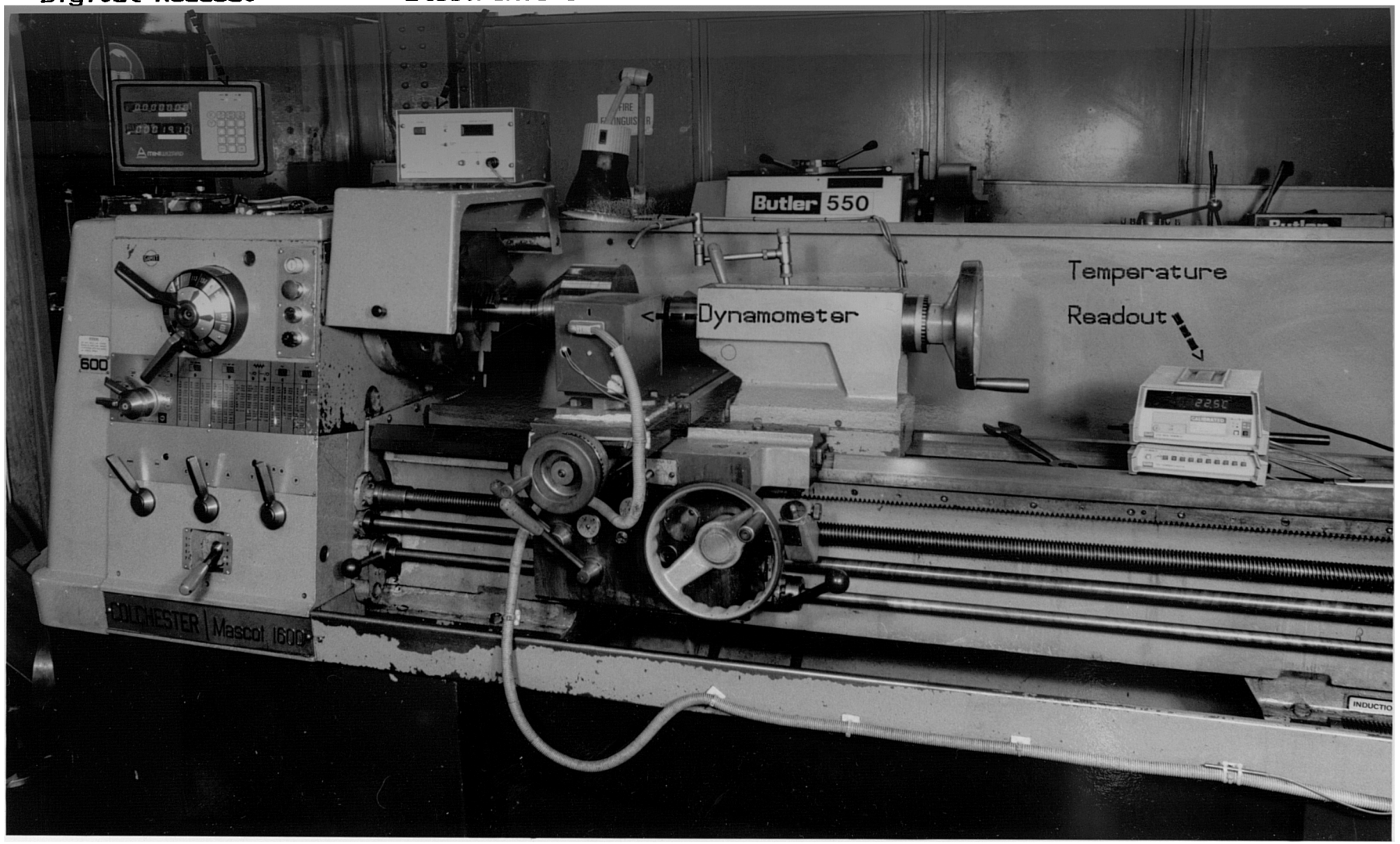

Fig. 3.35 A General View of the Centre-Lathe Used

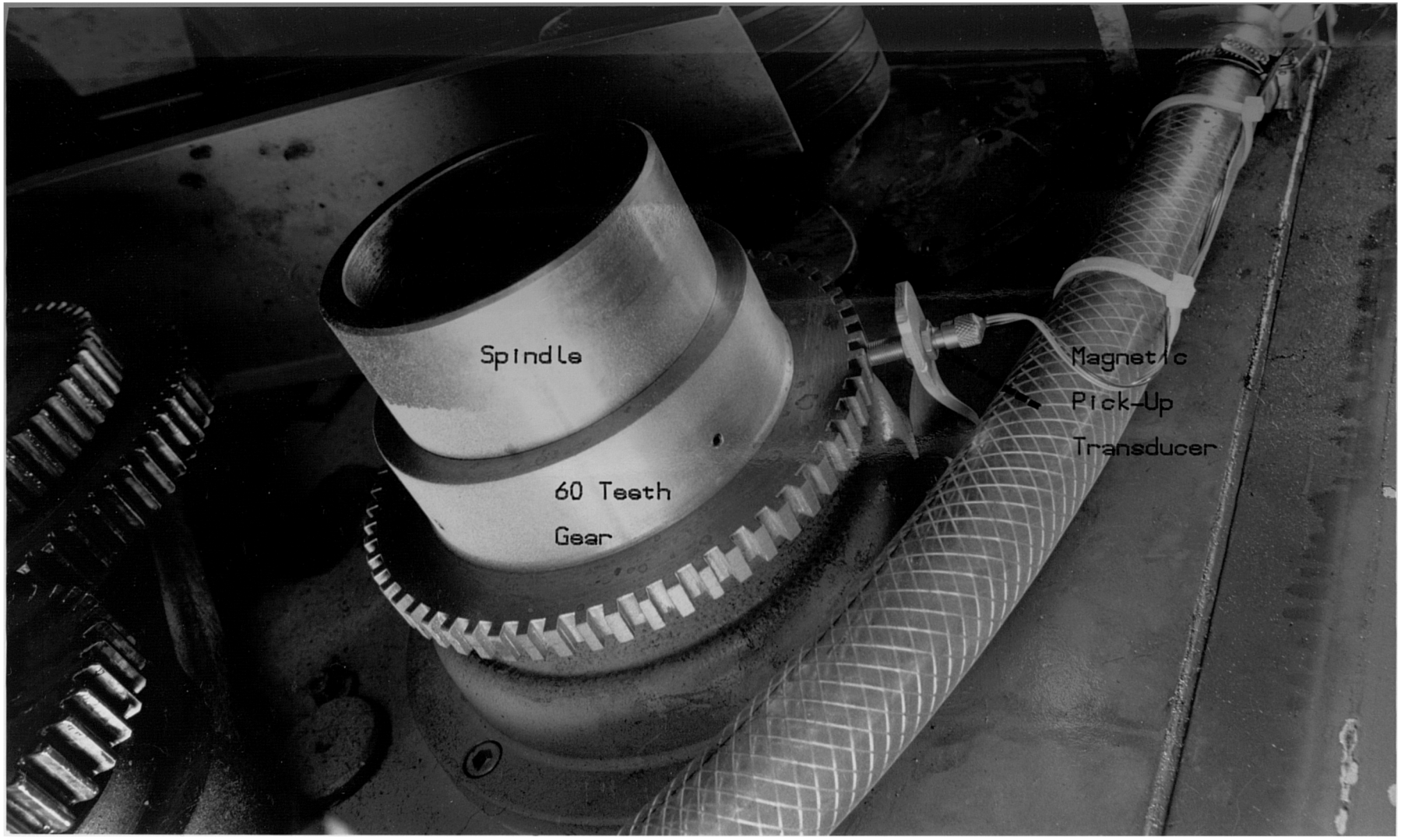

Fig. 3.36 Measurement of the Actual Spindle Revolutions

3.4 Tool Material and Tool Wear Measurement

The cutting tools used in this study was a multi-coated carbide inserts *(Sandvik GC435 - Gamma Coated)*. The chemical compositions and the mechanical properties of such inserts, as provided by *Sandvik*, are as follows:

Coating Layers	Substrate by Wt%				Hardness
	Co	WC	TiC	(Ta,Na)C	
$1\ \mu\ m$ TiN $3\ \mu\ m$ Al_2O_3 $5\ \mu\ m$ TiC	10.2	84.0	1.9	3.9	1400 HV

Table 3.5 Chemical Compositions and Mechanical Properties of GC435 Inserts

This type of tool inserts is ideally for steel cutting mainly within *ISO P35* area which includes steel, steel casting, long chipping malleable iron and stainless steel. The multiple coating layers with the tough substrate give the insert a wide application area especially when a higher productivity (greater metal removal rates) is required. The inserts were of the standard *SPUN* 12 03 12 with geometry as shown in *Fig. 3.37.a.* A set of compatible spare parts, such as top clamp, allen key, shim, shim pin, and chipbreaker were used to clamp the insert to the dynamometer. Each insert has four cutting edges but only one edge per insert was used since a cutting temperature for a specific cutting edge could affect the chemical properties and hardness of the others.

After each cut, the insert was taken away from the dynamometer in order to measure the wear scars developed on the cutting edge. Before taking this measurement, the cutting edge was carefully cleaned using kerosene to remove the sticking chips and grease.

As shown in *Fig. 3.37.b,* the wear scars on the tool clearance face were measured on three locations: the nose wear *NW;* the flank wear *FW;* and, the notch wear *NCW.*

The extension of nose area is usually determined by the cutting edge radius. The notch area determines the end of workpiece contact with the cutting edge. As indicated in *Fig. 3.37.b,* wear scar was measured in the vertical plane which contains the cutting edge.

A high precision *SIP* three-axis universal measuring optical microscope which has a measuring accuracy of ten-thousandths of a millimetre was used to measure these wear scars. To ensure that the wear level was read by the microscope accurately, a measuring kit was used to hold the tool-insert during measurement, *Fig. 3.38.* As shown, the angles were adjusted to simulate the insert geometry during cutting, 5^{o} clearance angle and 6^{o} side rake angle. The protuberant at the bottom of the block was used to secure it to the T-slots of the apparatus horizontal table. To ensure a permanent accurate reference line, a reference insert was clamped beside the worn tool. The difference between the measurement on the reference insert edge and the extent of wear level on the worn tool gave the wear value.

Also, for accurate and easy detection of the wear level, an extra external light was used.

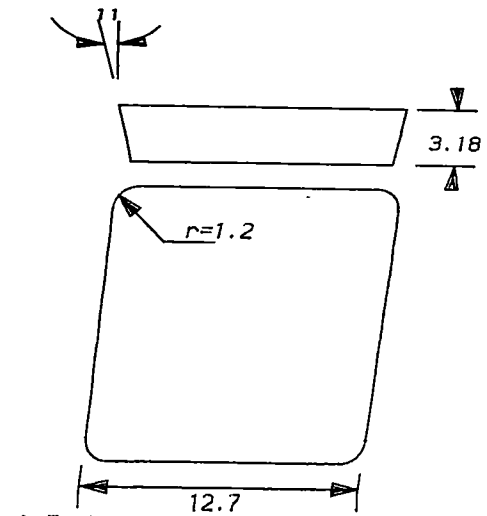

a) Tool Insert Geometry

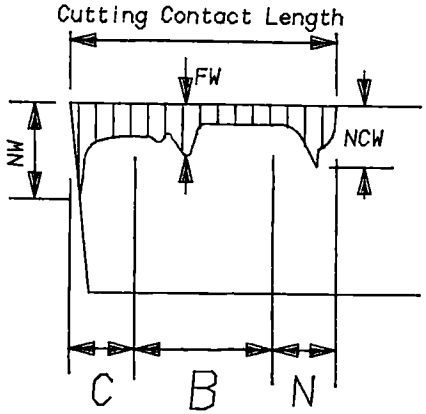

b) Flank Wear Elements

Fig. 3.37

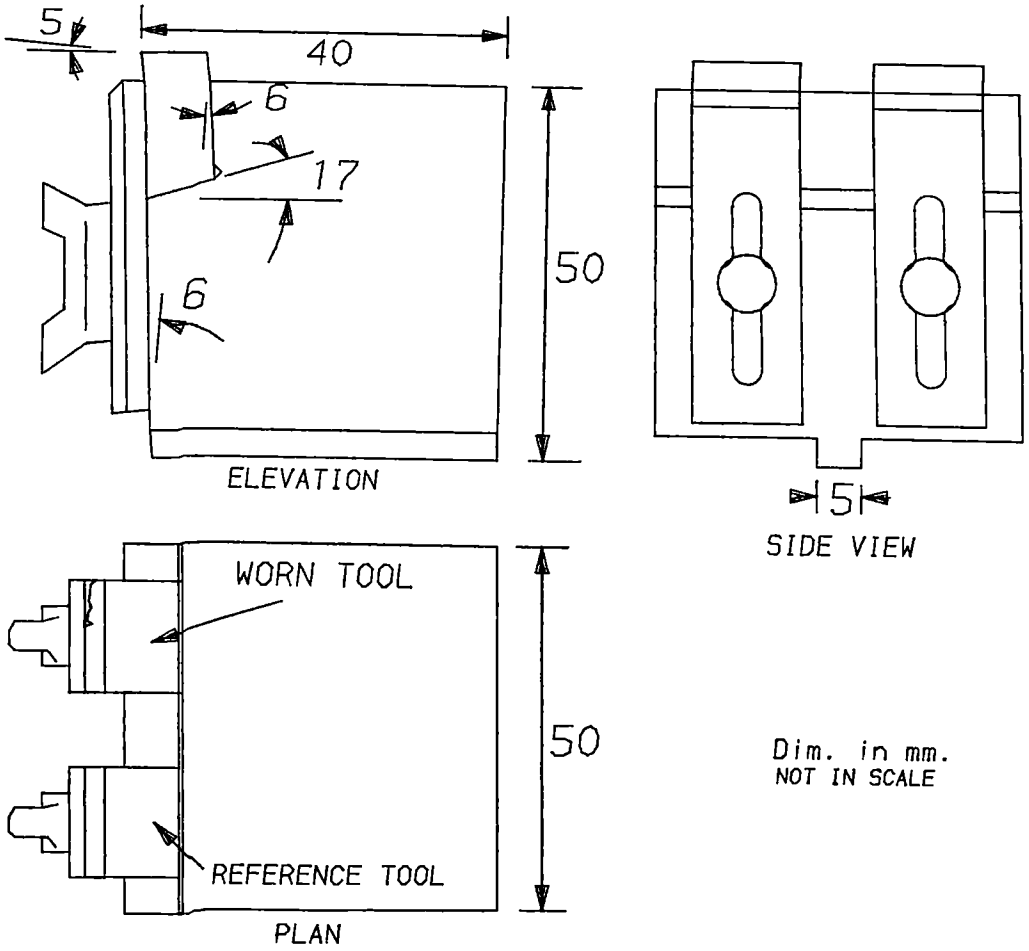

Fig. 3.38 Clamping Kit for Tool Wear Measurement

Chapter 4

REGRESSION ANALYSIS AND MODEL BUILDING TECHNIQUES

4.1 Introduction and Foreword

The selection of proper machining parameters still basically depends on human experience in spite of the rapid developments in automation. Even though there are many references to publications on the selection of appropriate cutting conditions, *[101]*, and on other sources of empirical data, it is not possible to achieve automatic selection of the optimal cutting conditions.

A more efficient alternative to the human approach, for a wide variety of engineering problems, is the mathematical model approach. This technique relates system output (response) to the corresponding independent cutting parameters such as speed, feed, and depth of cut. This approach is followed in this chapter and regression techniques will always be used as statistical tool to predict the parameters of the mathematical model. The main function of the regression model building technique is to find the best equation which will have sufficient variables capable of providing an accurate estimation of the response.

The selection of a consistent and reliable regression model depends very much on: the nature of experimental data, either planned or randomly collected; the validity of various phenomenological and statistical assumptions; and, the capability of distinguishing the best model from the wide range of possible alternatives using the proper criteria. Even though the approach of mathematical modelling of the turning operations has been investigated by many investigators *[11,17,19,50,102-111]*, an analysis such that described here has not been reported so far. Both linear and non-linear regression estimation procedures were used to formulate the responses of the rough-turning operation. Both weighted and ordinary least-squares estimation procedures have been used to take into account the possible superiority of certain observations over the others. This resulted in different forms of linear and non-linear models of tool wear; tool life; tool vibration; and, cutting force components. Most of these models represent a simultaneous continuous record of tool operating life history with the cut-

ting time as an extra parameter. Significance and adequacy of each model were checked using sophisticated statistical tests and criteria.

In this chapter, a review is presented of theoretical techniques and applications of regression analysis. Techniques are discussed for the design of laboratory experiments. For convenience of presentation, a practical modelling example has been presented in the theoretical analyses. This is to explain the sequence of the modelling strategy; and, the logical steps which were followed in developing of most of models in this study.

The presentation of study of mathematical modelling of the turning operations follows the sequence:

1. postulating of the mathematical model;
2. design of experiments;
3. choice of cutting parameters;
4. conduct of experiments;
5. estimation of model parameters; and,
6. examination of model significance and adequacy.

4.2 Postulation of Mathematical Models

The actual structure of the functional relationship between cutting response and cutting parameters is often unknown. The problem is to tentatively entertain an approximate relationship for an unknown response function, and then, using specific criteria, to check whether or not the assumed model is adequate. Generally, the problem can be mathematically expressed as:

$$R = \Phi(V_1, V_2, V_3, V_4, ..., V_p); \tag{4.1}$$

where R is the cutting response; V's are the independent variables. *Friedeman [109],* among others, suggested that the relationship between tool life and cutting variables -speed V, feed F, and depth of cut d - may take the form:

$$T = ao \ V^{a1} \ F^{a2} \ d^{a3}. \tag{4.2}$$

This equation is sometimes called the extended Taylor's equation. Generally, as proposed by many investigators, the tentative relationship between the machining responses and the machining variables for turning operations may take the non-linear form:

$$R = c \ V^{p} \ F^{m} \ d^{n}; \tag{4.3}$$

where c, p, m, n are constants to be predicted from the regression analysis using the experimental data. This form can be linearized using the logarithmic transformation so that it takes the linearized form:

$$Y = bo + b1 \ X1 + b2 \ X2 + b3 \ X3; \tag{4.4}$$

where $Y = \ln R$; $X1 = \ln V$; $X2 = \ln F$; and $X3 = \ln d$. Form *(4.3)* may take the general non-linear multiplicative form:

$$R = c \left[\prod_{j=i}^{p} \xi_j^{\beta j} \right] \bar{\varepsilon}; \tag{4.5}$$

where ξj are the natural machining variables, c and βj are the model parameters, p is the number of the independent variables, and $\bar{\varepsilon}$ is a multiplicative random error. To convert this non-linear model to the standard linear form, natural logarithms can be taken:

$$\ln R = \ln c + \sum_{j=1}^{p} \beta j \ \ln \xi j + \ln \bar{\varepsilon}; \tag{4.6}$$

which can be rewritten in the original form as:

$$Y = \beta o + \sum_{j=1}^{p} \beta j \ Xj + \varepsilon; \tag{4.7}$$

where $Y = \ln R$, $\beta o = \ln c$, $Xj = \ln \xi j$, and $\varepsilon = \ln \bar{\varepsilon}$. This equation is a linear polynomial of the first order, and multiple linear regression can be applied to estimate

the model parameters βo and βj's using the experimental data. Based on the estimated parameters, this equation can be written in the general predictive form as:

$$Y_i = bo + \sum_{j=1}^{p} bj\ Xij + \varepsilon; \qquad i = 1, 2, ..., n. \tag{4.8}$$

In terms of the natural variables, the prediction Eq. *(4.8)* becomes,

$$(\ln R_i)_{est.} = bo + \sum_{j=1}^{p} bj\ Xij; \qquad i = 1, 2, ..., n; \tag{4.9}$$

where bo and bj are the estimated model parameters, $(\ln R_i)_{est.}$ is the predicted response value, and n is the total number of data points. Although the model *(4.7)* can be fitted satisfactorily to many combinations of operations and work materials, experience *[18 & 112]* indicates that there is still a large number of machining cases where a model of the type described is not satisfactory because the data clearly shows the existence of non-linearities which cannot be ignored. Therefore, it is necessary to introduce models which take care of slight non-linearities. Therefore, Second-order and interaction terms were introduced by *Colding [18]* and *Wu [112]*. In his work to formulate cutting temperature as a function of cutting parameters, *Wu [112]* found that the first order model had some drawbacks, especially at higher temperature values, so that he used, what he called, a more comprehensive second-order model. He suggested that his first-order model presented in *[19]* could be extended to take the form:

$$\begin{aligned} Y \;=\; & bo + b1\ X1 + b2\ X2 + b3\ X3 + b11\ X1^2 + b22\ X2^2 + b33\ X3^2 \\ + \; & b12\ X1X2 + b13\ X1X3 + b23\ X2X3 + \varepsilon; \end{aligned} \tag{4.10}$$

where $X1^2$, $X2^2$, $X3^2$ are the quadratic effects of the three main cutting variables, and $X1X2$, $X1X3$, $X2X3$ represent their interaction effects. This second-order model may take the general form:

$$Y_i = bo + \sum_{j=1}^{p} bj\ Xij + \sum_{j=1}^{p} \sum_{k \geq j}^{p} bjk\ Xik + \varepsilon_i; \qquad i = 1, 2, ..., n. \tag{4.11}$$

The general second-order prediction equation expressed in terms of the natural variables is given by:

$$(\ln R_i)_{est.} = bo + \sum_{j=1}^{p} bj\ \ln \xi ij + \sum_{j=1}^{P} \sum_{k \geq j}^{p} bjk\ \ln \xi ij \ln \xi ik; \qquad i = 1, 2, ..., n. \tag{4.12}$$

All of the parameters of this second-order equation can also be estimated using multiple regression analysis. No prior statistical knowledge about the data is required to estimate the model parameters. However, to examine the adequacy of the developed model, there are some assumptions to be satisfied. These are:

1. the independent variables are errorless, that is, $V(\xi ij) = 0$;
2. the random errors $\tilde{\varepsilon}$ are additive, that is, $Y = (Y_i)_{est.} + \varepsilon_i$;
3. the errors have zero mean and a constant variance, that is, $E(\varepsilon_i) = 0$, $V(\varepsilon_i) = \sigma^2$;
4. the errors are uncorrelated, that is, $cov(\varepsilon_i, \varepsilon_j) = 0$ for $i \neq j$; and,
5. the errors have normal distribution, that is, $\varepsilon_i \sim N(0, \sigma^2)$.

The logarithmic linear transformation is necessary in the linear regression technique since it is impossible to use this technique to estimate model parameters in a non-linear form. A logarithmic transformed model of any order is still defined as a linear model since the transformation affects only the variables of the model.

In contrast to linear estimation, non-linear one does not require a specific model structure and no restriction is imposed on the number of variables or the relative relations among them. In non-linear estimation, the model parameters are dealt with in their natural forms. Equivalent statistical criteria, to those used in linear estimation, are developed and used to examine the significance and adequacy of the developed non-linear models.

4.3 Design of Experiments

To obtain an experimental data base which can be used to build mathematical models which have statistical significance over a specified domain, it is necessary to design the experiments accordingly. The data from carefully designed experiments are always

well conditioned and no serious problems exist when they are analyzed. As stated by *Balakrishnan [113],* the unplanned or happenstance data arising from non-designed experiments might not have the desired properties needed for regression analysis, and hence cause ambiguities during model building.

There are many methods for design of experiments *[114]* such as factorial design, fractional factorial design, central composite design, and non-central composite design. The central composite design *CCD* is the most appropriate to the purpose of metal cutting modelling, and therefore, it was used in this study to design the experiments. Central composite design has been initially proposed by *BOX [115].* For three independent variables, the complete *CCD* consists of twenty-four tests in four blocks, each block containing six tests. The *CCD* is diagrammatically shown in *Fig. 4.1.* To build a first-order model, only the first two blocks can be used. These blocks represent the conventional 2^3 factorial design located at the vertex of a cube with an added centre point repeated four times to determine the experimental error. The design of the first twelve tests provides three levels for each variable. For convenience, these levels are denoted to as high, medium, and low, *Table 4.1.*

To make a design for a second-order model, the twelve experiments are extended to 18 or 24 tests. To develop a design for an 18 tests, six experiments are added. These additional tests are called the augmented points, and may be referred to as highest and lowest. Whenever increased precision is required, a 24-tests design can be developed sequentially by repeating the last six augmented tests.

4.4 Selection of Cutting Parameters Levels and Conditions

The ranges of cutting speeds and feeds used in this study were selected so as to conform reasonably well with actual production roughing machining operations. Also, the choice was made considering the capacity of the lathe and its limiting conditions. The selected

Parameter Level	Speed (V) m/min.	Feed (F)	D.O.C (d) mm
Lowest	50	0.06	1.50
Low	72	0.12	2.00
Medium	104	0.20	2.25
High	145	0.30	2.50
Highest	206	0.60	3.00

Table 4.1 Different Levels of Cutting Parameters

ranges are given *Table 4.1.* In order to obtain adequately spaced points, a geometrical series with an exponent of 1.4 was used to determine the speed levels. The actual values of cutting parameters for the entire *CCD* are listed in *Table 4. .* The feed levels selected combined the characteristics of being large enough to accelerate tool wear, but being small enough to prevent chatter. Choice of maximum feedrate was arranged to satisfy the *BS 5623 [ ]* recommendations not to exceed 80% of the tool-tip corner radius.
The depth of cut was determined to satisfy many requirements. Larger values of depth of cut when combined with higher speed levels cause chatter to occur. Since it was thought that it had the least effect on the turning responses, values of depth of cut were selected to preserve the workpiece materials. A minimum value was selected not to be less than tool-tip corner radius, since a smaller depth of cut may make measurement of tool wear more difficult and less accurate.

4.5 Conducting the Experiments

Each test in *Table 4.2* consists of a number of sub-tests. Each sub-test lasted for about two minutes per cut. The test duration was terminated by either tool catastrophic failure or reaching a certain level of wear land *(at least 0.3 mm)* on any location of the clearance face, the nose, the flank, or the notch.
The trials and their sub-tests were carried out randomly as described by the sequence

Test No.	Cutting Speed m/min.	Feed mm/rev.	D.O.C mm	Tool Life min.
1	72 [72.35]	0.12	2.00	119.0
2	145 [144.67]	0.30	2.00	13.00
3	145 [145.89]	0.12	2.50	20.00
4	72 [71.97]	0.30	2.50	30.00
5	104 [104.51]	0.20	2.25	36.00
6	104 [104.72]	0.20	2.25	65.00
7	145 [148.22]	0.12	2.00	37.00
8	72 [72.69]	0.30	2.00	79.00
9	72 [72.32]	0.12	2.50	79.00
10	145 [144.72]	0.30	2.50	7.000
11	104 [103.67]	0.20	2.25	50.00
12	104 [103.06]	0.20	2.25	35.00
13	206 [206.94]	0.20	2.25	4.000
14	50 [50.04]	0.20	2.25	140.0
15	104 [101.71]	0.60	2.25	9.000
16	104 [104.15]	0.06	2.25	96.00
17	104 [104.66]	0.20	3.00	24.00
18	104 [102.67]	0.20	1.50	55.00
19	206 [206.85]	0.20	2.25	4.500
20	50 [50.36]	0.20	2.25	119.0
21	104 [103.55]	0.60	2.25	8.000
22	104 [104.80]	0.06	2.25	65.00
23	104 [103.75]	0.20	3.00	31.00
24	104 [103.40]	0.20	1.50	48.00

Table 4.2 The Central Composite Design and Tool Life Values

number in *Appendix A*. The first twelve tests (the first and second blocks of *CCD*) were first completed followed by the third block, and finally the fourth block was performed. The experiments were performed without using cutting fluids. This is to simulate industrial practice. This was recommended by Sandvick tool manufactrur when the inserts were supplied.

A chip-breaker was used to prevent long chips from wrapping around the workpiece which ruin the surface produced and disturb the whole operation.

For each sub-test, simultaneous records were obtained of vertical force component F_y, feed component F_x, radial component F_z, tool vibration acceleration in horizontal direction A_x, and tool vibration acceleration in vertical direction A_y. Following machining in each sub-test, the measurement of tool wear was performed as previously described in *section 3.4*.

4.6 Multiple Linear Regression Technique

4.6.1 Linear Least-Squares Estimation Procedure

In multiple linear regression analysis, a linear model is developed that summarizes the relationship between a dependent variable and a set of independent variables. The coefficients for the independent variables are computed by least-squares procedure so that the sum of squared differences between the observed and predicted values of the dependent variable based on the model is as small as possible. For instance, a simple case can be expressed as shown in *Fig. 4.2* where a single independent variable is involved in the estimation procedure. The regression line $(Y)_{est.} = Bo + B1\ X$ represents the predicted values of the response Y. Consider two points of the data used in estimating the coefficients Bo and $B1$ these are (X_i, Y_i) and (X_k, Y_k). The least-squares technique is designed to estimate the coefficients so as that to minimizes the error components $[Y_i - (Y_i)_{est.}]$ and, $[Y_k - (Y_k)_{est.}]$. However, since absolute values of the errors may lead to mathematical difficulties, a better least-squares method defines the line in such a

way that $\sum[Y - Y_{est.}]^2$ has the smallest value.

Generally, the linear forms *(4.8)* and *(4.11)* may be converted to the matrix form:

$$[Y] = [X][B] + [\varepsilon]; \tag{4.13}$$

where Y is an $(n \times 1)$ vector of the n data observations, X is an $(n \times p)$ matrix of the levels of the p independent variables, B is a $(p \times 1)$ vector of regression coefficients, and ε is an $(n \times 1)$ vector of random error.

For this arrangement, the least-squares estimator of B takes the form:

$$B_{est.} = (X'X)^{-1} X'Y; \tag{4.14}$$

where $B_{est.}$ is the $(p \times 1)$ of the parameter estimates, X' is the transpose of X, $(X'X)^{-1}$ is the inverse of $(X'X)$, and Y is the matrix of measured response on a logarithmic scale. Details about least-squares estimation procedure are found in *ref. [116].*

The total observed variability in dependent variable is subdivided into two components: that is attributed to the regression analysis and, that which is not. For point (X_i, Y_i) in *Fig. 4.2,* the distance from Y_i to Y_{mean} can be subdivided into:

$$Y_i - Y_{mean} = [Y_i - (Y_i)_{est.}] + [(Y_i)_{est.} - Y_{mean}]. \tag{4.15}$$

The distance from Y_i to $(Y_i)_{est.}$ is zero if the regression line passes through the point itself. It is called the residual from the regression. The second component $[(Y_i)_{est.} - Y_{mean}]$ is the distance from the regression line to the mean of the Y's. This distance is explained as the improvement in the estimate of the dependent variable achieved by the regression. It can be shown that:

$$\sum_{i=1}^{n}(Y_i - Y_{mean})^2 = \sum_{i=1}^{n}[Y_i - (Y_i)_{est.}]^2 + \sum_{i=1}^{n}[(Y_i)_{est.} - Y_{mean}]^2. \tag{4.16}$$

The first quantity is called the total sum of squares *SST,* the second is the residuals sum of squares *SSE,* and the third is the regression sum of squares *SSR.*

The effectiveness of regression model depends on the relationship between these three components. A commonly used measure of the quality of fit of a linear model is R^2,

sometimes called *the coefficient of determination or, R Square,* and can be expressed as:

$$R^2 = 1 - \frac{SSE}{SSE + SSR} = 1 - \frac{SSE}{SST}. \tag{4.17}$$

This coefficient of determination indicates how much of the total variation in Y has been explained by the linear relationship between X and Y. As can be seen from Eq. *(4.17),* the greater R^2, the better or more accurate and significant. the model will be. Another criterion used to determine the effectiveness of the model and the significance of the independent variables is the *F-ratio.* This ratio takes the form:

$$F - ratio = \frac{Regression\ \ Mean\ \ Squares}{Error\ \ Mean\ \ Squares} = \frac{M_{SR}}{M_{SE}}. \tag{4.18}$$

The mean squares for each entry is the sum of squares divided by its number of degrees of freedom *DF.* This number of degrees of freedom indicates how many independent pieces of information involving the n observations are required to compile the sum of squares.

If the regression assumptions are met, the ratio of the mean squares regression to the mean square residuals is distributed as an *F-statistic* with p and n-p-1 degrees of freedom. The *F-ratio* is equivalent to the value of *t-statistic* of the coefficients of the variables allowed in the model, since the *F-statistic* and the *t-statistic* are connected through the relation $F = t^2$. The *t-statistic* of the coefficient defined as the ratio of the coefficient to its standard deviation.

4.6.2 Model Building Techniques

Model building algorithms should be capable of selecting the best subset of variables for a given data set from the original variables. There are many techniques to select the suitable subsets of variables. All these techniques select the best set of variables to be included in the final equation and provide the appropriate statistical parameters and residuals analysis. In the commercial statistical computer package *SPSSX [117],* there are many regression techniques such as Forward Selection, Backward Elimination, Stepwise , Enter, and Remove procedures. Among these, the most practical and

well-known are the Forward selection, Backward Elimination, and Stepwise regression techniques.

Forward Selection starts with no variables in the equation. The first variable to enter into equation is the one with the largest correlation (or the smallest sum of squares of error *SSE* with the dependent variable. The significance of the variable is checked by its *F-statistic* or *t-statistic.* If the first variable selected for entry meets the criteria, forward selection continues; otherwise, the procedure terminates with no variables in the equation. Once a variable is entered, the partial correlation between the dependent variable and each of the independent variables not included in the equation are examined. This procedure is repeated until no variables qualify for entry or all the independent variables have been entered.

The most widely used criterion for assessing whether the reduction of *SSE* is sufficiently small to terminate the Forward Selection process is an *F-statistic.* At the first stage, the *F-statistic* is calculated as in form *(4.)*. At subsequent stages, the *F-statistic* is slightly modified to $F_j = (SSE_{j-1} - SSE_j)/M_{SEj}$, where M_{SEj} are the mean square residuals of the step *j*. Therefore, the number of variables in the final equation is completely dependent on the value of F_j. This criterion is called *F-change* and in the case of Forward Selection is called *F-to-enter (FIN).* Both from statistical and practical points of view, the significance of the *t-statistic* for all of the coefficients in the model should be high.

Backward Elimination procedure, in contrast to Forward Selection method, begins with all variables in the prediction equation. The variables are then eliminated one at a time until either all the variables have been excluded or some selected criterion is satisfied. A partial *F-test* for each predictor variable is calculated as though it was the last variable to enter the regression equation. At stage one, the predictor variable is discarded that, when eliminated, yields the smallest *SSE* for the remaining variables. It is noted that the predictor variable, that corresponds to the smallest *SSE,* is the one with the smallest *t-statistic.* At subsequent stages, the predictor variable that is a candidate for removal from the equation is that which has the smallest *t-statistic,* and

its *F-test* is smaller than the specified *F-to-remove (FOUT)* value. *FOUT* is calculated as : $F_j = (SSE_{j+1} - SSE_j)/M_{SE}$, where M_{SE} is the error mean squares of the full prediction equation.

Stepwise Regression procedure is a method that combines the Forward Selection and the Backward Elimination approaches. It is essentially a forward selection procedure but, at each step of the process, the predictor variables in the chosen subset are re-examined for possible deletion in a manner similar to that used in the backward elimination method. Hence, after each variable is added, consideration is given to discard one of the previously accepted variables. At each step of the Stepwise technique, a predictor variable is added to the prediction equation, as in the forward selection, as it is the largest one calculated and exceeds *FIN*. Next, each predictor variable already chosen is reconsidered and eliminated from the selected subset, as in the backward elimination, if its *F-statistic* is smaller than the specified *FOUT*. The next step is to consider for entry the variables not included in the equation, followed by the examination for removal of the variables included in the equation. Variables are removed until none remain that meet the removal criterion. To prevent the same variable from being repeatedly entered and removed, *FIN* must be greater than *FOUT*. Variable selection terminates when no more variables meet the entry and removal criteria.

Throughout the rest of this chapter a numerical example is introduced to explain and interprete the aspects under investigation. This represents the steps which should be followed to build a tool life model. The term of tool life *T*, used here as a dependent variable (response), was considered as the time taken to reach a certain level of average wear *AW*. The average flank wear was considered as the mean value of the three wear readings, nose, flank, and notch. A criterion average wear value of *0.25 mm* was used to determine the corresponding value of cutting time from the experimental wear-time curve. The observed tool life values for different observations are listed in *Table 4.2.*

Each of the model building techniques, Forward selection, Backward Elimination, and Stepwise Regression was used in turn to estimate the model parameters for both the

	First-Order Model [12-Tests]			Second-Order Model [24-Tests]		
	Forward	Backward	Stepwise	Forward	Backward	Stepwise
bo	13.95	13.95	13.95	-7.74	-9.99	-7.74
b1	-2.06	-2.06	-2.06	7.33	8.14	7.33
b2	-0.92	-0.92	-0.92	-	-	-
b3	-2.86	-2.86	-	-		-
b11	-	-	-	-1.12	-1.21	-1.12
b22	-	-	-	-0.36	-0.39	-0.36
b33	-	-	-	-	-0.85	-
b12	-	-	-	-0.46	-0.49	-0.46
b13	-	-	-	-	-	-
b23	-	-	-	-	-	-
R^2	0.89	0.89	0.89	0.96	0.96	0.96
F-ratio	21.2	21.2	21.2	84.3	93.4	84.3
SE	0.317	0.317	0.317	0.24	0.228	0.240

Table 4.3 Model Parameters and Statistical Characteristics of Tool Life Model

first and second-order models using different sets of data points. *Table 4.3* summarizes the results from these procedures.

For a first-order model of the form *(4.4)*, the first block of data trials *1-6* was first used. Low correlation factor of *0.53* and high standard error of *0.61* indicated that the six tests were insufficient to build a significant and adequate first order model. Therefore, the second block of data was added and the procedure was repeated. A considerable improvement in the model statistics was achieved with all of the three coefficients included into the final equation, *Table. 4.3.* When a second-order model was built using different sizes of data sets, it was evident that the model using full *CCD* of *24*-tests was better than the model with only *18*-tests (blocks *1,2,* and *3).*

It is evident from the results given in *Table 4.3* that the best model selected by the various model building techniques for a given set of data is not always the same. The behaviour of the Forward Selection and Stepwise techniques seems to be the same. This is to be expected since the Stepwise procedure uses the Forward Selection technique for entering the variables as already discussed. One disadvantage with the Forward Selection technique is that a variable once entered into the model is never removed,

even though the *t-statistic* of its coefficient becomes unacceptable after entering another variables. The Stepwise procedure seems to be superior to Forward Selection since it is capable of removing non-significant variables from the model before entering any new variables. Thus, the choice for the best technique has been confined to only the Backward Elimination and the Stepwise techniques. Examination of the results given in *Table 4.3* indicates that the Backward Elimination technique seems to be superior to the Stepwise procedure since it produces higher values of correlation factor and lower values of standard error.

Balakrishnan [113] and *Draper and Smith [118]* agreed with the fact that only Stepwise Regression and Backward Elimination techniques were of more practical importance. Based on this fact, only these two techniques were recommended for use in this study.

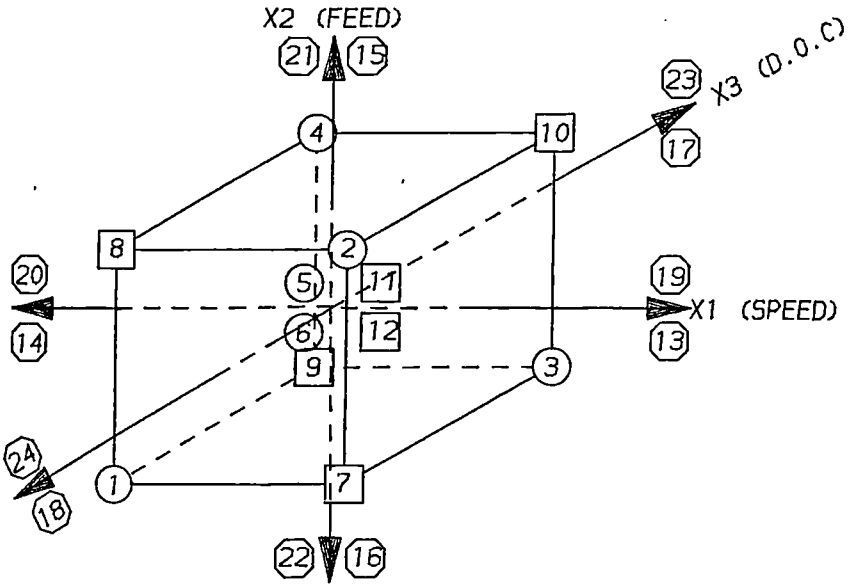

Block	Trial Number
1	1, 2, 3, 4, 5, 6
2	7, 8, 9, 10, 11, 12
3	13, 14, 15, 16, 17, 18
4	19, 20, 21, 22, 23, 24

Fig. 4.1 Central Composite Design Of Experiments

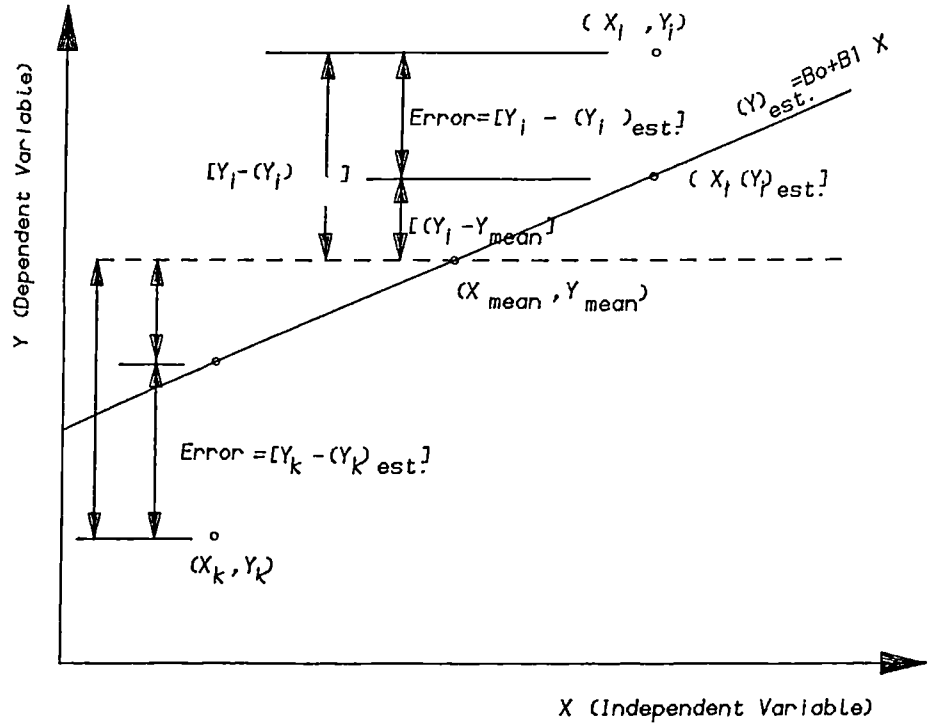

Fig. 4.2 Variables Used in the Least-Squares Procedure

Multiple R	.94253		
R Square	.88836		
Adjusted R Square	.84650		
Standard Error	.31732		
Analysis of Variance (ANOVA)			
	DF	Sum of Squares	Mean Square
Regression	3	6.41024	2.13675
Residual	8	.80554	.10069
F = 21.22038			

Table 4.4 Correlation Factor and ANOVA Table for the First-Order Linearized Tool Life Model

4.7 Examination of the Model Significance

The quality of fit of a linear (or linearized) model is often measured by its correlation factor R^2 and standard error *SE*. *Table 4.4* is an actual output from *SPSSX* package for the first-order tool life model using twelve tests using Stepwise technique.

4.7.1 Correlation Factor R^2

A commonly used measure of the quality of fit of the model is the correlation factor R^2 as given by *Eq. (4.17)*. In the current example of first-order tool life model, the correlation factor is *0.89* or *89%*, *R Square* in *Table 4.4*, which is fairly high suggests a good linear correlation between the independent variable (tool life) and the independent variables (speed, feed, and depth of cut).

Since the number of data points governs the number of degrees of freedom on which the correlation factor is based, a misleading correlation factor may result when too many data points are used in the analysis. To cope with this, an adjusted correlation factor $AdjR^2$ is introduced to maintain the relative ratio between the number of data points

and the number of the regressors in the final regression equation.

$$AdjR^2 = R^2 - \frac{p(1-R^2)}{n-p-1}; \tag{4.19}$$

where n is the number of data points, and p is the number of predictors in the final model. Here the value of $AdjR^2$ of *0.84* is considered to be fairly high.

4.7.2 Standard Error of the Estimates SE

Another criterion used to examine the quality of fit is the value of the standard error of estimates *SE*, labelled Standard Error in *Table 4.4*. This is given by:

$$SE = \sqrt{\frac{\sum_{i=1}^{n-p-1}[Y_i - (Y_i)_{est.}]^2}{n-p-1}} = \sqrt{M_{SE}}. \tag{4.20}$$

In the example under investigation, the value of *SE* is *0.31732, Table 4.4*. This is a large value considering it is on a logarithmic scale. However, the confidence intervals of the response in its natural form (tool life) should be analyzed to study the effect of this higher standard error value on the predictive capability of the model.

4.7.3 Confidence Intervals of the Estimates

Due to the existence of the experimental error, the predicted response is subject to some uncertainty. Hence, it is necessary to indicate the precision of the estimated response. Such an indication is achieved by calculating the confidence intervals of the predicted values which is given by:

$$\left[(Y_i)_{est.} \pm t_{(DF,1-\alpha/2)} \sqrt{V[(Y_i)_{est.}]}\right]; \tag{4.21}$$

where $(Y_i)_{est.}$ is the estimated response on a logarithmic scale for trial i, t is the *t-statistic, DF* is the number of degrees of freedom used to estimate the residuals variance S^2 (residuals mean squares M_{SE}, α is the significance level, and $V[(Y_i)_{est.}]$ is the variance of the predicted value. The values of both M_{SE} and its degrees of freedom

Trial No.	Observed Life (min.)	Predicted Life (min.)	Error (min.)	95% Confidence Interval	
				Lower	Upper
1	119.00	163.05	-44.05	78.44	338.93
2	13.00	16.64	-3.64	8.00	34.58
3	20.00	20.32	-.32	9.78	42.25
4	30.00	37.21	-7.21	17.90	77.35
5	36.00	34.76	1.24	16.72	72.25
6	65.00	34.76	30.24	16.72	72.25
7	37.00	38.49	-1.49	18.52	80.01
8	79.00	70.48	8.52	33.90	146.50
9	79.00	86.09	-7.09	41.41	178.95
10	7.00	8.78	-1.78	4.23	18.26
11	50.00	34.76	15.24	16.72	72.25
12	35.00	34.76	.24	16.72	72.25

Table 4.5 The 95% Confidence Interval of The First-Order Tool Life Model

are shown in the ANalysis Of VAriance table *ANOVA, Table 4.4.* From the statistical tables, the *t-statistic* at *95%* confidence interval with eight degrees of freedom *(8, 1,0.05/2)* is *2.306.* The resulting model takes the form:

$$Y = 13.95 - 2.058\ X1 - 0.915\ X2 - 2.862\ X3,$$

and the model in its natural form is given by:

$$(\ln T_i)_{est.} = 13.95 - 2.058\ \ln V - 0.915\ \ln F - 2.862\ \ln d. \tag{4.22}$$

Therefore, the *95%* confidence interval of the response estimates can be expressed as:

$$\left[(\ln T_i)_{est.} \pm 2.306\sqrt{0.10069}\right].$$

Table 4.5 shows the *95%* confidence interval of the response after transformation back to its natural form (tool life). It is clear that the *95%* intervals are too wide. This degrades the model predictive capability when it is used to estimate tool life values in the practical situations. This indicated that a first-order model is not good enough to fit the tool life data. Therefore, the second-order form was thought to achieve a better prediction capability.

As shown in *Table 4.3,* the best second-order model was obtained the backward elimination technique was used. This model has the predictive form:

$$(\ln Y_i)_{est.} = -9.999 + 8.137\ \ln V - 1.213\ [\ln V]^2 - 0.391\ [\ln F]^2$$
$$- \ 0.845\ [\ln d]^2 - 0.487\ \ln V\ \ln F. \qquad (4.23)$$

Higher correlation factor and lower standard error were obtained, *Table 4.3.* Also, the mean squares error is only *0.05206* with *18* degrees of freedom. From statistical tables at *(18,1,0.05/2)*, the *t-statistic* is *2.101.* According to *Eq. (4.21)*, the *95%* confidence interval equation in this case takes the form:

$$\left[(\ln T_i)_{est.} \pm 2.101\sqrt{0.05206}\right].$$

This confidence region is more compact than that for the first-order model. This suggests that, up to this point, there is nothing against the significance of the second-order model, and the examination procedures should be continue to check up other aspects such as lack-of-fit, and residual analysis.

4.7.4 Pure Error and Lack-Of-Fit

One of the methods used to confirm the significance of a model is the lack-of-fit test. This test indicates how much of the total error is due to experimental procedure and how much is due to the fitting procedure.

Lack-of-fit uses repeated experimental tests to obtain an estimate of the true variance of the estimates σ^2. Such an estimate is said to represent the pure error because, if the setting of X is identical for two observations, only the random variation can influence the results and provides differences between them. For this reason it was employed when designing experiments to make repeated observations.

As indicated by *Eq. (4.16)*, the total sum of squares *SST* consists of the residual sum of squares *SSE* and the regression sum of squares *SSR*. The residuals sum of squares can further be divided into the pure error sum of squares *SSP* and the lack-of-fit sum of squares. The pure error sum of squares *SSP* from the *X1* reading is given by *[118]:*

$$\sum_{u=1}^{n1}(Y_{1u} - Y^2_{mean1})^2 = \sum_{u=1}^{n1} Y^2_{1u} - n1\ Y^2_{mean1}; \qquad (4.24)$$

Source	DF	Sum of Squares	Mean Squares	F-ratio
Total	23	25.3		
Regression	5	24.2	4.87	
Residual	18	0.94	$0.052=\sigma^2$	93.62
Pure Error	9	0.398	$0.044=SE^2$	1.355
Lack-Of-Fit	9	0.539	$0.060=M_{SL}$	

Table 4.6 The ANOVA Table Showing Lack-of-Fit Test

where *n1* is the number of repeating observations, and $Y_{mean1} = (Y_{11} + Y_{12} + ... + Y_{1n1})/n1$. This sum of squares has *(n1-1)* degrees of freedom. Since this test is not provided by *SPSSX*, a computation procedure is introduced to compute the pure error sum of squares of the developed second-order model. According to the *CCD* design, the observation at the centre of the cube was repeated four times (trials *5, 6, 11, 12), Table 4.2,* and each of the augmented tests was repeated twice. The pure error sum of squares of the central observations may be computed according to *Eq. 4.24* as:

$$SSP1 = (Y_5)^2 + (Y_6)^2 + (Y_{11})^2 + (Y_{12})^2 - 4[(Y_5 + Y_6 + Y_{11} + Y_{12})/4]^2 = 0.2549;$$

with three degrees of freedom. Also, the pure error sum of squares due to augmented tests may be computed as:

$$\begin{aligned} SSP2 = \quad & 1/2\,[(Y_{13} - Y_{19})^2 + (Y_{14} - Y_{20})^2 + (Y_{15} - Y_{21})^2 \\ & +(Y_{16} - Y_{22})^2 + (Y_{17} - Y_{23})^2 + (Y_{18} - Y_{24})^2] = 0.14315; \end{aligned}$$

with six degrees of freedom.

The total pure error sum of squares is *SSP1+SSP2=0.3905* with nine degrees of freedom. The *ANOVA* table may be rearranged to include the information about lack-of-fit test as shown in *Table 4.6.* The $F-ratio$ (M_{SL}/SE^2) is *1.355* which is not significant since the *F-value* from the statistical tables at *(9,9 ,0.05)* is *3.18.* Thus, on the basis of this test, there is no reason to doubt the model significance. This means that the hypothesis that the model is incorrect is rejected and $S^2 = 0.052$ can be used as an estimate of σ^2, which is used to determine the confidence intervals of the estimates. However, since

the new approach of time-variant response is introduced in this study, it is hard to find real identical replicates (repeated observations). The cutting time as an independent variable is a floating parameter and moreover, the wear level as an independent variable is an uncontrollable parameter and cannot be classified in planned levels. To examine the lack-of-fit in such situations, *Daniel and Wood [119]* have suggested a method for measuring pure error in those cases where there are no exact repeated points. The procedure searches for points in the *X-space* that are near neighbours, that is, sets of observations that have been taken with nearly identical levels of *X1, X2,...,Xk.* The responses Y_i from such near neighbours can be considered as repeat points and used to obtain an estimate of pure error. As a measure of the distance between any two points $Xi1, Xi2, ..., Xik$ and $Xi'1, Xi'2, ..., Xi'k$, Daniel proposed the following weighted sum of squared distance

$$D^2_{i'i} = \sum_{i=1}^{k} \left[\frac{\beta j_{est.}(Xij - Xi'j)}{S} \right]^2 . \tag{4.25}$$

Pairs of points that have small values of $D^2_{i'i}$ are near neighbours; that is, they are relatively close together in *X-space.* The residuals of two points with a small value of that distance can be used to obtain an estimate of pure error.

Since it is not provided by *SPSSX,* an efficient computer algorithm was developed using *FORTRAN 77,* and used to compute the pure error. The data were arranged in increasing order of predicted values, then, the value of $D^2_{i'i}$'s were computed for all the resulting twenty-three points with adjacent values of $Y_{est.}$. This operation was repeated for the pairs of points separated by *1, 2,* and *3* of $Y_{est.}$ values. This produced 80 values of $D^2_{i'i}$. The results of a sample computation are shown in *Table 4.7.* Values of $D^2_{i'i}$ were arranged in ascended order, together with the values of the resulting standard error which was computed as proposed by *Daniel* using the equation:

$$\sigma_{est.} = \frac{0.886}{m} \sum_{u=1}^{m} \varepsilon_u . \tag{4.26}$$

The m values of residuals used in calculating the standard deviation was determined after inspecting the values of $D^2_{i'i}$. The values of ε_u which lead to large value of $D^2_{i'i}$ should not included in the calculation since they do not belong to near neighbour. Thus, as shown in *Table 4.7,* the standard deviation of the pure error is found to be

Iteration No.	SE Of Pure Error	$D^2_{i',i}$	Error ε_i
1	0.292380	0.000000E+00	0.330000
2	0.155050	0.000000E+00	2.000046E-02
3	0.180153	0.000000E+00	0.260000
4	0.170555	0.000000E+00	0.160000
5	0.161252	0.000000E+00	0.140000
6	0.221500	0.000000E+00	0.590000
7	0.267066	0.000000E+00	0.610000
8	0.272445	0.000000E+00	0.350000
9	0.266784	0.000000E+00	0.250000
10	0.249852	0.000000E+00	0.110000
11	0.236804	0.000000E+00	0.120000
12	0.239647	9.254554E-02	0.305787
13	0.230244	0.178521	0.132518
14	0.250663	0.178521	0.582518
15	0.234394	0.178521	7.482528E-03
16	0.238283	0.216011	0.334770
17	0.238089	0.216011	0.265230
18	0.225612	0.216011	1.523018E-02
19	0.230006	33.8517	0.348868

Table 4.7 Pure Error Estimation from "Near Neighbours"

0.226 for iteration no. *18*. This value is very close to the standard error of the model from regression analysis, *Table 4.3*. This suggests that there is no lack-of-fit of the second-order model. However, the residuals analysis, as a standard procedures, should be performed.

4.8 Examination of Model Adequacy

In regression analysis, the true error ε_i are assumed to be independent normal values with zero mean and a constant variance of σ^2. If the model is appropriate for the data, the observed residual $\tilde{\varepsilon_i}$, which are estimates of the true errors ε_i, should have similar characteristics. Therefore, it is necessary to investigate if the assumptions are violated.

The relative magnitudes of residuals are easier to judge when they are divided by estimates of their standard deviation. The resulting standardized residuals *ZRESID*

are expressed in standard deviation units above or below the mean. For example, the fact that the maximum positive residual in the second-order tool life model under investigation is 0.47 provides little information. If its standardized value $\varepsilon/S = 2.06$ is known, it may be understood not only that the predicted value is less than the observed one, but also that the observed value is 2.06 units, of the standard deviation, apart from the regression line. While standardized residual *ZRESID* involves a constant standard deviation for the entire set of observations, the studentized residual *SRESID* is the true residual ε divided by an estimate of its standard deviation that varies from point to point, depending on the distance of *X's* from the mean X_{mean}.

Fig. 4.3 is an output from *SPSSX* to indicate the residuals history for each data points, together with the corresponding observed values, predicted value *PRED*, true residual *RESID*, standardized residual *ZRESID*, studentized residual *SRESID*, adjusted predicted value *Adj PRED*, deleted residual value *DRESID*, Mahalanobis's distance *MAHAL*, and Cook's distance *COOK D*. The scatterplot on the left is called *"casewise plot "*, where its horizontal axis represents the value of standardized residual *ZRESID* for each of the data points which are represented by the vertical axis. In the following section a description is presented to explain how the residuals and their functions can be used to examine the adequacy of a linear regression model.

4.8.1 Examination of Model Linearity

In *SPSSX* the model linearity is checked by plotting the residuals, or one of their entries, against the observed *Y* or the predicted *PRED* values. If the assumption of model linearity is met, there should no relationship with the residuals. The residuals should be randomly distributed in a horizontal band around its zero mean. The width of the residuals band is a good indication of the model accuracy and quality of fit. The narrower the band, the more accurate the model will be. *Fig. 4.4* shows the scatterplot to indicate whether a relationship exists between the standardized residual *ZRESID*, in the vertical axis, and the predicted values from the resulting regression model $Y_{est.}$ (*PRED* as it is called in *SPSSX* package). The residual band is almost

	-3.0 0.0 3.0					Z-	S-	D-	ADJ-		COOK
	0:.....:.....:0	Y	PRED	RESID		RESID	RESID	RESID	PRED	MAHAL	D
1	. *. .	4.78	4.86	-.08		-.35	-.38	-.09	4.87	2.19	.0040
2	. . * .	2.56	2.37	.19		.84	.90	.22	2.34	2.20	.0218
3	. *. .	3.00	3.10	-.10		-.48	-.52	-.12	3.12	2.55	.0082
4	. * . .	3.40	3.83	-.43		-1.90	-2.04	-.50	3.90	2.17	.1102
5	. * . .	3.58	3.70	-.12		-.52	-.55	-.13	3.71	1.22	.0054
6	. . * .	4.17	3.70	.47		2.06	2.16	.52	3.65	1.22	.0824
7	. . * .	3.61	3.40	.20		.88	.96	.23	3.37	2.61	.0284
8	. . * .	4.37	4.13	.23		1.01	1.08	.26	4.10	2.23	.0320
9	. * . .	4.37	4.55	-.18		-.82	-.88	-.21	4.58	2.15	.0206
10	. * . .	1.95	2.06	-.12		-.54	-.58	-.14	2.08	2.17	.0090
11	. . * .	3.91	3.70	.20		.91	.95	.23	3.68	1.22	.0161
12	. * . .	3.56	3.70	-.14		-.65	-.68	-.16	3.71	1.22	.0082
13	. * . .	1.39	1.50	-.12		-.52	-.67	-.19	1.58	8.13	.0502
14	. . * .	4.94	4.76	.17		.77	1.00	.29	4.64	8.25	.1129
15	. .* .	2.20	2.12	.06		.30	.39	.12	2.07	8.90	.0200
16	. . * .	4.56	4.34	.21		.94	1.25	.37	4.18	8.83	.1944
17	. *. .	3.18	3.23	-.06		-.26	-.32	-.08	3.26	6.16	.0079
18	. *. .	4.01	4.12	-.11		-.49	-.58	-.15	4.16	5.58	.0228
19	. * .	1.50	1.50	-.003		-.01	-.01	-.004	1.50	8.13	.0000
20	. * .	4.78	4.76	.01		.06	.08	.02	4.75	8.25	.0008
21	. *. .	2.08	2.12	-.04		-.21	-.28	-.08	2.16	8.90	.0100
22	. * . .	4.17	4.34	-.17		-.75	-1.00	-.30	4.47	8.83	.1243
23	. . * .	3.43	3.23	.19		.85	1.02	.28	3.15	6.16	.0786
24	. * . .	3.87	4.12	-.24		-1.09	-1.29	-.34	4.21	5.58	.1105
	0:.....:.....:0	Y	PRED	RESID		Z- RESID	S- RESID	D- RESID	ADJ- PRED	MAHAL	COOK D
	-3.0 0.0 3.0										

Fig. 4.3 Casewise Plot and Residuals Analysis for the Second-Order Tool Life Model

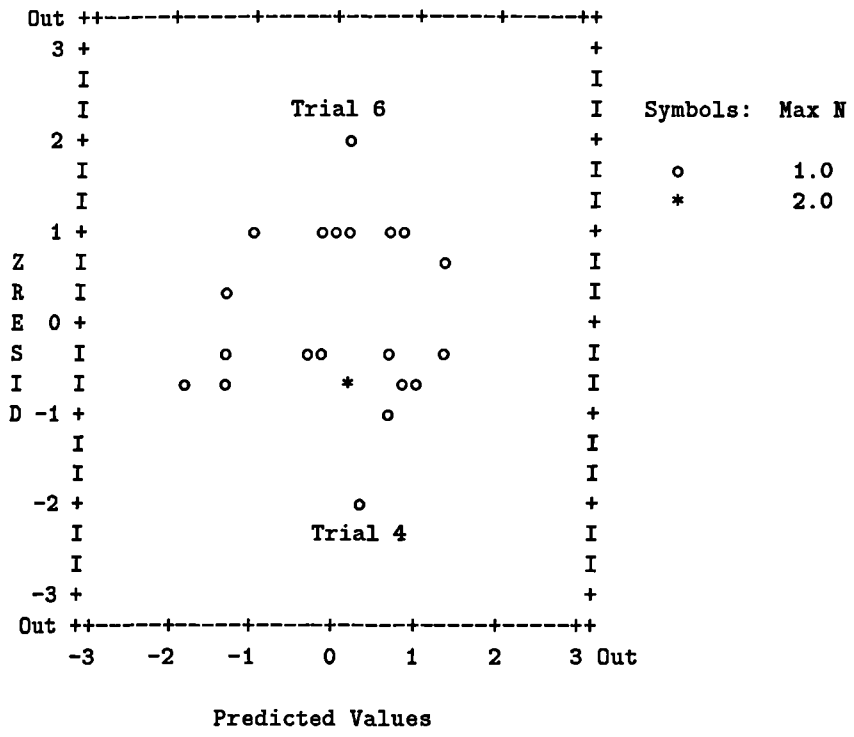

Fig. 4.4 Examining Linearity of the Second-Order Tool Life Model

horizontal around the zero mean revealing nothing against the assumption of model linearity. As indicated by the location of individual residuals in *Fig. 4.4*, twenty-two residuals elements are between ± 1 unit of the standard error, while the other two are between ± 2 units. The point of maximum positive error is attributed trial *no. 6* in the *CCD* design. This centred point was repeated four times *(Trials 5,6,11, and 12)*. The high error value was a result of the fact that its observed value was *65* minutes tool life, while for the other three observations it was between *35* and *50* minutes, *Table 4.3*. However, this error was attributed to the experimental error (pure error) rather than to lack-of-fit as explained earlier. The maximum negative residual belong to trial *no. 4* in the *CCD* design. The observed tool life for this test was only *35* minutes while it was *79* for similar conditions (trial *no. 8)*. This was due to the early chipping of the tool edge, which had been treated as gradual wear during measurement. From this discussion, the residuals distribution can be considered as a horizontal band of two unit of standard deviation and this is considered satisfactorily low. However, *Draper [118]* suggested some solutions when the linearity assumption is violated. The possible plots of residuals may take one or more of the patterns shown in *Fig. 4.5*. For case *(a)*, the variance is not constant but increases with time, implying that a weighted least-squares analysis should have been used. For case *(b)*, a linear term in time should have been included in the model. In case *(c)*, linear and quadratic terms in time should have been included in the model.

4.8.2 Examination of the Residuals Independency

The error components ε_i are assumed to be uncorrelated random variables. The variation in the accuracy of the measuring apparatus; in measuring skills; and, in experience over time, may affect the residuals. Variables that exhibit correlation over time are referred to as autocorrelated.

The occurrence of positively correlated errors has several potentially consequences. The ordinary least-squares estimates of the parameters are affected in such a way that they no longer have minimum variance. Furthermore, the mean squares error M_{SE} may

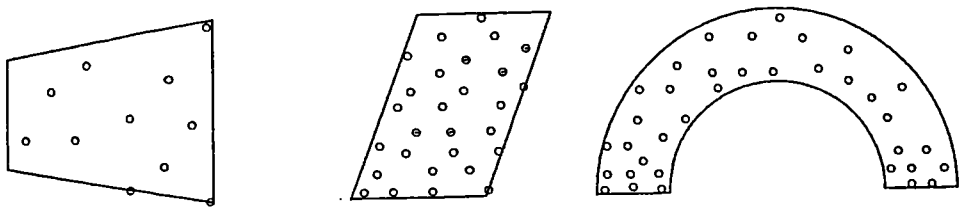

Fig. 4.5 Residuals Patterns as an Indication of Model's Abnormality

underestimate the variance. Also, confidence intervals and other tests of hypothesis, which are developed assuming uncorrelated errors, are not valid if autocorrelation is present. One way to determine the error autocorrelation is by using the *Durbin-Watson* test as given by:

$$D = \frac{\sum_{i=2}^{n}[\varepsilon_i - \varepsilon_{i-1}]^2}{\sum_{i=1}^{n}\varepsilon_i^2}. \tag{4.27}$$

This is a test to detect any time effect of sequential correlation of adjacent error terms. The differences between successive residuals tend to be small when terms are positively correlated and large when error terms are negatively correlated. For a suitable value of significance level α, the critical values D_{upper} and D_{lower} are obtained from tables of *D-statistic [120]* according to the sample size and the number of the estimators included in the final model. If $D > D_{upper}$, the model is accepted; but if $D < D_{lower}$, the model is rejected. If $D_{lower} \geq D \leq D_{upper}$, the test is inconclusive, and the implementation is that more data must be collected.

For the second-order tool life model under investigation, Eq. *(4.23)*, the computed *Durbin-Watson* value is *1.89* which is larger than D_{upper} value of 1.77 from statistical tables at *(0.025,5,24)*. Therefore, the hypothesis is rejected that the error are correlated or the residuals are autocorrelated.

4.8.3 Examination of the Residuals Normality

One of the assumption when the model is tentatively entertained is that the residuals are random variables with normal distribution variables. The *SPSSX* regression package investigates the residuals normality in two ways. The first is to construct a histogram of the residuals. *Fig. 4.6.b* indicates histogram of the tool life model. This contains a tally of the observed number of residuals (labelled *N*) in each interval and the number expected in the normal distribution with the same mean and variance as the residuals *EXP N*. A histogram of expected *N's* is superimposed on that of the observed *N's*. Expected frequencies are indicated by a period. When observed and expected frequencies overlap, a colon is displayed. Through examining this histogram,

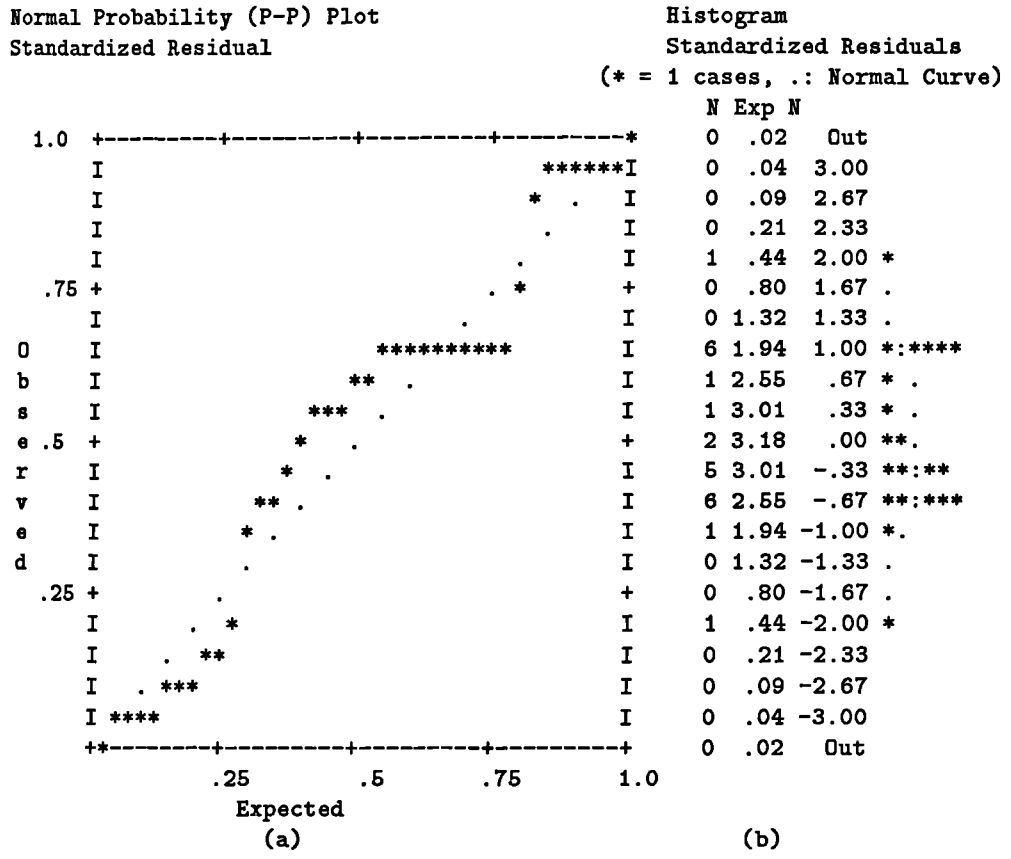

Fig. 4.6 Residuals Normality of the Second-Order Tool Life Model

the normality assumption seems to be violated for the second-order tool life model.

The second way is to plot the two cumulative distributions, observed and expected, against each other for a series of points, *Fig. 4.6.a.* By observing how points scatter around the expected straight line, the residuals normality can be judged. In *Fig. 4.6.a,* the observed residuals are initially below the straight line revealing that there are a smaller number of large negative residuals than expected. Once the greatest concentration of residuals is approached, the observed points tend to move above the line revealing that there are a larger number of positive residuals than expected. Although there is no serious deviation from normality, it cannot be said with confidentiality that the residuals are normally distributed.

However, in many cases, the distribution of the residuals may not appear to be normal for reasons other than actual non-normality: mis-specification of the model, or non-constant variance. These aspects are examined in detail in the following sections.

4.8.4 Examination of the Equality of Variance

One of the model's assumptions is that its residuals are of constant variance. With variance inequality, the analysis of data from a model would be very complicated. Furthermore, confidence intervals which were based on a constant variance, are no longer reliable.

Since the studentized residuals *SRESID* is the residual value divided by its individual standard deviation, which varies from data point to another, the variance equality may be examined by observing its distributions when they are plotted against the magnitudes of the predicted values, *PRED, Fig. 4.7.* The spread of the residuals with the magnitudes of the predicted values is again affected by the existence of the two components which belong to trials *nos. 4* and *6.* However, for the second-order tool life, even though there is no serious deviation of the variance equality, a conclusion may be reached that the residuals variance is not constant, and weighted least-squares analysis may help in finding a remedy for this problem. However, further investigation

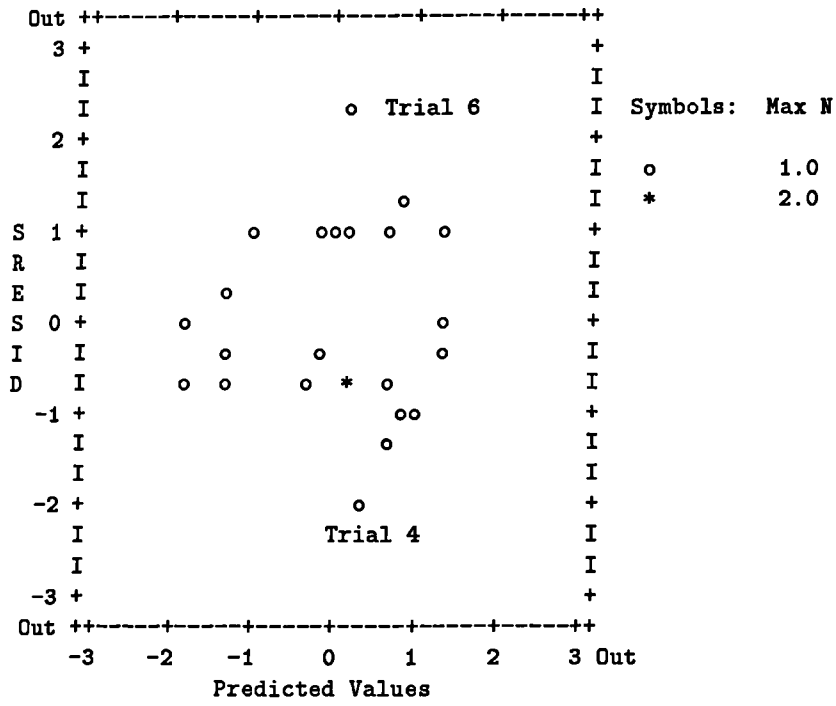

Fig. 4.7 Examining Equality of Variance of the Second-Order Tool Life Model

of the residuals behaviour is required before taking further action.

4.8.5 Location of the Outliers

An outlier among residuals is one that is far greater than the rest in absolute value. The outlier is a peculiarity and indicates a data point which is not at all typical of the rest of the data. It follows that an outlier should be submitted to particularly careful examination to see if the reason for its peculiarity can be determined.

Rules have been proposed for rejecting outliers by removing the corresponding observations from the data and repeating the model fitting. However, automatic rejection of outliers is not always a very wise procedure. Sometimes the outliers provide information which other data points cannot, due to the fact that they arise from unusual combination of circumstances which may be of vital interest and require further investigation rather than rejection.

In *SPSSX* regression analysis, any residual which is equal or greater than *3.16* units of the standard error *SE* is considered as an outlier. Consequently, no outlier was found for the tool life model since the max *ZRESID* was found ≈ 2. However, the magnitudes of residuals indicated a wide difference between trials *nos. 4* and *6* from one side, and the rest of data points from the other side revealing some peculiarity. Since trial *no. 6* is a repeated test, it could be removed and analysis repeated accordingly. Although some statistical criteria were improved when the outliers had been discarded, examination of the residuals normality and equality of variance showed no improvement. In this case, the implementation is that examination of more residuals is required to trace out the reason behind the residuals inhomogeneity.

4.8.6 Identification of the Influential Cases

Certain observations in a set of data can have a large influence on estimates of the parameters. The regression line obtained for the data is quite different if the point is omitted. One way to identify an influential case is to compare a case when the suspected term is included in the equation and when it is not. Some criteria and computation, to identify the influential cases for the tool life model are as shown in the casewise plot, *Fig. 4.3.* The *Adj PRED* is the adjusted predicted value for case *i* when it is not included in the computation of the regression line. The residual calculated for a case when it is not included is called the deleted residual *DRESID.*

Although the difference between the deleted and ordinary residual for a case is useful as an index of the influence of that case, this measure, however, does not reflect changes in residuals of other observations when the case *i* is omitted. Cook's distance *COOK D* does consider changes in all residuals when case *i* is deleted. It is defined as:

$$C = \frac{\sum_{j=1}^{n}[(Y_j^{(i)})_{est.} - (Y_j)_{est.}]^2}{(p+1)\ SE^2}; \tag{4.28}$$

where the superscript *i* indicates that the *ith* case is excluded.

The casewise plot for the tool life data in *Fig. 4.3* shows that neither case *4* nor *6* are of the most influential points despite their higher values of error. The first six influential cases were found, in descending order, as 16, 22, 14, 24, 4 and 6. The strong influence of these points on the model parameters; variance inequality; and residual non-normality may be diminished by using the weighted least-squares method. In the following sections, these strategies are discussed in more details.

4.9 Violation of Assumptions

When evidence of violation of one of the assumptions appears, one can pursue one or more of the following strategies:

4.9.1 Modifying the Model Structure

When the variance is not constant over the operational region, *Draper and Smith [118]* proposed a variety of remedial measures such as:

- When the variance is proportional to the mean of the predicted values for given independent variable, it is better to use the square root of Y if all Y's are positive.
- When the standard deviation is proportional to the mean, the logarithmic transformation may be employed.
- When the standard deviation is proportional to the square of the mean, the reciprocal of Y may be the solution.
- When Y is a proportion or rate, the arc sine transformation may stabilize the variance.

In the case of the tool life model, it seems that the first case applies. Therefore, the model was re-fitted considering $Y = \sqrt{\ln(T)}$ as a dependent variable instead of $Y = \ln(T)$. However, the problem of variance inequality seemed not to be improved. Again, the higher values of residuals for trial *4* and *6* disturbed the variance distribution. Therefore, it was thought that a weighted least-squares estimation procedure might help in stabilizing the variance.

4.9.2 Robust Regression Via Iterative Reweighted Least-Square

This technique is used to find a remedy for an existing ill-conditioning linear model of influential observations and/or inequality of the residuals variance. If a point is influential, it pulls the fit toward it, so that the magnitude of the residual is not as large as it would be otherwise. Robust regression procedure weights the data points differentially in such a way that points with large residuals have less impact on the parameter estimates than in the ordinary least-squares solution.

Robust regression via iterative estimation is first proposed by *Hoaglin et al. [121].* While ordinary least-squares minimizes the sum of squared residuals, robust regression minimizes some function of the residuals in such a way as to dampen the effect of observations that would be very influential if an ordinary least-squares method was used. The procedures of robust regression can be expressed in sequential functional steps as follows:

Firstly residuals components are scaled so as to be scale-free values. Therefore, rather than work with the residuals directly, it is useful to scale residuals to come up with scale-invariant estimates. To scale the residuals, *Hoaglin [121]* proposed the robust estimate of scale ν which is given by:

$$\nu = \frac{[Median \mid \varepsilon_i - Median(\varepsilon_i) \mid]}{0.6745}; \tag{4.29}$$

where *Median* is a statistical function which determines the central tendency or the point at which the sample is divided into two halves. For a sample of $X_{(1)}, X_{(2)}, ..., X_{(n)}$, the *Median* is defined as:

$$M = \begin{cases} X_{([n+1]/2)} & \text{if n odd} \\ \frac{X_{(n/2)}+X_{([n/2]+1)}}{2} & \text{if n even.} \end{cases} \tag{4.30}$$

Then, the error element ε_i is transformed into the scaled function Z_i, as follows:

$$Z_i = \frac{\varepsilon_i}{\nu}; \tag{4.31}$$

Secondly the weighting function may be constructed so as to dampen the effect of data points which have higher values of residuals. The *Ramsay's* function with an appropriate exponent can be used. *Hoaglin* proposed the weighting function as given by:

$$WT_i = e^{-0.3|Z_i|}. \tag{4.32}$$

Thirdly the iterative non-linear regression is employed to obtain the modified parameters of the final model.

The resulting model from these procedures takes the form:

$$\begin{aligned} (\ln T_{AW})_{est.} &= -7.953 + 7.275\ \ln V - 1.121\ [\ln V]^2 - 0.371\ [\ln F]^2 \\ &- 0.81\ [\ln d]^2 - 0.4685\ \ln V\ \ln F. \end{aligned} \tag{4.33}$$

Trial No.	Observed Life (min.)	Predicted Life (min.)	Error (min.)	95% Confidence Interval		Weighting Value
				Lower	Higher	
1	119.00	126.32	-7.32	87.01	183.40	.900243
2	13.00	10.44	2.56	7.19	15.16	.679834
3	20.00	21.39	-1.39	14.73	31.05	.888779
4	30.00	46.58	-16.58	32.08	67.62	.460915
5	36.00	39.16	-3.16	26.97	56.85	.862353
6	65.00	39.16	25.84	26.97	56.85	.409746
7	37.00	28.61	8.39	19.70	41.53	.635735
8	79.00	62.31	16.69	42.92	90.46	.658389
9	79.00	94.43	-15.43	65.04	137.10	.730417
10	7.00	7.81	-.81	5.38	11.33	.825507
11	50.00	39.16	10.84	26.97	56.85	.650321
12	35.00	39.16	-4.16	26.97	56.85	.820625
13	4.00	4.44	-.44	3.06	6.44	.833074
14	140.00	121.77	18.23	83.87	176.79	.782215
15	9.00	8.53	.47	5.88	12.39	.910235
16	96.00	74.31	21.69	51.18	107.88	.636991
17	24.00	25.09	-1.09	17.28	36.43	.924565
18	55.00	58.39	-3.39	40.22	84.78	.899986
19	4.50	4.44	.06	3.06	6.44	.975562
20	119.00	121.77	-2.77	83.87	176.79	.960298
21	8.00	8.53	-.53	5.88	12.39	.892864
22	65.00	74.31	-9.31	51.18	107.88	.790110
23	31.00	25.09	5.91	17.28	36.43	.689233
24	48.00	58.39	-10.39	40.22	84.78	.708180

Table 4.8 Results of the Robust Regression Second-Order Tool Life Model

A correlation factor of *0.97* and a standard error of *0.177* were found to be better than those for ordinary second-order model. Also, lower values were resulted of the partial standard error of the coefficients. Summary results and confidence intervals for the robust regression model are listed in *Table 4.8.* Note that the differential weighting of the data points accomplished through the use of robust regression with *Ramsay's* function as a criterion. In particular, points *6* and *4* were downweighted much more than any of the other points. Also, as would be expected, the low value of standard error resulted in a more compact confidence interval.

4.10 Non-Linear Regression Technique

In the previous sections, a linear least-squares method was used to estimate the coefficients of a model which was linear in its parameters. While the linear equation can represent a wide variety of relationships, there are some situations in which a model of this form in not appropriate. When definite information is available about the non-linearity of the model, it is prefered to fit such a model rather than to fit an alternative, perhaps less realistic, linear model.

4.10.1 Non-Linear Estimation Procedure

Generally, the non-linear model takes the form:

$$R = \Phi(\xi 1, \xi 2, \xi 3, ..., \xi k; \theta 1, \theta 2, \theta 3, ..., \theta p) + \varepsilon; \tag{4.34}$$

where R is the response or the dependent variable; ξ's are the independent variables; θ's are the parameters to be estimated; and, ε is a random error term with $E(\varepsilon) = 0$, $V(\varepsilon) = \sigma^2$. When there are n observations of the form $R_u, \xi 1_u, \xi 2_u, ..., \xi k_u, u = 1, 2, ..., n$, available, the model may take the general form:

$$R_u = \Phi(\xi 1_u, \xi 2_u, \xi 3_u, ..., \xi k_u; \theta 1, \theta 2, \theta 3, ..., \theta p) + \varepsilon_u. \tag{4.35}$$

This model can be abbreviated to:

$$R_u = \Phi(\xi_u, \Theta) + \varepsilon. \tag{4.36}$$

The residuals sum of squares to be minimized by non-linear squares method may be denoted as:

$$SSE(\Theta) = \sum_{u=1}^{n} \{R_u - \Phi(\xi u, \Theta)\}^2. \tag{4.37}$$

Since R_u and ξu are fixed observations, the sum of squares SSE(Θ) is a function of Θ. The non-linear estimate of Θ is $\Theta_{est.}$, that is a value of Θ which minimizes SSE(Θ).

In contrast to linear regression, non-linear regression requires a prior knowledge of the exact model structure that best fits the functional relationship between a response and a number of independent variables. Furthermore, good estimates of initial values of the model parameters are necessary. The closer these initial values to the final unknown ones, the more rapid the procedure will converge, resulting in a more precise and reliable model. Computational difficulties, such as overflow and underflow, may be avoided by good selection of initial values of the parameters. Poor initial values may result in no solution, a local rather than global solution, or physically impossible solution.

Draper and Smith [118] proposed a number of ways to determine initial values of the parameters. These can be summarized as:

1. Linearizing of the model using some transformation functions, and then using the linear regression to estimate the model's coefficients. These coefficients are transformed back to the non-linear form and considered as initial values for the non-linear procedure.

2. Using the prior knowledge and experience of the nature and behaviour of the true model. Examination of the the behaviour of the equation at its extremes, as well as the behaviour when all X's approach zero and infinity, may give good insight for initial values.

3. Solution of a system of equations by taking as many data points as the number of parameters and solving them simultaneously.

Non-linear procedures in the *SPSSX* statistical computer package estimate the values of the parameters for the model, and provide computational output in form of the *ANOVA* table. However, the usual statistical tests which are appropriate in the linear model case are, in general, not appropriate when the model is non-linear. However, the significance of a model can be still examined by comparing the residuals mean squares to the regression mean squares. While in linear models this is compared to the cor-

responding *F-value* from the statistical tables, this is not correct in non-linear model. The pure error of estimate can still be computed from repeated tests as indicated in *section 4.6.4.* However, the *lack-of-fit* test is not applicable here, but it can be used only as a measure of comparison *[118].*

Unfortunately, standard error levels of predicted values and residuals; and special residuals used for outlier detection; and, influential case analyses have not yet been established for non-linear estimation. However, as an intermediate solution, all these statistics can be calculated using the ordinary linear regression using information provided by non-linear procedure. Even it was a very expensive computation procedure, it provided very good information about the model adequacy.

The idea was to make use of the linear relationship between the parameters derivatives and the residuals from the non-linear procedure. An explanation may be offered considering the non-linear least-squares procedure when it produces an estimate of Θ. To find the least-squares estimates $\Theta_{est.}$, differentiation of Eq. *(4.37)* with respect to Θ is required. This provides P normal equations, which must be solved for $\Theta_{est.}$. According to *Draper and Smith [25],* the normal equations take the form:

$$\sum_{u=1}^{n} \{R_u - \Phi(\xi u, \Theta_{est.})\} \left[\frac{\delta\Phi(\xi u, \Theta)}{\delta\Theta_r}\right]_{\Theta=\Theta_{est.}} = 0; \qquad (4.38)$$

for *r=1,2,....,p,* where the quantity denoted by brackets is the derivative of $\Phi(\xi u, \Theta)$ with respect to Θ_r, with all Θ's replaced by the corresponding prediction values, which have the same subscript. For a particular case, the difference between the asymptotic residual and its derivative may give the true error. Therefore, if one consider the residual as a dependent variable and derivatives as independent variables, one can use the results to examine the model adequacy as explained in *section 4.8.*

In the following a possibility is expressed to fit a tool life model by the non-linear regression using the same set of data as that used in the linear estimation.

Source	DF	Sum of Squares	Mean Square
Regression	4	90085.87253	22521.46813
Residual	20	2939.37747	146.96887
Uncorrected Total	24	93025.25000	
(Corrected Total)	23	35645.98958	

R squared = 1 - Residual SS / Corrected SS = .91754

Parameter	Estimate	Asymptotic Std. Error	Asymptotic 95 % Confidence Interval Lower	Upper
A0	123251.00903	85739.730934	-55598.93567	302100.95374
A1	-1.777665598	.149486945	-2.089489900	-1.465841295
A2	-.681920203	.098764815	-.887939996	-.475900410
A3	-1.208640656	.338716505	-1.915190904	-.502090407

Table 4.9 Non-Linear Regression Summary Statistics for Non-Linear Tool Life Model

4.10.2 Tool Life Non-Linear Model

The Non-linear regression technique was used to estimate the tool life coefficients which resulted in a model of the form:

$$T = 123251 \ V^{-1.778} \ F^{-0.682} \ d^{-1.21}. \tag{4.39}$$

Table 4.9 lists summary statistics of the non-linear tool life model. The analysis of variance table *ANOVA,* together with the parameters estimates and their *95%* confidence interval are also shown. A statistical based comparison between this non-linear model and the linear one developed in previous sections is rather complicated, and the model should be examined either as a stand-alone non-linear model or compared to another non-linear model.

The ratio between regression and residuals mean squares is *(22521.5/ 146.97= 153.24)* suggesting a very high quality of fit. The corrected correlation factor is *0.92* which is fairly high. However, while the asymptotic standard errors of parameters are reasonably low, the one for the constant parameter is relatively high, *Table 4.9.*
In contrast to linear regression, residual mean squares is no longer the standard error

of estimates. This is due to the fact that the correct distribution properties in the non-linear case in unknown. The determination of the confidence intervals is extremely difficult especially when more than a single parameters is involved. This is because the confidence region is an ellipsoidal contour rather than a straight line as in linear regression, and sectional drawings should be constructed. However, standard error value for individual cases of predicted values can be used as an approximation. The total value of the prediction variance can be approximated as the summation of the residual individual variance and the residuals mean squares as follows:

$$V(T_{est.i}) = M_{SE} + (SEp_i)^2; \tag{4.40}$$

where $V(T_{est.i})$ is the variance of the predicted tool life value; M_{SE} is the residuals mean squares; and, SEp_i is the individual standard error. *Table 4.10* summarizes the results for tool life non-linear model. This includes the observed, the predicted, and the residual, together with their variance and its ratio to the regression mean squares. The ratio of individual variance to the regression mean squares is equivalent to, but is not, the *F-ratio* in the linear regression case. The ratio is very high for all cases, revealing nothing against the significance of the model.

The pure error estimation, from repeated tests, can be computed as follows:

$$SSP1 = (36)^2 + (65)^2 + (50)^2 + (35)^2 - 4[(36 + 65 + 50 + 35)/4]^2 = 597; \quad \textit{and},$$

$$\begin{aligned} \text{SSP2}= \quad & 1/2[(4 - 4.5)^2 + (140 - 119)^2 + (9 - 8)^2 + (96 - 65)^2 \\ & +(24 - 31)^2 + (58 - 48)^2] = 750.6. \end{aligned}$$

Thus, *(SSP=SSP1+SSP2=1347.6)*; with nine degrees of freedom. The pure error mean square is *(1347.625/9 =149.36)*. This value is almost equal to residuals mean squares, *Table 4.9*. This indicates a zero lack-of-fit of the model, and the experimental error is the only source of the deviation between the observed and the predicted values. Therefore, it may be concluded that there is nothing against the correctness of the non-linear tool life model.

Trial No.	Observed Life (min.)	Predicted Life (min.)	Error (min.)	Individual Variance	Total Variance	Ratio of Reg. and Res. Mean squares
1	119.00	112.10	6.90	6.61927	190.78	118.04
2	13.00	17.25	-4.25	3.88508	162.06	138.96
3	20.00	24.60	-4.60	3.28484	157.76	142.75
4	30.00	45.83	-15.83	5.80554	180.67	124.65
5	36.00	36.19	-.19	3.40187	158.54	142.05
6	65.00	36.19	28.81	3.40187	158.54	142.05
7	37.00	32.21	4.79	3.19991	157.21	143.25
8	79.00	60.01	18.99	5.69928	179.45	125.50
9	79.00	85.60	-6.60	5.97128	182.63	123.32
10	7.00	13.17	-6.17	4.68420	168.91	133.33
11	50.00	36.19	13.81	3.40187	158.54	142.05
12	35.00	36.19	-1.19	3.40187	158.54	142.05
13	4.00	10.60	-6.60	5.73524	179.86	125.21
14	140.00	131.37	8.63	7.91240	209.58	107.46
15	9.00	17.11	-8.11	3.86678	161.92	139.09
16	96.00	82.25	13.75	7.32753	200.66	112.23
17	24.00	25.56	-1.56	3.99297	162.91	138.24
18	55.00	59.07	-4.07	7.39061	201.59	111.72
19	4.50	10.60	-6.10	5.73524	179.86	125.21
20	119.00	131.37	-12.37	7.91240	209.58	107.46
21	8.00	17.11	-9.11	3.86678	161.92	139.09
22	65.00	82.25	-17.25	7.32753	200.66	112.23
23	31.00	25.56	5.44	3.99297	162.91	138.24
24	48.00	59.07	-11.07	7.39061	201.59	111.72

Table 4.10 Summary Results of the Non-Linear Tool Life Model

As previously described, the residuals of a non-linear model can be examined by establishing a linear relationship between the residuals as a dependent variable and the parameters derivatives as independent variables. However, it should be emphasized that when a linearized form of a non-linear relation is developed, all the results obtained are only valid to the extent that linearized form provides a good approximation to the true relationship.

The results obtained from such a strategy showed that trial *nos. 6* and *4* were the worst. Furthermore, this technique traced the most influential cases as trials *22,16,4,20,24,14*. A similar conclusion was reached when the linear tool life model was developed in previous sections.

The *Durbin-Watson* value is *1.95* which is higher than the one for the linearized model. This may indicate a better distribution of residuals independency.

The residuals normality indicates much better distribution than that of the linear model.

However, the residuals revealed a trend of increasing magnitude with the predicted values suggesting a non-constant variance. A similar conclusion was reached for the linearized model, and robust weighted regression was introduced. Therefore, a weighted non-linear model was thought to stabilize the residuals.

4.10.3 Tool Life Weighted Non-Linear Model

Weighted regression procedure minimizes some functions of residuals in order to eliminate the effect of observations that would be very influential if ordinary regression was used.

In the current model, the inverse of residual value was chosen to weight the different data points. This procedure resulted in a weighted non-linear tool life model of the form:

$$T = 158873 \; V^{-1.88} \; F^{-0.803} \; d^{-1.276}. \tag{4.41}$$

Source	DF	Weighted SS	Weighted MS
Regression	4	64633.29258	16158.32314
Residual	20	1591.46017	79.57301
Uncorrected Total	24	66224.75274	
(Corrected Total)	23	27587.86443	

R squared = 1 - Residual SS / Corrected SS = .94231

Parameter	Estimate	Asymptotic Std. Error	Asymptotic 95 % Confidence Interval Lower	Upper
A0	158873.11802	112531.35781	-75863.18105	393609.41709
A1	-1.880013153	.153408474	-2.200017622	-1.560008684
A2	-.803361305	.108327815	-1.029329167	-.577393444
A3	-1.276410897	.316647377	-1.936925752	-.615896042

Table 4.11 Summary Statistics of the Weighted Non-Linear Tool Life Model

Table 4.11 represents *ANOVA* table, along with the parameters estimates and their standard errors and confidence intervals. Much improvement were achieved in residuals mean squares, corrected correlation factor, and parameters standard errors values relative to those for the unweighted non-linear procedure. *Table 4.12* summarizes the obtained results from weighted non-linear estimation procedure. The most influential observations, which were determined as trials *22,16,4,20,24,* and *14,* were downweighted much higher than any other observations. This technique was found to stabilize the residuals variance distribution. No pattern was detected which revealed that the residuals distribution was not affected by the influential and outlier cases.

Trial No.	Observed Life (min.)	Predicted Life (min.)	Error (min.)	Weighting Value
1	119.00	115.08	3.92	.87
2	13.00	14.74	-1.74	.94
3	20.00	23.15	-3.15	.90
4	30.00	41.46	-11.46	.68
5	36.00	33.38	2.62	.91
6	65.00	33.38	31.62	.34
7	37.00	30.78	6.22	.81
8	79.00	55.12	23.88	.44
9	79.00	86.56	-7.56	.77
10	7.00	11.09	-4.09	.87
11	50.00	33.38	16.62	.57
12	35.00	33.38	1.62	.95
13	4.00	9.11	-5.11	.84
14	140.00	130.53	9.47	.72
15	9.00	13.81	-4.81	.85
16	96.00	87.82	8.18	.76
17	24.00	23.12	.88	.97
18	55.00	56.01	-1.01	.97
19	4.50	9.11	-4.61	.85
20	119.00	130.53	-11.53	.67
21	8.00	13.81	-5.81	.82
22	65.00	87.82	-22.82	.46
23	31.00	23.12	7.88	.76
24	48.00	56.01	-8.01	.76

Table 4.12 Summary Results of the Weighted Non-Linear Tool Life Model

4.11 Concluding Remarks

4.11.1 Tool life Modelling Recommendations

To develop a tool life model using the experimental data, the following remarks and recommendations may be suggested:

1. A first-order linearized model using twelve tests of the centrally designed experiments may be insignificant and inadequate to represent the functional relationship between tool life and cutting conditions, speed, feed, and depth of cut.

2. The entire arrangement of *24*-tests of central composite design *CCD* is required to fit a second-order linearized model using either the Stepwise or Backward Elimination regression techniques.

3. Although the second-order linearized tool life model might fit the data very well, examination of the residuals indicated some drawbacks such as variance inhomogeneity.

4. A robust regression technique via iteratively weighting data points was used to reduce effects of outliers and influential cases on the estimated model. High improvement was achieved especially residuals normality and variance homogeneity.

5. A non-linear regression technique was used to estimate a non-linear tool life model. Even though the resulting model was significant, the problem was noticed of residuals inhomogeneity.

6. A weighted non-linear regression technique resulted in highly significant and adequate non-linear tool life equation. This technique stabilizes residuals and produces some other advantages such as higher residuals normality and independency. Besides, using the model with variables in their natural forms may reduce computational difficulties which are involved in data transformation and transformation back operations.

4.11.2 Modelling Strategy Of Metal Cutting Responses

Responses of metal cutting may put challenge to choose, from the many alternatives of forms, the model which is most appropriate to the nature of the true relationship. Some steps that might help in choosing, building, fitting, and examining the equation may be summarized as follows:

1. Whenever a strong indication is available about the functional relationship between the dependent variable (response) and the independent variables, it is prefered to use the appropriate regression technique (either linear or non-linear) to estimate the model parameters in their natural forms.

2. Whenever the relationship is obscured or unknown, a linear, or linearized, form may be a good approximation to look at the problem. Further statistical analysis may confirm; conditionally accepted; or, reject the assumed form of model. When the model is conditionally accepted, further modification of the model structure may be required. These modifications depends on the type of variables, but to large extent, the use of logarithmic transformation, the introduction of quadratic and interaction terms (second-order terms), or the use of different mathematical functions such as square root or reciprocal of the dependent variable, may lead to a better model.

3. The use of robust regression technique with appropriate weighting function is recommended in case of linear models. This may help in treating some problems such as those resulted from the existence of outliers and influential cases.

However, whenever possible, it is of interest that different forms of model, such as linear, linearized, or non-linear, are built using different techniques such as linear, robust, non-linear, or weighted non-linear. The superiority of a particular model over the others should be based on both statistical and technical interpretation aspects. *Fig. 4.8* shows a flow chart in which logical steps are followed in this study to formulate the response of turning operations.

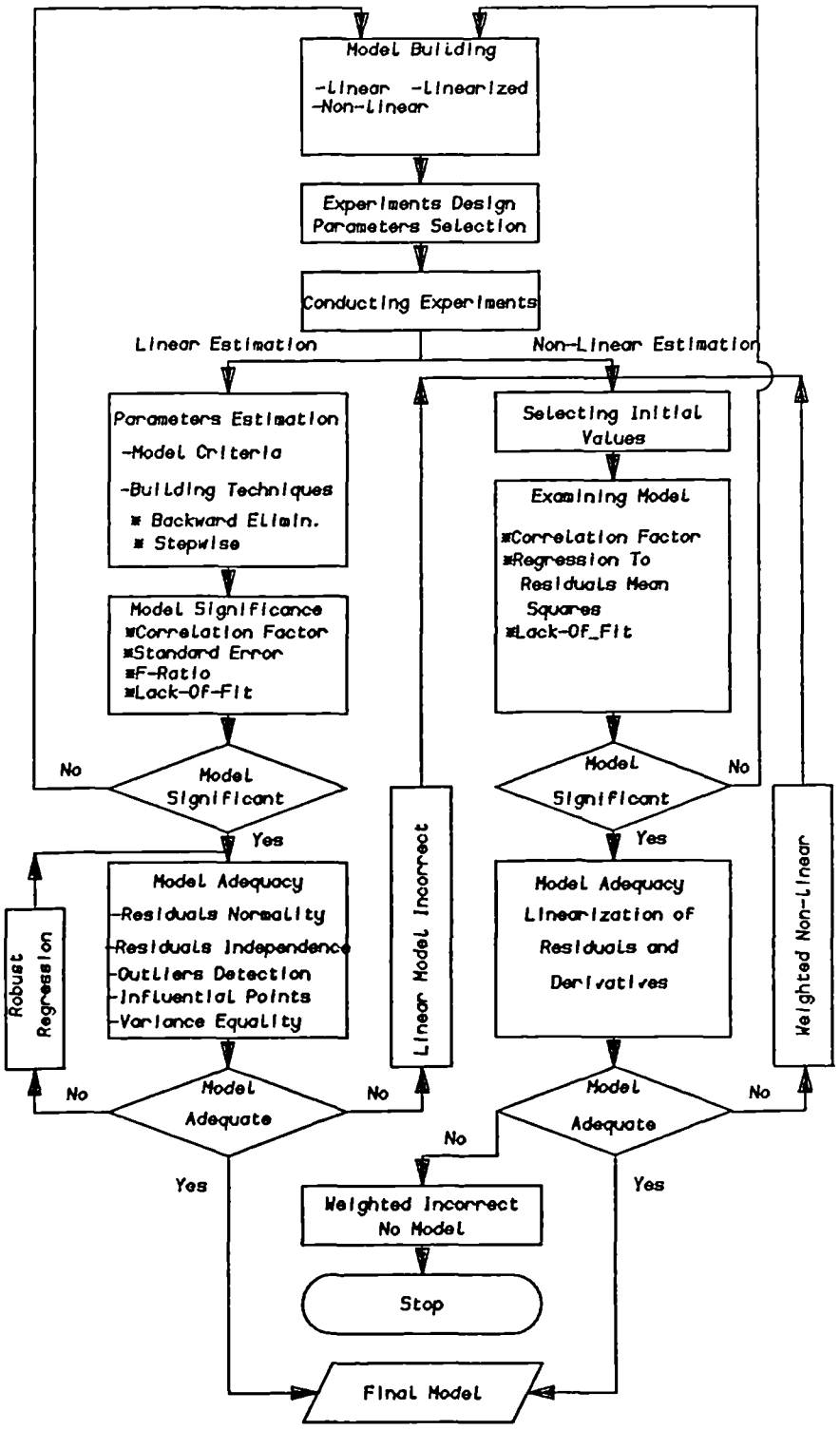

Fig. 4.8 Modelling Strategy and Logic Steps Used in This Study

Chapter 5

MATHEMATICAL MODELS OF TOOL WEAR, TOOL LIFE, AND CUTTING FORCE

5.1 Foreword

In turning operation, the wear developed on the tool clearance face is one of the principal factors affecting production optimization. Improved understanding of wear behaviour will lead to enhanced tool life and reliability and to safer and more efficient operation. Tool wear mechanisms for newer tool and workpiece materials are still very little understood, making it difficult to fulfill the target of manufacturing optimization. For conventional materials, the determination of the optimal tool life has been made difficult due to ambiguity of defined wear processes and to inaccuracy in their quantification. Although there are many descriptive theories for metal cutting, few have been well documented and used to improve decision making on the workshop floor. None of the available theories of the mechanics of the cutting process, which consider only perfectly sharp tools, are capable of describing all the observed data quantitatively; since they neglect the changes brought about by the added complications of wear. An intelligent system in which the model of the cutting process adapts itself to the changes in the system characteristics has great potential to enhance the optimization of the entire process.

The introduction of the computerized numerical control machine tools *CNC* fitted with a host computer has added to the flexibility of control of the machining operation. More recently, the advent of adaptive control of machine tools *AC* has offered a unique opportunity to achieve the ultimate targets of unmanned manufacturing and production optimization. To make full use of these advanced technology, compatible approaches are required to deal with the problem of when to remove or change the cutting tool, with minimal degradation of the efficiency of the entire process. Among the possible solutions are in-process monitoring of the tool state; and, the use of the machinability data base systems. These approaches require accurate predictive models which link the un-measurable parameters such as tool wear with more easily detectable variables such as tool forces and tool vibration. Mathematical modelling of the cutting operation may produce a practical solution to achievement of such requirement since it capable

of simulating industrial metal cutting processes.

This chapter is devoted to the presentation and to the analysis of collected experimental data of tool wear and cutting forces; and the following topics will be covered:

1. The understanding and the characterization of the tool wear behaviour for the multi-coated carbide tips employed in the experiments.
2. The search for the best tool life model which can be confidentiality employed in predicting both of the useful tool life and the optimal cutting variables for certain production situations.
3. The study of cutting forces characteristics within the different phases of the tool working life.
4. The investigation of the possible use of the variation in cutting force, due to wear progress, for in-process monitoring of tool wear.

5.2 Mathematical Models of Tool Wear and Tool Life

Tool wear can be defined in terms describing the size or extent of the wear scars on the tool faces, or in terms of the shape of the cutting edge, (see *Fig. 2.1*). The term "tool wear" considered in this analysis is the width of wear scars on the tool clearance face when the tool is in continuous contact with the workpiece. As discussed in **Chapter 2**, the crater wear on the tool face are not likely to exist when coated tools are used. Moreover, the wear scars on the clearance face are the most reliable and common by used criterion. In addition, it affects almost all output parameters such as cutting forces; temperature; tool vibration; and, surface quality and dimensional accuracy of the workpiece.

5.2.1 Experimental Results and Discussion

As discussed in **Chapter 3, section 3.4,** the wear scars were measured on three different locations of the tool clearance face at regular intervals of two minutes. These measures, as shown in *Fig. 3.37,* are: the nose wear *NW* at the insert radius at its point of maximum projection into the work material; the flank wear *FW* as the maximum wear land at the tool flank; and, the notch wear *NCW* at the point of intersection of the depth of cut with the clearance face. The wear-time curves for each of these wear elements, for each test of the central composite design *CCD* (see *Table 4.2*), together with the average value of these elements *AW,* are shown in *Fig. 5.1.(a-c).*

All the curves reveal the general three-region wear-time trend (see *Fig. 2.5*). At the beginning, when a new tool is used, the tool edge is quickly broken down and a finite wear land is established. The amount of this initial wear W_o is dependent on cutting conditions but, for a given tool, the values of the initial wear developed on the different locations- nose, flank, and notch- are generally similar.
Following this primary stage, the tool wears progressively at an almost constant rate until it reaches the final stage at which wear develops at an increasing rate leading to the tool failure. At the second stage, the tool wears at rates which depend on the variables employed in such a way that the time required for a tool to attain a certain wear level, or to reach its final stage of life span, is less for more severe conditions.

Among the three wear elements, the nose wear *NW* is not only the most severe but, in most cases, for instance Test# 3, 9, and 12, determines the tool lifetimes. Moreover, the time required for nose wear level to reach the failure zone is less than that for the other elements. In other words, tool failure always originates at the nose area and, is subsequently triggered on the the flank and notch areas. This observation may be explained by the experimental results of tests no. 3, *Fig. 5.1.a,* and no.9, *Fig. 5.1.b.* At the early stages of cut, the level of the nose wear is lower than that of the notch wear. At later stages, its level is rapidly increased while the flank and notch wear rates are constant. Two minutes later, the flank wear is triggered and a higher level is

attained.

In practice, the notch wear *NCW* is lower and the tool seldom fails by this mechanism. In some cases, however, high level of notch wear are noticed and this is due to random disturbances, such as chipping and fracture, which occur in the early stages of cutting.

In summary, the wear developed on the clearance face is not of a uniform pattern and the frequent chipping and fracture of the cutting edge complicates this mechanism. However, a degree of reliability and repeatability should be achieved when a reliable approach has been developed to the characterization of the tool wear mechanism. Investigation of the individual characteristics of a particular case, rather than identifying the general trend, usually adds little towards the establishment of a universal solution. Therefore, any mathematical formulation should provide the functional relationship between the parameters over the entire operational region.

5.2.2 Mathematical Models of the Wear-Time Behaviour

It has been suggested by many investigators *[47,48,65,122]* that the first two regions of the wear-time curve can be adequately approximated by a straight relation line of the form:

$$W = W_o + mt, \tag{5.1}$$

where W is the wear scar, W_o is the initial wear, m is the slope of the linear portion of the curve in the second region, and t is the cutting time. However, experience, *Fig. 5.1*, has indicated that the second stage of the wear-time curve is seldom characterized by a straight line, since it always exhibits some non-linearity which cannot be ignored. Therefore, higher order terms in time have frequently been proposed *[17]* so as Eq. (5.1) becomes:

$$W = W_o + m1\ t + m2\ t^2 + ... \tag{5.2}$$

Test No.	Parameters Coefficients					Statistical Criteria	
	ao	a1	a2	a3	a4	R^2	SE
a) Second-order polynomial [model (5.2)]							
1	0.145	0.0004	$3.7\ 10^{-6}$			0.97	0.009
6	0.134	0.0024	$-9.0\ 10^{-6}$			0.94	0.010
13	0.966	-.59	0.105			1.00	0.000
14	0.107	0.0006	$2.5\ 10^{-6}$			0.90	0.017
b) Second-order polynomial with exponential term [model (5.3)]							
1	0.148	0.003	$4.0\ 10^{-6}$	-2.285	-2.207	0.98	0.009
6	0.291	-0.003	0.00004	-0.1788	-0.053	0.96	0.008
13	0.546	-0.637	0.1002	0.413	0.116	1.0	0.000
14	0.111	0.0006	$2.9\ 10^{-6}$	-2.405	-2.196	0.905	0.171

Table 5.1 Non-linear Estimation of the Wear-Time Polynomials

However, as an attempt to include both of the early and the last stages of wear-time curve, an exponential term in cutting time was thought to improve the quality of the model.

$$W = W_o + a1\ t + a2\ t^2 + a3\ e^{a4t}. \tag{5.3}$$

Non-linear regression procedure is used to determine the coefficients estimates for each of *Eqns. (5.2) and (5.3)* for each test in turn. Different models result for each of the wear elements- nose, flank, notch, and average wear. *Table 5.1* lists the values of the coefficients, together with their statistical criteria as resulted from the regression analyses, for some selected tests. These tests represent the boundary of the operational region of the central composite design. The results in *Table 5.1* are for the average wear *AW* which has been found to have the best criteria among the various wear elements. This is expected since the use of the average wear apparently dampen the effect of the random disturbances which are usually occur unexpectedly. This, however, has the disadvantage that it does not accurately reflect the actual state of the tool.

The experimental *AW-t* data together with the predicted values from each of models (5.2) and (5.3) are plotted as shown by *Fig. 5.2.* Between the second-order polynomial (5.2) and the relation with the extra exponential term (5.3), the latter

seems to have a slightly better capability to fit the experimental data, especially at the very early and the very late stages of cutting. However, in most cases, both models fail to reasonably estimate the wear level at the end of tool life when a tool fails catastrophically. The tool fails almost instantaneously attaining a very high level of wear and this sudden change in wear-time attitude cannot be estimated by the wear-time models. Moreover, the mathematical formulation of an individual test is always influenced by the local characteristics of the tool and does not reflect the global effect of the entire operational region. Thus, a more generalized approach is required to formulate the tool wear behaviour as has been affected by the cutting variables: speed, feed, and depth of cut.

Equation (5.1) may be generalized to take the form:

$$W = W_o + \Delta W, \tag{5.4}$$

where ΔW is the wear increase at particular cutting time and it is dependent on the cutting conditions employed.

$$W = W_o + ao\, V^{a1}\, F^{a2}\, d^{a3}\, t^{a4}, \tag{5.5}$$

where V, F, and d are the cutting speed, the feed, and the depth of cut respectively. Another approach is to assume a model in which the variation in the initial values of wear is embodied within the effects of the cutting conditions.

$$W = bo\, V^{b1}\, F^{b2}\, d^{b3}\, t^{b4}. \tag{5.6}$$

Instead of dealing with the individual tests, the entire set of data of the central composite design *CCD* (669 data points for 24-test in Appendix A), is used, in association with the regression procedures, to determine the coefficients estimates of models (5.5) and (5.6).

To develop a model of the form (5.5), both of the initial wear, and the wear increase, are dealt with separately. The initial wear for each test is determined as the intercept of the wear-time curve shown in *Fig. 5.1* by projecting the curve back to zero

cutting time. As mentioned earlier, similar values of initial wear are found for all the wear elements and therefore, the average initial value AW_o is considered to reasonably represent each of the three wear elements. Non-linear regression procedure has resulted in a model of the form:

$$W_o = 9.3 \times 10^{-3}\ V^{0.5133}\ F^{0.0059}\ d^{-0.0597}\ D^{0.0371}, \tag{5.7}$$

where D is the workpiece diameter in mm. Statistical criteria indicate a moderate value of the correlation factor of 0.75 and a relatively high value of standard error of estimates. However, this model gives a very good explanation of the tool wear behaviour in the first few moments of cutting. The values of initial wear is positively affected, to different extents, by the values of each of the speed, the feed, and the workpiece diameter, while it is negatively affected by the value of the depth of cut. While the effect of the cutting conditions on the value of initial wear is essential, the effect of the workpiece diameter needs some explanation. Since the hardness of a workpiece varies so that harder material is found for larger diameters *[30 & 123]*, the initial wear seems to be hardness dependent for a given set of cutting conditions *[50]*.

To determine the coefficients $a's$ and $b's$ in equations (5.5) and (5.6), first-order linearized models are found to adequately fit the experimental data. However, the models are found to be influenced by the behaviour of certain data points of higher values of the residuals, which increase the values of standard errors of estimates. These influential cases are found to belong to the points at which the sudden increase in wear level has occurred. Removal of these cases from the experimental data has improved the statistical characteristics of the models without affecting their predictive capability. The resulting models are as follows:

A) Models for wear increase

$$\Delta W_{NW} = NW - W_o = 7.44 \times 10^{-4}\ V^{0.698}\ F^{0.403}\ d^{0.606}\ t^{0.602}; \tag{5.8}$$

$$\Delta W_{FW} = FW - W_o = 3.83 \times 10^{-4}\ V^{0.786}\ F^{0.398}\ d^{0.513}\ t^{0.609}; \tag{5.9}$$

$$\Delta W_{NCW} = NCW - W_o = 5.83 \times 10^{-4}\ V^{0.613}\ F^{0.467}\ d^{1.004}\ t^{0.627}; \textit{and}, \tag{5.10}$$

$$\Delta W_{AW} = AW - W_o = 3.35 \times 10^{-4}\ V^{0.775}\ F^{0.427}\ d^{0.782}\ t^{0.652}. \qquad (5.11)$$

B) Models for wear level

$$NW = 8.873 \times 10^{-3}\ V^{0.559}\ F^{0.174}\ d^{0.159}\ t^{0.259}; \qquad (5.12)$$

$$FW = 7.205 \times 10^{-3}\ V^{0.585}\ F^{0.145}\ d^{0.165}\ t^{0.226}; \qquad (5.13)$$

$$NCW = 9.08 \times 10^{-3}\ V^{0.506}\ F^{0.165}\ d^{0.325}\ t^{0.234}; and, \qquad (5.14)$$

$$AW = 7.620 \times 10^{-3}\ V^{0.577}\ F^{0.168}\ d^{0.248}\ t^{0.245}. \qquad (5.15)$$

Statistical criteria of these two sets of models are summarized in *Table 5.2.* A relatively

	Models of Wear Increase				Models for Wear Level			
	ΔW_{NW}	ΔW_{FW}	ΔW_{NCW}	ΔW_{AW}	NW	FW	NCW	AW
R^2	0.78	0.70	0.65	0.83	0.73	0.74	0.64	0.84
SE	0.29	0.34	0.40	0.26	0.15	0.13	0.16	0.10
F-Ratio	568	376	296	790	441	455	289	831

Table 5.2 Statistical Criteria of Wear Models (5.8 - 5.15)

low values of the correlation factor R^2 and high values of standard error SE are resulted. A second-order model, achieved by including the quadratic and the interaction terms of the cutting variables, has added almost nothing to improve the models behaviours. However, the higher values of the *F-ratio* confirmed the significance of these models to be used in tool wear prediction. Analyses of the residuals of the models do not reveal any inadequacies.

Among the wear elements, the models for the average wear AW gives better statistical criteria. *Fig. 5.3* shows plots of the predicted values for each of the models (5.11) and (5.15), together with the relevant experimental data. It is seen that a better predictive capability is obtained when the wear level is estimated according to the models of wear increase ($W = W_o + \Delta W$). However, for *Test#13,* both models fail to give a reasonable estimation of tool wear level. A high value of cutting speed of 206 m/min of this test has caused the tool to be plastically deformed after only four minutes of cut. The final

wear level at the end of six minutes cut is 1.2 *mm*, and this is found among the outliers and influential cases which have been eliminated from the experimental data.

In summary, tool wear estimation based on models of wear-time or wear-time-cutting conditions has shown to well predict the wear levels within only the first two stages of wear-time trend. The third stage, at which a very high wear rate occurs, is usually not detectable using this technique.

5.2.3 Mathematical Models of Tool Life

The term "tool life" can be defined as the ultimate time after which tool is no longer able to perform an efficient cut. The appropriate criterion to determine the end of the useful tool life usually depends upon the production requirements. Whilst a certain variation in the magnitudes of cutting forces can be used as a criterion to measure wear in rough cutting, specification of an acceptable level of surface finish and dimensional accuracy is more suitable in finish cutting. However, the criterion of specifying a fixed wear level on the cutting edge may combine the two objectives since wear progress affects the tool forces; and, the workpiece surface finish and dimensional accuracy.

Tool life was first characterized by *Taylor's equation* which relate the life of the *HSS* tools to the cutting speed by a power transformation. Even though this technique is still widely used as an approximate index of machinability, many obstacles are practiced when it is applied to metal cutting data. Generally these difficulties may be classified being due to: *Taylor's* approach; and, to the nature of tool wear and tool life data. The invalidity of *Taylor's equation* has been experienced when it is applied for machining data of newer tool and workpiece materials and also, when a more severe feeds were employed *[21 & 22]*. Furthermore, *Taylor's equation* covers only a narrow range of cutting speed *[20]* and this is economically undesirable in today's production engineering. Besides, from experimental viewpoint, *Taylor's* approach of one-variable-at a time is very time and material consuming.

Aside from these drawbacks, the in-deterministic nature of tool wear mechanism has added more complication in determining the tool life. For a set of identical tools under nominal identical machining conditions, a large variation in tool lives may be obtained. This difficulty may result from many possible sources such as: the slight variation in hardness and machinability from one workpiece to another, or from one cut to another; the variation between cutting tools of the same compositions; the variation due to different measuring accuracies; the variation due to the different criteria used to assess the wear level at which tool life is terminated; and, the variation due to slight differences in the nominal values of cutting parameters from one cut to another. These may cause significant difference in machining performance between cuts, and between cutting tools of the same grade.

In this section, the approach of tool life determination is investigated through the establishment of the mathematical models which relate the tool life to the cutting variables- speed, feed, and depth of cut. Different model building techniques and statistical analyses are used to develop and carefully examine the models. More advanced regression techniques, such as robust regression, described in *Section 4.9.2* for differentially weighting the experimental observations, are used to detect the sources of tool life variation and to dampen their influence on the resulting models.

The selection of a suitable wear level criterion has long been investigated for a reliable description of the tool lifetime. It has been found that the optimal tool life may be practically defined as the cutting time required for the tool to enter the third stage of the wear-time curve (see *Fig. 2.5*). This was described by points *P's* in *Fig. 2.6* in **Chapter 2.** These points represents the limits between the temperature insensitive wear region at which wear rate is likely to be constant, and the temperature sensitive region at which wear is rapidly accelerated resulting in tool failure and breakage *[12]*. However, the determination of the beginning and the end of this failure zone is extremely difficult *[124]*. Furthermore, tool failure is almost instantaneous and the point at which the tool fails does not follow any regular pattern or physical mechanism. However, it has been well established and accepted to use a fixed wear level on the cutting

edge as an indication of tool life. However, the appropriate wear value of this level usually depends on the machining system and on the production requirements. Whilst specifying a low wear level may be economical undesirable, the selection of high wear criterion value should be checked against the capacity, the rigidity, and the strength of the different elements involved in the machining process. Also, the selection of the appropriate type of wear on the clearance face is of crucial factors in tool life determination. Experimental data in *Fig. 5.1* indicate that the wear on the nose area is always predominated and, that the tool may already have failed due to excessive nose wear while the flank and notch wear elements are still within the accepted range. Therefore, it may be concluded that both the flank wear FW and the notch wear NCW cannot be used as a reliable tool life criteria.

A fixed level of 0.25 mm is used to determine the experimental values of tool life for each test in *Fig. 5.1.* This value of wear level has been chosen to adequately cover both the average and the nose wear data for all the 24 tests. This has resulted in 24 data points for each of the nose wear NW and the average wear AW and these data, have been used to develop the tool life models.

In **Chapter 4,** tool life model was developed and examined using different model building techniques and tests of hypothesis. The average wear AW was used as a criterion tool life measure. The robust regression procedure via iteratively re-weighting least-squares (see *Section 4.9.2*), resulted in the best second-order model of the form *(4.33):*

$$\ln T_{AW} = -7.953+7.275 \ln V-1.121 [\ln V]^2-0.371 [\ln F]^2-0.81 [\ln d]^2-0.469 \ln V \ln F.$$

With a correlation factor of 0.97 and a standard error of 0.177, the robust regression was found to stabilize the residuals through reducing the effects of the influential cases and outliers. This eliminated the effect of tool life variation which were noticed in the experimental tool life values of the repeated tests. Also, tests of hypothesis of residual normality, independency, and lack-of-fit revealed nothing against the adequacy of the developed model. Details of the steps which were followed to develop and examine this

model are found within the text of **Chapter 4.**

The same steps are followed to develop a tool life model using the nose wear as a tool life measure. The first-order linearized model has been found inadequate to fit the experimental data. Plot of the residuals against the predicted values revealed a parabolic pattern which suggested that a second-order model might lead to better results *[118].* Therefore, a second-order model was assumed and, linear regression in association with the experimental data has resulted in a model of the form:

$$\ln T_{NW} = 8.271 - 0.357\,[\ln V]^2 - 0.448\,[\ln F]^2 - 0.53\,\ln V \ln F. \qquad (5.16)$$

The statistical criteria of this model are as follows:

Correlation Factor	R^2	$= 0.88$
Adjusted Correlation Factor	Adj. R^2	$= 0.86$
Standard Error	SE	$= 0.42$
F-Ratio		$= 47.0$

The lack-of-fit test confirmed the model significance to be used in predicting tool life data. The ratio of lack-of-fit mean squares to that of pure error is 0.11 and this value is found far less than the *F-value* from the statistical tables at $(3, 21, 0.05) = 3.47$. The residuals did not exhibit an autocorrelation among their successive values. The *Durbin-Watson* value of the model's residuals was 1.47 and this was found greater than D_{upper} from the statistical tables at $(0.01, 3, 24) = 1.41$. However, the high value of standard error of 0.42 raised doubts about the model quality. This lead to wider confidence intervals which degrade the predictive capability of the resulting model. Analyses of the residuals indicated that the cases which belonged to trials 19, 7, 11, and 2, (see *Table 4.2*), were of the highest error values. The examination of their standardized residual values *ZRESID,* which was defined in **Chapter 4** as the ratio between the error value to the regression standard deviation, has indicated that these points were not from the most influential cases. However, the *Cook's distance,* which indicates the effect of the elimination of a particular case on the predictive capability

of the rest of the observations (see *Section 4.8.6*), has indicated that trials 22, 19, and 16 were of the most influential. The examination of the experimental results in *Fig. 5.1.c* for *Test#22* indicated that a tool failure has occurred at the nose area after 26 minutes of cutting. This resulted in almost instantaneous wear increase from 0.17 to 0.24 *mm*. For *Test#16* in *Fig. 5.1.b*, which is a repeated test with nominal conditions as for *Test#22*, the wear level at 28 minutes cutting is only 0.18 *mm*. Since error $\varepsilon = Y - Y_{est.}$, a maximum positive residual resulted from *Test#22* while it was negative for *Test#16*. A similar tool failure, to that which occurred for *Test#22*, has been found at the nose area of *Test#16* at 30 minutes cutting time. This indicates that the lowest level of feed of 0.06 *mm/rev* used in these two tests is not favourable. This causes higher vibrational amplitudes and machining instability which usually result in a local random disturbances of tool chipping and fracture. This indicates the abnormality involved with the experimental results of these two tests and therefore, a robust regression technique with *Ramsay's* damping function is used to re-weigh these two cases so as to reduce their influence on the resulting model. Details of the robust regression procedures can be found in *Section 4.9.2.*

These procedures have resulted in a second-order linearized tool *life model of the form:*

$$\ln T_{NW} = 8.12 - 0.341\ [\ln V]^2 - 0.33\ [\ln F]^2 - 0.45\ \ln V \ln F. \qquad (5.17)$$

An improvement is achieved in the value of the correlation factor from 0.86 in case of conventional regression to 0.91 when robust regression is used. Also, a reduction in the value of standard error is obtained from 0.42 to 0.3. However, a standard error value of 0.3 is still relatively high considering it is on a logarithmic scale.

Comparing the parameters of the conventional model (5.16) to those for the weighted model (5.17) shows that the feed parameter is the most affected by the weighting procedures. This confirms that the high error produced by trials 16 and 22 is basically due to the effect of the low value of feed employed in these two tests.

Between the two types of tool life models, the one using the average wear T_{AW}, (4.33), gives a better and more reliable predictability. The effect of cutting variables on tool life for both models, however, follows a similar trend. The cutting speed has

the strongest effect on the values of tool life followed by the feed. While the quadratic effect of the depth of cut is included in the average wear model (4.33), neither of its value nor its quadratic or interaction terms is significant to enter into the nose wear tool life model (5.17). This is essential; since the depth of cut usually governs the level of notch wear which is among the elements involved in the computation of the values of the average wear.

However, for a better understanding of the effect of the cutting variables on the values of tool life, the graphical representation of the response surface for both models is now explained. The values of tool life may be represented by a surface bound by the extremes of the experimental operational region. *Fig. 5.4* shows how the tool life surface for each model is influenced by the speed and by the feed. *Fig. 5.4.a* is for the average wear tool life model T_{AW} for a given value of the depth of cut of 2.25 mm, Eq. *4.33*, while *Fig. 5.4.b* is for the nose wear tool life model T_{NW}, Eq. *5.17*. Both surfaces show a similar trend to predict values of tool life using feed and speed. Generally, tool life values at the corners of the speed-feed plane are of similar magnitudes. The effect of the quadratic and the interaction terms of speed and feed is represented in the figure by the non-linear distribution of the surfaces. However, for the nose wear tool life model in *Fig. 5.4.b*, the cutting speed has a stronger negative influence on tool lives. A higher negative effect of feeds is observed at lower cutting speeds and this decreases non-linearly with speed increase. However, both of the surfaces reveals a very interesting observation of sudden change of its attitude below a cutting speed of 100 m/min. In this speed range, feed values less than 0.12 mm/rev tends to negatively affect the resulting values of tool life. The cutting conditions of both *Test#16* and 22 are of 104 m/min speed and 0.06 mm/rev feed and these values are within the region at which tool life surface reversed its trend. This confirms the conclusion already drawn that the use of low feeds, which are always accompanied by tool vibration, increases the wear level on the cutting edge and, as a result, reduces tool life.

Another way to obtain a quantitative information from the tool life models is by developing contours or surface projection in the speed-feed plane. As indicated in

Fig. 5.5, each line represents a certain level of tool life in minutes. The non-linear behaviour of tool life is more distinctive at lower values of feed and speed. The region at which the tool life reverses its attitude is characterized by the circular curves near the origin. However, the contour of the nose wear tool life model in *Fig. 5.5.b* indicates lower effects of low-to-moderate feed-speed combinations on the values of tool life than in the case of average wear tool life model in *Fig. 5.5.a.*

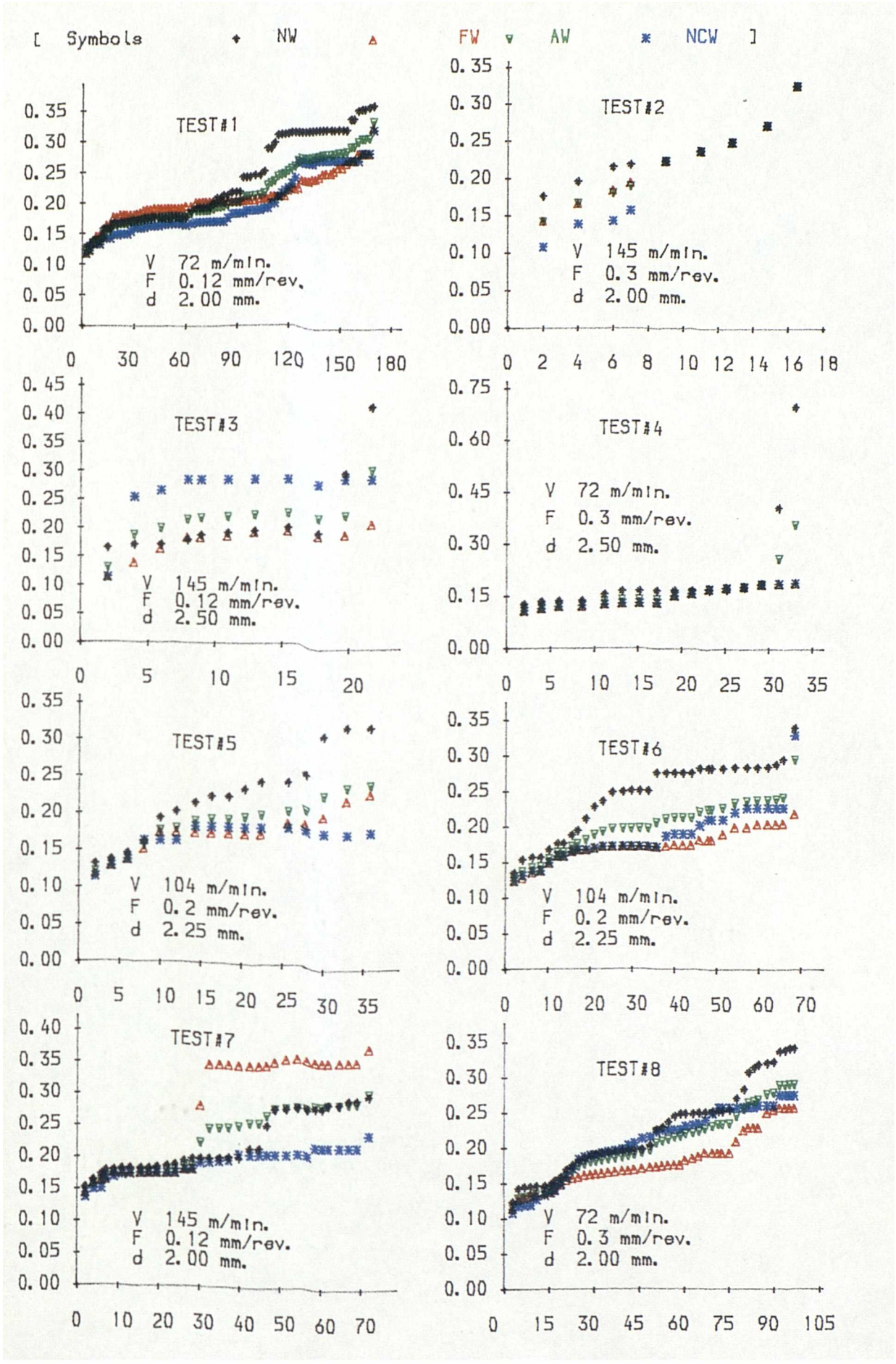

Fig. 5.1.a Wear-Time Curves for Different Wear Elements for Tests [1-8]

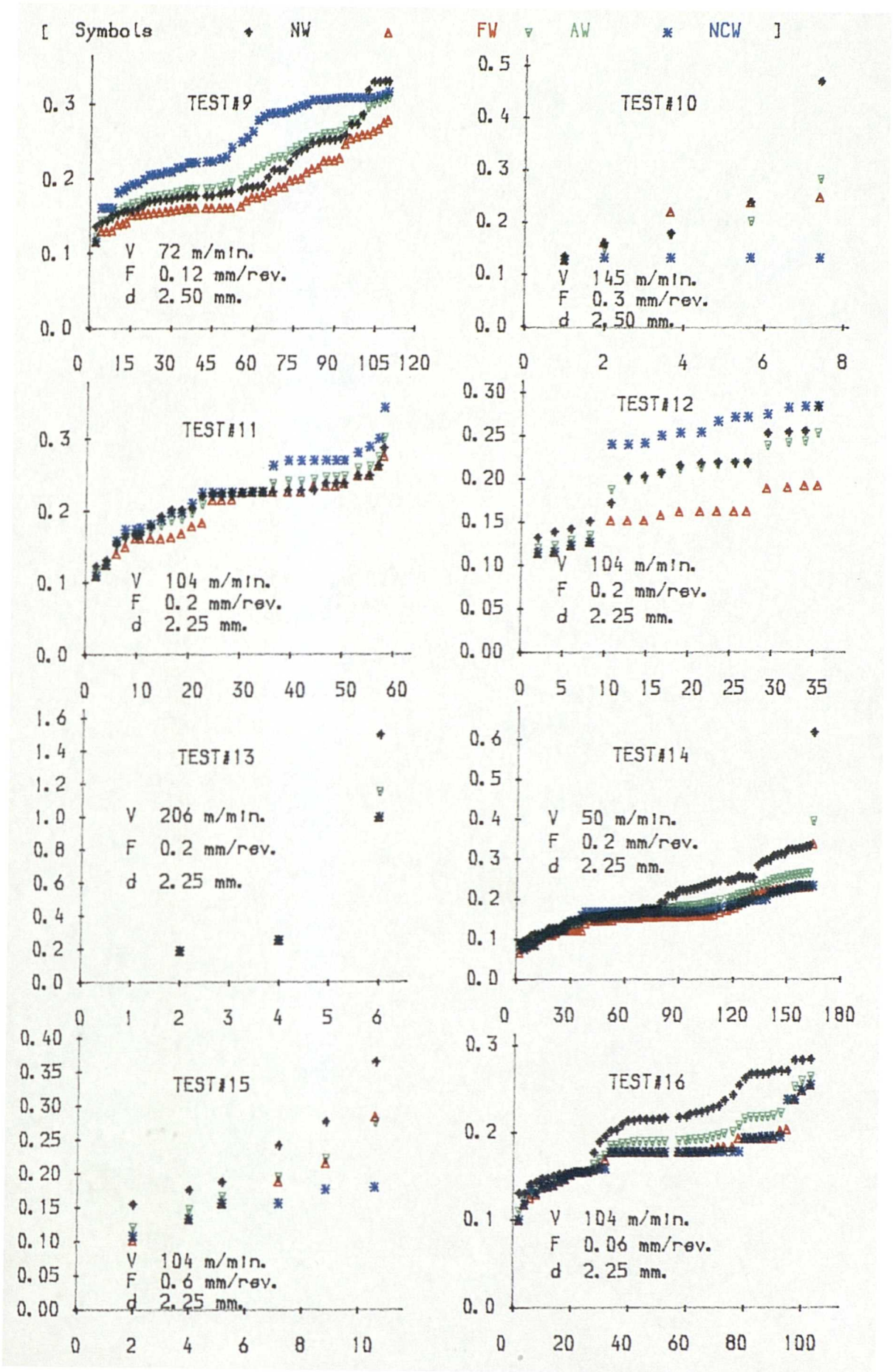

Fig. 5.1.b Wear-Time Curves for Different Wear Elements for Tests [9-16]

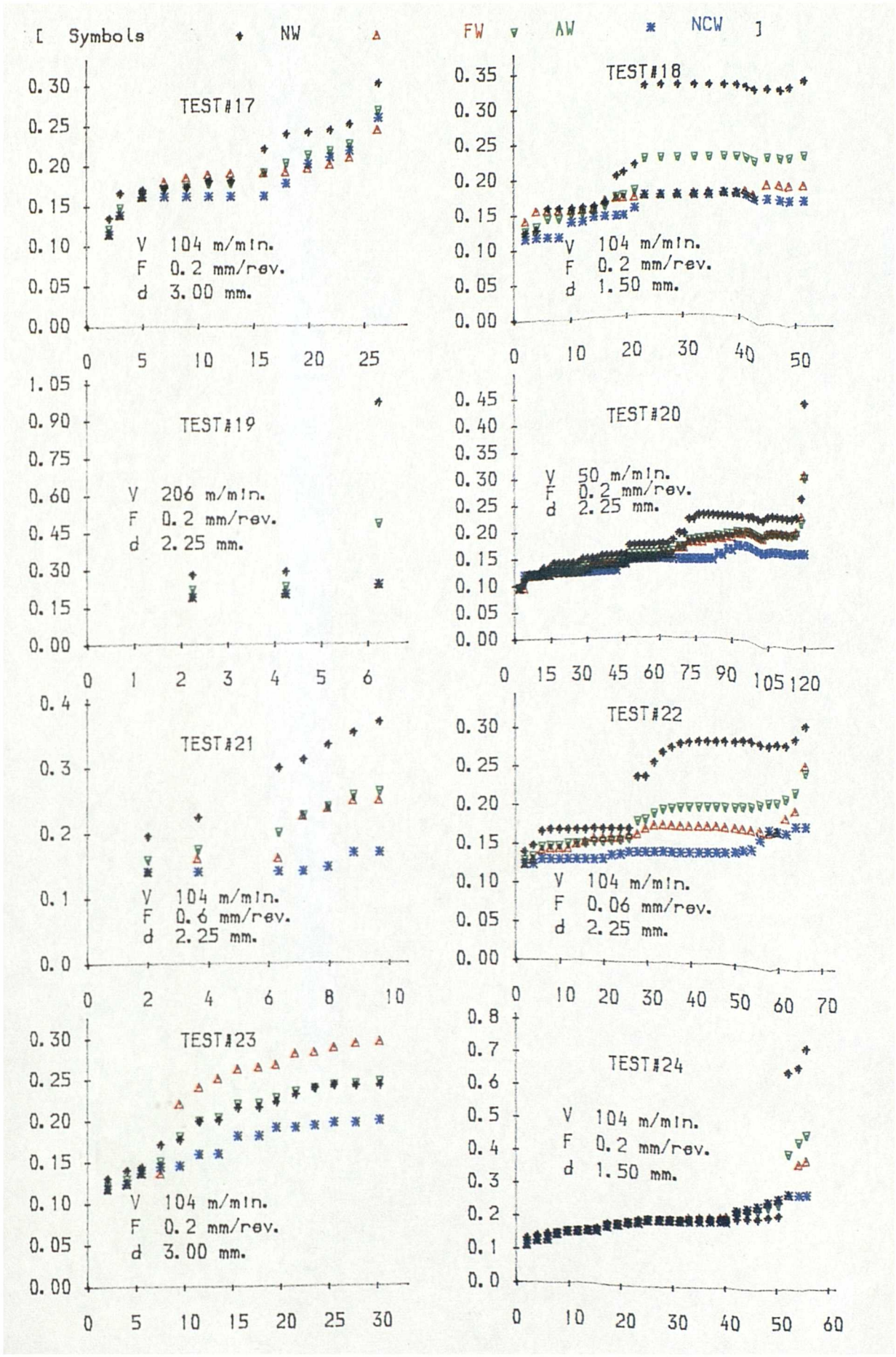

Fig. 5.1.c Wear-Time Curves for Different Wear Elements for Tests [17-24]

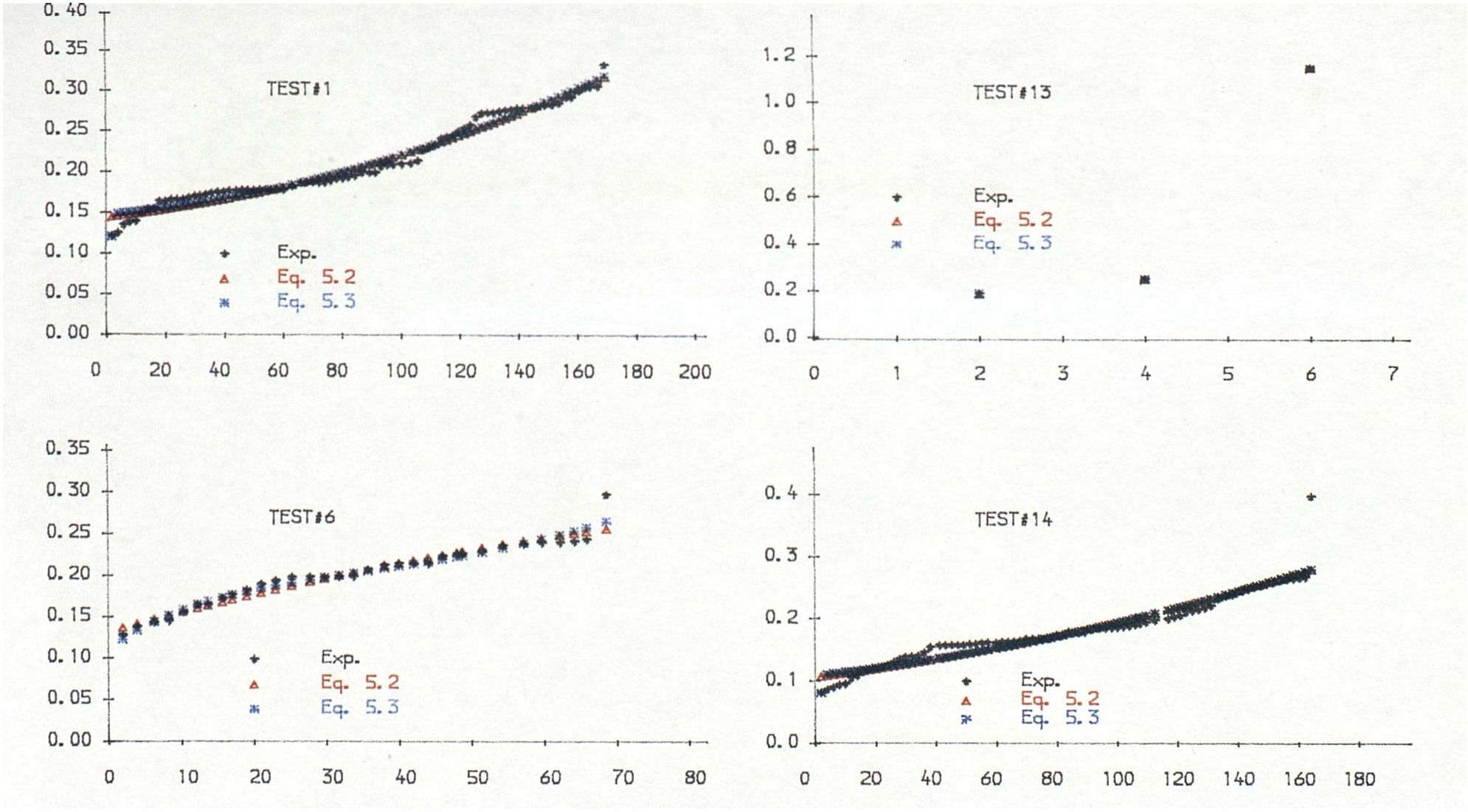

Fig. 5.2 Experimental and Predicted Average Wear Using Different Wear-Time Models

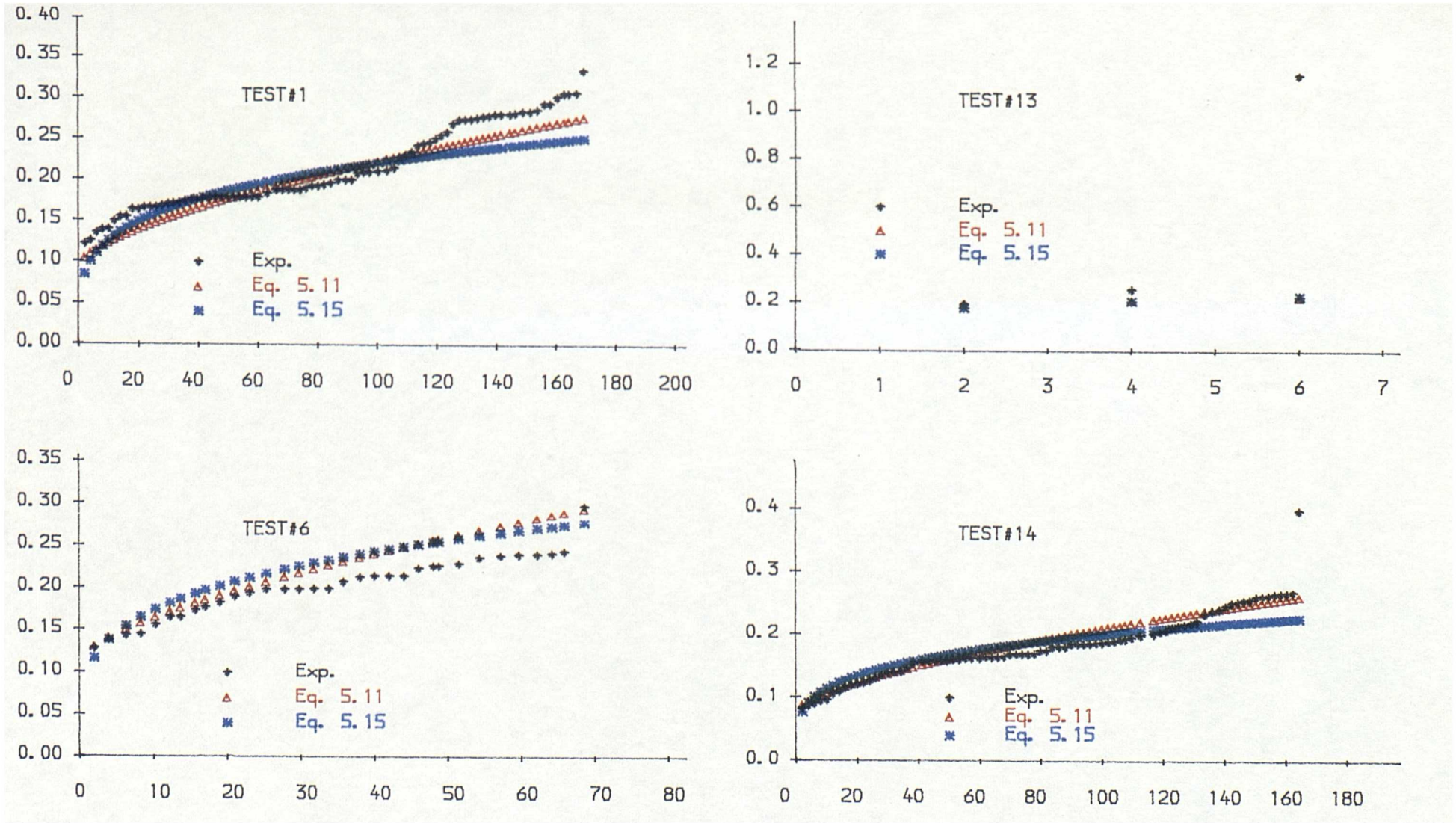

Fig. 5.3 Experimental and Predicted Average Wear Using Different Wear Models

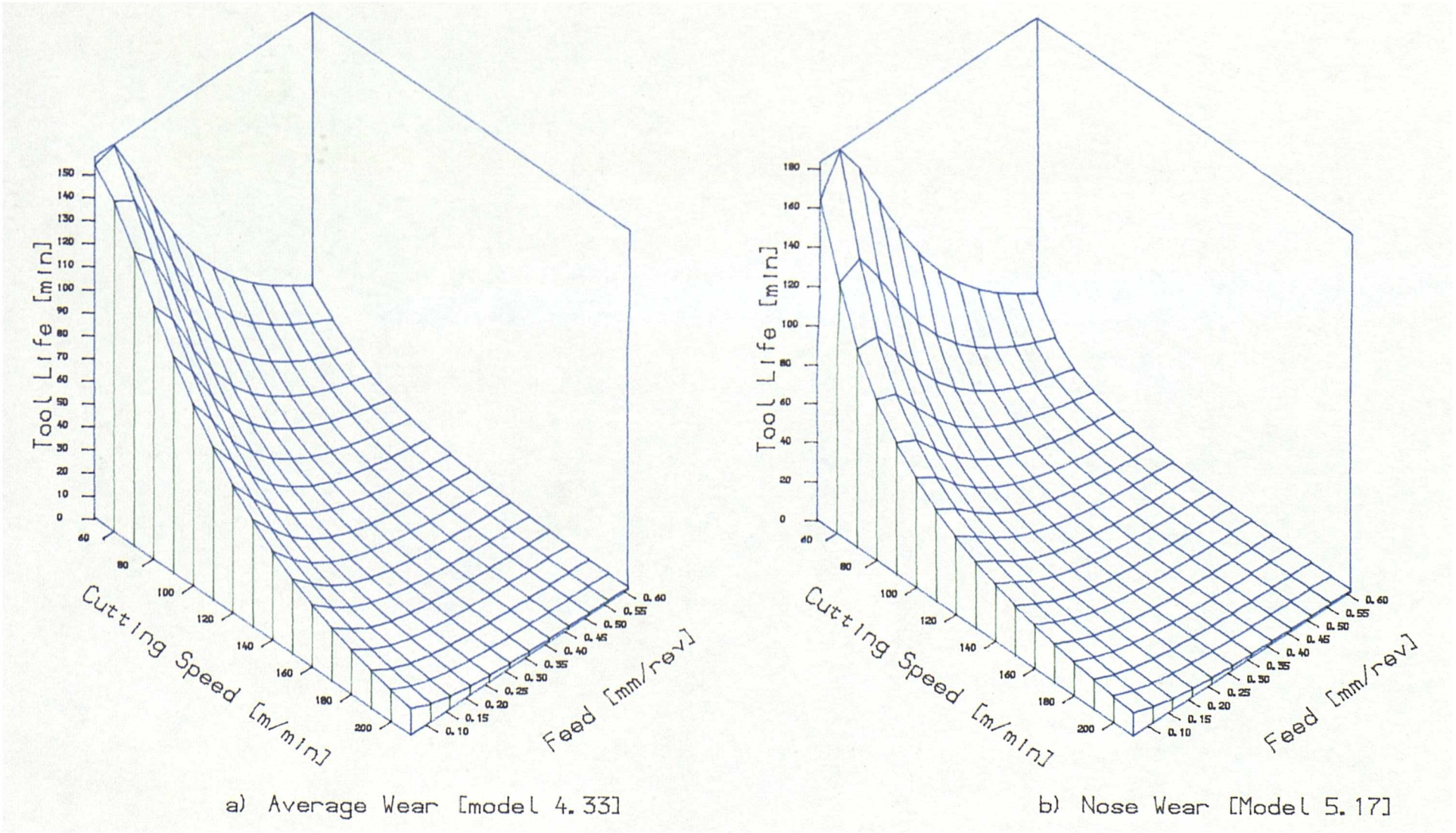

Fig. 5.4 Three-dimensional Representation of Tool Life Models

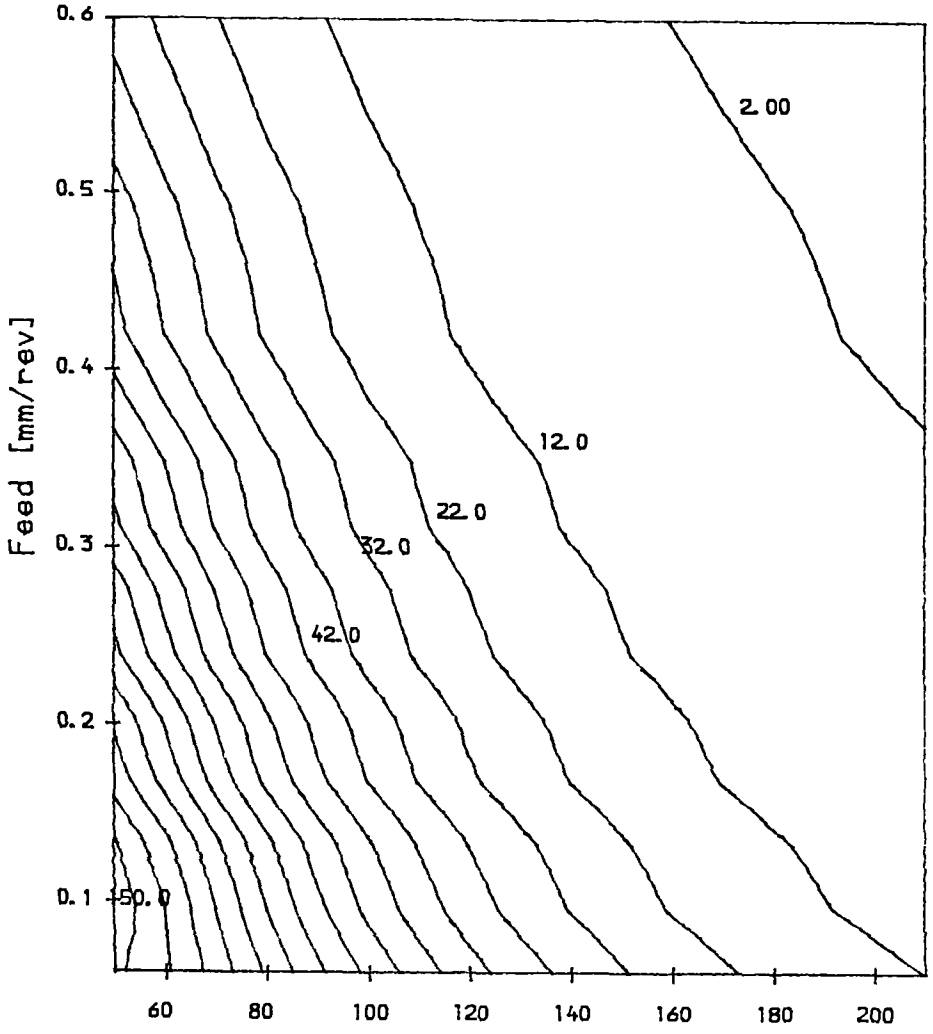

a) Average Wear [Model 4.33]

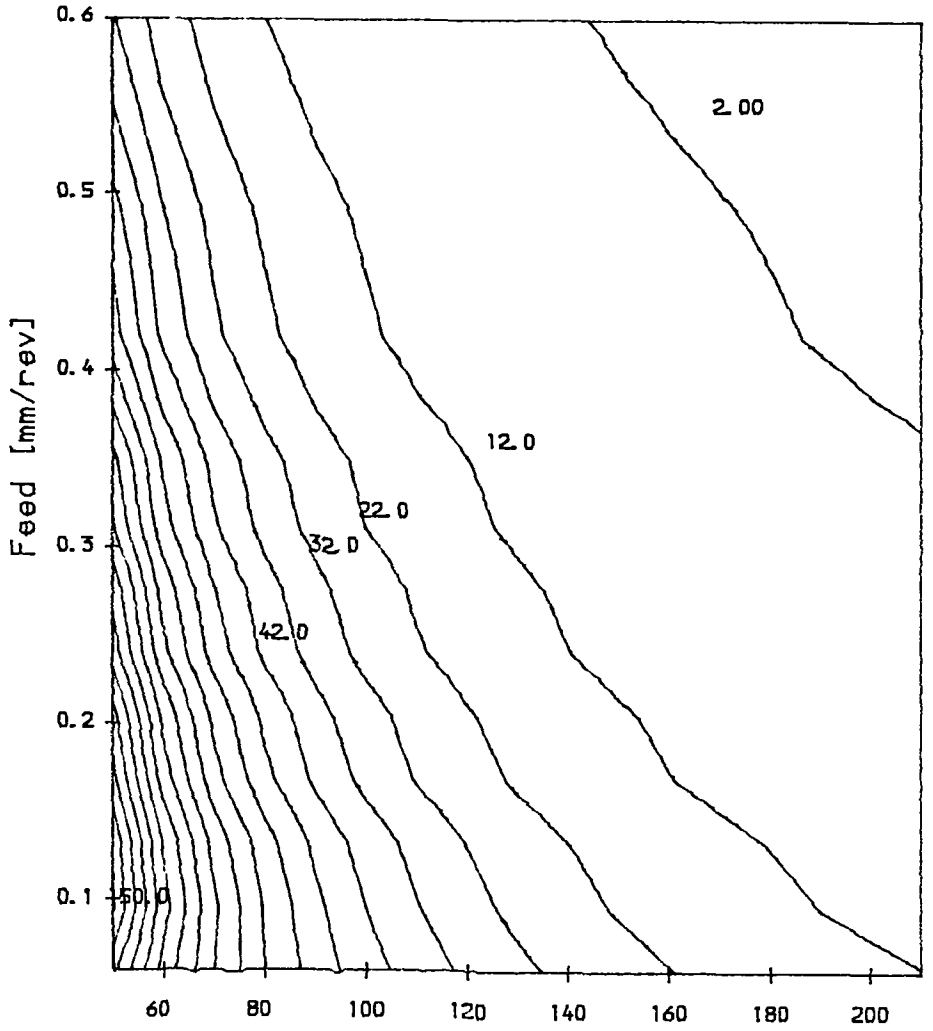

b) Nose Wear [Model 5.17]

Fig. 5.5 Tool Life Contours in Speed-Feed Plane

5.3 Mathematical Models of Cutting Force Response

In turning operation, cutting forces can be represented by a three-component system as: the vertical component F_y; the feed component F_x; and, the radial component F_z, see Fig. 3.1. For each sub-test, a simultaneous records of these components were collected and processed using the dynamometer and the data processing procedures which were explained in **Chapter 3.** A sample of the force signals are shown by *Fig. 5.6.* During stable cutting with sharp tool, force signals fluctuate around a constant level as shown in *Fig. 5.6.* The width of the dynamic force fluctuation is dependent on the wear level developed and on the cutting conditions employed. While higher cutting speed and wider wear land always reduce the band width, lower feed and speed tend to excite the system resulting in a wide band of force fluctuation. Also, the formation of discontinuous chips usually causes a larger variation in the force signals and consequently, leads to wider dynamic width. The effect of some disturbances during cutting on the behaviour of force signals is illustrated by a sample results as shown in *Fig. 5.6.* As shown in *Fig. 5.6.*a, a sudden increase in the magnitude of both feed F_x and radial F_z components was resulted from tool chipping and fracture. When chipping and fracture occurs, a new and wider tool-workpiece contact area is developed which increases the normal force on the clearance *[12]* (see *Fig. 2.7*). The vertical component F_y, however, shows almost no variation as a result of tool chipping. Nevertheless, vertical force F_y seems to be the most sensitive to the machining instability as shown in *Fig. 5.6.b* by the increased amplitude of force between the cutting time of 42-100s. At the end of this sub-test the workpiece surface was examined and it was found that at the region, between the times in question, three bright-spots were observed each of approximately 30 mm^2. These were associated with increased material hardness, i.e. hard spots, and were deemed responsible for the observed instability. *Fig. 5.6.c* shows the force signals for the last sub-test of *Test#3* where the local failure has occurred at the nose area while the other elements of the flank and the notch wear are of lower levels (see *Fig. 5.1.a).* This causes a sudden force increase followed by a steady fluctuation, but at a higher level. Again the vertical force component F_y is the least sensitive to local tool

failure. *Fig. 5.6.d* shows the force signals of the last sub-test of *Test#13* at which the tool failed catastrophically due to material softening or plastic deformation. The tool damage was spreading over the whole contact area so causing a rapid rate of increase of force for both feed F_x and radial F_z components. From the above discussion it may be concluded that a strong correlation exists between the force variation during cutting and the tool state.

In this section, the effect of several wear elements on the variation in the different force components, and on their ratios is investigated. Both linear and non-linear regression procedures are used to develop and examine the possible mathematical models of force and force-wear interrelationships. A complete set of force histories, for each test studied using the central composite design, (see *Table 4.2*), is shown in *Fig. 5.7.* For each sub-test, the static force value was determined by filtering and smoothing the corresponding dynamic signals using a specially written computer program. Each sub-test is represented by a single value at the end of cut and, for each test, the force-time curve consists of its successive sub-tests as shown in *Fig. 5.7.* Force-time curves shown in *Fig. 5.7* indicate a similar trend to that of wear-time relationship. After a few second of cut, a fixed value of initial force is attained followed by a second phase at which a longer period of uniform force rate is noticed. Finally, the force exhibits a higher rate of change near the end of the tool life. The magnitudes of initial forces are strongly dependent on the cutting variables used, particularly the feed and the depth of cut. Similar values of initial forces are found for both feed F_x and radial F_z components. The value of initial force for vertical component F_y is the largest in magnitude but typically, its ratio with F_x or F_z varies according to the conditions used, and to the levels of wear scars developed on the clearance face.

In the second phase of force-time curve, forces increase with rates depend on the cutting conditions employed especially the speed and the feed. The more severe these variables are, the higher the wear rates which will result and, as a result, greater variation is observed in the force values.

In the third region of the force-time characteristic, the forces vary differently for various force components. The radial component F_z is usually the most affected by the wear

level at the nose area. The effect of flank wear FW seems equal for each of the feed F_x and radial F_z components. However, a quantitative explanation of the characteristics of the force-wear-conditions interrelation may be obtained by the mathematical formulation of the relevant parameters.

5.3.1 Mathematical Models for Initial Forces

The initial force system can be defined as that which results when the workpiece is machined by a sharp tool. As explained by many investigators *[9 & 23]*, the initial force for a given tool-workpiece combination basically depends on the cross-sectional area of the cut. The effect of the cutting speed on the initial force has been studied as early as 1946 when *Arnold [125]* indicated that the force tended to decrease by increasing cutting speed up to certain limit after which the force magnitude was slightly affected by any further increase. At low cutting speed, high force are generally obtained due to the welding occurring between the tool and the chip thus forming a built-up-edge *[126]*. An increase in the cutting speed causes an increase in the shear angle which results in a shorter length of the shear plane and, in turn, causes a reduction in tool forces.

In this study, the initial forces for a particular component is considered as the intercept by projecting the force-time curves back to zero cutting time. A total of 24 data points is obtained for each force component and these are used to develop mathematical models which relate the initial force to the cutting conditions- speed, feed, and depth of cut.

A first-order model using linear regression procedure is found to adequately fit the experimental data for each force component in turn. Tests of significance and adequacy have revealed nothing against the characteristics of the models which take the forms:

$$F_{xo} = 318.62\ F^{0.33}\ d^{1.062}; \tag{5.18}$$

$$F_{yo} = 2344.9\ V^{-0.064}\ F^{0.729}\ d^{0.993}; \tag{5.19}$$

$$F_{zo} = 699.20\ V^{-0.146}\ F^{0.359}\ d^{0.880}; and, \tag{5.20}$$

	Correlation Factor R^2	Standard Error SE	F-Ratio
F_{xo}	0.89	0.091	86
F_{yo}	0.99	0.042	790
F_{zo}	0.90	0.090	59
F_{xzo}	0.91	0.082	68

Table 5.3 Statistical Characteristics of the Models of Initial Force

$$F_{xzo} = 727.8\ V^{-0.109}\ F^{0.324}\ d^{0.998}. \tag{5.21}$$

where F_{xo}, F_{yo}, F_{zo}, *and* F_{xzo} are the initial force for the feed, the vertical, the radial, and the thrust components respectively. Statistical criteria for these models are listed in *Table 5.3*. The thrust component F_{xzo} is the resultant cutting force in the horizontal plane normal to the cutting edge (see *Fig. 2.7*). This component is thought to have a better correlation with tool wear than if an individual component would has been used.

The models of the initial force (5.18 – 5.21) signify the strong dependence of the initial force on the cutting conditions, especially the depth of cut and the feed. For the feed component F_x, the influence of the cutting speed is not significant enough to be included into the model. However, both of the vertical F_y and the radial F_z components are negatively affected by the cutting speed for given values of feed and depth of cut. The depth of cut has the strongest effect on the force magnitude for all components. The effect of feed is found similar for the feed and the radial components, while similar effect of depth of cut is observed for the vertical and the thrust components. This indicates that the ratio of the initial values for each of the feed or the radial components to the vertical one depends only on the value of feed used. To confirm this phenomenon, the same set of data is used to establish a quantitative relationships of the ratios of various force components. This has resulted in the following set of equations:

$$(F_{xo}/F_{yo}) = \ 0.193\ F^{-0.4}; \tag{5.22}$$

$$(F_{zo}/F_{yo}) = \ 0.186\ F^{-0.37}; \textit{and}, \tag{5.23}$$

$$(F_{xzo}/F_{yo}) = \ 0.253 \ F^{-0.405}. \tag{5.24}$$

For the range of feeds used in this study ($0.06 - 0.6\ mm/rev$), the ratio of the feed to the vertical components (F_{xo}/F_{yo}) varies between 0.24 and 0.59, while for the radial to the vertical (F_{zo}/F_{yo}), it varies between 0.22 and 0.53. This contradicts the general idea which has been long established that the relative magnitudes of the different force component are constant and independent of cutting conditions. However, the fact that force ratio is independent of both cutting speed and depth of cut may help in isolating the effect of tool wear progress on the variation of cutting forces. However, these relationships represent merely the situation when the tool is sharp and further investigation is required to determine the force characteristic under various levels of tool wear.

5.3.2 Effect of Tool Wear on the Force Characteristics

The effect of wear progress on the instantaneous value of force components $F_i(t)$ is investigated through the establishment of the mathematical formulae to relate each of force component to the relevant parameters of wear elements; cutting conditions; and, cutting time. The whole set of data (669 data points) for the *CCD* are used to find the best possible functional relationships. Among the different structures of models, the first-order linearized model is found to give the best results. The resulting models are of the forms:

$$F_x(t) = 22248\ V^{-.45}\ F^{.24}\ d^{.93}\ t^{-.15}\ NW^{.45}\ FW^{.41}\ NCW^{.13}; \tag{5.25}$$

$$F_y(t) = 8400\ V^{-.96}\ F^{.36}\ d^{.83}\ t^{-.00}\ NW^{.12}\ FW^{.58}\ NCW^{.03}; \tag{5.26}$$

$$F_z(t) = 66138\ V^{-.50}\ F^{.25}\ d^{.51}\ t^{-.20}\ NW^{.69}\ FW^{.41}\ NCW^{.14}; and, \tag{5.27}$$

$$F_{xz}(t) = 47525\ V^{-.47}\ F^{.24}\ d^{.77}\ t^{-.17}\ NW^{.54}\ FW^{.41}\ NCW^{.13}. \tag{5.28}$$

When the average wear is used instead, the following models are resulted:

$$F_x(t) = 23861\ V^{-.450}\ F^{.235}\ d^{.883}\ t^{-.154}\ AW^{.982}; \tag{5.29}$$

$$F_y(t) = 8375\ \ V^{-.180}\ F^{.627}\ d^{.884}\ t^{-.049}\ AW^{.342}; \tag{5.30}$$

	Correlation Factor R^2		Standard Error SE		F-Ratio	
	Wear Elements	AW	Wear Elements	AW	Wear Elements	AW
F_x	0.84	0.84	0.116	0.117	492	672
F_y	0.97	0.97	0.060	0.062	3170	4156
F_z	0.83	0.81	0.130	0.137	456	563
F_{xz}	0.84	0.83	0.117	0.120	509	670

Table 5.4 Statistical Criteria for Models of Force Wear Relationship [(5.25)-(5.32)]

$$F_z(t) = 86509\ V^{-.526}\ F^{.243}\ d^{.440}\ t^{-.200}\ AW^{1.270}; and, \tag{5.31}$$

$$F_{xz}(t) = 55354\ V^{-.484}\ F^{.236}\ d^{.715}\ t^{-.173}\ AW^{1.099}. \tag{5.32}$$

Statistical criteria for this set of models are listed in *Table 5.4.* Among the various force components, the vertical component F_y seems to be the least affected by the tool wear. Among the different wear elements, the notch wear NCW has the least influence on all force components. The effect of the flank wear FW is found similar for both the feed and the radial components. The nose wear NW affects the radial component F_z more than it does for the feed component F_x. However, the global effect of tool wear as it is represented by the average value AW seems to be higher for the radial component F_z.

To investigate the effect of tool wear on the different force ratios, the following models are resulted:

$$(F_x(t)/F_y(t)) = 2.65\ V^{-.26}\ F^{-.39}\ d^{.07}\ t^{-.10}\ NW^{.28}\ FW^{.26}\ NCW^{.10}; \tag{5.33}$$

$$(F_z(t)/F_y(t)) = 7.87\ V^{-.32}\ F^{-.38}\ d^{-.35}\ t^{-.15}\ NW^{.51}\ FW^{.26}\ NCW^{.11}; and, \tag{5.34}$$

$$(F_{xz}(t)/F_y(t)) = 5.64\ V^{-.29}\ F^{-.39}\ d^{-.09}\ t^{-.12}\ NW^{.37}\ FW^{.26}\ NCW^{.11}. \tag{5.35}$$

For a given cutting conditions, force ratios are positively affected by the level of wear elements on the clearance face. The nose wear NW has the most influence on the force ratios with higher effect on the ratio (F_z/F_y). A similar effect is observed on the different force ratios of each of the flank wear FW and the notch wear NCW.

Generally, forces on the cutting tool are strongly influenced by wear progress on the tool's clearance face so that it can be applied for an in-process monitoring strategy. However, for a universal approach to be developed, the force variation due to only wear variation should be properly separated from other effects caused by the cutting conditions.

5.3.3 The Detection of Tool Failure by Force Variation

One disadvantage of the linear force models (5.25 – 5.32) is that the force variation is a function of too many interrelated variables. However, for an in-process technique to be more universal, the detector variable should rely on as a few parameters as possible and the variation due to other effects should be eliminated. One approach is to isolate the different effects from each other so that they can be dealt with and accounted for individually. Even though the implementation of such idea was almost impossible in the past due to computational and modelling difficulties, it is now possible since the non-linear regression techniques are well qualified to deal with such problems.

The force-time trend, as shown in *Fig. 5.7,* can be expressed by the following relationship:

$$F_i = F_{io} + bo\,(W - W_o)^{b1}, \tag{5.36}$$

where F_i can be either F_x, F_y, F_z, *or* F_{xz}, *and* F_{io} is the corresponding initial value. The wear W can be either NW, FW, NCW, or AW, while W_o is the initial wear in the running-in area.

As explained earlier, each of the initial wear and the initial force are cutting conditions dependent and therefore, Eq. (5.36) may be re-written to take the form:

$$F_i = ao\,V^{a1}\,F^{a2}\,d^{a3} + bo\,(W - co\,V^{c1}\,F^{c2}\,d^{c3})^{b1}. \tag{5.37}$$

Since this model cannot be linearized using a simple logarithmic transformation, the non-linear procedure was the only way to fit the data and then, to estimate the coefficients in the final equation. However, due to some computational difficulties such as

underflow and overflow involved in the non-linear estimation procedure, the structures of the models models were continuously adapted to give the best results. Although it was a very expensive computational procedures, non-linear models of very high quality are resulted. The final developed models are summarized as follows:

A) Feed Component F_x

$$F_x = 459\, F^{.32}\, d^{.96} + 3397\, [AW^{1.95} - .012 \ln V]; \quad (R^2 = .86). \tag{5.38}$$

$$= 294\, F^{.48}\, d^{1.39} + 3346\, AW^{1.99}; \quad (R^2 = .85). \tag{5.39}$$

$$= 327\, F^{.38}\, d^{1.22} + 1844\, NW^{2.19}; \quad (R^2 = .91). \tag{5.40}$$

$$= 386\, F^{.41}\, d^{1.11} + 4338\, FW^{2.56}; \quad (R^2 = .76). \tag{5.41}$$

$$= 354\, F^{.36}\, d^{1.14} + 1497\, NW^{2.64}\, FW^{-.72}\, NCW^{.41}; \quad (R^2 = .92) \tag{5.42}$$

$$= 629\, F^{.30}\, d^{.720} + 1199\, (NW^{3.58} - .023\, V^{.27}) \\ (FW^{-.66} - 0.23\, V^{.27})\, (NCW^{.03} - 0.23\, V^{.27}); \quad (R^2 = .94) \tag{5.43}$$

B) Vertical Component F_y

$$F_y = 1829\, F^{.97}\, d^{1.14} + 1373\, [AW^{.35} - .073 \ln V]; \quad (R^2 = .97). \tag{5.44}$$

$$= 1930\, F^{.90}\, d^{1.05} + 1049\, AW^{.95}; \quad (R^2 = .97). \tag{5.45}$$

$$= 1907\, F^{.87}\, d^{1.04} + 742\, NW^{.83}; \quad (R^2 = .97). \tag{5.46}$$

$$= 1995\, F^{.87}\, d^{1.00} + 1049\, FW^{.99}; \quad (R^2 = .96). \tag{5.47}$$

$$= 1916\, F^{.89}\, d^{1.05} + 1047\, NW^{.49}\, FW^{.23}\, NCW^{.22}; \quad (R^2 = .97). \tag{5.48}$$

$$= 1862\, F^{.94}\, d^{1.11} + 2677\, (NW^{.24} - .05 \ln V) \\ (FW^{.23} - .05 \ln V)\, (NCW^{.16} - .05 \ln V); \quad (R^2 = 0.94). \tag{5.49}$$

C) Radial Component F_z

$$F_z = 475\, F^{.69}\, d^{1.0} + 3914\, [AW^{1.73} - .004 \ln V]; \quad (R^2 = .86). \tag{5.50}$$

$$= 415\, F^{.82}\, d^{1.19} + 3893\, AW^{1.75}; \quad (R^2 = .85). \tag{5.51}$$

$$= 418\, F^{.58}\, d^{1.01} + 2351\, NW^{1.82}; \quad (R^2 = .93). \tag{5.52}$$

$$= 592\, F^{.60}\, d^{.750} + 4731\, FW^{2.22}; \quad (R^2 = .72). \tag{5.53}$$

$$= 425\, F^{.56}\, d^{.980} + 2247\, NW^{1.90}\, FW^{.18}\, NCW^{-.23}; \quad (R^2 = .93). \tag{5.54}$$

$$= 500\, F^{.46}\, d^{.810} + 2377\, (NW^{1.93} - 0.007 \ln V)$$
$$(FW^{.26} - .007 \ln V)\, (NCW^{-.33} - .007 \ln V); \quad (R^2 = 0.93). \tag{5.55}$$

D) Thrust Component F_{xz}

$$F_{xz} = 612\, F^{.42}\, d^{.97} + 4896\, [AW^{1.86} - .009 \ln V]; \quad (R^2 = .87). \tag{5.56}$$

$$= 442\, F^{.58}\, d^{1.31} + 4846\, AW^{1.89}; \quad (R^2 = .87). \tag{5.57}$$

$$= 479\, F^{.44}\, d^{1.15} + 2782\, NW^{2.02}; \quad (R^2 = .93). \tag{5.58}$$

$$= 604\, F^{.47}\, d^{0.99} + 6120\, FW^{2.41}; \quad (R^2 = .76). \tag{5.59}$$

$$= 500\, F^{.42}\, d^{1.11} + 2509\, NW^{2.23}\, FW^{-.18}\, NCW^{.03}; \quad (R^2 = .93). \tag{5.60}$$

$$= 472\, F^{.43}\, d^{1.15} + 2547\, (NW^{2.20} + 103\, V^{-2.29})$$
$$(FW^{-.18} + 103\, V^{-2.29})\, (NCW^{.03} + 103\, V^{-2.29}); \quad (R^2 = 0.94). \tag{5.61}$$

The strong correlation is clear between the force variation and wear progress. From the statistical standpoint, these models are more precise to represent the functional interrelation between the dependent variable F_i and the set of the independent variables. For instance, the values of the correlation factor for Eqns. (5.42), (5.48), (5.54), and (5.60) are 0.92, 0.97, 0.93, and 0.93 respectively while the corresponding values for the linear models (5.25 – 5.28) are only 0.84, 0.97, 0.83, and 0.84. This indicates that the force variation is more accurately detectable if the effect of the tool wear is properly isolated from the other effects of cutting conditions and cutting time. However, a careful investigation of these models is required to choose from the one which is most sensitive to wear progress.

The effect of excluding the cutting speed may be examined by comparing the models when it is included and when it is not. The results indicate that the cutting speed can be confidentiality removed without degrading the predictive capability of the models. The worst recorded case is for the pair of models (5.42) and (5.43) when a insignificant reduction in the values of the correlation factor from 0.94 to 0.92 is observed. Thus, it may be concluded that for a given tool-workpiece combination, the force variation, after attaining an initial value, which mainly depends on the cut cross-sectional area, corresponds only to the amount of wear developed on the clearance face.

As concluded previously, the force variation is found to be differentially influenced by the various wear elements. However, for the purpose of an in-process tool wear monitoring to be reliable and more accurate, both of the most predominant wear element and the most sensitive force component should be selected.

The rate of change due to wear progress of the vertical force F_y is noticed to be the least among all components, which makes it a less reliable for an in-process purposes. This is expected since the vertical component is predominantly determined by the cross-section of a cut and changes only slightly as a tool wears, while both the feed and the radial components are mainly penetrating and frictional loads and very sensitive to wear. Between the components of feed F_x and radial F_z, their resultant (the thrust component F_{xz}) tends to give slightly better results. However, a conclusion may be drawn that any of the feed component F_x, the radial component F_z, or the thrust component F_{xz} may be satisfactorily used to detect tool failure and to predict tool wear levels. *Fig. 5.8* shows the plots of the predicted values from both of the linear continuous model (5.28) and the non-linear discrete model (5.60), together with the experimental data, of the same set of tests used in producing *Fig. 5.2.* It can be seen that both models fit the experimental data very well. However, the non-linear model is superior at the end of tool life especially in the cases when the tool fails catastrophically. The poor fit for *Test#6* reaffirm that this test is abnormal and this conclusion was reached when a tool life model was processed. By observing the plots

for all the 24 tests of the *CCD,* this test was the least reliable in every respect. The tool used exhibited lower values of wear than those identical trials nos. 5, 11, and 12. Almost the same conclusion is noticed from *Fig. 5.9* when the average wear AW is used in place of the individual wear elements (models (5.32) and (5.57)).

However, the low values of correlation factor when only the flank wear FW is used as a regressor for the force variation may discard the idea of using it as an in-process detector. Again, either the nose wear NW or the average wear AW may be adequately used in the purpose of an in-process tool wear detection. This is noticeably from *Fig. 5.10* when both models of nose wear (5.58) and average wear (5.57) are plotted against the experimental data for the same set of tests used in producing *Fig. 5.9.* The high quality of the predictive capability of the models can be noticed especially at the end of the tool life when the forces rapidly increase due to the tool failure.

In the actual situation, the force transducer can be used to measure the various force components and the values of wear level may be estimated accordingly. This requires a mathematical formulation in which the tool wear is regressed on the variation of the cutting forces. This functional relationship can be approximated as:

$$W = W_o + ao\ (F_i - F_{io})^{a1}. \tag{5.62}$$

Since W_o and F_i are basically dependent on the cutting conditions, this equation may be re-arranged to take the form:

$$W = bo\ F^{b1}\ d^{b2}\ V^{b3} + ao'\ (F_i)^{a1'}, \tag{5.63}$$

where the coefficients bo and ao' usually depend on the tool geometry; the workpiece hardness; and, the type of lubricant. While both the tool geometry and the type of lubricant may be considered constant for the same set of tool and cutting conditions, the effect of the variation in the workpieces hardness may be dealt with by using the ratio of either the feed component F_x, or the radial component F_z, to the vertical component F_y *[90].* Thus, *Eq. 5.63* may be take the form:

$$W = bo\ V^{b1}\ F^{b2}\ d^{b3} + b4\ (F_i/F_y)^{b5}. \tag{5.64}$$

Non-linear regression procedure using the experimental data resulted in the following form of models:

$$AW = 0.132\ F^{0.58}\ d^{0.35} + 0.35\ (F_z/F_y)^{1.147}; and, \tag{5.65}$$

$$NW = 0.255\ F^{0.96}\ d^{0.23} + 0.48\ (F_z/F_y)^{1.321}. \tag{5.66}$$

The improvement gained by applying the force variation is clear from *Fig. 5.11* for average wear AW and, from *Fig. 5.12* for the nose wear NW. These figures are a re-production of *Fig. 5.3* after adding the non-linear model (5.65). Even though the linear model has a better capability to estimate wear levels in the early stages of the tool life, it fails to detect the tool failure and breakage at the end of tool life. This is accurately detected by the non-linear model using the ratio of the radial to the vertical components (F_z/F_y). The variation in this ratio is very sensitive to wear change on the clearance face. For *Test#1, Fig. 5.11,* no change is noticed in the estimated wear level until the point of 105 minutes cutting time where a higher increase in the ratio (F_z/F_y) is observed. As shown in the wear-time curves in *Fig. 5.1.a,* a sudden increase of the wear level from 0.24 to 0.29 mm occurred on the nose area at that moment. The same has happened for *Test#6* at 30 minutes time and this explains the increase in the estimated wear levels shown in *Fig. 5.11.*

For *Test#14* in *Fig. 5.11,* a sudden decrease in the estimated wear values is noticed within the period between 90 and 133 minutes cutting. This drop of force values is noticed in the magnitudes of each of the vertical and the radial components as shown by *Fig. 5.7.b.* During this period of cutting, a tool failure has occurred at the nose area as shown in *Fig. 5.1.b* and, the resulting recess was filled of workpiece material. The frequent formation and breakage of this weld junction caused tool chatter and machining instability. During the wear measurement it was very difficult to remove this hard spot from the tool edge lest for the damage of the tool. This gave a misleading setting of the depth of cut for the successive cuts so that less material was machined and therefore, lower cutting forces were resulted. The hostile conditions of low cutting speed of 50 m/min used in this test has maintained this mechanism until a further uniform deformation had occurred on the nose area resulting in higher force values.

This indicates that not only the wear progress and tool failure but also the random disturbances and machining instability can be detected by observing the variation in the force or in the force ratios.

In **Chapter 6,** however, the possible detection of the random disturbances and system instability are investigated using the tool dynamic characteristics.

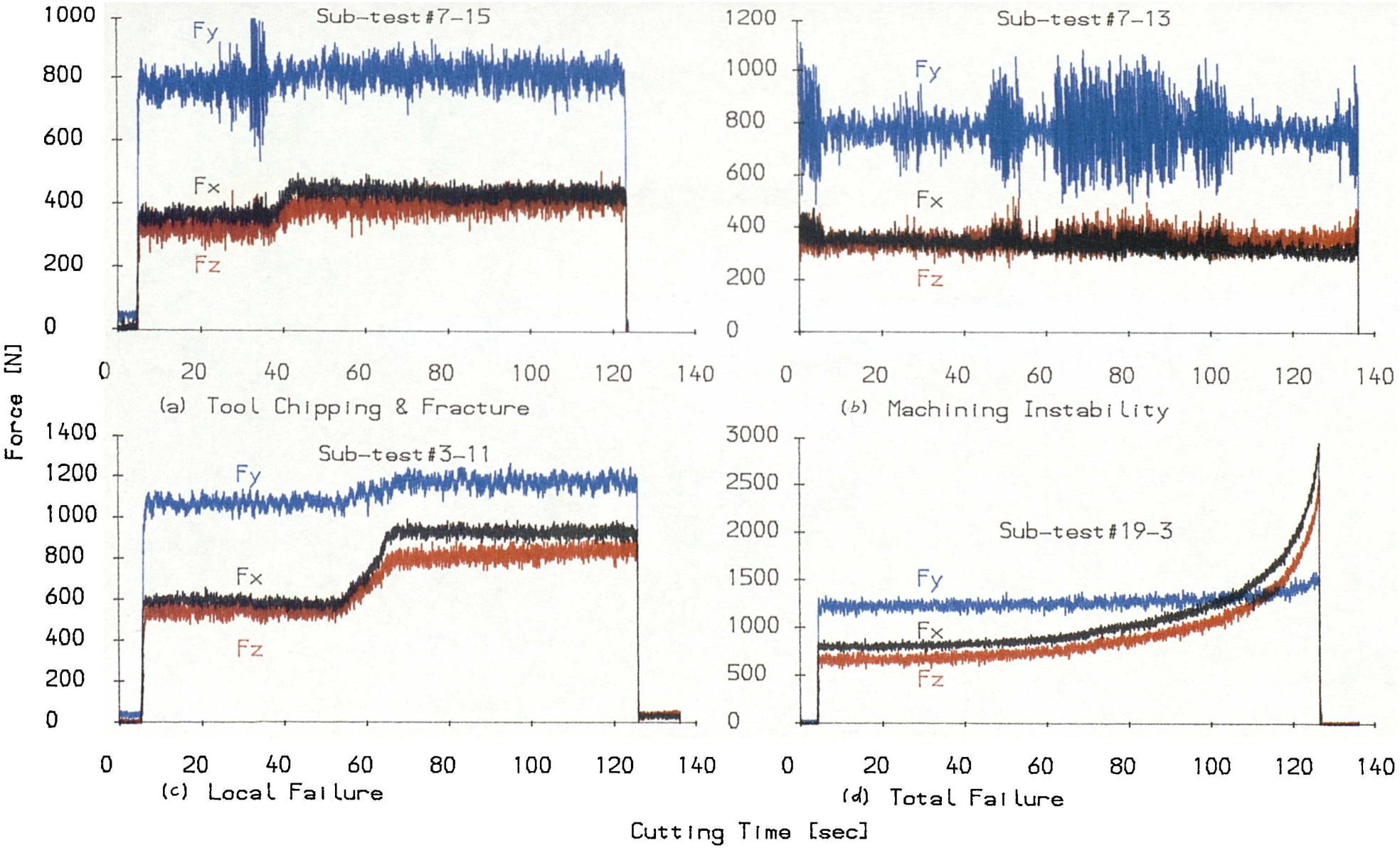

Fig. 5.6 Dynamic Force Signals as Affected by Cutting Disturbances

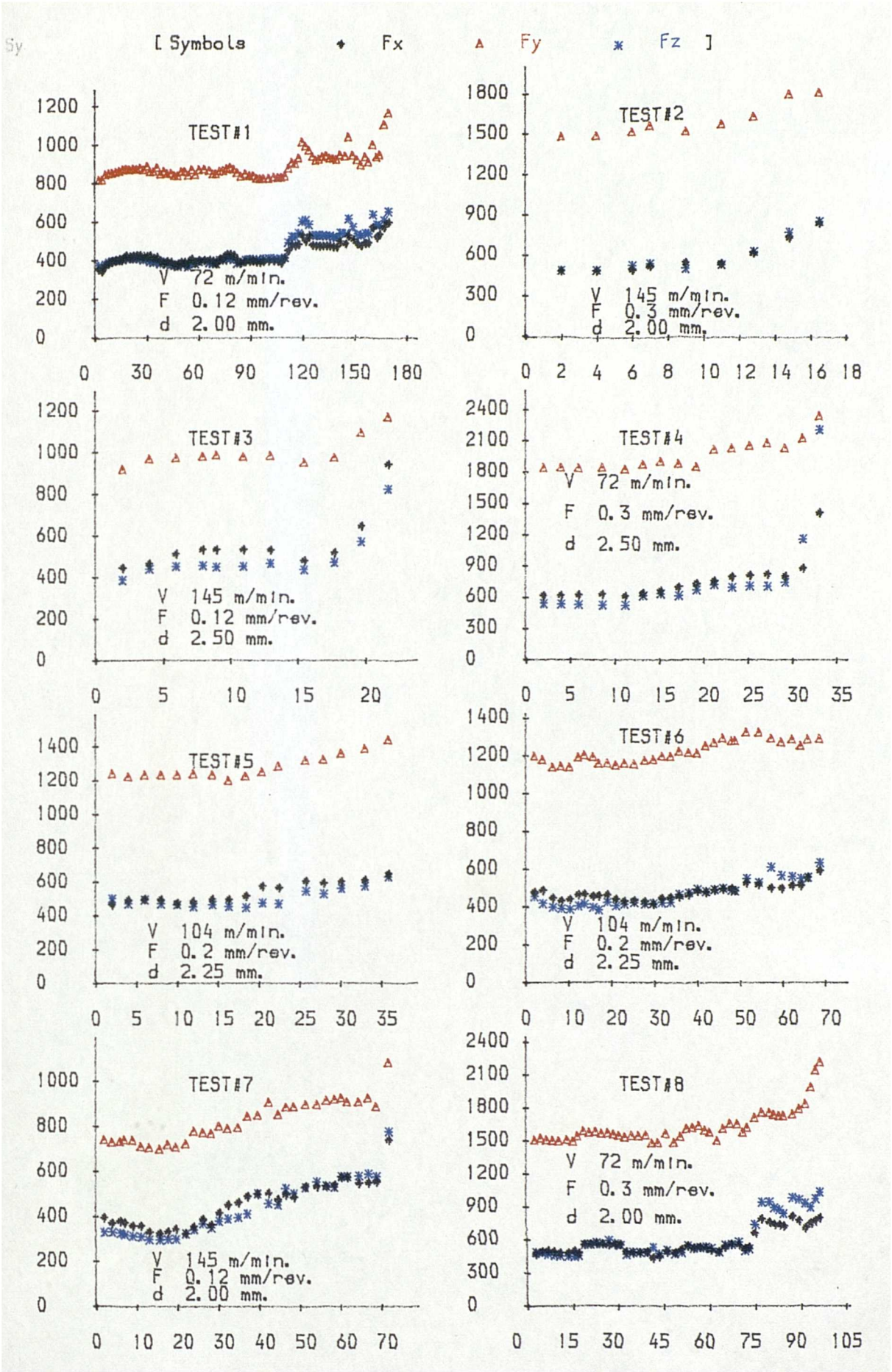

Fig. 5.7.a Force-Time Curves for Different Force Components for Tests [1-8]

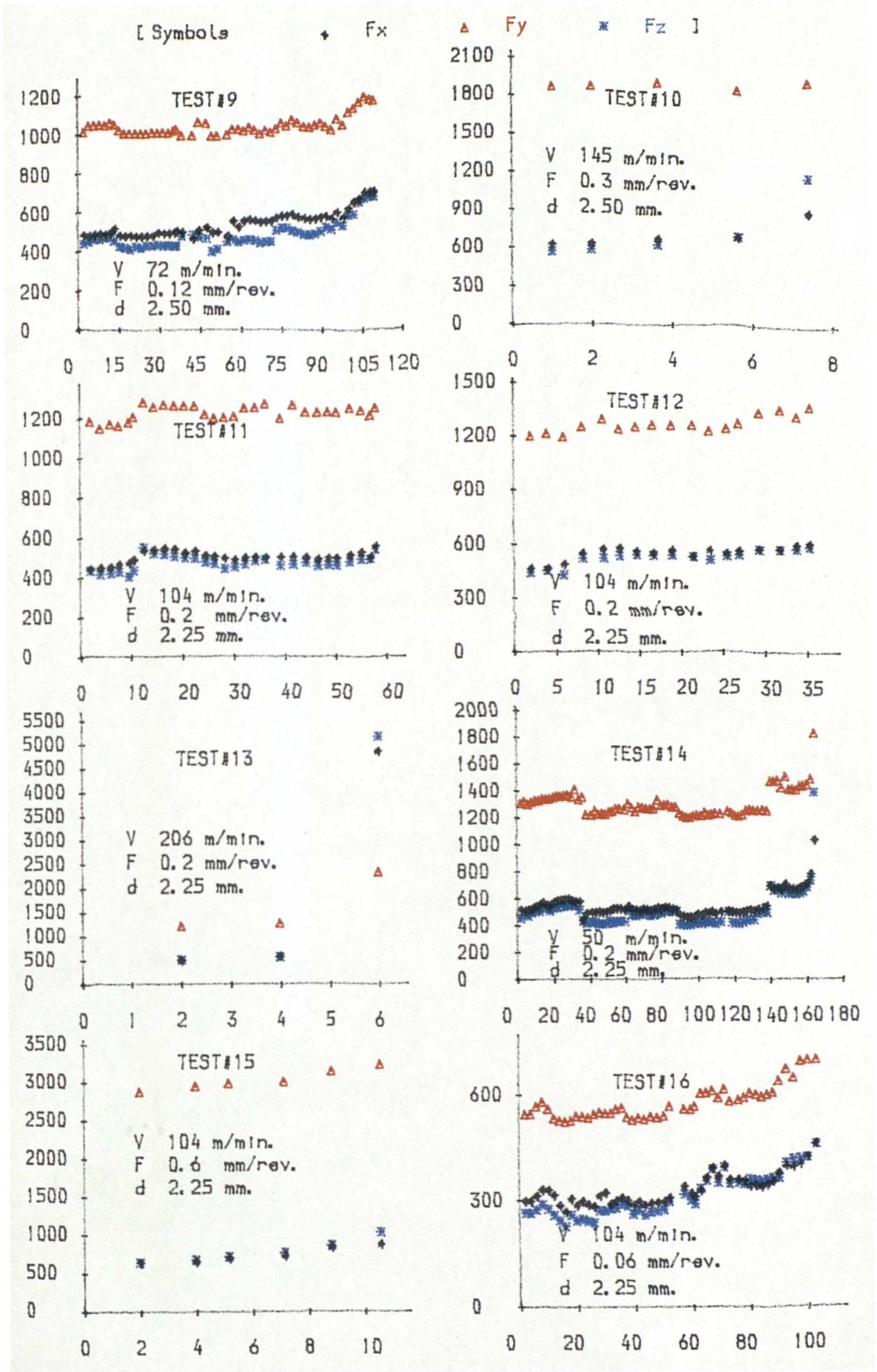

Fig. 5.7.b Force-Time Curves for Different Force Components for Tests [9-16]

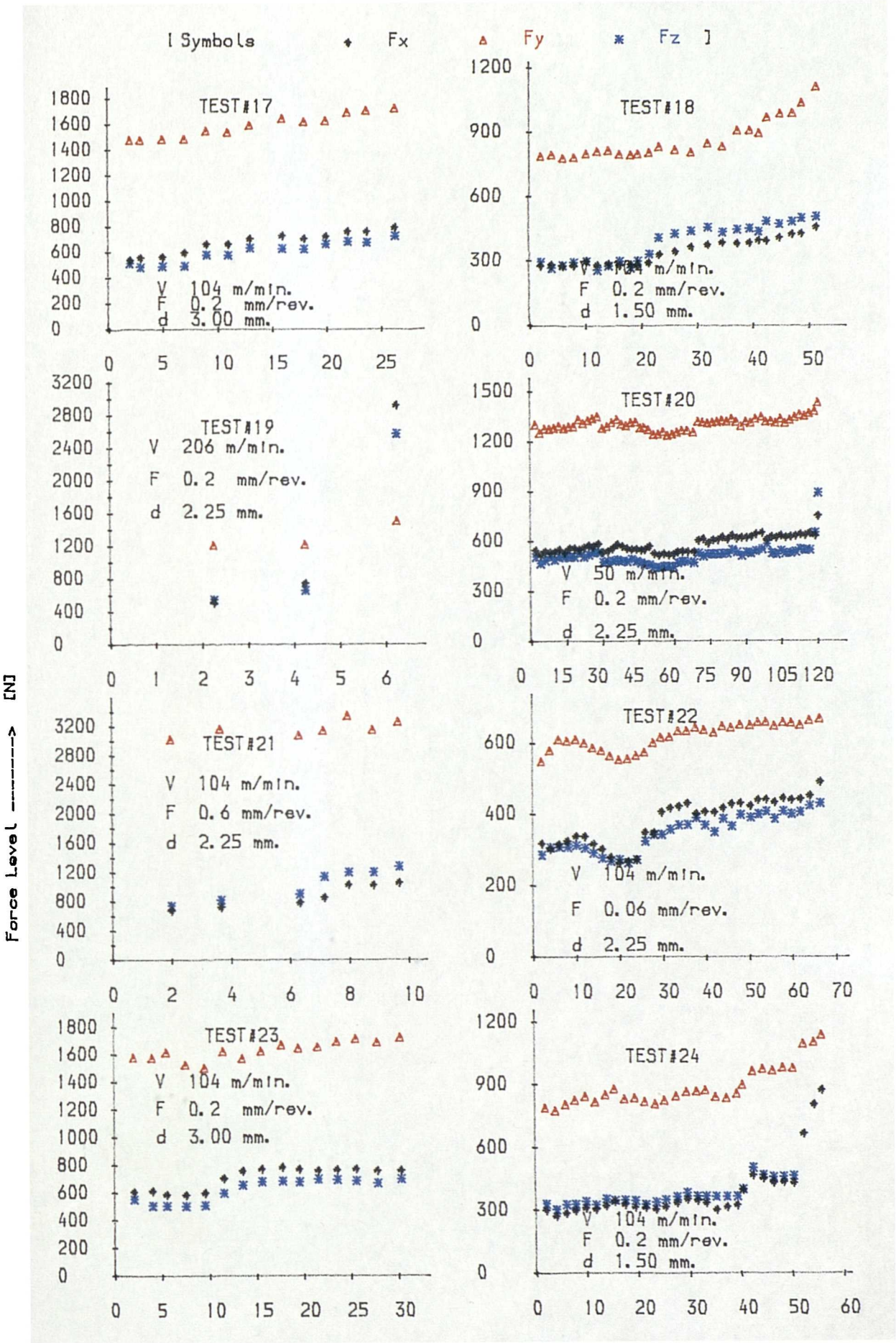

Fig. 5.7.a Force-Time Curves for Different Force Components for Tests [17-24]

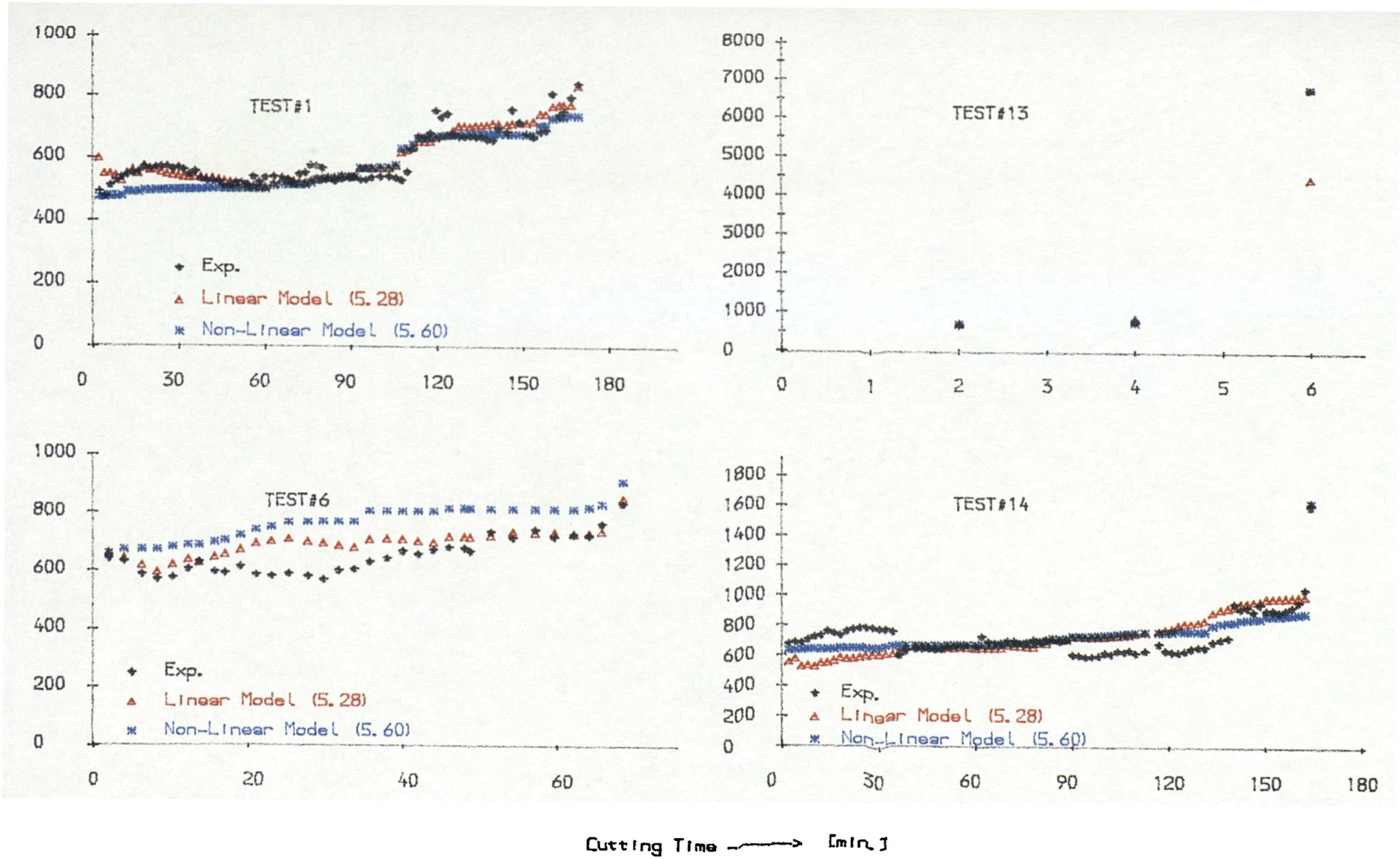

Fig. 5.8 Experimental and Predicted Values of Thrust Force using Linear and Non-linear Model

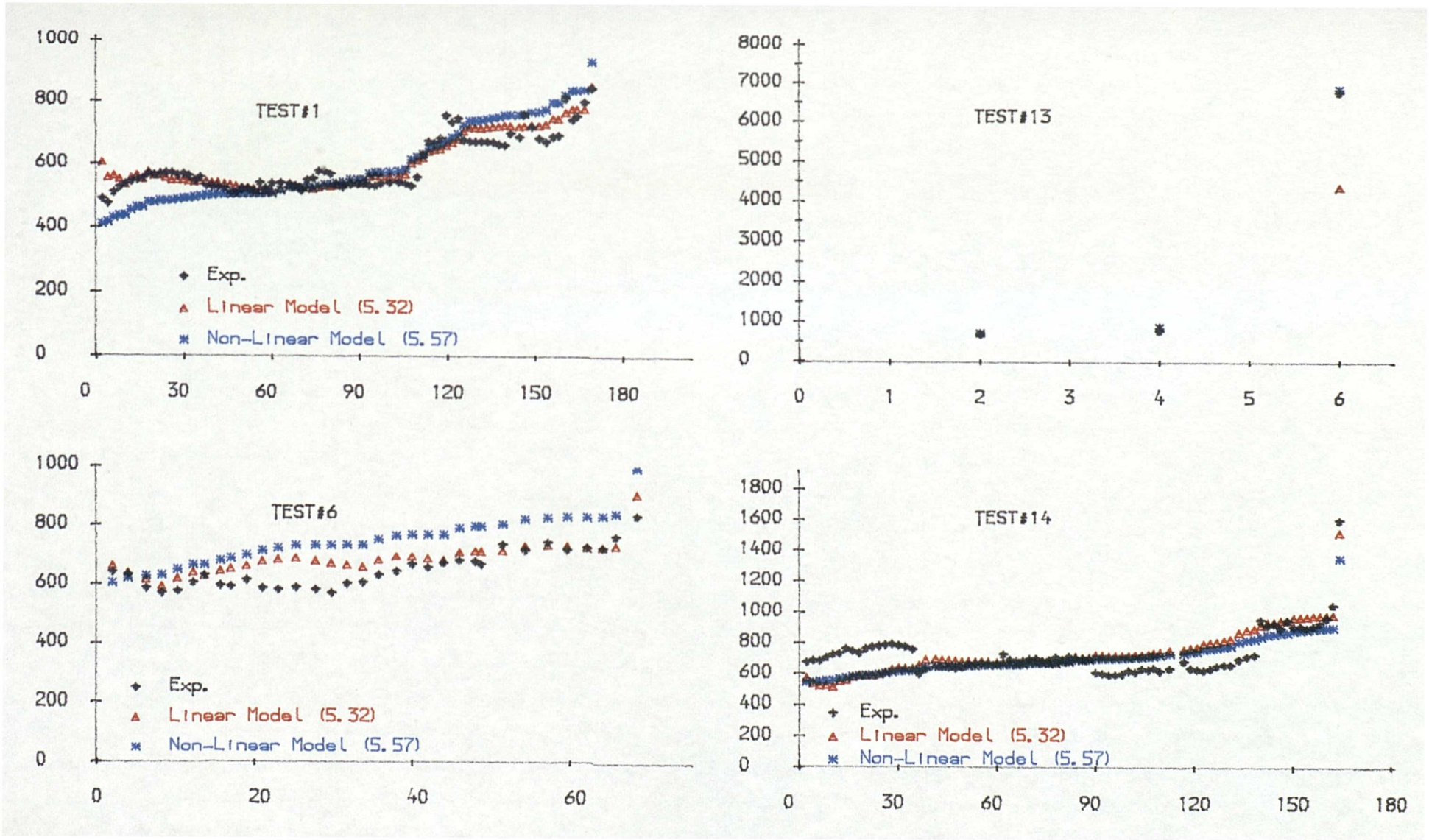

Fig. 5.9 Experimental and Predicted Values of Thrust Force using Linear and Non-linear Model

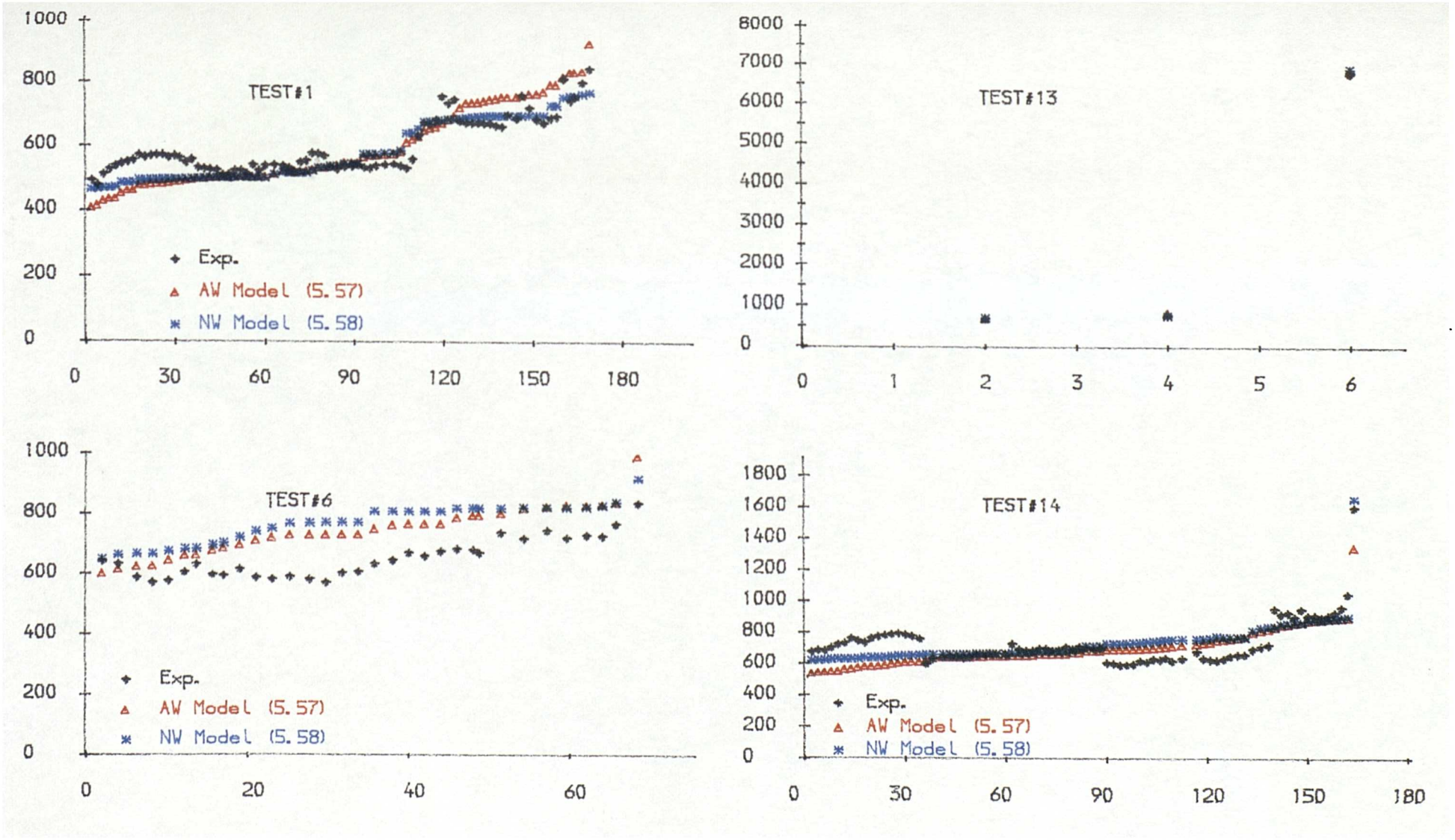

Fig. 5.10 Comparison Between Average and Nose Wear to Predict Thrust Force Component

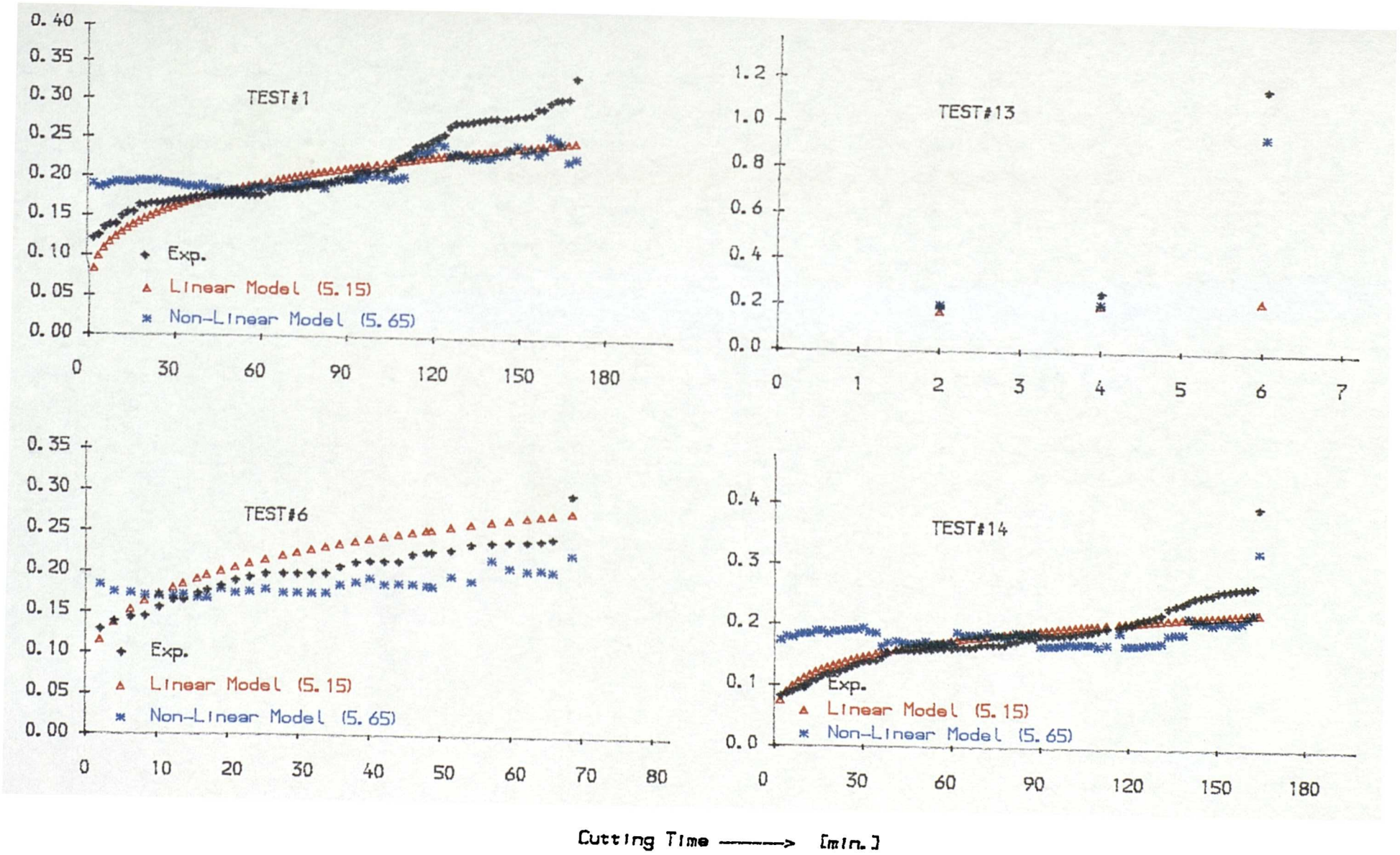

Fig. 5.11 Comparison Between Linear and Non-Linear Models to Estimate Average Wear

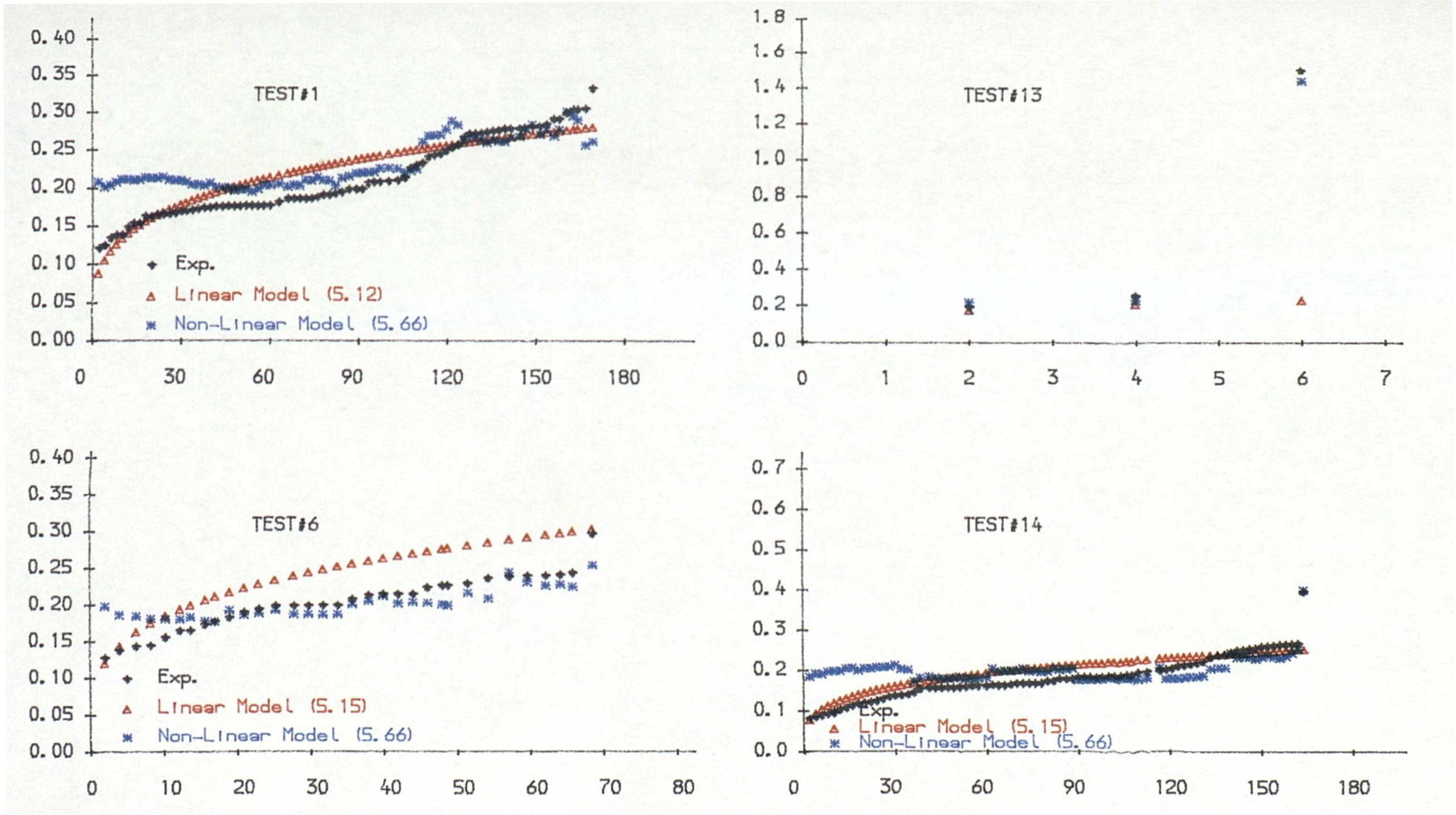

Fig. 5.12 Comparison Between Linear and Non-Linear Models to Estimate Nose Wear

5.4 Conclusions

In this chapter, mathematical models are developed of the tool wear and cutting forces. Results of this study may be summarized as follows:

1. The establishment of wear-time polynomial for an individual test has proved to be impractical since the resulting model is always affected by local characteristics of the test under investigation. In some cases, a first-order polynomial was adequate while in others, a polynomial of higher orders was required.

2. The mathematical models of the relationship between the wear level and the cutting conditions were found to be more appropriate in estimating the wear levels only within the region of constant wear rate. The point at which a tool fails catastrophically is usually not detectable by using this approach. Among the various wear elements on the clearance face, the average wear AW gives better results when it is used in models to simulate the functional variability in the wear-time conditions relationships.

3. Mathematical models are developed to relate the tool life to the cutting conditions-speed, feed, and depth of cut. Both of the nose wear NW and the average wear AW are found to be good criteria for tool life modelling. A first-order linearized model is found inadequate to fit the experimental tool life data. A second-order model is found to give better statistical criteria and to improve the models predictability. However, the resulting models are found to be affected by some outliers and influential cases. This increases the standard error of estimates and causes the residuals inhomogeneity. The careful examination of these influential cases indicates their abnormality and peculiarity and therefore, the robust regression procedures, via iteratively re-weighting least-squares, is used to minimize and dampen their influence. A considerable improvement is achieved in the statistical criteria and predictability of the models. Between the two types of tool life models, the one using the criterion average wear is found to be more consistent

and reliable.

4. The behaviour of tool lives within the operational region of speed and feed is examined by using the response surface methodology and surface contours. The tool life surface exhibits a non-linear trends especially at low-to-moderate range of cutting conditions. It has been found that for a low-to-moderate range of cutting speed, there is a certain value of feed of 0.12 mm/rev below it the tool life is positively affected by the value of feed employed.

5. The force variation during cutting has been found not only to well correlate with the wear level on the clearance face but to be very sensitive to any tiny disturbances such as tool chipping and machining instability. Mathematical models for various force components are developed to quantify such an interrelation. Each of the feed component F_x and the radial one F_z are found to be very sensitive to the gradual progress of tool wear. The effect of wear progress of the various wear elements on the different force components is investigated. The nose wear NW has the strongest influence on all force components with its highest effect on the radial component F_z. The flank wear FW equally affects both of the feed and the radial components. Among the various wear elements, the notch wear NCW has the least effect on all force components.

6. Mathematical models are developed to investigate the effect of cutting conditions and wear progress on the relative magnitudes of the force components. When the tool is new, each of the ratios (F_x/F_y) and (F_z/F_y) is found to be dependent on the value of feed employed. At later stages, the level of the nose wear has affected these ratios and with higher effect on the ratio (F_z/F_y). The ratio of (F_x/F_z) is found constant and insensitive to wear progress throughout the entire span of tool lives.

7. An approach of the tool failure detection using the force variation has been proposed. The force variation due to only the wear progress and tool failure has been properly isolated through the development of non-linear discrete models. The variation in the workpiece hardness is eliminated by using the force ratio as

an independent variable to detect the wear variation. The ratio of (F_z/F_y) has been found to give the best results when it is used in estimating and predicting both the gradual and the random forms of each of the nose wear and the average wear. The proposed approach has shown a good validity to be used for the purpose of an in-process monitoring of tool state for a wide range of cutting conditions and workpiece materials.

Chapter 6

MATHEMATICAL MODELS AND MONITORING STRATEGIES FOR TOOL CONDITION BASED ON TOOL VIBRATION CHARACTERISTICS

6.1 Introduction

The wear of a cutting tool in centre lathe turning operations is one of the most important limiting parameters in manufacture involving metal cutting. Since, as yet, the measurement of tool wear during continuous machining can not be made reliability, several attempts have been developed to monitor wear indirectly, which concentrated on the idea of finding a strong correlation between tool wear behavior, and one or more of the operating parameters. These parameters could be one or more of cutting variables; one or more of the system outputs (responses); or, one or more of the system characteristics. Details and an historical review of such techniques have been previously surveyed in **Chapter 2.**

Although some of the attempts have achieved part success in determining tool wear indirectly using cutting force and some other machining responses, such as those mentioned in *[72]*, further developments are still required before a computer aided tool management system can be realized for industrial applications.

In recent years, effort has been devoted to investigate the possibility of using tool vibration characteristics and system acoustic emission to predict; to estimate; or, to monitor manufacturing system conditions and tool wear behaviour.

The potential to use vibration to monitor tool wear drives from several reasons which are now discussed. Since in turning operations the tool is always in intimate contact with the workpiece, any change in the system vibration behaviour could lead to knowledge about the state of the cutting tool, and hence the technique provides a unique and attractive opportunity for monitoring the details of a cutting process. The considerable amount of information generated by vibration response provides, however, a formidable challenge to isolate; and, to characterize only those specific signatures and responses relevant to tool wear diagnosis.

Although the subject of the effect of tool wear on tool vibration has been handled

as early as *1946 [125]*, contradictory conclusions are the only outcome from reading through such literature. Some individual efforts claimed success in exploiting tool vibration to predict the tool state during cutting. A few years ago, *PERA [127]* revealed that a tool-breakage vibration-based device has been successfully built. Twenty years ago, Weller [128] claimed that there was a definite relationship between tool wear and the sound emitted during machining. Accordingly, tool wear detector hardware was built.

However, for a wear monitoring vibration-based approach to be universally accepted, a number of problems require solution. Firstly, one needs to isolate relevant information from the huge amounts of data in the noisy environments which the vibration signals are carried during industrial manufacture. Secondly, a flexible approach must be achieved which permits interchangeability among the different manufacturing systems; since different systems lead to variability in masses, weights, rigidity, stiffness, frequencies, etc. Thirdly, the designed strategy has to be economically feasible.

In this study, a tool wear monitoring vibration-based approach is investigated using advanced vibration analysis instrumentation such as the Fast Fourier Transform *FTT* analyzer; and, the Power Spectrum Technique *PST*. This includes the identification of the possible interrelation between the tool wear and tool vibration in stable centre lathe turning operation. The vibration element most sensitive to tool wear has been isolated. An in-process tool life determination vibration-based approach has been proposed. Finally a tool-wear prediction model using the force-vibration combination has been proposed which is capable of being used in real time manufacturing process control.

6.2 Tool Vibration In Centre Lathe Turning Operation

The cutting of metal in centre lathe turning is often considered as a steady state (static) process. As schematically shown in *Fig. 6.1.a*, it is a process in which cutting proceeds

with constant chip thickness; constant feed; constant cutting speed; constant cutting angles; and, with permanent sharp tool edge. Under these conditions, it is supposed that the resulting cutting force will remain constant. In practice, however, the cutting force fluctuates around an average value, *Fig. 6.1.b.* Such force variations are due to many factors, among them, variation in tool-chip friction; disturbances from out of balance rotating elements; tool striking a hard spot in the machined surface; cutting an existing irregular surface; etc. The tool thus changes its position relative to the chip and to the workpiece at periodic intervals. This in turn produces a variation of the chip thickness, feed, tool geometry, etc. This is referred as dynamic cutting.
When the tool vibrates it may achieve one or more of the shapes indicated in *Fig. 6.2.* Whether excessive vibration occurs depends on whether these initial oscillations will increase or decrease in amplitude. Therefore, dynamic cutting could be either stable or unstable. Unstable dynamic cutting produces high amplitude vibration which are known as chatter. Although the current work basically concerns stable dynamic cutting, a general review is next presented.

Tool vibration might be due to self-excited or to forced vibration or to both, and these two situations are now considered in turn:

6.2.1 Forced Vibration

Forced vibration results essentially from an external periodic force which is quite independent of the system on which it acts. The amplitude attained depends on the magnitude and frequency of this force and the inherent damping, but if the frequency is close to the natural frequency of the system, a large vibration may result from a relatively small force.
In other words, forced vibration is the response of the machine structure to the fluctuation of force acting on it. This is due to out of balance rotating masses; gear contact, varying chip thickness; discontinuous cutting (milling); etc. [129]. Therefore, forced vibration of machine tools can be remedied by accurate balancing, mounting on vibration

isolators, etc.

6.2.2 Self-Excited Vibration

A self-excited vibration results when the internal energy of a system varies in such a way that during a cycle of deformation, more energy is stored than is released during a single cycle.

Machine tool chatter is a self-excited vibration the amplitude of which can build up without the presence of any oscillatory force [130]. Chatter, therefore, results from the machine structure and the cutting force combining to form a dynamically unstable system, in which an infinitesimal amplitude of vibration can grow in an unbound fashion [130].

One of the most common forms of self-excited vibration in machine tools is regenerative chatter. Suppose, during cutting, the tool strikes a hard spot on the workpiece material, or the system is excited by any source of disturbances, then the machine is set into vibration to give relative tool-workpiece displacement, and hence a wave will be produced on the workpiece surface, Fig. 6.3.a. During the next revolution this wave causes a a variation of the chip thickness, Fig. 6.3.b, which produces a varying cutting force [130]. This varying force excites the system, and consequently, further relative displacement between tool and workpiece and hence the production of another wave in the machined surface. The surface is thus regenerated, on the leading edge in the case of turning, from one revolution to the next.
When the amplitude of the regenerated wave is larger than that of the generating wave, the amplitude will increase from one revolution to the next, and the system becomes unstable (chatter occurs). If, however, the amplitude decreases, the system is stable, and disturbances die out [130].

Tobias and Fishwick [131] considered machining chatter as a dynamic instability condition in which the force variations are brought about by the variation of chip

thickness (regenerative effect), by the variation in the feed penetration; and by the variation in the workpiece angular velocity.

Arnold [125] claimed that the only reason for the self-excited vibration was the decrease of the vertical cutting force F_y with increasing cutting speed, *Fig. 6.4.*, this is called the "falling characteristics ".

Jemielniak and Widota, [132], concluded that the spindle speed variation *(SSV)* during machining was one of the self-excited vibration sources. This confirmed the idea of falling characteristics proposed by *Arnold [125].*

However, *Marui et al. [133]* concluded that the chatter vibration occuring with turning tools is a self-excited vibration to which vibration energy is supplied due to the frictional force acting when the flank surface contacts the workpiece.

Tobias [134] stated that even with a falling characteristics, it is doubtful whether the negative damping introduced is large enough to overcome the positive damping of the system.

Doi and Kato [135] indicated that chatter is self-induced and caused by a lag in the fluctuation of horizontal cutting force F_x behind the horizontal vibration of work. Because of such lag, an amount of energy per cycle is maintained resulting in increased vibration of the workpiece. Also, it was ascertained by them, *[135],* that in some cases of cutting without chatter, the fluctuation in horizontal cutting force F_x lagged behind the variation of undeformed chip thickness. In recent research, *Mauri et al. [136]* have reached absolute agreement with the results of *Doi and Kato [135].*

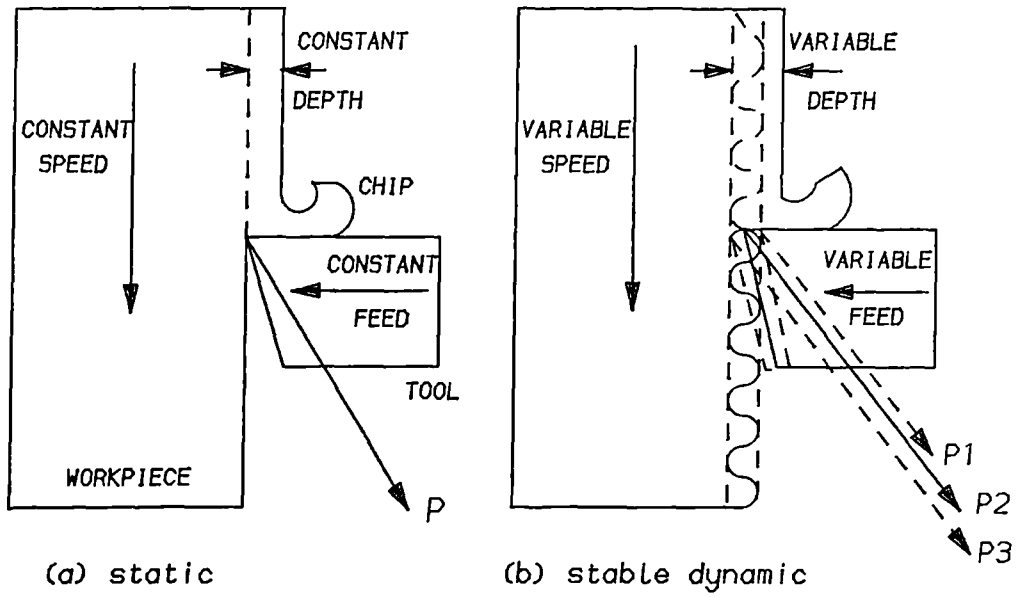

Fig. 6.1 Static and Dynamic Cutting

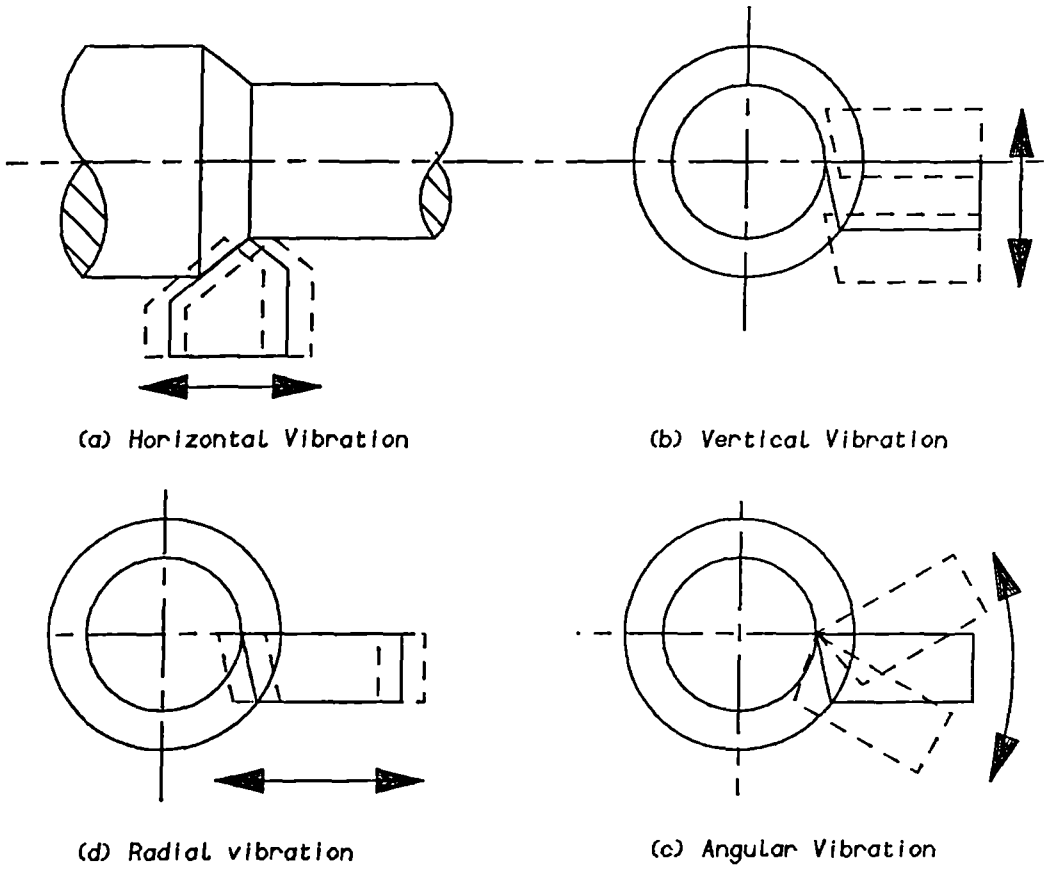

Fig. 6.2 Tool-Work Relative Oscillation Types

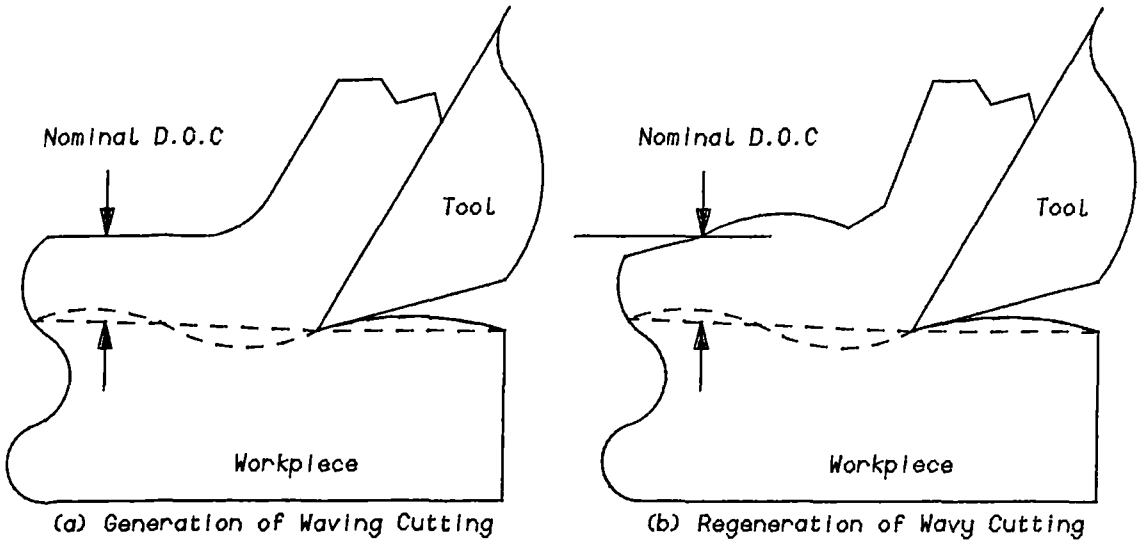

Fig. 6.3 Regenerative Chatter Due to Chip-Thickness Variation

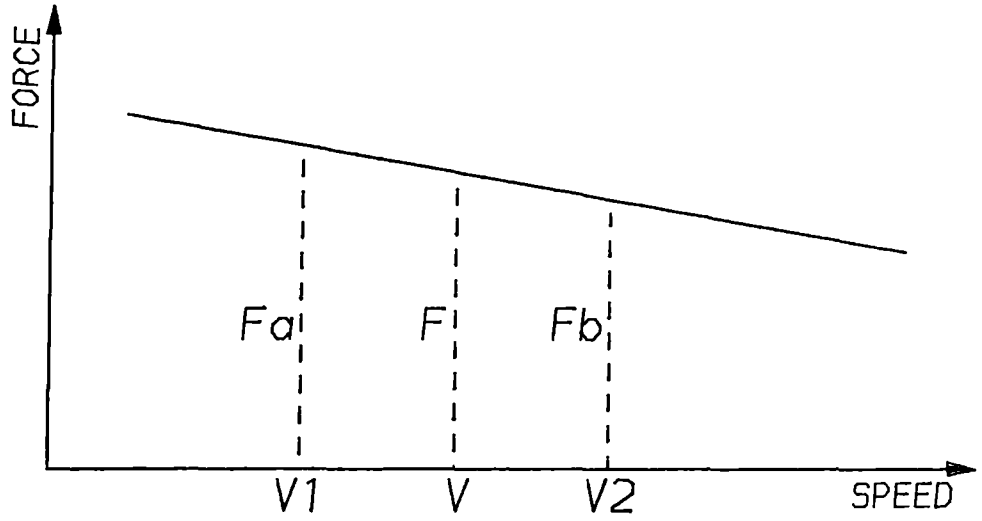

Fig. 6.4 Force Drop Due to Speed Increase

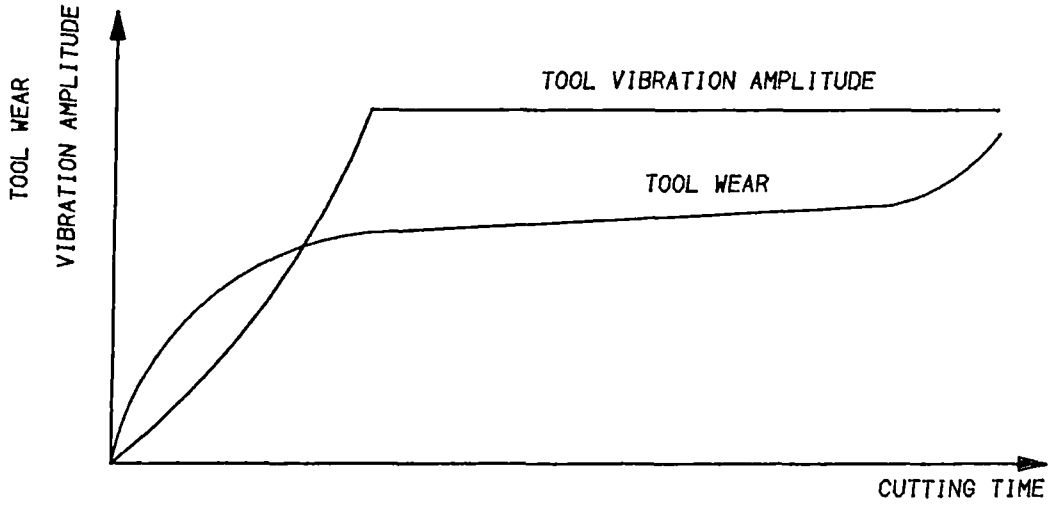

Fig. 6.5 Vibration Amplitude as Affected by Tool Wear
[After Arnold, 1946]

6.3 Historical Review Of Tool Wear-Vibration Relation

The effect of tool wear on the tool vibration was studied as early as *1946, [125],* and some studies were done between early $50's$ and late $60's$. Because of the complication involved in manipulating the tool vibration aspects, the possibility of finding a relation between the tool wear and the tool vibration was so low that efforts were directed toward finding the best conditions which would ensure the most stable cutting process rather than investigating the causes of such instability. However, due to the recent developments in instrumentation and in microcomputer interfacing, the possibility now exists to achieve these goals.

Arnold [125] was the first to try to build a qualitative relation between progressive tool wear during the turning operation and the tool tip vertical vibration amplitude. Tool oscillations have been found to correspond to the natural frequency of the tool. With the progress of tool wear, *Arnold* suggested the trend shown in *Fig. 6.5,* where two distinct phases are evident. In the first, the vibration is initially small and increases slowly; and, according to *Arnold,* is somewhat irregular. In this phase the wear of the tool edge continues to increase steadily.

In the second phase, a large steady vibration persists at almost constant amplitude, while the rate of wear increases significantly after a temporary pause. The transition period between low and high amplitudes was claimed to be short and was, in most cases, instantaneous. *Arnold* indicated that this merely indicated the general characteristics and, the high amplitude could be attained more quickly if higher cutting speed was used. This means that the jump point from low to high steady amplitude is reached after a certain wear level has developed at the tool edge. This implies that using a cutting speed which is much higher than that used by *Arnold* could lead to a constant vibration amplitude which is insensitive to tool wear progress.

Although it was the first fundamental study of tool vibration performed, *Arnold* faced strong criticism at that time and subsequently thereafter.

Tourret [126] suggested an explanation for *Arnold's* findings by stating that the wear on a clearance face, after reaching a certain level, might promote vibration by causing an additional periodic force to act on the tool, this means inducing an additional forced vibration which did not exist at the beginning when the tool was sharp. Twenty years later, *Tobias [134]* refuted *Arnold's* suggestion that a sharp tool exhibits virtually no vibration. *Tobias* stated that this contradicts the well-known workshop dodge whereby chatter can be remedied by rounding off the cutting edge. *Tobias* added that *Arnold's* experimental arrangement for studying tool vibration was arranged so that some of the disturbances were eliminated, and that the results were obtained under, what *Tobias* called, controlled conditions.

Five years later in *1969, Weller et al. [128]* published their work which was a part of a larger program to develop diagnostic techniques for many types of machinery and structures. It was thought by *Weller* that the same analysis and data reduction techniques, which had been successfully used to determine the internal conditions of machinery by studying their structure-borne sound emission, could be applied to metal cutting applications. In the first serious and effective study to address the problem, *Weller* recorded the vibration during turning operation using an accelerometer. They found that the signal obtained could be divided into low frequency band ($0-4\ kHz$) and high frequency band ($4-8\ kHz$). A worn tool exhibited a higher amplitude at high frequencies which was not observed with a sharp tool. A low frequency amplitude band was found to be insensitive to tool wear progress. They explained that the tool vibration in the $X-$Direction (horizontal) was initiated by the force increase in that direction after a certain level of wear was attained on the tool's clearance face. The greater the wear level was, the broader the flank wear land became, producing an increasingly greater rubbing effect and, in turn, more horizontal vibration. Also, *Weller* claimed that the worn tool vibrated in the vertical direction (Y) as a result of the cutting force falling characteristics proposed by *Arnold [125].* Although *Weller* agreed with *Arnold's* tool wear-vibration trend, *Fig. 6.5,* they stated that the jump point from low vibration amplitude, by a sharp tool, to a high one could not generally be calculated; and, the high-frequency high- amplitude was noticed only after a noticeable wear progress had

occured. However, they did not agree with *Arnold* concerning the constant vibration amplitude following the jump point. They noticed that the vibration amplitude increased rapidly with tool wear to the point where the workpiece surface waviness was beyond tolerance. However, they *[128]* reported some problems in the system performance due to the effect of the cutting heat; and, generally there some uncertainty about what the behaviour would be if different conditions were to be used. Besides, it was not clear how they distinguished between the frequency bands using the time-domain signals. Even though they claimed that the problem was entirely solved and a tool wear detector was build for the *GENERAL ELECTRIC COMPANY,* surprisingly it was found, twenty years later, that the same company was still looking for a solution for the same problem, *[131]*.

In his work, *Pandit et al. [138]* found that a vertical vibration mode in the frequency band of $4.3-4.7\ kHz$, which was found to be around their tool-holder's natural frequency, appeared in all three tests conducted and the area under this peak decreased at the early stages of wear and then increased at later stages. However, no attempts has been made to study the effect of the progressive tool wear on the vibration in the $X-$direction. Besides, only three tests were conducted representing a narrow range of cutting conditions; which, from an experimental data validity standpoint, is inadequate to draw any firm conclusions. Also, at that time, there was no other data available in the literatures to support such findings.

Taglia [139] examined the variation in the total vibration power in the frequency range $(0-2.5\ kHz)$ as a function of tool wear; and found that total power, expressed as the whole area underneath the frequency power spectrum, decreased as wear increased, reaching a minimum value at very advanced tool wear level, after which it increased. In his study, *Taglia* commenced with a relatively high wear level claiming that before this level the trend was ambiguous and contrary to that revealed by subsequent data. However, he was doubtful about using the term of *"total power"*, and he recommended a further study to be made to explain which specific band of frequency would be more sensitive to tool wear progress.

A somewhat different approach was suggested by *Rao [123],* and later by *Lindstrom et al. [140]* that a tool wear monitoring technique based on the vibration signal alone was not enough to represent the process; and, that a combination of the signals due to dynamic cutting force and to vibration amplitude (in the $X-$direction, in the case of *Rao* case, and in the $Y-$direction, in the case of *Lindstrom*) was required to achieve a good wear monitoring approach. *Rao [123]* also stated that the cutting force and acceleration signals, in directions other than the $X-$direction, did not reveal any useful information.

Micheletti et al. [141] presented the first results of research concerning the relation between the steady-state vibration of the form tool in an automatic screw machine, under normal cutting conditions, and the tool life corresponded to several machining parameters. Despite the accuracy involved in the data collection system and in the analyses, it was concluded that no correlation existed between tool vibration and wear. Reaching such a disappointed conclusion was a direct result of the proposed strategy to determine and to define tool life. For every cut, the tool vibration was measured in the first span of tool life (early stage of wear) in order to see whether the vibration pattern could be used for tool life forecasting. In fact this stage is much too early to obtain significant indication, and a record of the whole tool life may be necessary to find such a relation. For instance, if data had been collected for longer periods, or the signal had been ignored in the first few minutes of cut, as has been suggested by *Taglia [139],* a different outcome might be reached. Besides, in screw machining no overlapping of cuts exists (i.e. the situation is avoided where part of material from the previous revolution(s) is cut in the current revolution) then virtually no forced vibration is available to excite the system.

Martin et al. [142] used the total power of the vibration signals because it was impossible to isolate the variations due to cutting conditions from the experimental errors. The experiment showed that the vertical vibration of a lathe tool in the course of stable machining is almost sinusoidal, with frequency perceptibly equal to the natural frequency of the tool. In the range of values studied, the power of the acceleration signal

determined by spectral analysis was a linear function of the cutting speed, and of the tool wear; the signal increased in the ratio of $\{\frac{1}{10}\}$ between the new and worn tool.

In summary, the problem of finding a consistent trend of the tool vibration-tool wear has not been resolved. This is reflected in the contradictions encountered among those ideas which have emerged so far. Even though some investigations have reached agreement concerning few essential aspects, the problem of identification is still unsolved. Generally the situation may be expressed as follows:

1. what is the nature of tool vibration at different wear levels?;
2. which direction of tool motion is most dynamically affected by wear levels?;
3. what are the effect of cutting conditions and wear on tool vibration?;
4. what is the effect of the system characteristics on tool vibration?; and,
5. how can the approach of tool wear monitoring, if found, be implemented?

All these queries have to be answered if a universal approach is to be developed.

The current study is an attempt to make some progress in this way. This includes the identification of relevant information and its isolation; and of how, the in-process tool wear monitoring approach, based on tool vibration, could be more generally used. The study has been developed for tool vibration mechanism under several tool wear levels. Great attentions has been given to distinguishing the local dynamic characteristics of the individual machining system elements from the general dynamic characteristics of different systems.

In the following section, a study is produced to identify the tool's dynamic signature using the experimental vibration data in connection with the tool's dynamic characteristics which were determined during the dynamic calibration of the dynamometer.

6.4 Results Analyses and Discussion

6.4.1 Power Spectrum And Envelope Identifications

The vibration signals for both horizontal (X) and vertical (Y) directions were recorded and later analyzed using a *FFT* analyzer, as explained in *Section 3.2.* Both the vertical ($Y-direction$) and horizontal ($X-direction$) vibration signals were fed to the analyzer by playing back from magnetic tapes. The two signals were simultaneously processed using the dual channel mode of the *FFT* analyzer. Power spectrum of the input voltage in root mean squares *(RMS)* was produced.

The spectrum is considered as a measure of the energy distribution in the frequency domain. Several frequency ranges of the analyzer were chosen and it was found that, for all the available signals, frequency range up to of 10 kHz was adequate to fit the current system; and, no responses was found outside this range. Therefore, a 10 kHz frequency range was the limit of the useful frequency of the system. This range was well within the linearity ranges of the accelerometer, the recorder, and the tapes used in this study.

A power spectrum pattern for all the tests involved was found to have the form as shown in *Fig. 6.6.* Two frequency ranges can be recognized, lower frequency low-amplitude ($0-4\ kHz$) and higher frequency high-amplitude ($4-10\ kHz$). Also, it was found that there were six frequency bands which dominated the behaviour of the two spectra. For the horizontal (X) spectrum, *Fig. 6.6.a,* these were around the values of 1350, 1850, 2000, 3200, 6200, and 9800 Hz while for the vertical (Y) direction were 1350, 1850, 3200, 4500, 6200, and 9800 Hz, *Fig. 6.6.b.* However some shifting from these specific values may occur but generally, they are still around the central frequencies mentioned, and the patterns shown in *Fig. 6.6* pertain to all conditions. Also, it sometimes occured that one or more of these dominating bands, especially in the lower frequency low-amplitude section, lost their domination. In fact, they were immersed into the flat portion of the base power. For both spectra, it was found that

four of the six dominating frequencies were in the range of 1000 *to* 4500 Hz, while the remaining two peaks were in the range of 6000 *to* 10000 Hz.

Identification of such signature and recognition of pattern elements may be demonstrated in connection with the result of the dynamic calibration test of the dynamometer system which was done during the dynamometer design stage.

During the dynamic calibration of the dynamometer, *section 3.1.4,* it was found that the resonant frequencies ω_r for horizontal (X), vertical (Y), and radial (Z) directions were 1360, 750, and 3000 Hz respectively, (see *Fig. 3.20).* These were further confirmed by obtaining the equivalent damped natural frequencies ω_{nd} through applying a hammer blow on each direction and the number of oscillations per second were counted. The determined damping natural frequencies were 1650, 850, and 3046 Hz respectively.

The spectra shown in *Fig. 6.6* could be explained in the light of such dynamic aspects. The first dominating frequency band in both spectra, which is 1360 Hz, seems to be the first fundamental natural frequency of the tool-toolholder system in the horizontal (X) direction. The second one, 1850 Hz, is thought to be the first fundamental natural frequency for the $Z-$direction in which no accelerometer was fixed. As shown in *Fig. 3.20,* this frequency has only dominated in $Z-$direction; and, having appeared in both the horizontal (X) and the vertical (Y) spectra, *Fig. 6.6,* it appears to highlight dynamic cross-sensitivity between vibration in the radial Z and in each of the other directions. Also, confirmation of the idea that 1850 Hz corresponds to $Z-$direction is evident from *Fig. 3.20* where the cross-sensitivity due to the frequency 1850 Hz was higher for the $Y-$direction; and, a similar effect was found in the spectra where the frequency of 1850 Hz is generally greater in amplitude for the $Y-$spectrum. However, this peak at 1850 Hz, was not present in all spectra and this confirms the conclusion that it is a characteristics of the $Z-$direction. The frequency band 3200 Hz appears in both $X-$ and $Y-$spectra. This is thought to be the second fundamental frequency of the $X-$direction or, the first fundamental of $Z-$direction. The frequency band of *4500 Hz,* which has a higher amplitude than the preceding frequencies, appears only in

the spectra of the $Y-$direction. In fact this frequency represents the boundary limit between lower and higher amplitude frequencies in the Y pattern. However, there is insufficient evidence to identify the high frequency, high-amplitude bands of 6200, and 9800 Hz. Nevertheless, they could be attributed to the characteristics of one or more of the system elements such as tail-stock, head-stock, machine carriage, machine beds, or even the dynamometer base.

As a result of the above discussion, it can be concluded that each of the $X-$ and $Y-$spectra consists of individual frequency bands which represent the dynamic behaviour of the tool, toolholder, dynamometer, machine, workpiece system. As far as the effect of the toolholder and the dynamometer are concerned, the X and the Z natural frequencies and their harmonics have a major effect on the power spectrum while the vertical natural frequency in $Y-$direction has found to have a little effect. The high frequency responses of acceleration are several times higher than the lower natural frequencies of the dynamometer, which therefore, acts as an attenuator. This situation could be avoided if the accelerometers were located on the moving mass of the dynamometer. With regard to the location of the accelerometers it is the acceleration components of the mass of the dynamometer cutter head which should be measured, since these best reflect the cutting force components which act at the tool tip. Such forces, and their variations provide a direct measure of the influence of tool wear on the cutting process. However, it is not always practical to locate the accelerometers in close proximity to the cutter tip and in some applications a more remote location is necessary. Such conditions prevail in the research reported here, and the accelerometers were located at the back of the dynamometer as shown in Fig. 3.33. Since this location is not ideal due account has to taken in the interpretation of the results. The dynamometer is bolted to a clamping plate, and to a base, both of which have large mass, and so the accelerometers will measure the response of this system and will reflect forces which will be different from those encountered by the tool tip. Hence the acceleration measured in the experiments will be regarded as reflecting the response of a system which contains a variable element: namely the cutter-workpiece interaction.

However, in the following section a general discussion and analyses is produced to investigate the possible existence of an interrelation between the system's dynamic characteristics and the tool state.

6.4.2 Tool Wear-Vibration Interrelation - Data Reduction Technique

The output from the *FFT* analyser was obtained in the form of power spectra of *RMS* voltage values which represented a specific sub-test of the test involved. Originally, the signal was recorded at the beginning of each cut and lasted throughout the whole cutting time, which was about two minutes. A dynamic history of a specific test is represented by a group of spectra which represented its individual sub-tests.
A unique and consistent spectrum envelope, *Fig. 6.6,* was obtained for all the sub-tests through the wide variety of cutting conditions used. Analysis of power spectral plots along with the values of different dominating frequencies (peaks) were examined for the purpose of finding any trend that might exist among any mode of vibration, aggregated cutting time, cutting force, and the progress of tool average flank wear during machining. The area underneath each mode was examined using different pass band frequencies, 10, 5, and 2 kHz.
From now on, the test number refers to the test position in the central composite design *(CCD)* which was used in the experimental tests design. However, for some technical and economic reasons, not all the *(CCD)* set were tested. The experimental data used in this study are listed in *Appendix B*. Nine levels of cutting speed ($50 - 230$ $m/min.$), eight levels of feeds ($0.06 - 0.6$ $mm/rev.$), and six levels of depth of cut ($1.5 - 3$ mm) were used in this study. Different workpiece diameters (193 down to 50 mm) were employed to obtain the desired surface speed. Cutting was started and ended up at different locations on the workpiece length which was about (500 mm).

Although the wide variation in cutting conditions; system parameters; and, time effect, a consistent envelope pattern was obtained for all tests. This implied that the experimental set up was reliable and therefore, one of the obstacles which confronted

previous investigators had been eliminated. The problem of variation of the spectrum envelope, when one or more of the conditions were changed, has long been a very serious problem for many investigators. This problem would manifest itself if the approach were to be applied on an Adaptive Control system *AC*, where flexibility would be required to change one or more of the conditions at any time to satisfy the production requirements.

In the following is a try to investigate the possible existence of a correlation between one or more of these dominating frequencies (peaks) and the whole story of tool life. The tool state, represented by its wear level, has been investigated in association with the corresponding vibration amplitude at different frequency bands as it is explained next.

For each test, the power value underneath each of the dominant peaks has been plotted against cutting time; tool wear; and, cutting force. *Fig. 6.7* shows a typical arrangement for such procedures for *Test #2* which has the conditions $(145.88, 0.12, 2.5)$, which refers to speed; feed; and, depth of cut respectively. The vibration power amplitude for each peak, along with their ratios, are plotted against the cutting time; the average wear *AW;* and, the thrust force component F_{xz}. As seen from *Fig. 6.7,* the only trend, which is consistent with the all other tests, is the one in plot (a) for the frequency band of 1350 Hz which is the the dynamometer first natural frequency for $X-$direction. The other plots, $(b-f)$ in *Fig. 6.7,* which represent the other dominant peaks and their ratios, do not reveal much useful information. The same conclusion is obtained if all the other tests are considered. The power spectra for this test are collected together as shown in *Fig. 6.8.* While *Fig. 6.8.a* is for the $X-$direction, *Fig. 6.8.b* is for $Y-$direction. Also, power spectra for *Test #13,* which has the conditions $(206, 0.2, 2.25)$, are shown in *Figs. 6.9.a & b.* Analysis of different vibration modes of this test, as affected by the wear progress and force variation, are shown in *Fig. 6.10.* As a result of analysing all tests involved $(13-test)$, the following observations can be extracted:

- At the beginning of each test when the tool was new, the total power of the

spectrum for the vibration signal from the $Y-$direction was higher than that from the $X-$direction. Once some wear had developed on the cutting edge, both values became closer until, in many cases, they reached an identical value, *Fig. 6.8.a & b* and *Fig. 6.9.a & b*. In fact, this could be due either to an increase in X total power or to a decrease in Y total power. The analysis of individual sub-tests did not give a firm answer. However, the domination of the total power for the $Y-$direction at the very beginning was anticipated for the following reasons: First, the magnitude of the vertical force component F_y was the largest among the others and therefore, any slight variations would cause large vibration amplitudes; this may be observed from the time-domain dynamic cutting force signals for almost all the tests (see *Figs. 3.31 & 5.6*). Second, the natural frequency of the $Y-$direction was the least among the others (760 Hz); consequently, it was the least rigid direction, and a larger amplitudes may be produced for a given source of excitation. However, this may be due to the fact that the vibration principal direction is not coincident with either X or Y directions, and probably in the thrust direction XZ. As a result, the response in each of X and Y directions are only components of the superposition of motion in the actual force principal direction [129].

- In some stages, when a 10 kHz band pass frequency of the analyzer was selected, some of the low-frequency peaks were difficult to be distinguished from the base power. Using a lower band pass, such as 2 kHz or 5 kHz, these peaks were amplified and then became more detectable.

- The peak corresponds to the natural frequency of the $X-$direction was the only mode in the power spectrum to reveal a significant general trend between power amplitude and either wear or force history, *Figs. 6.7-6.10*. Generally the power amplitude at this frequency decreases by increasing the tool wear. The reduction in the power amplitude continued until it reached a limit after which it tended to increase. The point at which the amplitude was later increased was found to be in good agreement with the point at which both the wear and the force underwent

a rapid rate of increase. However, this rate of increase in the power amplitudes seemed to be dependent upon cutting conditions. Higher rates were noticed in some cases, lower rates in others, and even constant rates were also observed. Generally, the conditions which induce higher wear rates tended to cause higher increase of the vibration amplitudes after changing its direction. Similarly, the rate at which the amplitude decreased before reaching the minimum limit was also cutting conditions dependent.

- Since the mode of tool natural frequency in $X-$direction (1360 Hz) always appeared in both the X and Y spectra while the one in $Y-$direction (750 Hz) appeared only in the Y spectra, an approach based on vibration in only the $X-$direction was more reliable. This idea was supported by the fact that the vertical force component F_y was the least sensitive to tool wear which initially had controlled the tool vibration.

In summary, only the power amplitude at the frequency band of 1350 Hz in the $X-$direction exhibited a strong correlation with both tool wear and cutting force. Therefore, the analyses were confined only to investigate the effect of wear progress on the variation of this mode of vibration.

In the following section, an analytical discussion is produced of the phenomenological interrelation between this mode of vibration and the cutting state. This is to shed some lights on the dynamic characteristics of the cutting tool as affected by the variation in each of tool wear and cutting force.

6.4.3 Tool Wear Characteristics Under Oscillating Conditions

Fig. 6.11 shows the the plot of the time history of the vibration power amplitude, at a frequency band of 1350 Hz in $X-$direction, and each of the corresponding average wear flank and cutting force for *Test #2* which has already discussed. It can be seen that the vibration power amplitude decreases by increasing the level of flank wear reaching a minimum value, after which, the trend is reversed and the amplitude starts to increase. It is clear how good the agreement is between the point at which the amplitude changes its direction and the point at which both wear and force value enter the last stage of tool life. Again, *Fig. 6.12,* which represents *Test #13,* indicates that the same conclusion is quite evident. Generally, such trend has been revealed among all tests performed, (13−test), except for some minor disturbances which are next discussed.

Fig. 6.13 represents the relationship between the vibration power amplitude at 1350 Hz for $X-$direction, and each of the average wear AW and the thrust force F_{xz} for *Test #3.* The cutting conditions for such test are $(145.88, 0.12, 2.5)$. This figure shows a deviation from the general wear-vibration trend which is already discussed. However, there were some points suggested that these plots should be discussed in an association with the individual tool wear values at the different locations of tool clearance face. As mentioned before, the average wear considered here is the mean of three values of wear developed in three locations, nose, flank, and notch. In practice, these wear elements are not of equal levels, and irregular wear distribution over the clearance face is frequently observed, (see *Fig. 3.37.b*). When a certain element dominates over the others, this will not be faithfully reflected by the average wear value. This one disadvantage of using the term of average wear as a tool life termination criterion. However, as far as *Test #3* is concerned, a sudden edge chipping in the notch area NCW occured during the second sub-test after four minutes cutting (see *Fig. 5.1.a* for *Test#3*). As a result, a rough contact existed between the tool and the rotating workpiece. This continued through the third and fourth sub-tests. The resulting crevices caused a machining instability which started at the second sub-test and lasted for a while during the third sub-test. By

the end of the fourth sub-test, the irregular asperities were rubbed out which resulted in a more homogenous and smooth contact between the tool and the workpiece. This regained the machining stability and then, the vibration amplitude started to again decrease taking the same general trend as that observed in stable conditions.

The vibration mode at a frequency band of 1350 Hz was the most affected by the system instability, and that confirmed its reliability to represent the dynamic characteristics of the cutting operation. Also, a frequency band of 6200 Hz was also affected by such instability, which suggests that this mode may be one of the dynamometer modes.

Also, *test #14* did not produced good agreement with all the other tests neither for vibration amplitude nor the wear force component, *Fig. 6.14*. This was a result of the hostile cutting conditions under which the test was conducted, (50.2,0.2,2.25). A low cutting speed with a relatively high feed and depth of cut produced thick broken chips. This imposed a cyclic variable force on tool face every time the chip separated from the work material. Besides, the speed used in this test, 50.2 $m/min.$, is well within the range in which the force falling characteristics is likely to occur. All these features contributed to instability during *Test #14* and consequently, made such a low speed as 50.2 m/min used in *Test #14*, outside the speed range in which the proposed phenomenon might be expected to occur. Although the instability was noticed throughout the whole test, as shown in *Fig. 6.14*, there was a specific period in which the instability reached its ultimate level. As indicated, the instability started when a chipping occured and lasted for about ten sub-tests forward. This agrees with the observations for *Test #3* that the sudden increase of wear is always accompanied by cutting instability. This mechanism of tool chipping suggests that not only the gradual wear, but tool fracture and chipping could be detected using the tool vibration criterion. To distinguish between the higher vibration amplitude which is due to local disturbances such as chipping, fracture, etc., and that which results from actual gradual wear, the cutting force should be considered. It surprisingly was found that the instability due to chipping was always accompanied by drop in the corresponding force values. In normal situation (stable cutting), the force increases if such instability was resulted from gradual wear. This is evident from the force-vibration plot in *Fig. 6.14* within the interval from 39 to 64 minutes cutting

time. However, this force drop may be due to the fact that less material is cut when the tool loses some of its material. As explained in Chapter 5, page 141, the force drop in Test#14 was noticed due to the tool fracture and chipping, and to the frequent formation and breakage of workpiece materials which filled the crevices. This gave a misleading setting of the depth of cut for the successive cuts so that less materials was machined. Measurement of the machined workpiece diameters confirmed this fact.

However, a common trend has been elicited for the variation of vibration amplitude against the tool wear behaviour for the first fundamental frequency of the toolholder. While cutting continued, the average tool wear level increased and power amplitude decreased. At a later stage of tool wear, the power amplitude reached its minimum limit after which it tended to increase again. In most tests it has been found that the point at which the amplitude changed its behaviour corresponded to the point at which the wear entered the region of rapid wear rate, the failure zone (see *Fig. 2.5*).

6.4.4 Phenomenological Analyses of the Tool Wear-Vibration Behaviour

This trend of the vibration amplitude in relation to the tool wear is very similar to the well-known trend of the tool wear rate. In the light of this fact, an explanation is now given:

The initial higher vibration amplitude exists during the initial region of tool wear, region *A*, *Fig. 6.15.* After some wear has developed, the second phase commences in which the amplitude continues to decrease. This stage is terminated when the tool exhibits a considerable wear level. Beyond this point, the amplitude enters its third phase in which an amplitude increase is produced due to the higher wear rate. Using this fact, one can consider the point of minimum amplitude to be the the critical wear limit. Therefore, the end of the useful life of the cutting edge can be determined by observing the vibration behaviour.

Pandit et al. [138] reached a similar trend for the power amplitude corresponding to the natural frequency in the $Y-$direction. However, they did not investigate $X-$direction. Providing their tool system had a square cross-sectional area, both Y and X natural frequency would be the same and the mode of vibration appeared in the $Y-$direction was, in fact, a dynamic cross-sensitivity of the $X-$direction. Also a similar trend might have been observed by *Taglia [139]* if he had not ignored the vibration signal in the first part of tool wear. *Taglia* commenced investigating the relation between wear and vibration at a very advanced stage of tool wear of 0.4 *mm*. However, he noticed that the total vibration power was decreasing until it reached a minimum value at the tool failure region, and then, it increased.

This provides a very attractive in-process solution to the problem of tool life termination. Tool wear is by no means a deterministic parameter and therefore, in-process approach is the most suitable. Among those approaches, the current vibration approach seems to be most favourable for several reason. First, the approach can easily be achieved on-line using a small accelerometer, which can be safely located anywhere in the cutting vicinity; and, using suitable software, which could be included in the memory of the host computer of any *CNC* or *DNC* machine tool. Second, the vibration

based wear monitoring approach proved to be sufficiently sensitive to detect not only gradual tool wear, but also any tiny disturbances to the system during the actual cutting. Third, the hidden system instability could then be detected, saving the product, tooling system, and even the machine and the operator. Finally, a vibration approach could produce a very good early warning system giving an opportunity for operator actions to be taken.

Also, it is very important to emphasise here that a good agreement between cutting force-wear behaviour and vibration amplitude-wear trend is evident and confirmed. However, and for the emerged approach to be trusted, a good understanding of the nature of the physical behaviour should be established.

Pandit et al. [143] tried to investigate the variation of the dynamic coefficient of friction when the tool vibrates vertically. The friction force and friction coefficient were computed to show that they decrease at the initial stages of wear, reach a minimum near the critical wear; and, then increase again. It is clear that this trend is identical to that trend revealed in this project for the tool wear-vibration relationship. However, since *Pandit's* work was devoted for the $Y-$direction and due to to the high scatter involved in his data, the validity of applying his idea to the $X-$direction requires further explanation. However, in conjunction with the available information the following explanation could be offered: at the beginning of cut when the tool is sharp, then the tool-workpiece contact area is small, being almost line contact, flexibility exists for the tool to vibrate freely and hence attain higher amplitudes. Moreover, the first engagement between the tool and the workpiece has the nature of a discontinuous machining which leads in the case of sharp tool to the initiation of a chipping mechanism *[33]*. This induces more forced vibration into the system causing the tool to oscillate with higher amplitudes. As cutting continuous, a wider contact area is developed on the tool flank area causing an increase in the feed force. Such an increase acts as a damping force or as a resistance to tool vibration. As wear increases more and more, the feed force continues to increase, and consequently, a higher damping force is produced generating a stronger restriction on the tool movement. This phenomenon

is supported by the fact that, for a given test, the dynamic force signals exhibited a narrower bands at higher wear levels as indicated in **Chapter 5.** As the tool reaches the high wear region, an external factor is involved; this is the high increase in the dynamic coefficient of friction in the $Y-$direction, *Pandit [143]*. Then, the system stability is disturbed, and the input vibration power exceeds the resistance (internal damping) power. This produces higher vibration amplitudes in both the $Y-$ and the $X-$directions. This might be the reason why the amplitudes in the $Y-$direction is larger than of $X-$direction when a very high wear level is developed, *Figs. 6.9 (a & b).*

These findings of tool wear-tool vibration trend, and tool wear characteristics under oscillating conditions are best described by formulating or mathematical modelling of the relevant parameters. This may provide a quantitatively understanding of the emerged ideas. These are explained in the following sections, and include: *i*) the formulation of the effect of the cutting variables on the initial vibration amplitude when the tool is sharp; *ii*) the determination of the useful tool life using the approach of tool vibration and dynamic characteristics; and, *iii*) the establishment of an in-process vibration based approach for detecting and predicting tool wear using the force-vibration combination.

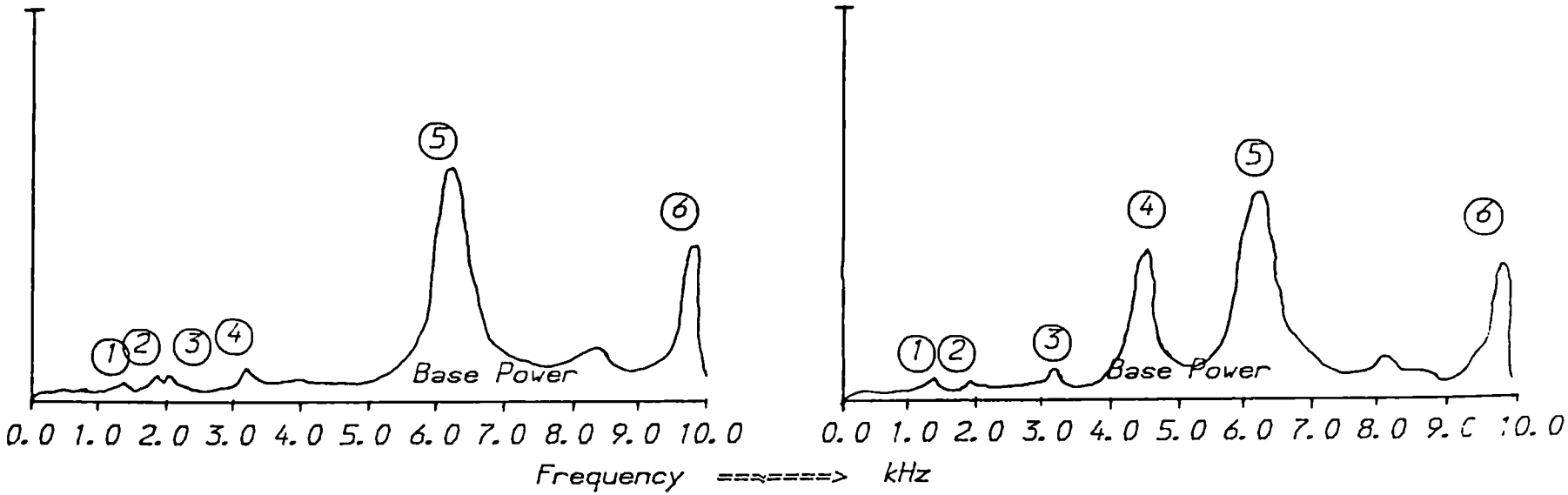

Fig. 6.6 Typical Vibration Power Spectra for Both X- and Y-Directions

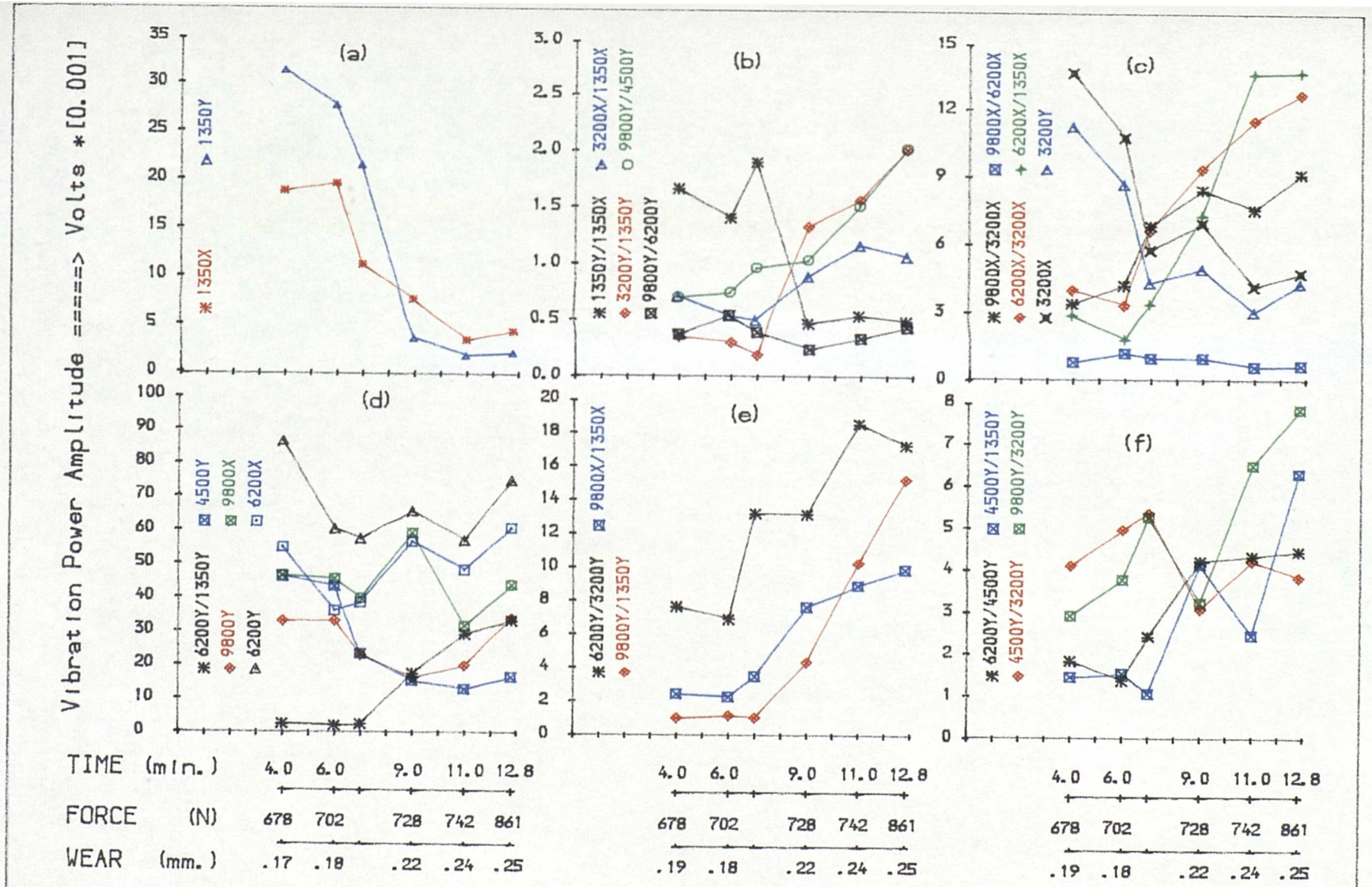

Fig. 6.7 Different Frequency Behaviours with Time, Wear, and, Force, for Test #2

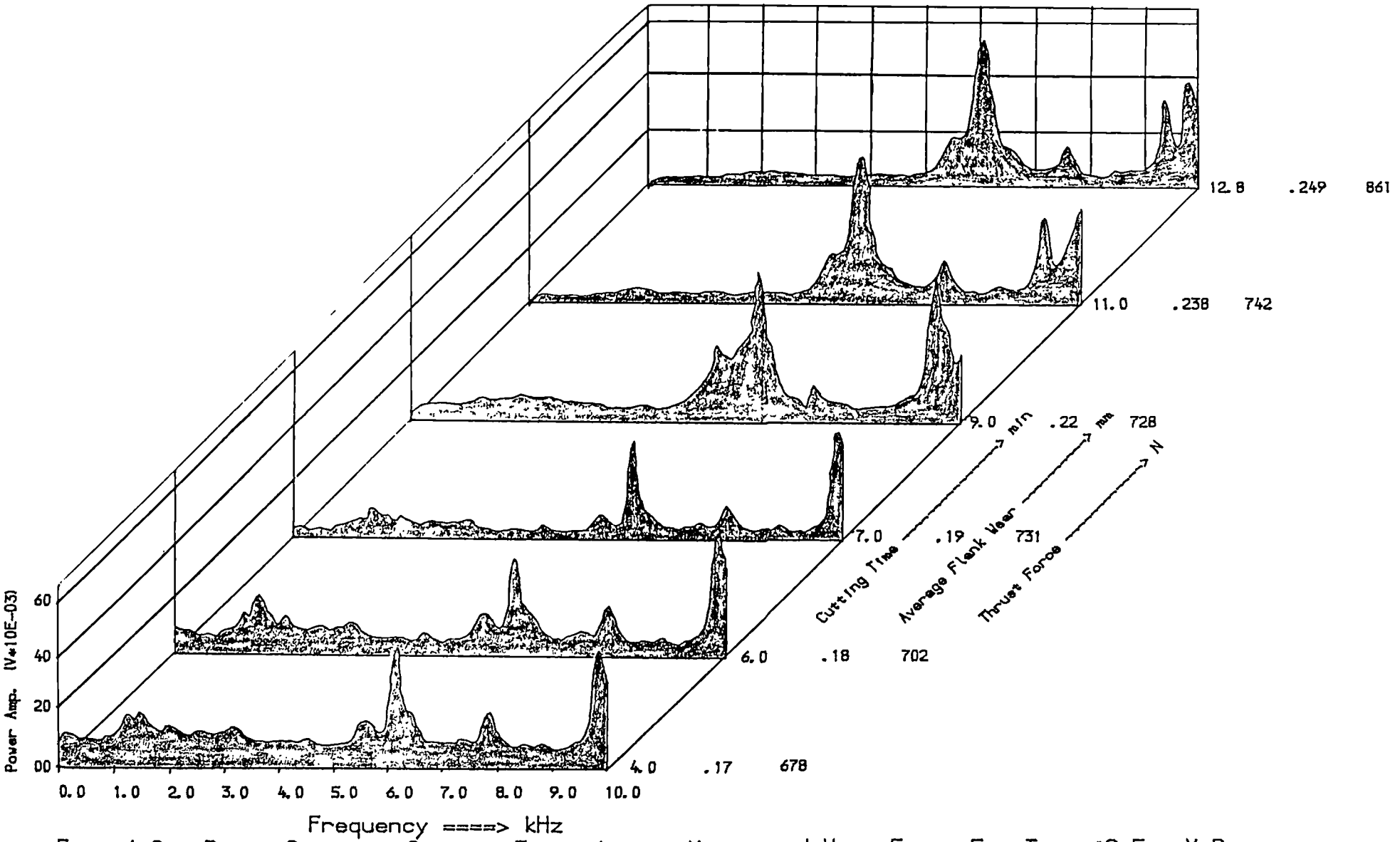

Fig. 6.8.a Power Spectra, Cutting Time, Aveage Wear, and Wear Force For Test #2 For X-Direction

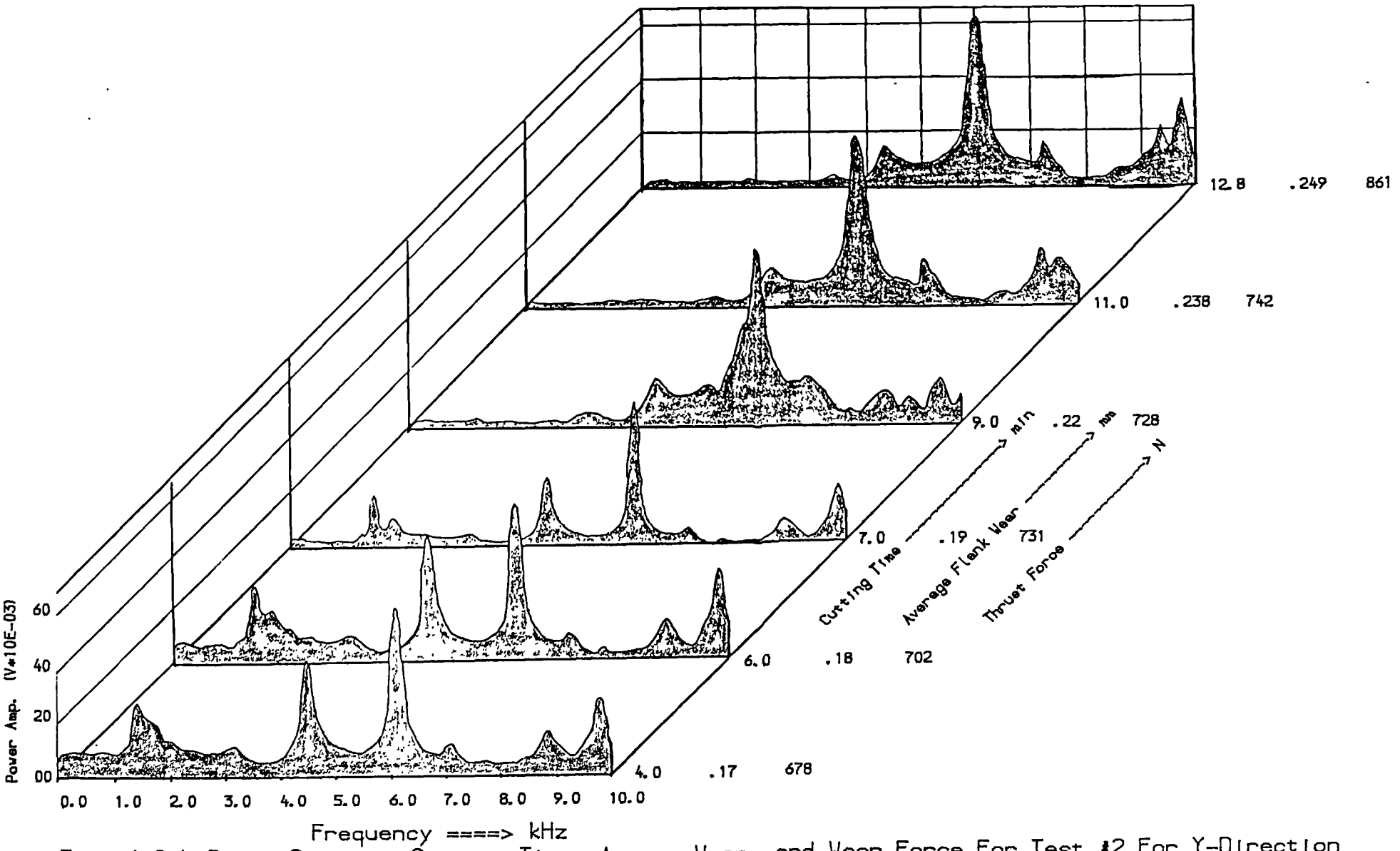

Fig. 6.8.b Power Spectra, Cutting Time, Aveage Wear, and Wear Force For Test #2 For Y-Direction

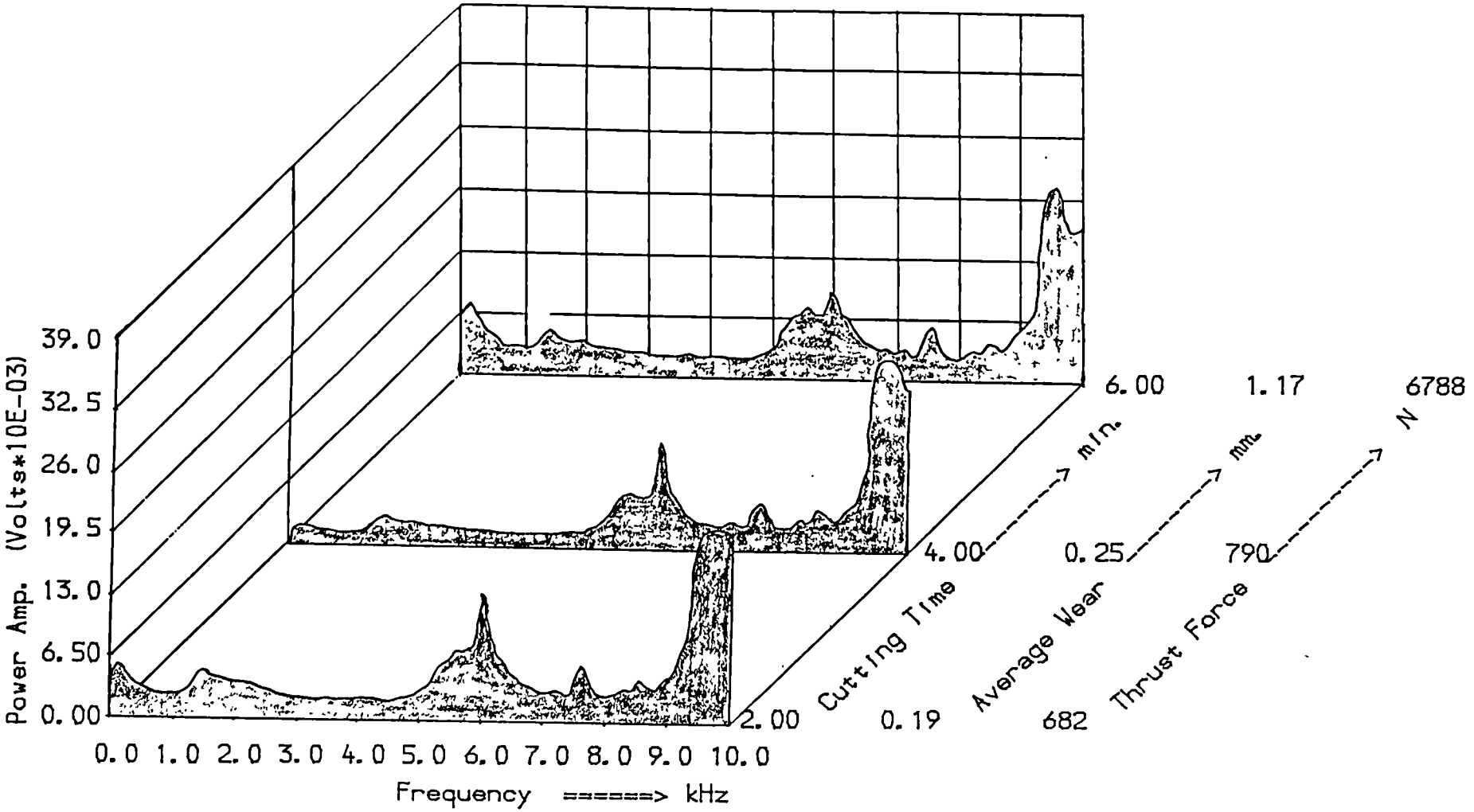

Fig. 6.9.a Power Spectra for X-Direction for Test #13

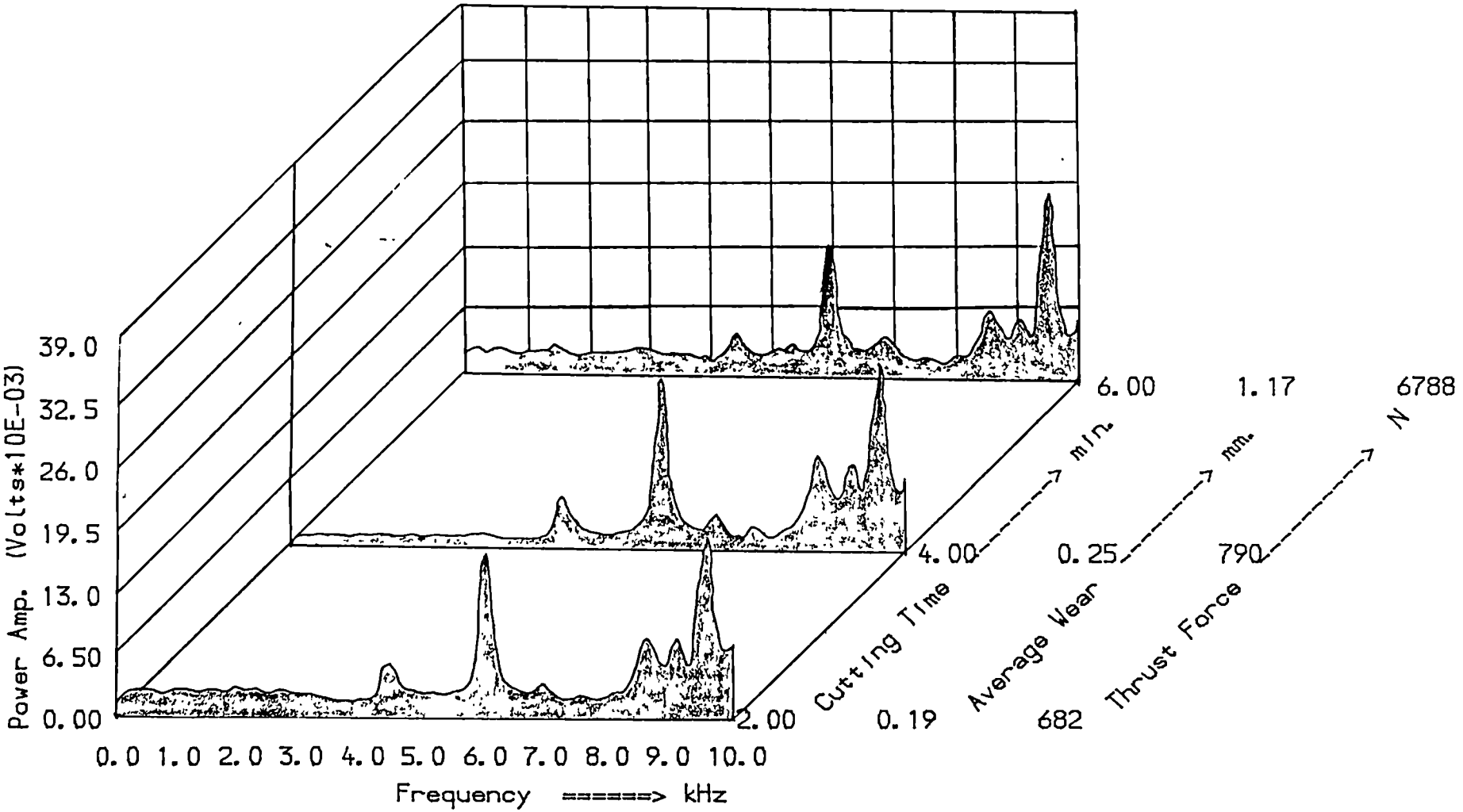

Fig. 6.9.b Power Spectra for Y-Direction for Test #13

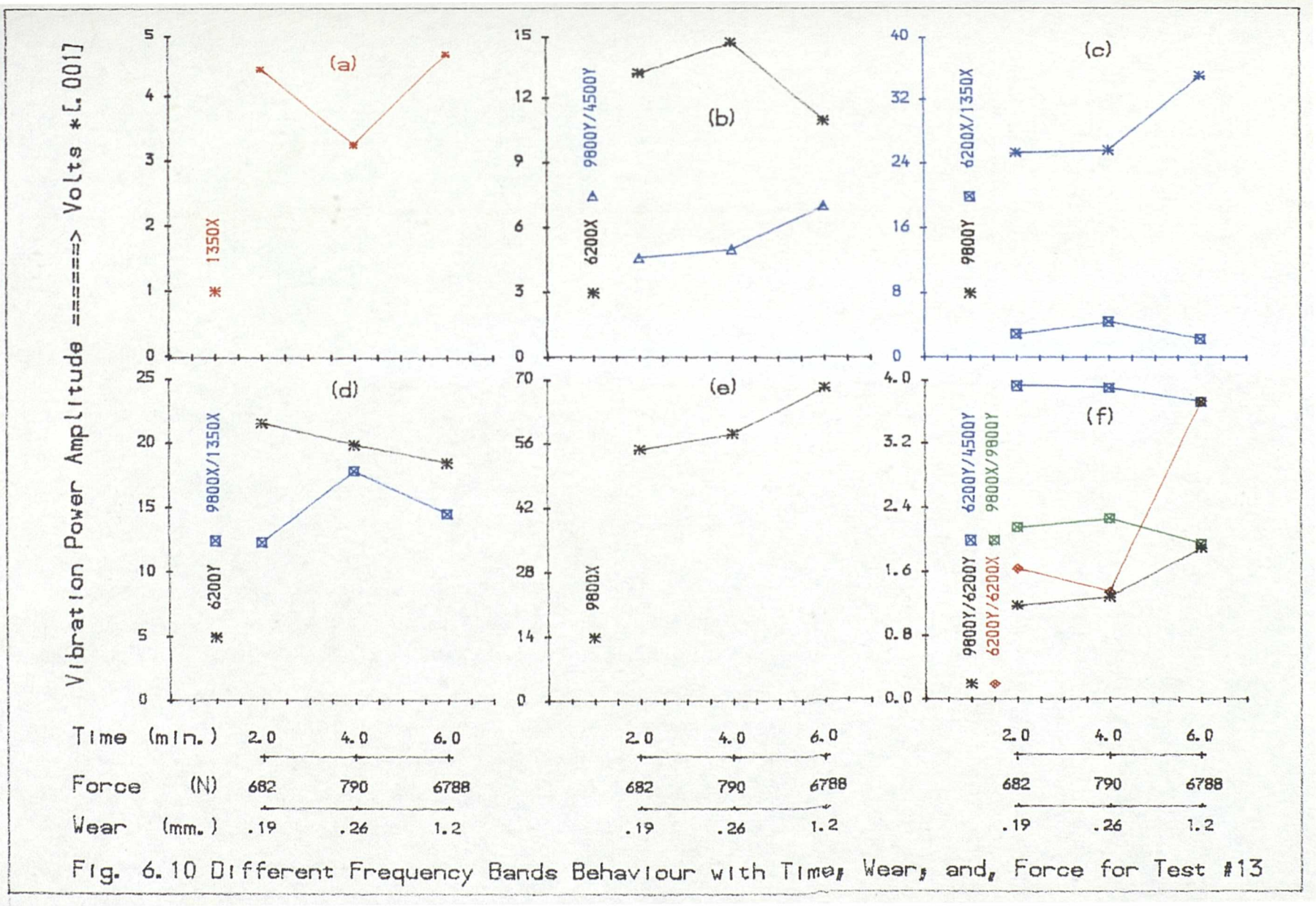

Fig. 6.10 Different Frequency Bands Behaviour with Time, Wear, and, Force for Test #13

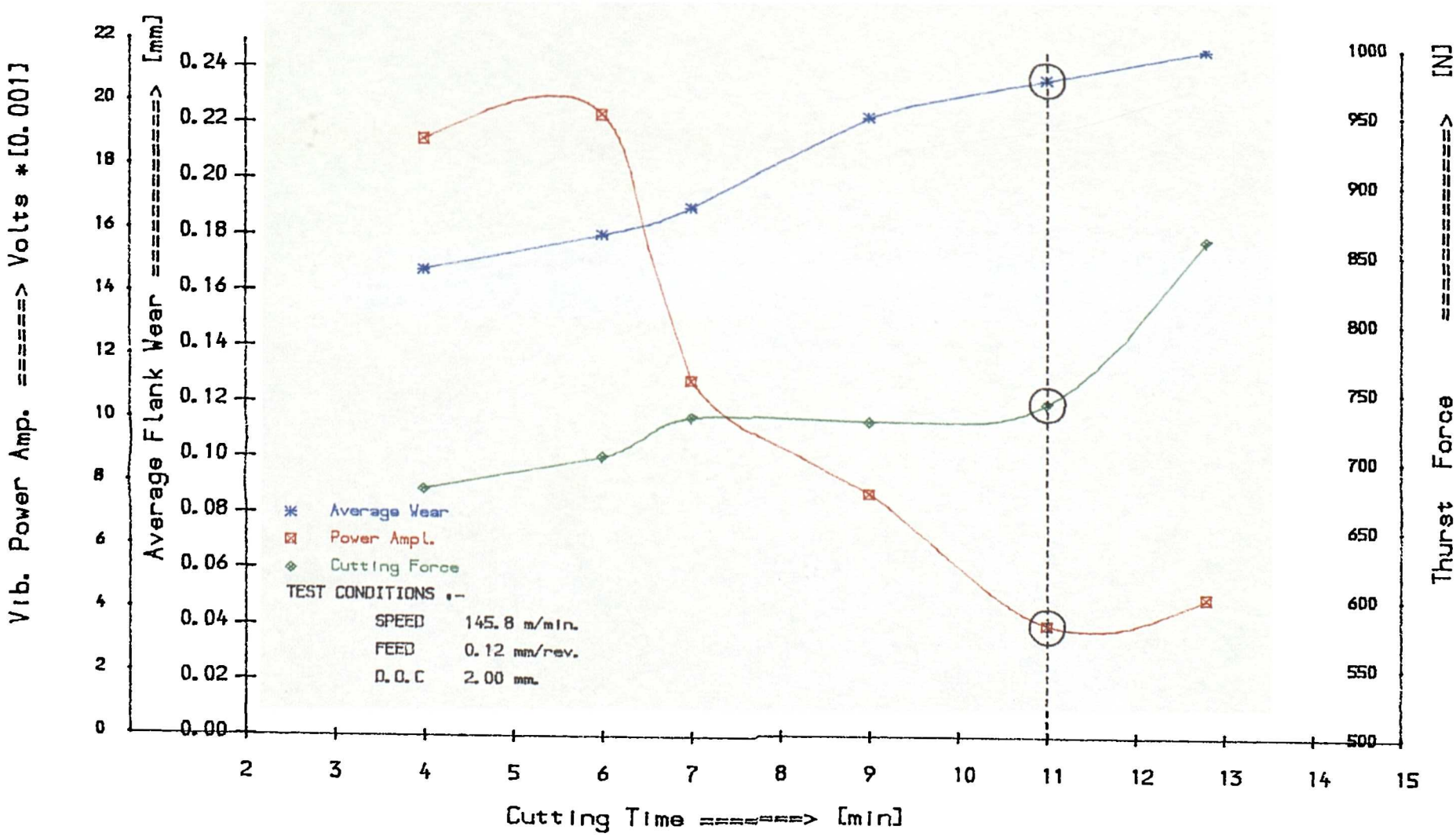

Fig. 6.11 Vibration Amplitude-Wear-Force Relationship For Test #2 For X-Direction

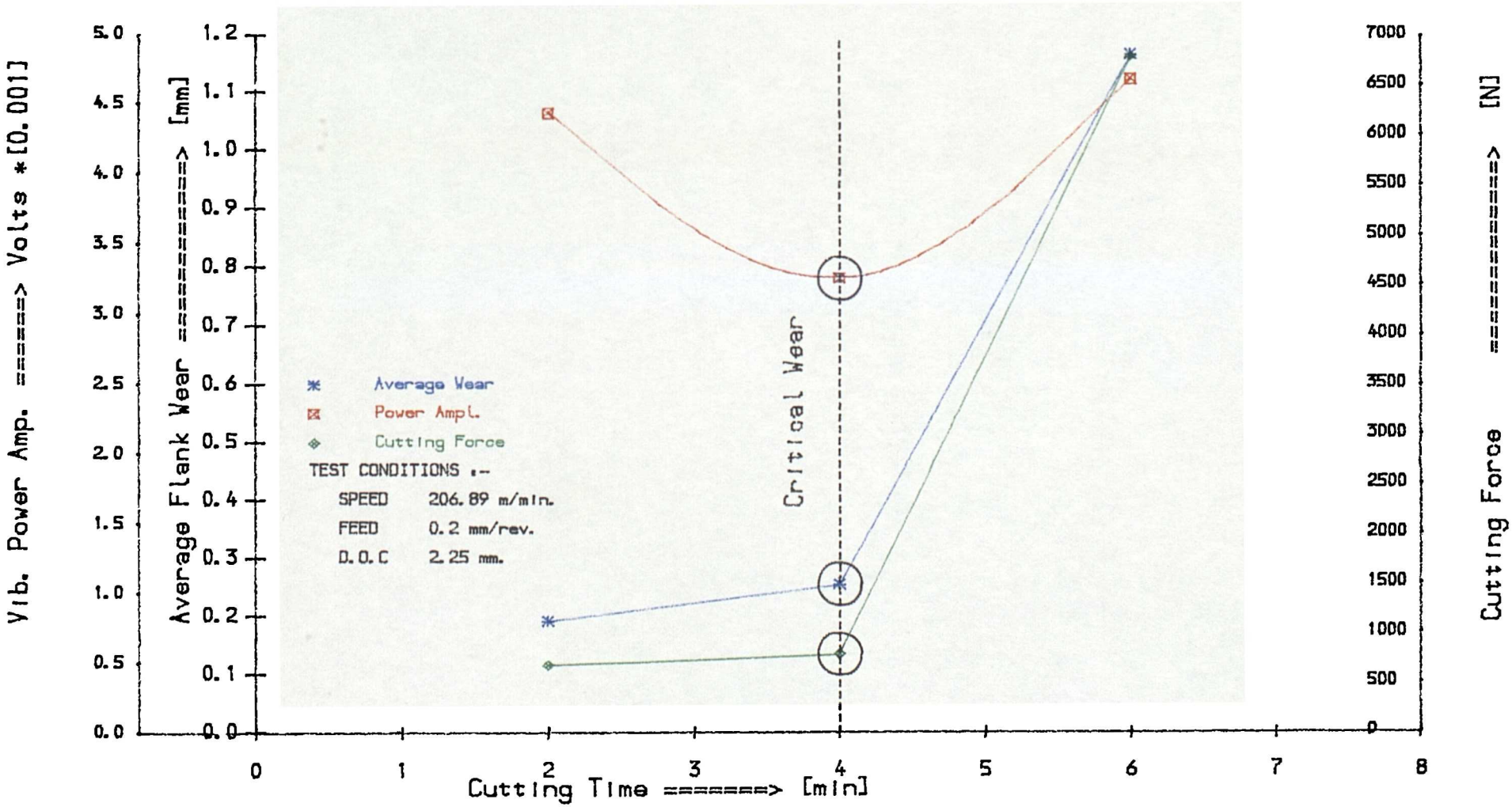

Fig. 6.12 Vibration Amplitude-Wear-Force Relationship For Test #13 For X-Direction

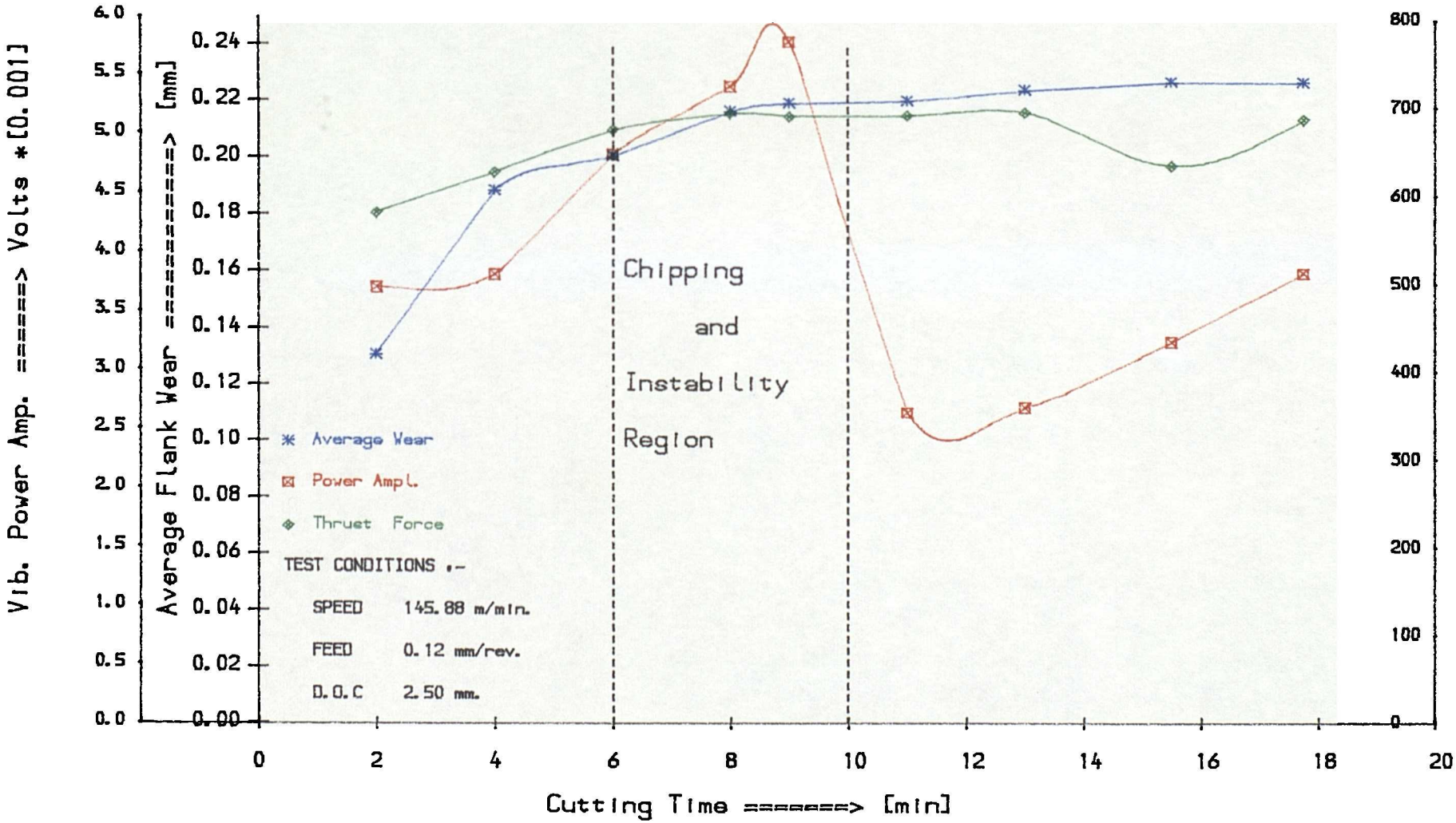

Fig. 6.13 Vibration Amplitude-Wear-force Relationship For Test #3 For X-Direction

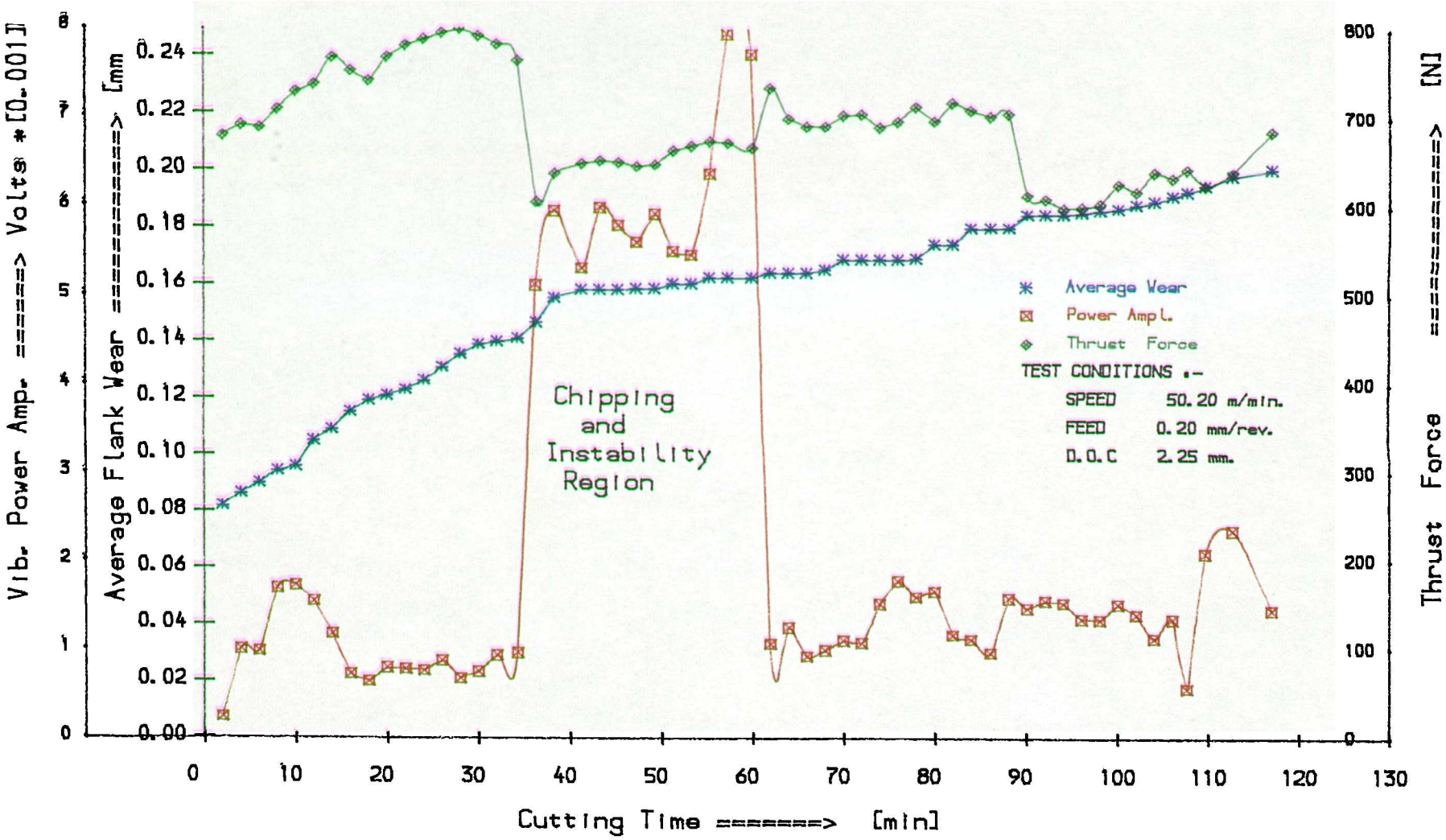

Fig. 6.14 Vibration Amplitude-Wear-force Relationship For Test #14 For X-Direction

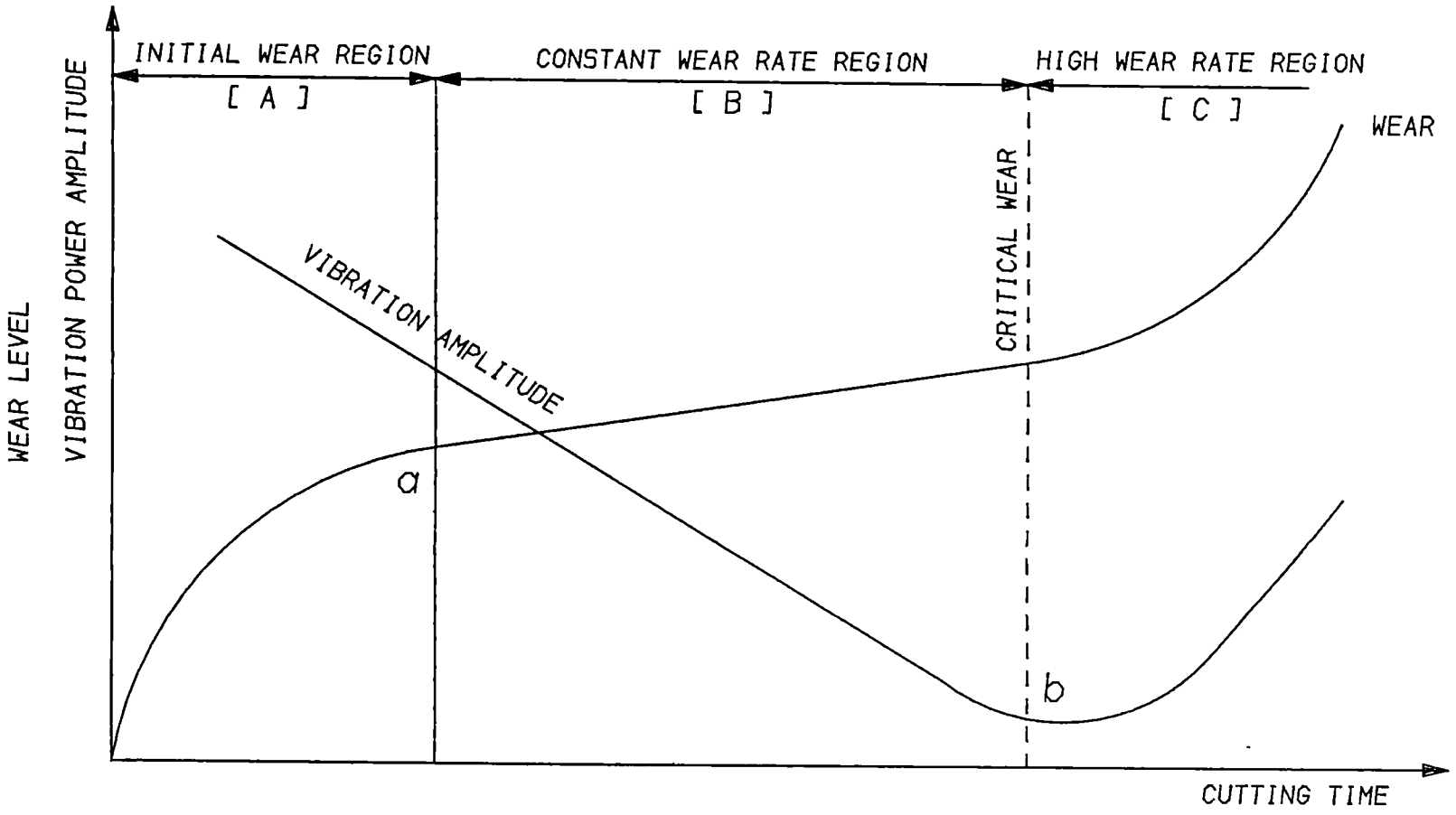

Fig. 6.15 Wear-Time and Vibration Amplitude Trend Proposed in this Study

6.5 Mathematical Models for Tool Wear-Vibration Relationships

The aforementioned findings might be further explained by mathematical modelling of the relevant data. Such models, having proved to be statistically significant enough, might shed the light on the whole aspect of relating the tool wear level to its vibrational characteristics. Therefore, the cutting operation could be monitored, tool wear level could be estimated, and moreover, any deviations from stable conditions could be detected on-line.

6.5.1 Effect of Cutting Conditions on Tool's Initial Vibration

The effect of the cutting conditions: speed, feed, and depth of cuts, along with workpiece diameter, on the tool vibration amplitude was studied for possible interrelation among these parameters. Using the experimental data listed in *Appendix B*, in association with the linear regression modelling technique, resulted in the following second order linear model:

$$\begin{aligned} R &= 0.914 - 5.826\,d - 2.4\,10^{-4}\,V\,D - 0.108\,V\,F + 0.153\,D - 4.45\,10^{-4}\,D^2 \\ &+ 1.74\,10^{-4}\,V^2 + 3.6\,10^{-2}\,V\,d - 7.0\,10^{-2}\,F\,D \end{aligned} \tag{6.1}$$

The vibration acceleration amplitude in millivolts during the first five seconds for each test was used as a dependent variable R, while the set of dependent variables included : speed V; feed F; depth of cut d; and, workpiece diameter D. This model characterizes the tool dynamic behaviours when it is sharp. The ranges of the independent variables used to develop this model were as follows:

- Cutting Speed (V) $50 - 230\ m/min.$
- Feed (F) $0.06 - 0.6\ mm/rev.$
- Depth of Cut (d) $2 - 3\ mm.$
- Workpiece Diameter (D) $53 - 186\ mm.$

The whole set of data contained *24* data points for *24* separate tests of the central composite design *CCD*. The statistical criteria for such model are as follows:

- Correlation Factor R^2 = 70.35.
- Adj. R^2 = 54.533.
- Standard Error SE = 1.30369.
- F-Ratio = 4.45

This model reveals some important aspects which are now discussed. The vibration amplitude for sharp tools R increases by decreasing the depth of cut d, by increasing the workpiece diameter D, or by decreasing the speed-feed product VF. The amplitude increase at lower values of the depth of cut d can be explained as follows: increase the depth of cut causes the tool to be more tightly engaged with the workpiece which reduces its freedom to vibrate. However, there is a boundary limit for such mechanism to be stable. Higher depth of cuts, when it is accompanied by higher speeds produce higher vibration amplitudes. This is indicated in the model by a positive coefficient of the term involving the product of depth of cut and cutting speed Vd.

Also, the model (6.1) indicates that the tool tended to induce higher oscillating amplitudes when higher values of speeds were used. This higher amplitudes at higher speeds are thought to be due to the falling cutting force characteristics, introduced by *Arnold [125]*. This leads to a self-induced vibration of the tool in which high instability is sustained due to the variation in the force magnitudes when tool oscillates upward and downward, *Fig. 6.3*.

The higher amplitude at higher workpiece diameter is thought to be due the fact that the workpiece hardness is less for smaller diameters for the billet of material, *Rao [123]*. Such facts reveal that the vibration amplitude may be hardness dependent. However, in most practical production situations, metal removal using multi-passes using different workpiece diameters is not a desirable economic.

The effect of feed seems to be dependent on other parameters involved in the machining operation such as cutting speed and workpiece diameter. *Fig. 6.16* shows a

3-dimensional representation of model (6.1). Both depth of cut and the workpiece diameter are kept constant, and the initial vibration amplitude is plotted against the two main cutting parameters which are speed and feed.
Vibration amplitude is positively affected by speed and negatively by feed. However, the vibration attained higher amplitudes when higher values of speed-feed combination are used. Also, while amplitudes surface reveals a slight non-linearity with the cutting speed, a linear attitude is observed with the feed. This is expressed in model (6.1) as a second-order speed term.

6.5.2 Tool Life Determination using a Vibration Based Approach

As concluded before, a vibration power amplitude for stable turning operation using the normal cutting conditions reveals a significant interrelation with the level of the tool wear. As tool wear increases, such vibration power amplitude decreases until a certain limit is reached after which it tends to increase. It was explained that this limit could be used as an on-line criterion to determine the end of the tool life. An absolute agreement was found between tool life vibration-based criterion and those which were developed using both wear-time and cutting force relationships.
In order to clarify the aspect, a quantitative mathematical formulation is followed in this section to determine the tool life using the tool vibration and its dynamic characteristics.

The early reduction in the vibration power amplitude with increasing the wear was described as an increase in the damping resistance due to the increase the cutting force in the $X-$direction. Such an increase in feeding force component is, in turn, due to the wider flank wear land. Therefore, such damping resistance DR could be approximated as the instantaneous ratio of the vibration amplitude at early wear stage to the amplitude at any time within the tool working life.
Using such a ratio rather than the absolute value of the amplitude, eliminates the variability which may results among the repeated tests with the same nominal conditions.

Besides, any noisy signal could be cancelled. Moreover, the effect of the cutting conditions on the initial values of the amplitudes sometimes disturb the whole result. This is what forced *Taglia [139]* to ignore the vibration signals until a very advanced tool wear limit had been reached. However, using such damping resistance ratio produced more meaningful definition to the problem than if an absolute amplitude were used.
To retain the same trend of amplitude-wear, and consequently the wear rate trend, an inverse of the damping resistance DR was selected to be used in the analysis $\{A_c = \frac{1}{DR}\}$. Mathematically, A_c can be defined as the ratio of the vibration amplitude at any wear level to the initial vibration amplitude R when the tool was sharp.
Since A_c resembles the amplitude-wear trend, *Fig. 6.15,* a mathematical model of the following form can be suggested.

$$A_c\ (AW) = B1\ e^{(-C_1\ AW)} + B2\ e^{(C_2\ AW)} \tag{6.2}$$

The early decreasing trend of the A_c with the average wear AW, can be accounted for by a decaying exponential with a negative exponent whereas the subsequent increasing part can be modelled by an increasing exponential with positive exponent.

Since this model cannot be linearized by a simple transformation, such as a logarithmic transformation, non-linear estimation procedures were used to find the parameters, $B1$, C_1, $B2$, and C_2. Fitting of this model showed a very high correlation between estimates of C_1 and C_2, with their values being fairly close. This indicated over-parameterization and therefore a more parsimonious model was selected by setting $C_1 = C_2 = C$.

$$A_c\ (AW) = B1\ e^{(-C\ AW)} + B2\ e^{(C\ AW)} \tag{6.3}$$

Initial values of the parameters $B1$, C, and $B2$, which were necessary for the the non-linear estimation, were first determined by the linear regression by neglecting the part of the equation which had the positive exponent term. Such an assumption was based on the fact that the first exponential should dominate at the beginning which normally represented a wider range of data for each test.

The critical values of tool wear, AW_{cr}, at which A_c is a minimum, or the damping

resistance DR is a maximum, can be found by differentiating *Eq. (6.3)* and equating to zero as :

$$\frac{d\,(A_c)}{d\,(AW)} = 0.00 = -C\ B1\ e^{(-C\ AW_{cr})} + C\ B2\ e^{(C\ AW_{cr})}, \tag{6.4}$$

and thus

$$AW_{cr} = \frac{1}{2C}\left(\ln \frac{B1}{B2}\right) \tag{6.5}$$

The corresponding value of $A_{c_{min}}$ is obtained by back substitution of AW_{cr} into *Eq. (6.3)* , and hence

$$\begin{aligned} A_{c_{min}} &= B1\sqrt{\frac{B2}{B1}} + B2\sqrt{\frac{B1}{B2}} \\ &= 2\sqrt{B1B2} \\ &= 2B1\ e^{(-C\ AW_{cr})} \\ &= 2B2\ e^{(C\ AW_{cr})} \end{aligned} \tag{6.6}$$

Final values provided by the non-linear least squares procedure for each test along with the experimentally determined of critical wear are shown in *Table 6.1.* The first column shows the test number. The second, third, and fourth columns show the non-linear estimates of the parameters in *Eq. (6.3),* whereas the fifth column shows the corresponding correlation factor R^2. Column six and seven indicate the estimated critical wear, AW_{cr}, and the corresponding values of $A_{c_{min}}$. Finally, columns eight, nine, and ten show the experimental critical wear values based on wear-time curves; the experimental critical wear values based on force-time curves; and, the value $A_{c_{min}}$ if the experimental critical wear based on wear-time curves were used in form *(6.6).* The experimental critical tool wear value was taken as the value at which a higher rate of increase was observed in the curve.

From the results shown in *Table 6.1,* a very good agreement has been achieved, on one hand, between the critical wear values predicted by the non-linear model, column 6, and that from the experimental records, columns 8 and 9; and on the other hand, the model reveals a good ability to calculate the damping resistance values, column 7, which are very close to the actual experimental ones, column 10.

Generally, a very good agreement was found between the approach of using tool vibration, as a tool life determination criterion, and those using either wear-time or force-time criteria. These results support the hypothesis of using the vibration power amplitude at the natural frequency of the tool as an on-line index to monitor tool wear level during a continuous stable turning, and to determine the useful limit of the tool life without going further into the higher wear rate area.

Although the difference between the predicted and experimental critical wear values, *Table 6.1,* are not significant, and are far less than tool life variability observed during the conventional laboratory testing, an attempt to explain the sources of such differences is required for any further enhancement of the approach.
Essentially the error sources could be due either to the independent variable, the average wear AW, or to the dependent variable A_c. Between them, the former produced a greater effect due to several factors: Firstly, the wear progress was not equally distributed along the flank area as explained before. Secondly, the tool vibration mechanism seemed not to be affected equally by each element of nose wear NW; flank wear FW; and, notch wear NCW used in calculating the average value. Experimental results proved that nose wear NW was the most predominant one. Also, in most cases, the notch wear at the depth of cut NCW was not as large as the other two wear elements. Moreover, tool chipping and fracture could lead to an instantaneous instability as explained before.
However, *Test #12, table 6.1,* shows the worst case in which 0.06 mm difference exists between predicted and experimental values. This error is, in fact, less than any error if a conventional off-line method was used.

Fig. 6.17 shows the plots of both the experimental and the predicted values from model *6.2,* against the measured average wear. *Fig. 6.17.a & b* represents the best model predictions which are for *Test #2* and *Test #13,* while *Fig. 6.17.c & d* are the worst model predictions, which are for *Tests #3 & 14* where the cutting stability conditions were disturbed, as discussed before.

To the authors best knowledge this work is the first attempt to relate the tool dynamic characteristics to the average tool wear during the actual machining conditions which have produced encouraging results. The idea of using such a model to monitor tool wear, and to determine the end of tool life adds the advantage of being independent of cutting conditions and workpiece diameter. Providing on-line vibration signals are available, such a non-linear model could be on-line, self-built, and tuned. The point of changing direction along with change of the coefficients could be determined on-line. In computerized numerical CNC machin tools, the initial signature of a new tool can be stored in the host computer and then, continuously compared to the instantaneous tool signature at subsequent stages. The point at which the trend reverses its direction can be considered as the beginning of the failure zone at which the tool should be changed. Besides, this model can be used to detect cutting instability through observing of any deviation from the normal conditions at stable cutting. This strategy could be established probably in association the measurement of force signals, as a secondary in-process measure as is discussed next.

6.5.3 A Vibration-Force Tool Wear Estimation Approach

A combination of vibration, as represented by the coefficient of power amplitude variation A_c, and the thrust force component F_{xz}, which was previously found to be most sensitive to tool wear, was thought to produce a good tool wear predictor as already mentioned. In contrast to the last approach, such an approach represents the whole domain of operating parameters in which the data were collected.

The independent variable was suggested to be either the average flank wear AW or one of its components - nose wear NW, flank wear FW, or notch wear NCW. The independent variables involved were the coefficient of power amplitude variation A_c, thrust force component F_{xz}, cutting time t, and the cutting conditions: speed, feed, and depth of cut. The suggested model was of the form:

$$WEAR = C_o \; A_c^{C_1} \; F_{xz}^{C_2} \; t^{C_3} \; V^{C_4} \; F^{C_5} \; d^{C_6}. \tag{6.7}$$

Such a model can be linearized by a logarithmic transformation and therefore, a multiple linear regression routines can be used to determine its coefficients. Linear regression of such a model indicated some lack of fitness due to the non-linear nature of some of the data and it was thought that a second-order model was the remedy. However, a second-order model finished with twenty-six variables in the equation with slight improvement in the prediction capability over the first-order one. However, there were still some non-linear effects which were not detected by such a model, especially when the extreme value were to be estimated. Therefore, it was thought that a non-linear estimation procedure might overcome the problem.

Nose wear NW rather than the average wear AW was found to be best correlated with all the independent variables involved. The final model was as follows:

$$NW = 2.8 \times 10^{-3} A_c^{0.017} F_{xz}^{0.846} \left(\frac{t}{100}\right)^{0.194} \left(\frac{V}{100}\right)^{0.339} F^{0.053} d^{-1.005}. \qquad (6.8)$$

Statistical criteria are:

- Residual Sum of squares RSS = 0.17937.
- Corrected Correlation factor R^2 = 94.222.
- Standard Error SE :

  $SE(C_o) = 0.001$ $SE(C_1) = 0.023$

  $SE(C_2) = 0.016$ $SE(C_3) = 0.017$

  $SE(C_4) = 0.051$ $SE(C_5) = 0.041$

  $SE(C_6) = 0.068$

The corresponding model using the ordinary multiple linear regression takes the following form:

$$NW = 1.36 \times 10^{-4} A_c^{-0.015} F_{xz}^{0.847} t^{0.172} V^{0.423} F^{-0.088} d^{-0.987}. \qquad (6.9)$$

Statistical criteria are :

- Correlation Factor R^2 = 86.4.
- Standard Error SE = 0.1207.
- F-Ratio = 206.

Good improvement has been achieved in the correlation factor from 86.4, for ordinary multiple linear regression *(6.9)*, to 94.22 using the non-linear regression model *(6.8)*. *Fig. 6.18* represents typical plots of the experimental nose wear values against the cutting time for *Tests #4* and *10*. This figure also indicates both the corresponding linear and non-linear estimates. Good agreement are observed between the experimental and the predicted values. Between the linear and non-linear models, the latter is more accurate especially at later stages of the tool life. During this stage the tool wear exhibits some non-linear behaviour with the cutting time which is better detected by a non-linear model.

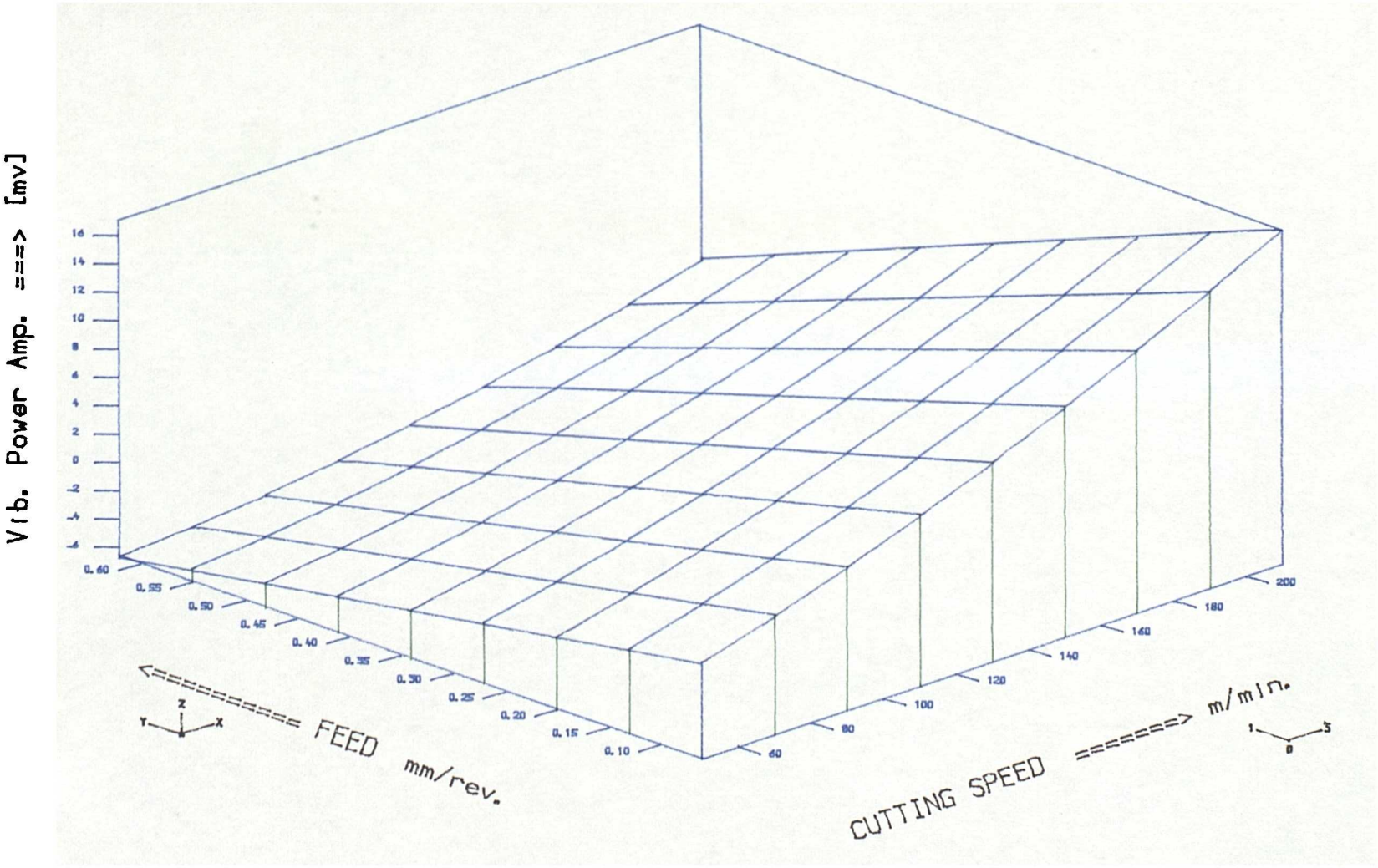

Fig. 6.16 Effect Of Speed and Feed on The Amplitude of Initial Vibration Value

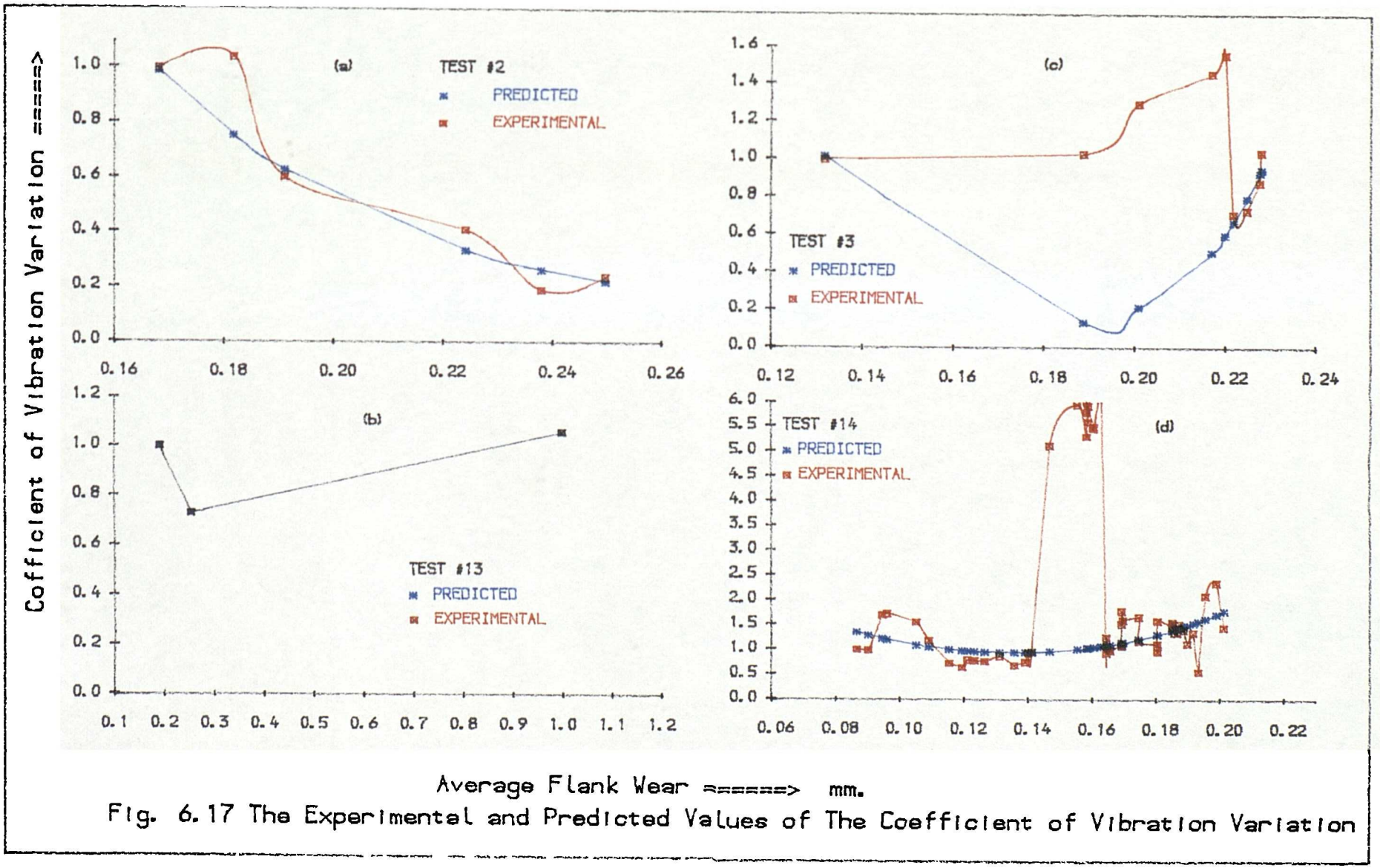

Fig. 6.17 The Experimental and Predicted Values of The Coefficient of Vibration Variation

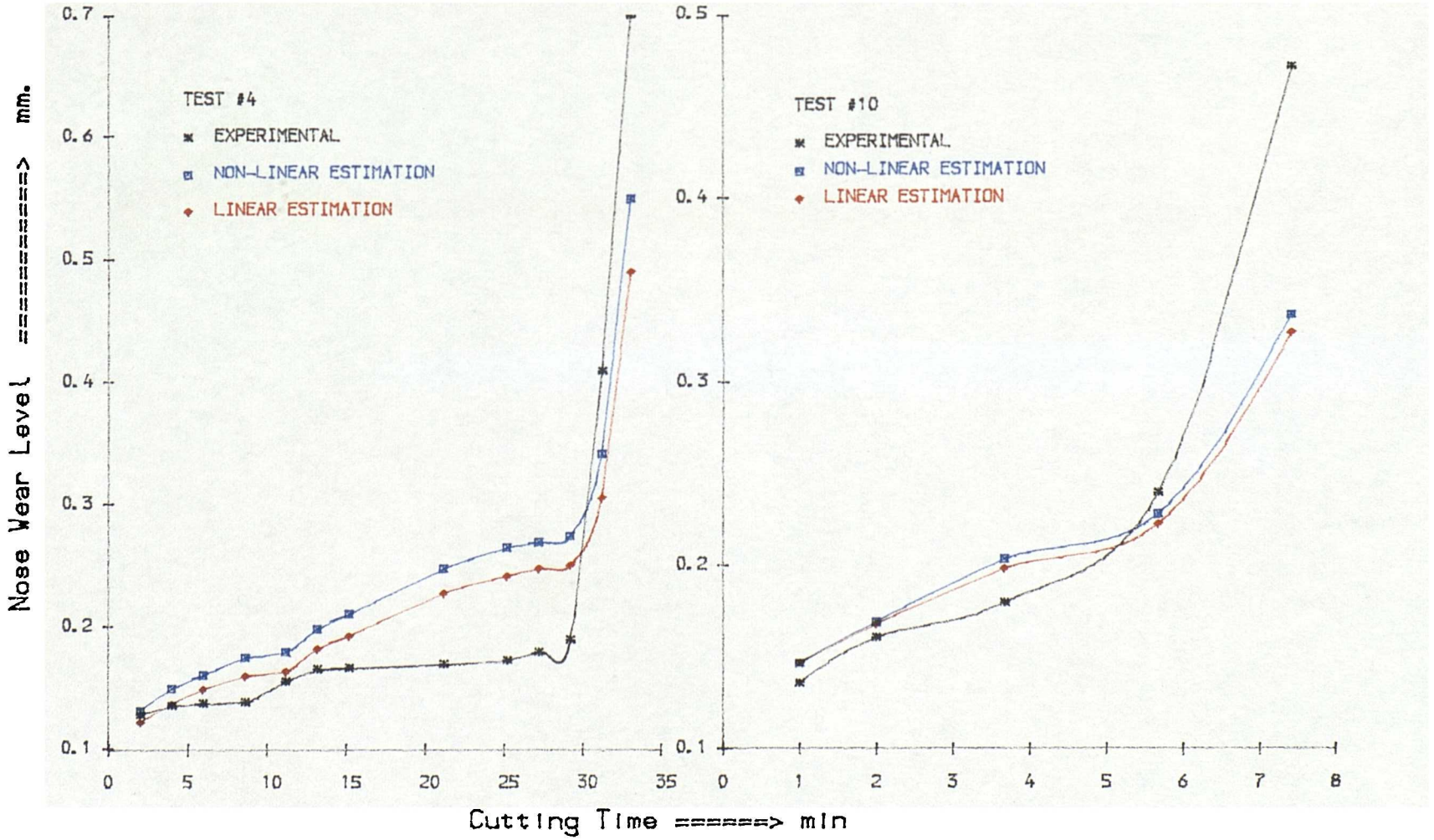

Fig. 6.18 Experimental and Predicted Linear and non-linear Nose Wear Vibration-Based Models

TEST NO.	COEFFICIENTS			CORRELATION FACTOR R^2	CRITICAL WEAR AW_{cr}(mm.)	Ac_{min}	EXPERIMENTAL RESULTS		
	B1	C	B2				CRITICAL WEAR		AC_{min}
							WEAR CURVE	FORCE CURVE	
2	29.41	20.21	0.0002	97.16	0.295	0.152	0.240	0.240	0.188
3	2090.	57.95	1.7E-6	79.00	0.185	0.120	0.230	0.230	0.696
4	5.32	16.15	0.0002	59.63	0.249	0.190	0.200	0.200	0.234
5	4.33	11.63	0.0103	85.96	0.260	0.422	0.238	0.245	0.190
7	11.65	17.92	0.0066	48.34	0.209	0.553	0.183	0.183	0.496
9	4.81	12.96	0.1700	52.42	0.223	0.572	0.243	0.243	0.451
10	2.81	9.10	0.0347	93.10	0.241	0.628	0.234	0.234	0.689
11	20.80	20.88	0.0027	76.19	0.215	0.470	0.263	0.200	0.313
12	3.59	13.41	0.0493	25.98	0.160	0.841	0.218	0.218	0.874
13	2.70	5.22	0.0056	100.0	0.591	0.247	0.500	0.500	0.734
14	5.93	18.8	0.0373	32.49	0.135	0.942	0.195	0.195	0.557
18	3.69	11.30	0.0218	76.37	0.227	0.567	0.235	0.235	0.455
23	17.74	24.70	0.0066	81.33	0.160	0.682	0.200	0.200	0.717

Table 6.1 Non-Linear Estimates and the Corresponding Experimental Values

6.6 General Discussions And Conclusions

The vibration during normal conditions of stable centre lathe turning operation has been investigated. The vibration signals for a wide range of operating conditions were recorded using two accelerometers in the $X-$ and $Y-$directions. The recorded signals were later analyzed by a Fast Fourier Transform *(FFT)* analyzer. The output from the analyzer, in forms of power spectra in the frequency domain, were fully investigated, and an interrelation has been found between tool vibration characteristics and the evaluation of the tool wear. Such studies resulted in important conclusions which may be summarized as follows:

1. A frequency range of 10 kHz was found to represent the dynamic characteristics of the system used in this study; outside this range no frequency response was found.

2. A unique and consistent power spectrum characteristic was found for the wide range of machining parameters. The components of the characteristic were identified using the dynamic calibration of the dynamometer.

3. Among the vibration signature which appeared in the power spectrum envelope, the component at the frequency (1250 *to* $1360Hz$) was found to be most affected by the tool wear. Such a frequency band was previously denoted as the first fundamental natural frequency of the dynamometer in the $X-$direction. Although this signature appeared in both $X-$ and $Y-$spectra, its amplitude in the X spectrum was found to have a more reliable and consistent trend with both the wear and the force characteristics.

4. The analysis of the individual tests revealed that the value of the power amplitude at frequency 1250 to 1360 Hz was decreasing as the tool wear was increased; then the amplitude reversed its direction and tended to increase at advanced wear levels. The point at which the power amplitude reached its minimum value was found to be in a good agreement with the moment at which higher rates of both

the wear and the force were obtained. However, the rate of increase of the power amplitude, after reaching its minimum value, was found to be dependent on the the wear rate, and consequently, on the cutting conditions.

5. The proposed vibration approach demonstrates a high capability to detect any disturbances to the system stability. Moreover, an early warning strategy is one of the advantages produced by using the tool vibration detection techniques.

6. The proposed approach was found to be valid only for relatively high speed range of more than 70 m/min.; the observed trend was more consistent for the higher cutting speeds.

7. The tool vibration and dynamic characteristics was further quantitatively explored by mathematical modelling of the experimental data. A multiple linear regression technique was used to estimate the parameters required for a second-order model relating the initial absolute values of the power amplitude to the machining parameters. Such an initial amplitude, when the tool was sharp, was positively affected by speed-feed product and workpiece diameter, whilst it was negatively affected by the value of depth of cut.

   A non-linear least-squares routine was used to build a non-linear model which relates the variation of the power amplitude to the corresponding average wear values. Using such model, a critical wear value were determined which was in good agreement with experimental values of both wear-time and force-time relationships. This could be the first step to establish an approach in which tool life is determined on-line.

   Finally, a non-linear model was built, using a non-linear least squares routine, to predict the values of the nose wear during cutting. A combination of the power amplitude variation coefficient, wear force component, cutting time, and cutting conditions were used to build such a model. A highly significant model was established; the gain achieved using non-linear estimates rather than the ordinary multiple linear regression was justified.

Chapter 7

TECHNOLOGICAL APPLICATIONS OF THE DEVELOPED MATHEMATICAL MODELS

7.1 Foreword

The mathematical models developed in this study have the capability to be applied and interpreted in many technological applications such as adaptive control of machine tools and creation of machinability data bank systems.

This chapter is devoted to the investigation of how the developed models can be used as a powerful information source for a prospective turning system using the latest advanced machine tools technology. The latest state of arts is surveyed. This is followed by the way by which the current study may help in enhancing some vital aspects, such as: the validation of mathematical models to be used in adaptive control strategies; the application of models in on-line detection of the tool wear; the use of models in maximizing the system productivity; the capability of models to be applied in attaining the pre-specified tool life during cutting; and, the model contribution in solving some of the problems of the existing technique of machinability data bank systems. Also, it is explained how the developed models can be used within a suitable computer software to obtain a prior expectation of the system behaviour.

7.2 Adaptive Control Applications

In the following is a general review of the latest state of the arts of modern machining facilities and techniques.

7.2.1 Introduction

The introduction of super-hard materials, used in manufacturing aircraft parts, nuclear constructions, weapons, etc., along with the complication of workpiece configuration, and the extreme accuracy required, were the reasons behind looking for new machining methods and techniques. As a result of many efforts, the first Numerically Controlled

NC milling machine was introduced in 1952. Since then, the most significant development in manufacturing has been the advent and wide-scale adaption of numerically, tape-, and computer-controlled machine tools.

The first generation of such *NC* machines, used punched paper tapes to input the part program. This part program is processed and interpreted in the hardwired machine controller. The controller sends out signals to the axes motors producing linear and/or circular interpolation movements. In the early years the part program was manually prepared by the part programmer and that was a time consuming procedure, especially for complex operations such as contouring and three-dimensional machining. It was also necessary to check the tape on the machine tool several time to ensure that it was error free. Therefore, a computer-assisted part program replaced the manual preparation. This was done using special languages such as *APT, EXAPT 1, EXAPT 2, COMPACT II*, which were designed for most *NC* controllers. The result being a punched paper tape produced in a reasonable time. As a result of the rapid developments in the computer technology, mini- or micro-computers have replaced the *NC* hardwired controllers. This has achieved more flexibility in the machining process. The result was the computerized numerically controlled machine tool type *CNC*. With *CNC* machine tools, additional functions, to those available with *NC* machine tools, are accessible which permit editing and storing of programs.

Direct numerically controlled machine tools *DNC* were developed subsequently to *CNC* type. They enabled several machines to be operated just by one operator because the program and the machining instructions are loaded directly from central computer. Moreover, information about the state of the workshop floor can be fed back to the central computer so that the whole operations can be synchronized. In *DNC* a well qualified operator or engineer is required. Such a person should have a good knowledge about the production process; machinability data selection; and, any other relevant information.

However, even with all of these developments, the choice of the cutting conditions still depends on human experience and on some machinability data references. In order

to preserve the tool, even under the most adverse conditions, the part programmer prefers to select conservative values for the operating parameters which consequently slow down the system productivity. Inherent in these procedures are the following drawbacks:

i. the un-repeated part of the machining environment;
ii. new tool and workpiece materials have to be handled;
iii. human interface has not been eliminated; and,
iv. improvement in the productivity is not proportional to the cost of equipment.

As a result, a new development in the form of adaptive control AC of machine tools has been proposed. In AC the optimal cutting speed and/or feed can be chosen automatically, and modified whenever the need arises. The idea is that the adaptive control system seeks the best on-line cutting conditions for an individual machine for each specific operation as it is being performed, and thus, it provides the machine with much more flexibility especially for products with complicated configurations in terms of:

i. greater safety where fewer failure are likely to occur;
ii. time-saving in terms of maximum utilization of the operating and program preparation;
iii. minimum human interfacing;
iv. reduced wear rate through optimizing the operating parameters; and,
v. overall efficiency improvement.

Such developments have enabled considerable progress to be made towards the achievement of optimal productivity at minimum cost.

The main idea in adaptive control of machine tools is based on the measurement of process variables in real time, followed by on-line adjustment of the operating parameters subject to machining constraints in order to optimize the performance of the overall

system. Whereas on the one hand numerical facilities guide the sequence of tool position or the tool path during machining, adaptive control, as a feedback system on the other hand, chooses the operating parameters as a function of variations in such factors as work material hardness; width or depth of cut; and, air gaps in the part geometry. *Fig. 7.1* shows a schematic view of the basic aspects of adaptive control system in which the operating parameters have automatically been selected for the actual conditions of the process.

As shown in *Fig. 7.2*, the subject of adaptive control of machining process can be split into two major distinct topics; geometrical adaptive control *GAC*, and technological adaptive control *TAC*.

Geometrical adaptive control *GAC* is referred to as the control techniques in machining to achieve stability of dimensional accuracy; and, to improve the surface roughness of machined parts. Most applications of *GAC* are restricted to the dimensional measurement of a workpiece during machining, and compensatory decisions are taken accordingly. *Shiraishi [144]* used an optical method to measure the workpiece radius and to report any deviation from the programmed value to the machine controller for compensatory action. *Szafarczyk [145]* measured the workpiece radius on a stationary workpiece during interruption between subsequent cuts. However, Szafarczyk reported some difficulties such as the thermal deformation of the machine tool elements which affected the workpiece dimensional accuracy. Besides, the time taken for such measurement may delay the total production time and adds extra time and labour cost. Moreover, other factors which have generally delayed the widespread application of this technique may be summarized as follows:

i. a large-scale equipment is required to build the overall system;

ii. the complex geometry cannot dealt with;

iii. the outcome depends on the basic accuracy of the machine system;

iv. using laser beams requires ultimate safety requirements; and,

v. the reflected signals may contain noise generated from chip and coolant accumulation.

These inherent difficulties restricted the application of *GAC* to end-milling and grinding where the workpiece or tool deflections is easily recognised.

Technological adaptive Control *TAC* can be divided into two subsystems; adaptive control constraints *ACC* and adaptive control optimization *ACO*. Adaptive control constraints *ACC* is based on maximizing the operating parameters, such as cutting speed and feedrate, subject to process and machine constraints, such as cutting force on the tool, or maximum power of the machine. One of the functions of the *ACC* is to maximize the feedrate while maintaining a constant load on the tool, despite variations in width and depth of cut. This achieves maximum productivity while minimizing the probability of cutting tool breakage. Also, *ACC* systems can improve the part dimensional accuracy by limiting tool deflections.

ACC was initially designed for milling machines and was based on analog hardware. The increasing use of *CNC* machine tools offered the possibility of integrating the constraints control in the computer which is already available. On one hand, powerful control algorithms with *AC* modifications can be facilitated, and on the other hand the amount of the additional hardware required is kept minimal. Several investigators have manipulated *ACC* systems using different strategies *[146-156]*.

Adaptive control optimization techniques *ACO* present a high level of process control and organization. *ACO* has the task of optimizing machine time and cost during the manufacturing process through controlling the tool wear variable. In contrast to *ACC*, *ACO* requires intensive computation algorithms. The elements required for such technique are the optimization computer, performance computer, data reduction system, along with the sensors, interfaces and other logic functions. The performance index, usually in terms of minimizing cost or wear rate or maximizing *MRR*, is stored in the performance computer. The optimizer usually contains the relevant models and/or data along with information concerning the production environment and machining constraints. The sensors system may include torque, force, or temperature. The signal from such sensors are processed producing the present state of tool wear rate, machining cost, and/or *MRR*. These values are compared to the desired objectives through

the performance computer. Any deviations can be dealt with in the optimization computer which produces the corrected values of feedrates and/or speeds.
As explained, the heart of *ACO* system is the tool wear sensor and due to the lack of a reliable one, *ACO* systems have not produced much practical contribution to the manufacturing technology. Few experimental investigations have been done which have been concerned with the development and applications of *ACO* systems *[157 & 158]*. A survey by *Milner [159]* indicated that adaptive control constraint *ACC* has been the only method developed which is suitable for general application. This is because, according to *Milner*, the development of adaptive control optimization systems depends heavily on the on-line measurement of tool wear and this problem has never been solved satisfactory. A summary of *Milner's* survey is presented in *Table 7.1.*

In summary, in *AC* systems, the machinability software program is stored in the machinability preprocessor which is used to compute the optimal spindle speed and maximum feedrate. The computations are performed by using the built-in algorithms and mathematical models of the cutting process and require input information such as workpiece material, tool material, depth of cut, maximum allowable power. To be useful and reliable, the mathematical models and algorithms must be developed based on previously collected machining data which relates machining operating parameters, (e.g. speed, feed, and depth of cut), to one or more of the operation responses, (e.g. tool wear, tool wear rate, cutting force, surface finish, tool life, tool vibrations). Therefore, for an adaptive control system to be established, the following elements should be available;

1. A computerized numerically controlled *CNC* or direct numerically controlled *DNC* machine tool with a closed-loop feedback circuit. However, an existing conventional machine tool can be retrieved using a suitable processor and *DC* motor.
2. An adaptive controller, in a form of separate hardware or a robust software, to be included in the existing host computer.
3. Group of sensors such as cutting force dynamometer, watt- meters, thermocou-

ples, vibration accelerometer, or current meters.

4. Mathematical models which represent the process. Such models must cover the whole range of operating parameters and relate them to the system outputs. The accuracy of the overall system depends on the accuracy of the model, therefore the more significant the model the better the enhancement of the system will be.

5. Strategy algorithms to organize the overall operation. Such algorithms contain the group of logic steps required to receive information concerning the machining state; to compare it with the current information; and to provide a quick response to allow the corrected parameters to be implemented in the process. Also, it may include the performance index or the operating functions.

6. Set of electronics and software interface such as digital to analog converters *DAC* and analog to digital converters *ADC*, amplifiers, clocks, and data processing software.

This project basically deals with the aspect of building a new approach based on mathematical models for turning operation shop-floor conditions. Such models must be capable of characterizing, and being used in multi-purpose environments in a practical *AC* system.

In what follows is an account of the *AC* system, based on the mathematical models developed in this study. The models developed in previous chapters will be re-stated whenever necessary; they relate the system outputs such as: cutting force; tool wear; tool wear rate; tool life; and, tool vibration to each other and/or to cutting conditions such as: speed; feed; depth of cut; and, cutting time. These models were designed, postulated, and fitted to the collected experimental data using either the conventional linear or the new non-linear least-squares computer regression packages to predict the models coefficients.

The idea is to adapt the developed models to some of the production performance functions in order to integrate a software to be used in *CNC* machine tools, which meet

the aforementioned adaptive control requirements.

First, a study is introduced of the validity of the developed models for use in adaptive control system where machining parameters are subject to change for the same tool in the same operation.

Second, the structure of three adaptive control systems are proposed, which use the developed models, along with the appropriate strategies and algorithms.

7.2.2 Validity of Models for Use in Adaptive Control Systems

In this study, mathematical models are developed in which the tool wear; the cutting forces; and the tool vibration are the dependent parameters to be measured. Such models were developed using the experimental data collected from constant parameter tests in which the speed, feed, and depth of cut were kept constant throughout the entire test until tool wear reaches a critical value after which the tool is no longer capable of efficient cutting. However, in practice the same tool is used for a succession of different cutting parameters. This situation applies for tools used in adaptive control strategies where speed and/or feed are subject to modification when the need arises during the same cut. Also, these procedures are essential in flexible manufacturing systems, and even in conventional and automatic machining. To predict tool life in such situations, it is usually assumed that the further wear of a partly worn tool is independent of previous cutting conditions. The assumption makes possible the assessment of the tool wear increments during consecutive cutting periods. The resultant wear is calculated by the summation of these increments. Such independence is often assumed without verification, and sometimes leads to significance error. The verification of such assumption has been investigated by *Jemielniak et al [67]* for coated and uncoated carbide tools. He concluded that the assumption of sequence independence depends on tool material, and on the tool life criterion. For uncoated tools, where the spread of feed values is not too wide, there is a possibility of using tool wear characteristics, obtained for cutting with constant parameters for the prediction of tool wear under variable cutting speeds and feeds. However, this is not the case for coated carbide tools *(TiC-TiN)* where further

progress of wear in a partly worn tool is dependent on previous cutting conditions. However, the validity is examined of the idea that models developed could be accurately used for on-line control of cutting conditions.

First, an analytical investigation is produced of a tool working under variables conditions within the different stages of its working life.

Consider three different tools cutting under three different cutting conditions, speed, feed, and depth of cut, which is referred as (Vk, Fk, dk), where k denotes cutting conditions and takes the values 1,2, or 3. For the tool no.1 which has conditions $(V1, F1, d1)$, the wear-time curve may be assumed as the curve 1 in *Fig. 7.3.* Whilst for tools nos. 2 and 3, which working under the conditions $(V2, F2, d2)$ and $(V3, F3, d3)$, the wear-time curves are 2 and 3 respectively. The current investigation deals mainly with the straight line region of wear-time curve in which tool wear rate is almost constant, since it is the region where most of tool working life lies in; and is often described as the commercial region.

Now, assume that a particular cutting tool is to be used under these three conditions for different cutting periods within the span of its useful life, as follows:

- Cut No. 1 $(V1, F1, d1)$ for $t1$ minutes cutting; then,
- Cut No. 2 $(V2, F2, d2)$ for $(t2 - t1)$ minutes cutting; then,
- Cut No. 3 $(V3, F3, d3)$ for $(t3 - t2)$ minutes cutting; then,
- Cut No. 4 $(V1, F1, d1)$ for $(t4 - t3)$ minutes cutting; and finally,
- Cut No. 5 $(V2, F2, d2)$ for $(t5 - t4)$ minutes cutting.

As shown in *Fig. 7.3,* wear rate slope is changed every time the conditions is changed to suit the new conditions. After a total of $t5$ cutting time, the actual wear curve takes the broken dotted line with final wear level of $AW5$. As shown in *Fig. 7.3,* the partial wear increment for each step are $d10$, $d21$, $d32$, $d43$, and $d54$ respectively. Thus, the following relationships can be obtained:

$$
\begin{aligned}
AW1 &= F(V1, F1, d1, t1) \\
AW2 &= AW1 + d21 \\
AW3 &= AW2 + d32 \\
AW4 &= AW3 + d43 \\
AW5 &= AW4 + d54 \\
&= AW1 + d21 + d32 + d43 + d54. \qquad (7.1)
\end{aligned}
$$

where dij is the wear increment as a result of changing conditions from (Vj, Fj, dj) to (Vi, Fi, di) for $(ti - tj)$ minutes cutting, and generally,

$$
\begin{aligned}
dij &= AWi - AWj \\
&= F[Vi, Fi, di, (ti - tj)], \quad j = i - 1. \qquad (7.2)
\end{aligned}
$$

where, AWi is the total wear for conditions (Vi, Fi, di) for $(ti - tj)$ minutes, and AWj is the accumulated wear after using the tool for tj minutes using either variable or fixed cutting conditions.

At this stage, the question is posed: can the mathematical model based on constant cutting conditions be applied to situations where cutting conditions are subject to change at any time within the same cut? To answer such a question, verification procedures of the models are next discussed.

Consider that the following three sets of test conditions are to be used randomly for the same cutting tool.

[Set1] has conditions of (100, 0.2, 3.0) with a cutting time of 3 minutes;

[Set2] has conditions of (130, 0.1, 2.5) with a cutting time of 5 minutes; and,

[Set3] has conditions of (80, 0.3, 2.0) with a cutting time of 10 minutes.

Suppose that these three different conditions are to be used for different cutting periods for the same tool as the need arose. The possible different sequences are set out as follows:

[Tool No.1]	Set1,	followed by	Set2;	and then,	Set3.
[Tool No.2]	Set1,	followed by	Set3;	and then,	Set2.
[Tool No.3]	Set2,	followed by	Set1;	and then,	Set3.
[Tool No.4]	Set2,	followed by	Set3;	and then,	Set1.
[Tool No.5]	Set3,	followed by	Set1;	and then,	Set2.
[Tool No.6]	Set3,	followed by	Set2;	and then,	Set1.

A model for the average wear AW is selected just to verify the current aspect.

$$AW = 6.7 \times 10^{-3} \; V^{0.605} \; F^{0.180} \; d^{0.223} \; t^{0.246}. \tag{7.3}$$

This model is for the entire set of the experimental data (669 data points listed in Appendix A). Using this model, the average wear values for the above different arrangement can be computed. *Fig. 7.4* shows the result of such computations for each tool for a total cutting time of 18 minutes on three steps, using the conditions stated above.

When cutting started and finished with similar conditions, an almost identical wear level is obtained at the end of the cutting periods. This is clear for tools 1,2,3, and 4 from one side and for tools 5 and 6 from the other side. However, as shown in *Fig. 7.4*, there is a slight difference ($\approx 0.02\ mm$) in the predicted values between the two groups. It has been noticed that the gap is wider when the difference in the starting conditions, especially the cutting speed, is larger. The starting speed for tools 5 and 6 is 80 m/min, while it is 100 for tools 1 and 2 , and 130 for tools 3 and 4. Although the maximum deviation, which represents at most 10% of the mean value at its worst condition, is not significant and is still well within the permissible allowances in the metal cutting field; in the following section an attempt is made to elucidate this aspect.

Consider two wear-time cases in which two different cutting conditions are used, as shown in *Fig. 7.5*. The first tool starts with condition $(V1, F1, d1)$ for cutting time $t1$ and then changes to condition $(V2, F2, d2)$ for some cutting time ti, where higher speed and feed are applied, path CBA. In the second case the situation is reversed, path FED. Theoretically, the developed wear levels at ti for both cases should be the

same. However, as shown in *Fig. 7.5*, at any time *ti* within the area in which the condition changes its direction, the total developed wear level for each case is different where;

$$d = AW21 - AW12. \tag{7.4}$$

This difference, d, is zero only at a certain cutting time T, *Fig. 7.5*, at which there is no effect for changing conditions. Below this point the difference is positive due to commencement of cutting with higher condition, whilst beyond it, the case is reversed due to the longer cutting time involved. To investigate the effect of such wear prediction errors, which result from the fact that random cutting periods are used, another extensive verification procedure is arranged.

Consider the following ranges of cutting conditions:

- Cutting Speed (V) $80, 150, 200\ m/min.$
- Feed (F) $0.1, 0.3, 0.5\ mm/rev.$
- D.O.C (d) 2, 2.5, 3 *mm.*
- Cutting Periods 15, 5, 3 *minutes.*

These conditions are to be arranged so that two aspects are to be examined, these are: the prediction error of the mathematical model when cutting conditions are applied for fixed cutting periods; and, the prediction behaviour when conditions are applied for variable cutting periods.

To investigate the first aspect using the above set of conditions, a particular parameter, speed, feed, or depth of cut is used for a certain time interval while the sequence of applying each pair, the parameter and its indispensable time, is changed from one tool to another. When a parameter is used as a variable, the other two parameters are kept constant. A Summary of such arrangements, along with the computations using the same wear mathematical model (7.3), in conjuction with relations (7.1) and (7.2), are listed in *Table 7.2*, groups (1-A), (1-B), and (1-C). Group (1-A), *Table 7.2*, represents the arrangement when the cutting speed is used as a variable parameter,

while groups (1-B) and (1-C) are for the feed and the depth of cut respectively. As shown in *Table 7.2,* the final wear level for each group is almost identical whatever the sequence is. This indicates that for any tool used in machining with different cutting conditions, but with fixed cutting intervals, the final wear level is not affected by such variation of conditions. *Fig. 7.6* shows plots for different tool wear paths for group (1-A). As can be seen all tools have the same final wear levels.

For groups (2-A), (2-B), and (2-C), where the sequence of conditions for all tools is kept constant while the cutting intervals are varied, the final wear level developed for each tool is different from the others. *Fig. 7.7* shows plots for tools in group (2-A) and indicates that the final wear on the tool after many cuts with different conditions for random cutting intervals depends on the applied conditions and the time intervals. Also, as indicated in *Table 7.2*, the maximum error in the predicted value of the final tool wear for the different tools is most affected by speed, less affected by feed, and least affected by by values of depth of cut.

In summary, the computed final values of tool, for different cutting conditions with un-prespecified cutting intervals, depends on the present conditions, the previous conditions, and on the cutting time taken for each period of the process.

As can be seen from *Fig. 7.5*, such a conclusion agrees with the fact that the deviation exists for any individual cut as long as its cutting time in not equal to T. Moreover, due to the effect of using different cutting conditions in the first step, the initial tool wear in the break-in region should be introduced.

As concluded before, (see *Section 5.2.2*), the initial wear W_o is dependent upon the cutting conditions and is given by (5.17).

As shown in *Fig. 7.5*, total average wear developed after cutting time ti for the first case when conditions change from $(V1, F1, d1)$ to $(V2, F2, d2)$ is :

$$AW12 = W_{o1} + m1 \times t1 + m2 \times (ti - t1). \tag{7.5}$$

while for the second case when conditions change from $(V2, F2, d2)$ to $(V1, F1, d1)$,

$$AW21 = W_{o2} + m2 \times t1 + m1 \times (ti - t1). \tag{7.6}$$

where $m1$ and $m2$ are the curves slopes for the first and the second cases respectively. Since $W_{o1} \neq W_{o2}$ and $m1 \neq m2$, then, $AW12 \neq AW21$. By letting $ti = T$, we get:

$$AW12 = W_{o1} + m1 \times t1 + m2 \times (T - ti). \tag{7.7}$$

and

$$AW21 = W_{o2} + m2 \times t1 + m1 \times (T - ti). \tag{7.8}$$

Hence by equating both *RHS* of (7.7) and (7.8) are obtained:

$$T = \frac{W_{o2} - W_{o1}}{m2 - m1} + 2 \times t1. \tag{7.9}$$

Equation *(7.9)* indicates that the deviation or the error in wear at the end of cut, for conditions which are different from preceding conditions, depends not only on previous cut $m1$ and its time $t1$, but also on the difference in the initial wear values which result from such conditions variation. Therefore, if absolute accuracy is required, the difference in both the initial wear values and time periods could be taken into consideration. However, the accumulated errors at the end of the tool working life do not exceed, at worst, the standard deviation of any developed mathematical model or the tool wear variability due to the use of different tools of the same type.

Fig. 7.8 is a re-production of *Fig 7.4* after compensating for such factors. The difference is slightly improved at the end of the tool working time, but such improvement is not worthy of inclusion in a complicated adaptive control strategy software.

Therefore, it may be concluded that the tool wear error, if it exists, is due to the the nature of the metal cutting rather than to predictive capability of the model.

The same may be applied to all the mathematical models developed in this study, and thus, they are valid to be used in adaptive control situations where cutting conditions are subject to change at any instant to meet the system requirements.

In the following section adaptive control strategies are proposed using the mathematical models which are developed in this study.

7.2.3 On-Line Tool Wear Monitoring Adaptive Control System

The proposal is to use the measured cutting force signals as an input to the AC algorithms, which may be included in the machine tool computer, to predict the current state of the tool wear. Cutting force signals may be measured using a cutting force dynamometer. *Fig. 7.9* shows a block diagram of the structure of the proposed system. The adaptive controller could be either a self-contained unit or an integrated unit within the machine tool processor. The AC controller will contain both the system software and operating strategies. System software will include the relevant mathematical models along with the part program. The operating strategies include the logic sequence of commands which organize the entire operation, and the optimization algorithms which determine the objective functions and the operating constraints.

Fig. 7.10 summarizes such an AC strategy for on-line tool wear monitoring under tool cutting force constraint. The idea is to estimate tool wear levels and tool wear rates during continuous turning while maintaining the level of the cutting forces within a permissible region $F \leq F_{cr}$. This allows on-line tool life determination and correction of the cutting parameters to preserve the cutting edge. Tool life and wear rate criteria are supplied to the system according to the production requirements.

As concluded in **Chapter 5,** cutting forces which are: the feed component F_x; radial component F_z; the thrust component F_{xz}, or one of their ratios to the vertical component F_y, proved to have the capability to detect and predict tool wear, breakage, and failure. such tool random forms of failure. According to the proposed strategy in *Fig. 7.10,* a critical cutting force value F_{cr} may be specified to avoid higher values of wear and to protect the toolholder and the machine tool. During the cutting operation, tool wear is continously monitored and a tool change decision is taken following the violation of the wear limit W_{cr}. The cutting force which has been used in this strategy should be the ratio (F_z/F_y); since, as explained in **Chapter 5,** it proved to correlate most clearly with the tool wear (see relation (5.65)). Alternatively, the same strategy could be applied to the individual local wear elements such as the nose wear NW as is given by the relation (5.66). As shown in *Fig. 7.10,* information about depth of

cut and the criterion wear level AW_{cr} are entered as an input requirements. Once the system is activated, the measured force values are received by the AC controller and both initial values of wear and 1 force are first computed using models equations (5.7) and (5.23), which was developed in **Chapter 5**. The measured force is continuously checked to ascertain whether it is still within the safe range. In the current example, *Fig. 7.10,* a 50% increase in the cutting force is taken as a critical value F_{cr} after which the tool should be changed. The wear rate TWR can be obtained by rearranging and differentiating (5.31), which was developed in **Chapter 5,** so that:

$$\begin{aligned} TWR &= \frac{d(AW)}{dt} \\ &= 3.29 \times 10^{-5} \, [F_z(t)]^{0.787} \, V^{0.668} \, F^{-0.309} \, d^{-0.556} \, t^{-0.746}. \end{aligned} \tag{7.10}$$

Models (5.7), (5.23), (5.65), (5.31), and (7.10) represent the heart of the AC software in which the tool wear rate is minimized constraining the force change, which can be achieved by variation of speed and feed.

7.2.4 Maximization of Productivity using Adaptive Control Constraints ACC system

Adaptive control AC of machine tools holds promise as a technique for improving productivity, since no high capital investment or drastic changes in manufacturing process and techniques are involved.

An adaptive control system to increase the system productivity is discussed in this section which is based on the developed mathematical models. The productivity can be defined as the output per unit time for individual machine tool. In *NC, CNC,* or *DNC* machining process, fixed values of V and F are used, within the part program or by operator's manual data input, whilst in the proposed strategy these parameters are modified so as to maximize MMR under the machining constraints of machine capacity and tooling safety.

Frequently, metal removal rate MRR is used to determine productivity in roughing

machining operation as follows:

$$MRR = 100 \times V \times F \times d \qquad mm^3/min. \tag{7.11}$$

where; V is the cutting speed in m/min.;

F is the feed in mm/rev.; and,

d is the depth of cut in mm.

Thus, MRR is dependent on the cutting conditions where an increase in any of these parameters leads to an increase in MRR. System constraints always place limits on such increase; for instance, machine tool power limit or the safety of its elements.
In the following sections it is shown how the mathematical models, developed in **Chapter 5,** may be used to build such AC system.

The power consumed during machining can be specified as the product of the instantaneous force and the corresponding cutting speed.

$$Power = Co \times F_y \times V \tag{7.12}$$

where F_y is the vertical (main) cutting force component and V is the cutting speed. If F_y has units of Newtons and V m/min, then $Co = (1/60000)$, and the power P will be in kW. A model of F_y , as a function of cutting conditions and tool average wear, was developed to have the form (5.30).

$$F_y = 8375\, V^{-0.180}\, F^{0.627}\, d^{0.844}\, t^{-0.049}\, AW^{0.342}.$$

Substitution of (5.30) into (7.12), thus;

$$P = 0.140\, V^{0.180}\, F^{0.627}\, d^{0.844}\, t^{-0.049}\, AW^{0.342}. \tag{7.13}$$

Also, tool force model was found to take the form (5.32):

$$F_{xz} = 55354\, V^{-0.484}\, F^{0.236}\, d^{0.715}\, t^{-0.173}\, AW^{1.01}.$$

A model of form (7.3), which is developed in *Section 7.2.2*, is used to compute tool wear level at any time as a function of cutting conditions.

Fig. 7.11 shows a flow chart of the proposed strategy to maximize metal removal rate MRR while *Fig. 7.12* shows the machining system in which the AC unit is independent of the rest of machining system elements, and could be activated or shut down separately. The AC unit, *Fig. 7.12*, is relatively simple to be built using microcomputer. It involves the measurement of three components of cutting force using a dynamometer, and a built-in interface, and suitable software to perform necessary computations. Such software could be divided into data base; operating models; tool change strategy; and, optimization strategies. Data files might contain the relevant mathematical models of the process, e.g. (7.11), (7.12), (5.30), and (5.32); the tool change strategy might include on-line tool wear estimation values, (7.3); and optimization algorithms might be included in the optimization processor as a sequence of operating commands.

In this case the object is to maximize the metal removal rate without causing damage to the machine tool, tooling system, and operator. Such an optimization algorithm may be explained as shown in *Fig. 7.13*. This figure shows four contours for the primary objective function MRR, as is expressed by form *(7.12)*; the secondary objective function, which is tool wear rate; the machine power constraint, as in model *(7.13)*; and the tool force constraint, as in model *(5.32)*. These contours represent the function values at any given cutting time and depth of cut. This graph is produced using *GHOST* graphical computer package available on *PRIME* computer using *FORTRAN77* language.

The MRR contours, in cubic millimetres per minutes, which is the function to be optimized, are superimposed on the contours of consumed power, and force on the tool, in the speed-feed operational plane. The machine tool capacity usually determines the extremes of such functions. Maximum machine power and the available range of speeds and feeds represents the machine constraints. Maximum allowable force on the tool represents another constraint. The intersection of such machine capacity and tool force constraints determine the visible region of feeds and speeds. Then the object is to full make use of such region to achieve the objective function.

In *Fig. 7.13*, under the machine power limit, say 4 kW; the maximum allowable

tool force of 1000 N; and machine parameters range of (50 – 200 m/min) speeds and (0.06 – 0.6 mm/rev) feeds, the working feasible region is bound by the borders $ABCDEA$. If tool wear is to be sacrificed, it can be seen that there are large number of combinations of speeds and feeds which produce the same amount of metal removal rate. If a secondary objective is to be specified, such as tool wear rate, this could result in achieving the first objective without violation of the second. Tool wear rate TWR is computed by model described by *(7.14)*, which is derived from *(7.3)*, and used as a secondary objective function.

$$TWR = 1.7 \times 10^{-3}\ V^{0.605}\ F^{0.180}\ d^{0.223}\ t^{-0.754} \tag{7.14}$$

For instance, as shown by *Fig. 7.13*, a 80000 cubic millimetres per minute metal removal rate is achieved by different speeds and feeds combinations causing different tool wear rate values, a, b, and c, to be developed. The use of an adaptive control algorithm enables the machine tool to be operated using the combination which achieves the primary objective of maximizing the metal removal, at best value of the secondary objective of minimizing tool wear rate. This results in the selection of the optimal values of feed and speed, as shown, of 80 m/min and 0.48 mm/rev respectively.
This figure is a graphical representation of the steps which should be followed to build an adaptive control software. Arrangement of such instructions in form of a sequence of program blocks could lead to an approach of MRR maximization AC system using the measured cutting force signals.

Such a technique of optimizing primary and secondary objectives under the system constraints is applicable to any sort of objectives such as tool life, surface finish, cutting temperature, tool vibrations, or even chip breakability as long as the relevant mathematical models are available.

In the following section is outlined another approach to achieve an AC system using the developed mathematical models with the objective of prolonging the tool life.

7.2.5 Attaining Tool Life Under System Constraints

Tool life is one of the most important aspects in metal cutting. Many efforts have been made to characterize the tool wear and tool life with little success. This is due to the indeterministic nature of metal cutting relationships. In-process or on-line tool wear control approach offers a practical solution of such a problem. In what follows is a study of the way in which a tool life value may be attained through in-process adjustment of cutting parameters.

The tool life model used in this approach, as a primary objective function to be optimized, takes the form (4.33) which was developed and examined in **Chapter 4**

$$\ln T_{AW} = -7.953 - 1.121[\ln V]^2 - 0.469 \ln V \ln F - 0.371[\ln F]^2 + 7.275 \ln V - 0.81[\ln d]^2.$$

This model which relates the tool life response, T_{AW}, to the machining conditions, has been achieved using a second-order multiple linear regression technique based on experimental tool lives. The secondary objective function is the maximization of the metal removal rate MRR, equation *(7.11)*. The system constraints are the same as those used in the last section, *Fig. 7.13*. As explained in the last section, the function and the constraint contours are superimposed to determine the feasible region, *Fig. 7.14*; and represent an adaptive control strategy where the tool life is the function to be optimized as a primary objective. The best metal removal rate, can be achieve as a secondary objective. For instance, a 31 minutes tool life can be achieved using many values of speeds and feeds. Using adaptive control technique based on the mathematical models, almost twice as much MRR can be achieved in moving from 40000 ,at point a, to 70000 mm^3/min at point d. These plots of responses contours, *Figs. 7.13 & 7.14*, could generally be used as a references for the selection of the operating parameters for other purposes of the selection of the optimal cutting conditions.

Generally, several AC approaches can be established using the mathematical models. In the following section is presented a use of the mathematical model when it plays the role of a computerized information data bank system.

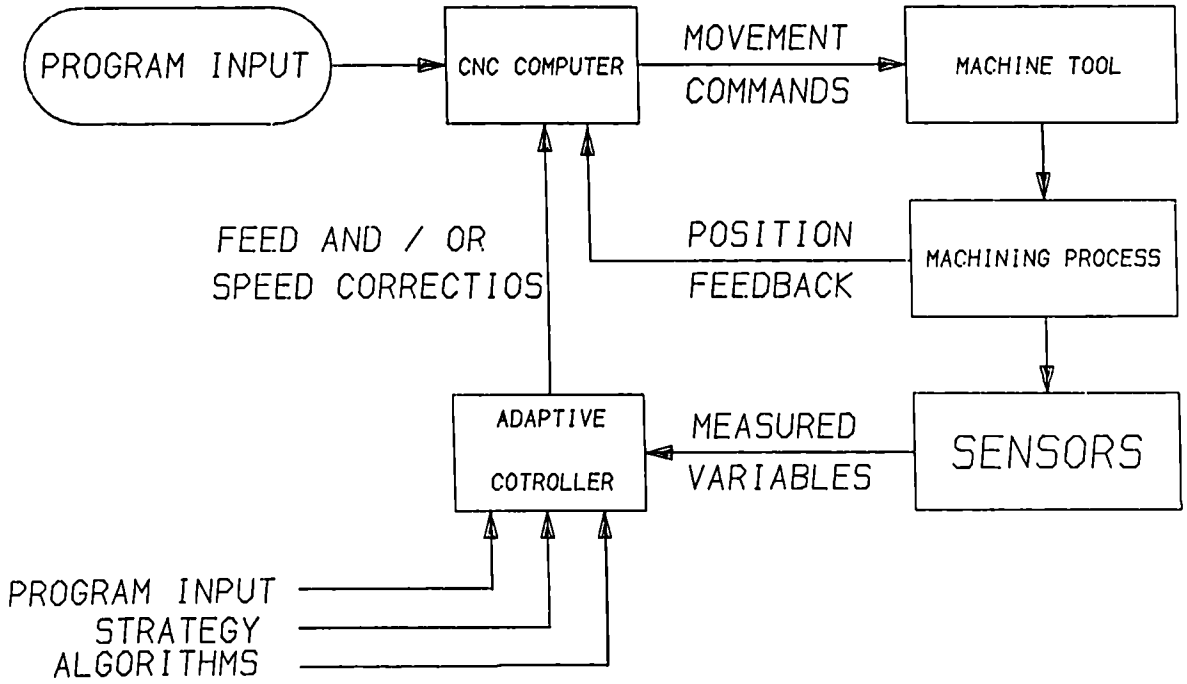

Fig. 7.1 Adaptive Control System for Machine Tools

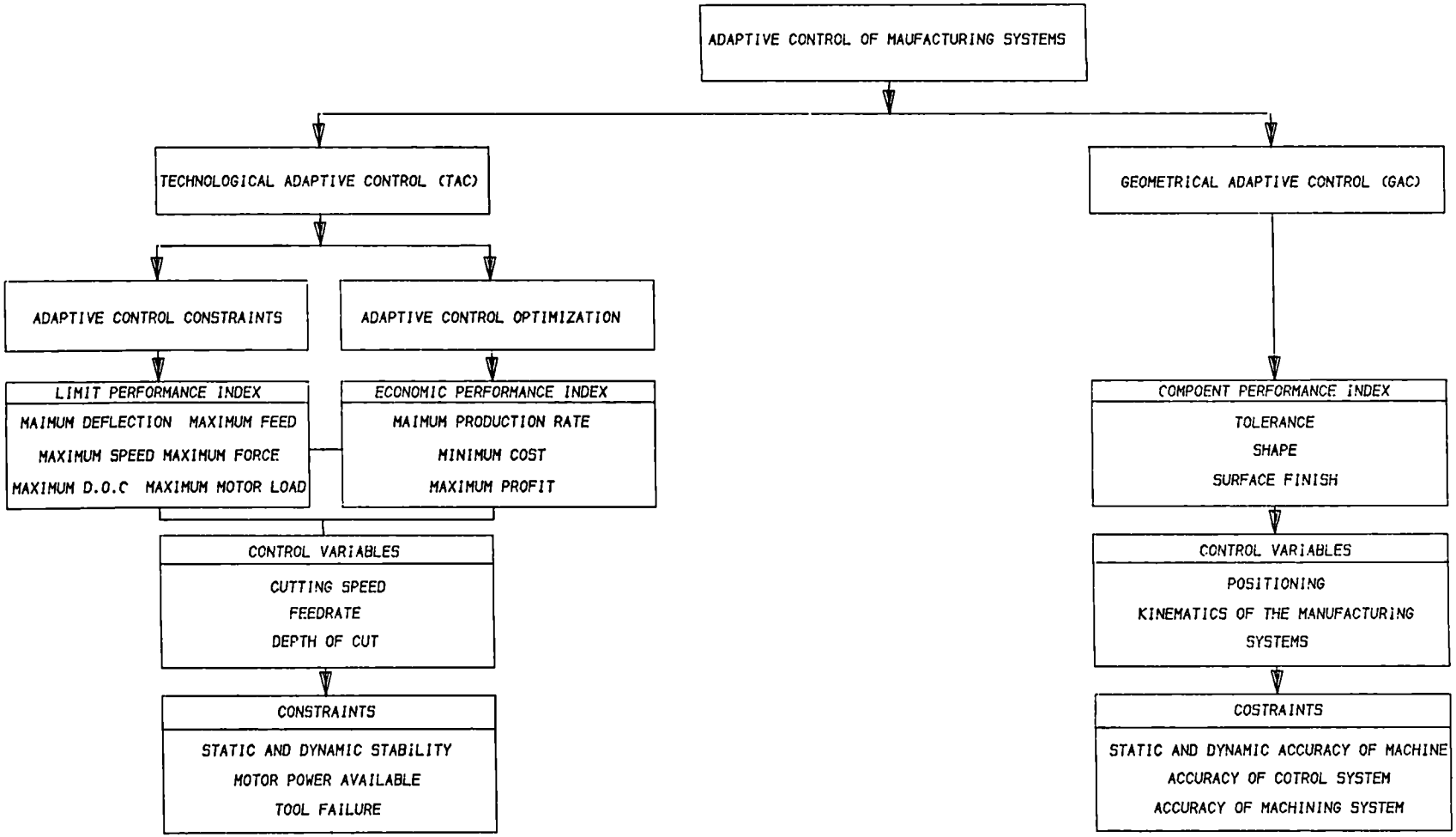

Fig. 7.2 Classification of Adaptive Cotrol Types

TURNING SYSTEM (Destination)	MEASURED PARAMETERS	CORRECTING VARIABLE(S)	OBJECT	ACC OR ACO
AEG - Pittler (Germany)	Motor Load	Feedrate	Maximum Utilization	ACC
Bath University (GB)	Cutting Speed	Spindle Speed	Constant Temp. at Cutting Edge	ACC
Bendix Dynapath System (USA)	Cutting Force, Motor Current, Motor Temp.	Feed	Maximum Utilization	ACC
Belfast University (GB)	Spindle Torque, Temp. at Cutting Edge	Spindle Speed, Feed	Maximum Utilization, Forecasting of Tool Wear Rate	ACC
General Electric (USA)	Motor Current, Motor Load	Cutting Speed or Feedrate	Mximum Utilization	ACC
Stavely (GB)	Spindle Torque	Spindle Speed and Feed	Maximum Utilization	ACC
USSR	Cutting Edge Temp.	Cutting Speed	Max Metal Removal Rate	ACO
Pisa Uni. (Italy)	Cutting Temp., Motor Load	Spindle Speed	Cutting Temp. at Edge	ACC
Royal Aircraft Est. (GB)	Temp. and Cutting Force	Spindle Speed and Feed	Max. Utilization and Const. Temp.	ACC

Table 7.1 Adaptive Control Systems for Turning Operations

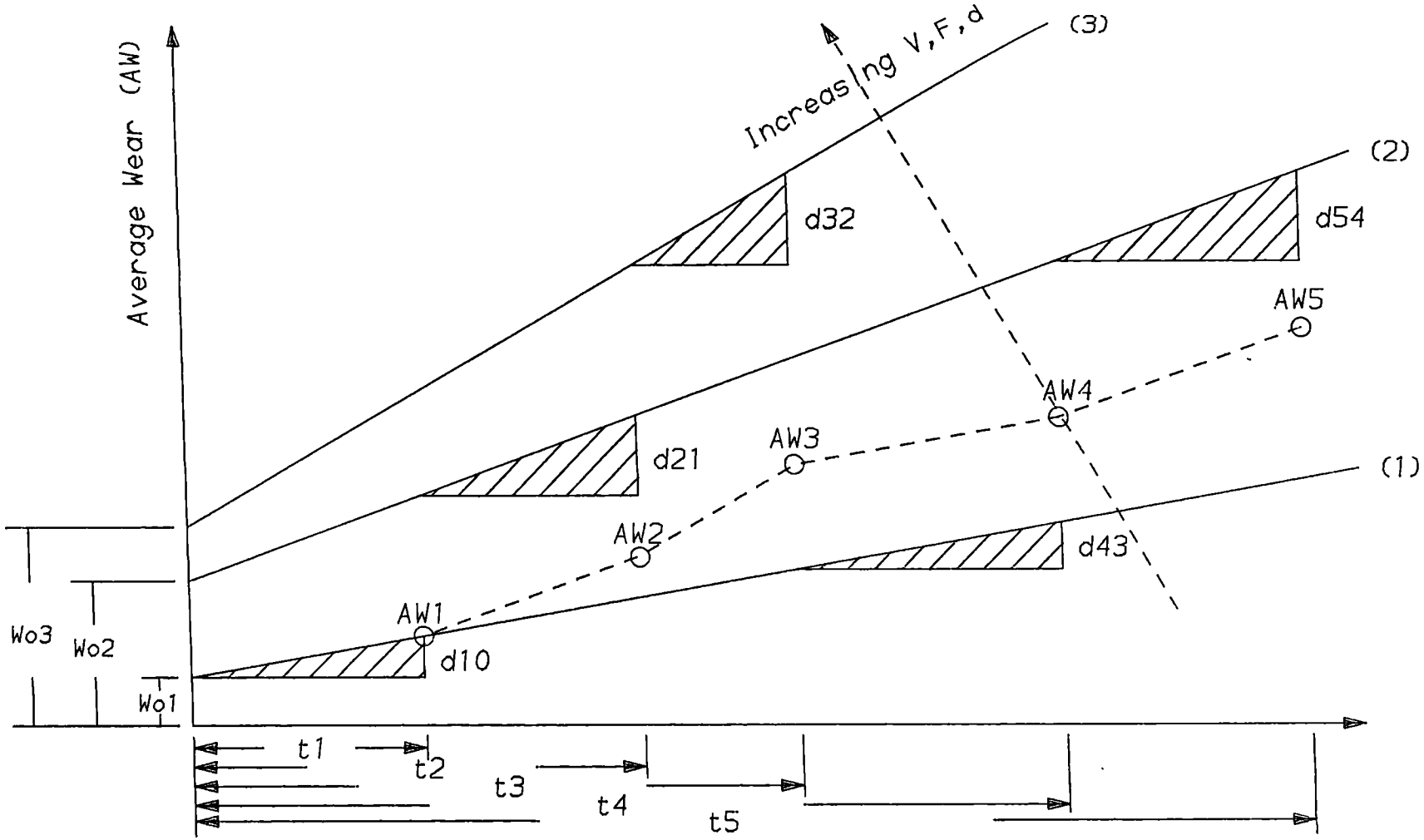

Fig. 7.3 Tool Wear Behaviour With Different Conditions

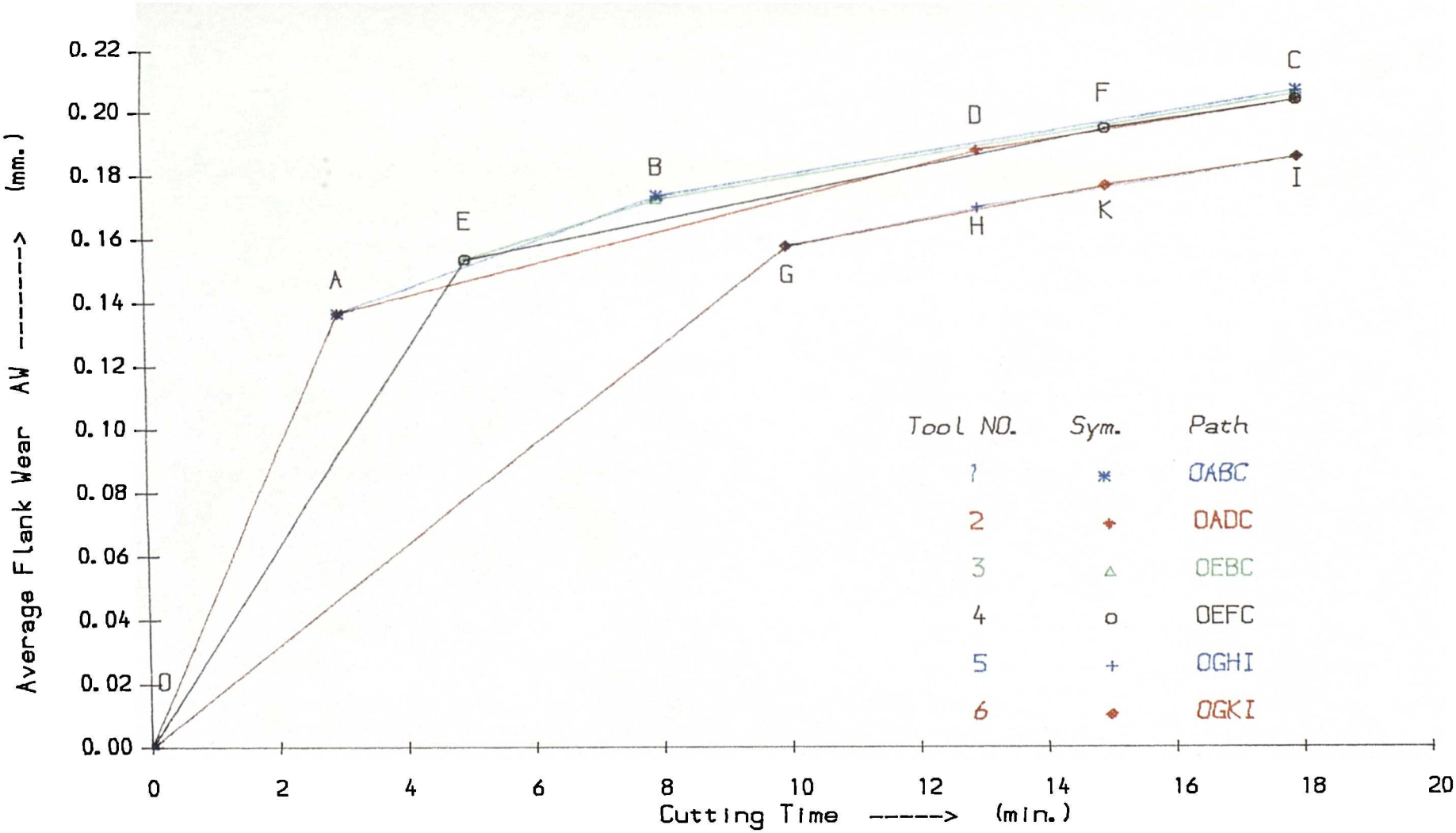

Fig. 7.4 The Effect of Changing Conditions on Developed Wear Level

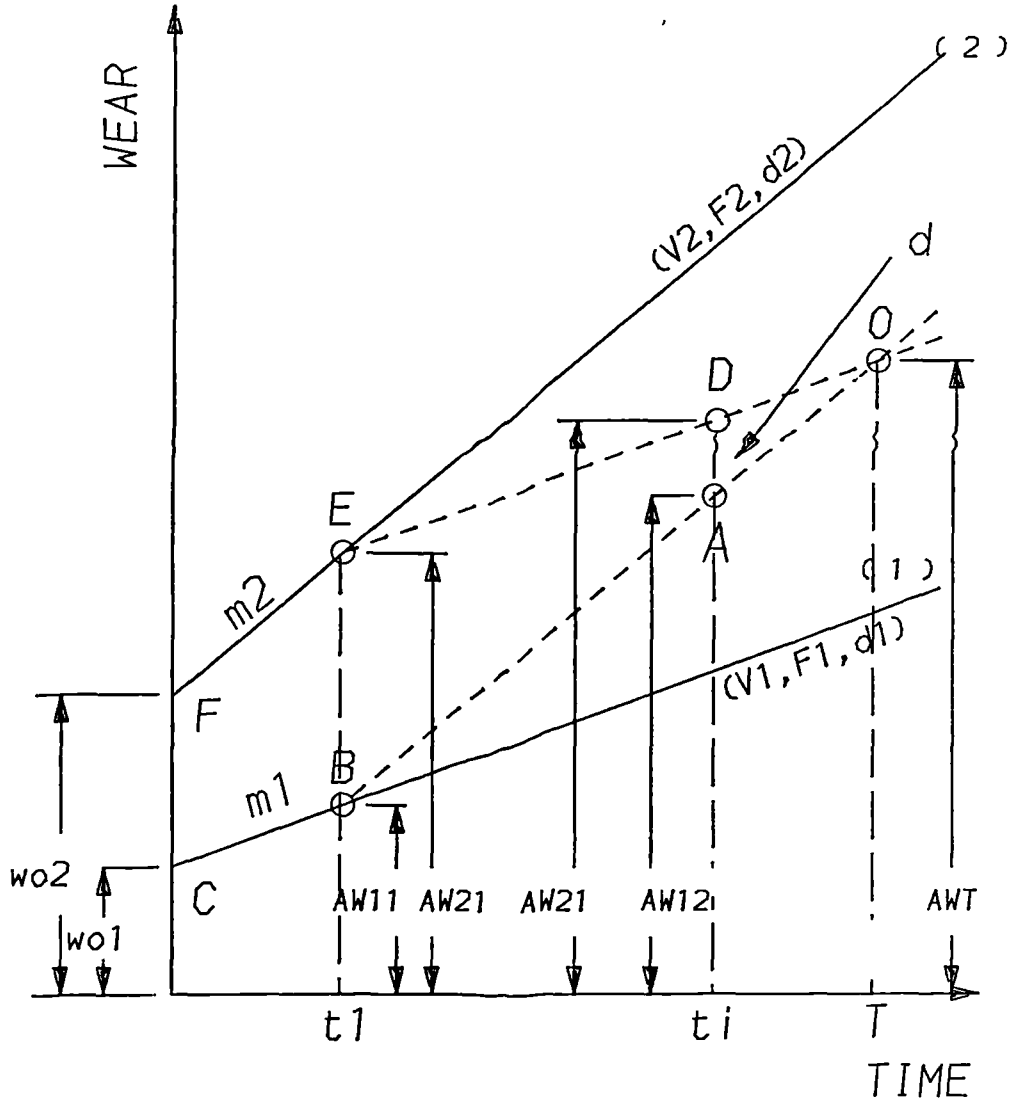

Fig. 7.5 Effect of Cutting Periods on Tool Wear Behaviour

A) CUTTING SPEED AS A VARIABLE

GROUP 1 VARIABLE SPEEDS WITH FIXED CUT TIMES

TOOL NO.	CUT NO.	SPEED	CUT TIME	TOTAL TIME	WEAR
1	1	80	15	15	0.17021
	2	150	5	20	0.36023
	3	200	3	23	0.55968
2	1	200	3	3	0.19945
	2	150	5	8	0.38948
	3	80	15	23	0.55968
3	1	150	5	5	0.19002
	2	80	15	20	0.36023
	3	200	3	23	0.55968
4	1	150	5	5	0.19002
	2	200	3	8	0.38048
	3	80	15	23	0.55968
5	1	200	3	3	0.19945
	2	80	15	18	0.36966
	3	150	5	23	0.55968
6	1	80	15	15	0.17021
	2	200	3	18	0.36966
	3	150	5	23	0.55968

GROUP 2 VARIABLE SPEEDS WITH VARIABLE CUT TIMES

1	1	80	15	15	0.17021
	2	150	5	20	0.36023
	3	200	3	23	0.55968
8	1	80	15	15	0.17702
	2	150	3	18	0.33778
	3	200	5	23	0.56395
9	1	80	3	3	0.11453
	2	150	15	18	0.36356
	3	200	5	23	0.58974
10	1	80	3	3	0.11453
	2	150	5	8	0.30456
	3	200	15	23	0.60097
11	1	80	5	5	0.12988
	2	150	15	20	0.37891
	3	200	3	23	0.57836
12	1	80	5	5	0.12988
	2	150	3	8	0.29745
	3	200	15	23	0.59386

MAX ERROR = 0.041 mm.

FEED = 0.2 D.O.C =2.5

B) FEED AS A VARIABLE

GROUP 1 VARIABLE FEEDS WITH FIXED CUT TIMES

TOOL NO.	CUT NO.	FEED	CUT TIME	TOTAL TIME	WEAR
1	1	0.1	15	15	0.21985
	2	0.3	5	20	0.42425
	3	0.5	3	23	0.62183
2	1	0.5	3	3	0.19758
	2	0.3	5	8	0.40198
	3	0.1	15	23	0.62183
3	1	0.1	15	15	0.21985
	2	0.5	3	18	0.41743
	3	0.3	5	23	0.62183
4	1	0.5	3	3	0.19758
	2	0.1	15	18	0.41743
	3	0.3	5	23	0.62183
5	1	0.3	5	5	0.20440
	2	0.1	15	20	0.42425
	3	0.5	3	23	0.62183
6	1	0.3	5	5	0.20434
	2	0.5	3	8	0.40198
	3	0.1	15	23	0.62183

GROUP 2 VARIABLE FEEDS WITH VARIABLE CUT TIMES

1	1	0.1	15	15	0.21985
	2	0.3	5	20	0.42425
	3	0.5	3	23	0.62183
8	1	0.1	3	3	0.21985
	2	0.3	5	8	0.40010
	3	0.5	15	23	0.62419
9	1	0.1	15	15	0.14794
	2	0.3	3	18	0.35234
	3	0.5	5	23	0.64598
10	1	0.1	3	3	0.14794
	2	0.3	15	18	0.41580
	3	0.5	5	23	0.63986
11	1	0.1	5	5	0.16776
	2	0.3	15	20	0.34800
	3	0.5	3	23	0.64164
12	1	0.1	5	5	0.16776
	2	0.3	3	8	0.43562
	3	0.5	15	23	0.63321

MAX ERROR = 0.024 mm.

SPEED = 150 D.O.C = 2.5

C) DEPTH OF CUT AS A VARIABLE

GROUP 1 VARIABLE D.O.C WITH FIXED CUT TIMES

TOOL NO.	CUT NO.	D.O.C	CUT TIME	TOTAL TIME	WEAR
1	1	2.0	15	15	0.23695
	2	2.5	5	20	0.42698
	3	3.0	3	23	0.60150
2	1	3.0	3	3	0.17452
	2	2.5	5	8	0.36454
	3	2.0	15	23	0.60150
3	1	2.0	15	15	0.23695
	2	3.0	3	18	0.41147
	3	2.5	5	23	0.69150
4	1	3.0	3	3	0.17452
	2	2.0	15	18	0.41147
	3	2.5	5	23	0.60150
5	1	2.5	5	5	0.19002
	2	2.0	15	20	0.42698
	3	3.0	3	23	0.60150
6	1	2.5	5	5	0.19002
	2	3.0	3	8	0.36454
	3	2.0	15	23	0.60150

GROUP 2 VARIABLE D.O.C WITH VARIABLE CUT TIMES

1	1	2.0	15	15	0.23695
	2	2.5	5	20	0.42700
	3	3.0	3	23	0.60150
8	1	2.0	15	15	0.23700
	2	2.5	3	18	0.40453
	3	3.0	5	23	0.60243
9	1	2.0	5	5	0.18081
	2	2.5	3	8	0.34838
	3	3.0	15	23	0.60774
10	1	2.0	5	5	0.18081
	2	2.5	15	20	0.42984
	3	3.0	3	23	0.60434
11	1	2.0	3	3	0.15944
	2	2.5	15	18	0.40848
	3	3.0	5	23	0.60638
12	1	2.0	3	3	0.15944
	2	2.5	5	8	0.34947
	3	3.0	15	23	0.60882

MAX ERROR = 0.007 mm.

SPEED = 150 FEED = 0.2

Table 7.2 Cutting Conditions Arrangement for Models Verification

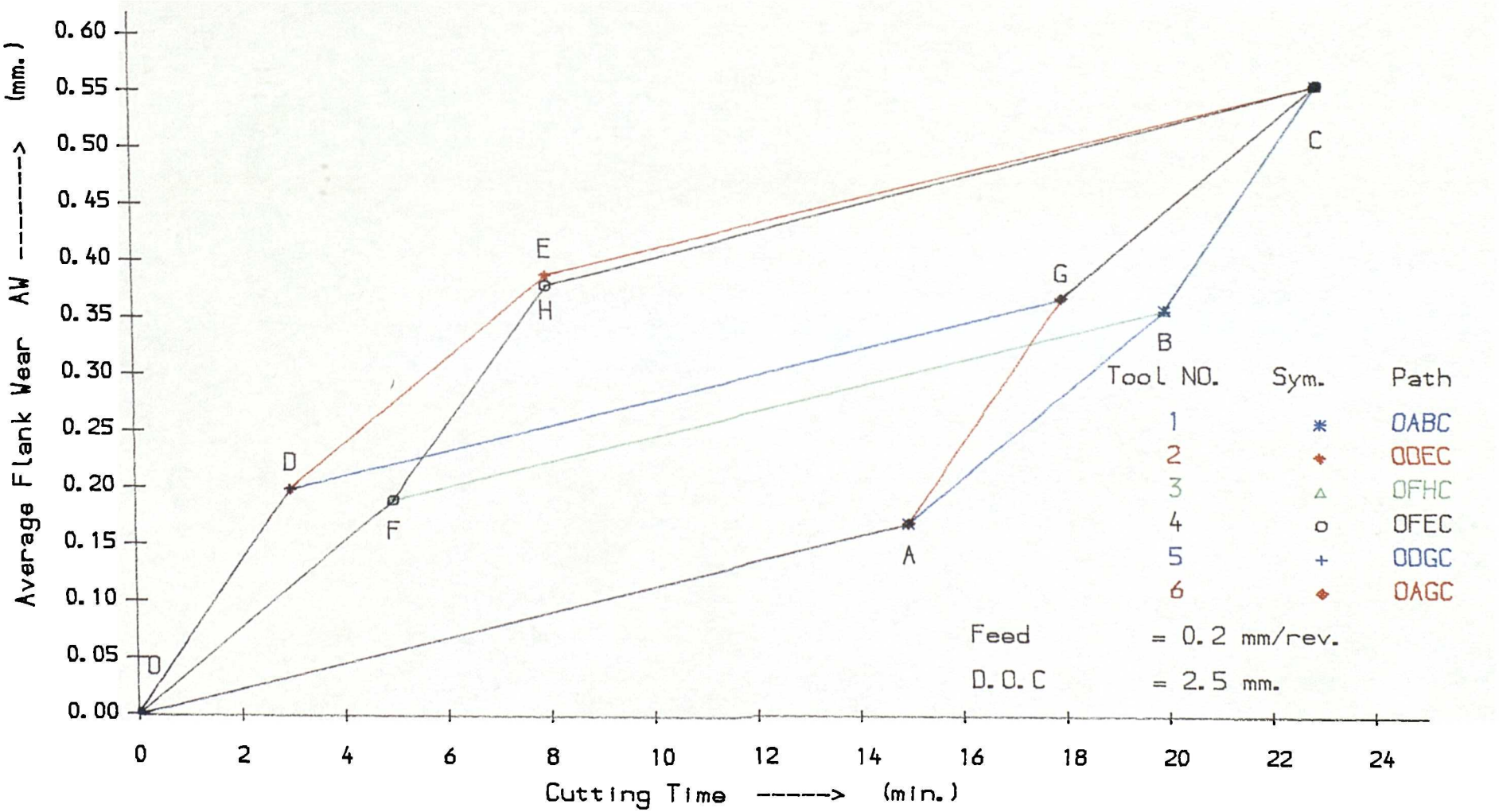

Fig. 7.6 The Effect of Fixed Cutting Periods With Variable Speeds

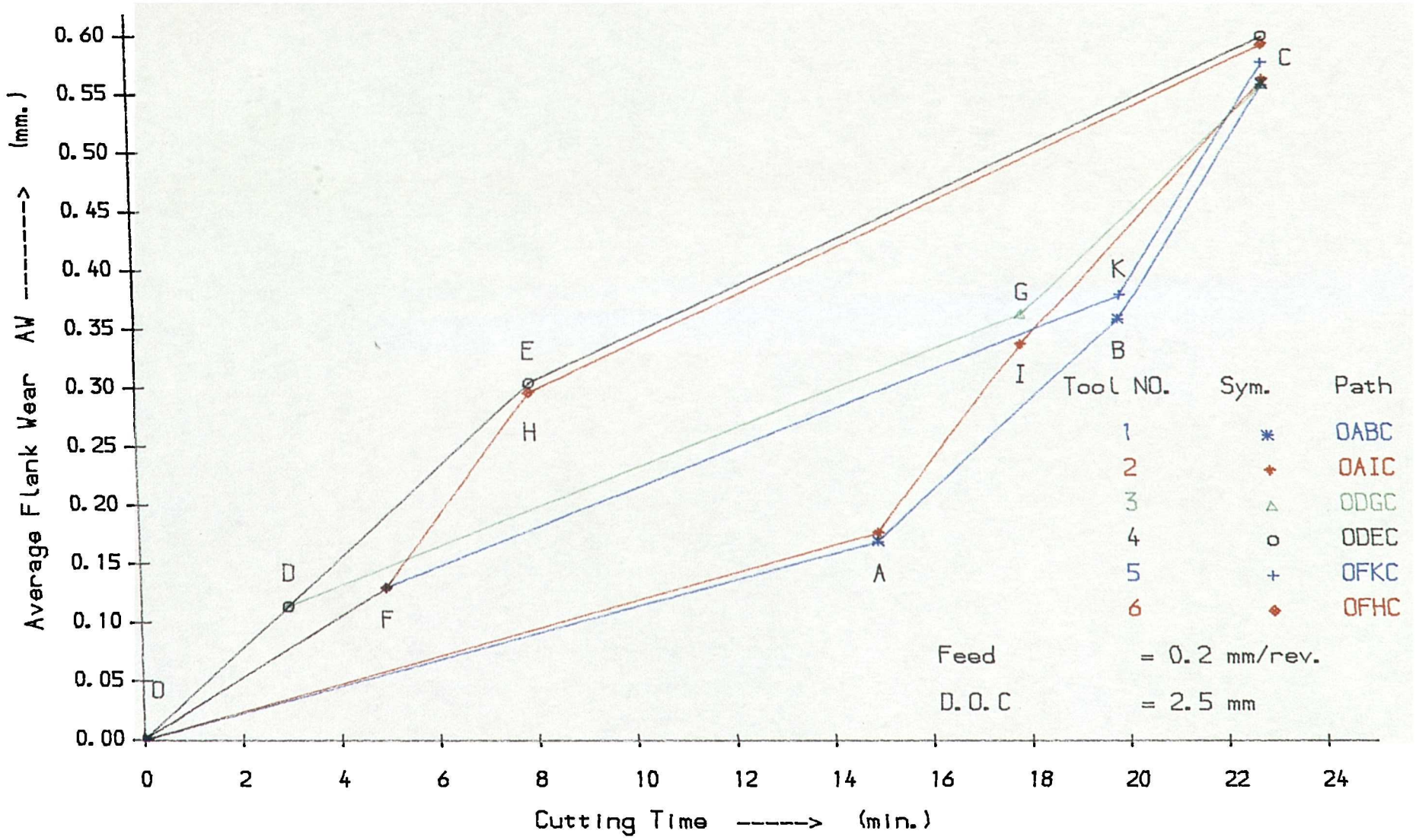

Fig. 7.7 The Effect of Fixed Speed with Variable Cutting Periods

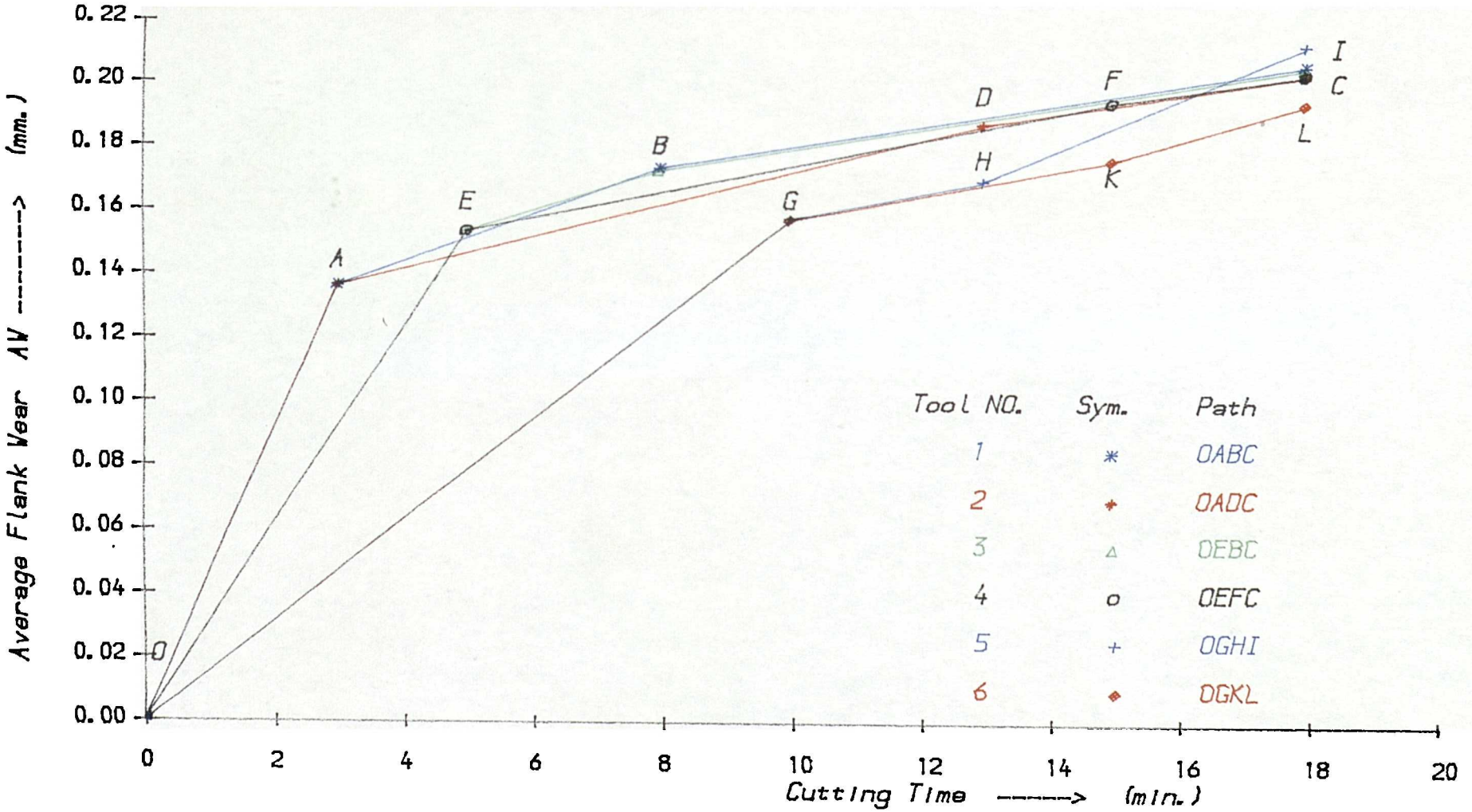

Fig. 7.8 The Effect of Compensating for Initial Wear Difference

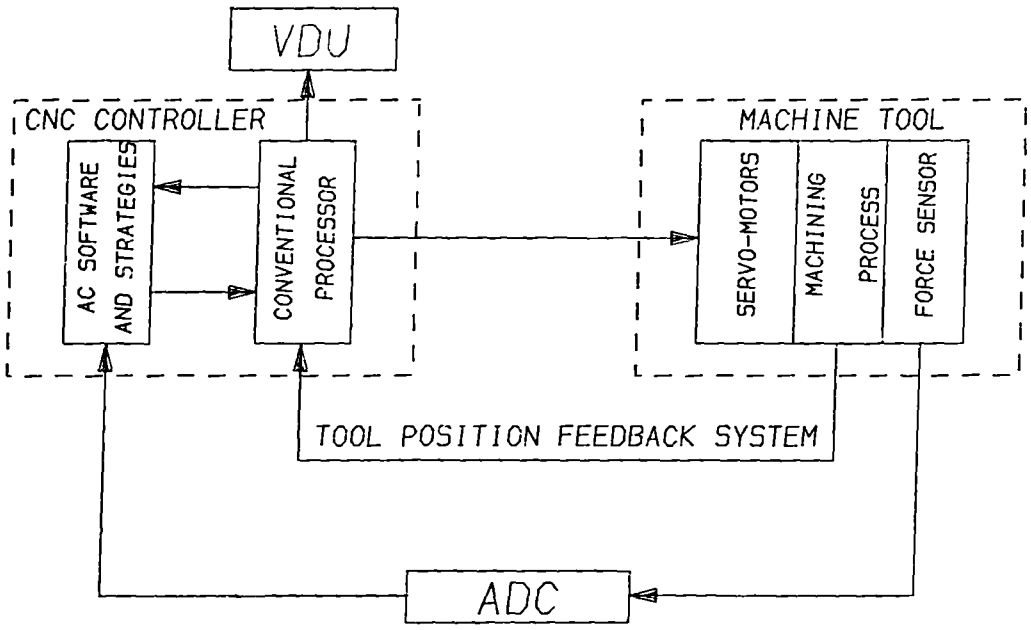

Fig. 7.9 Proposed Tool Wear Monitoring AC System

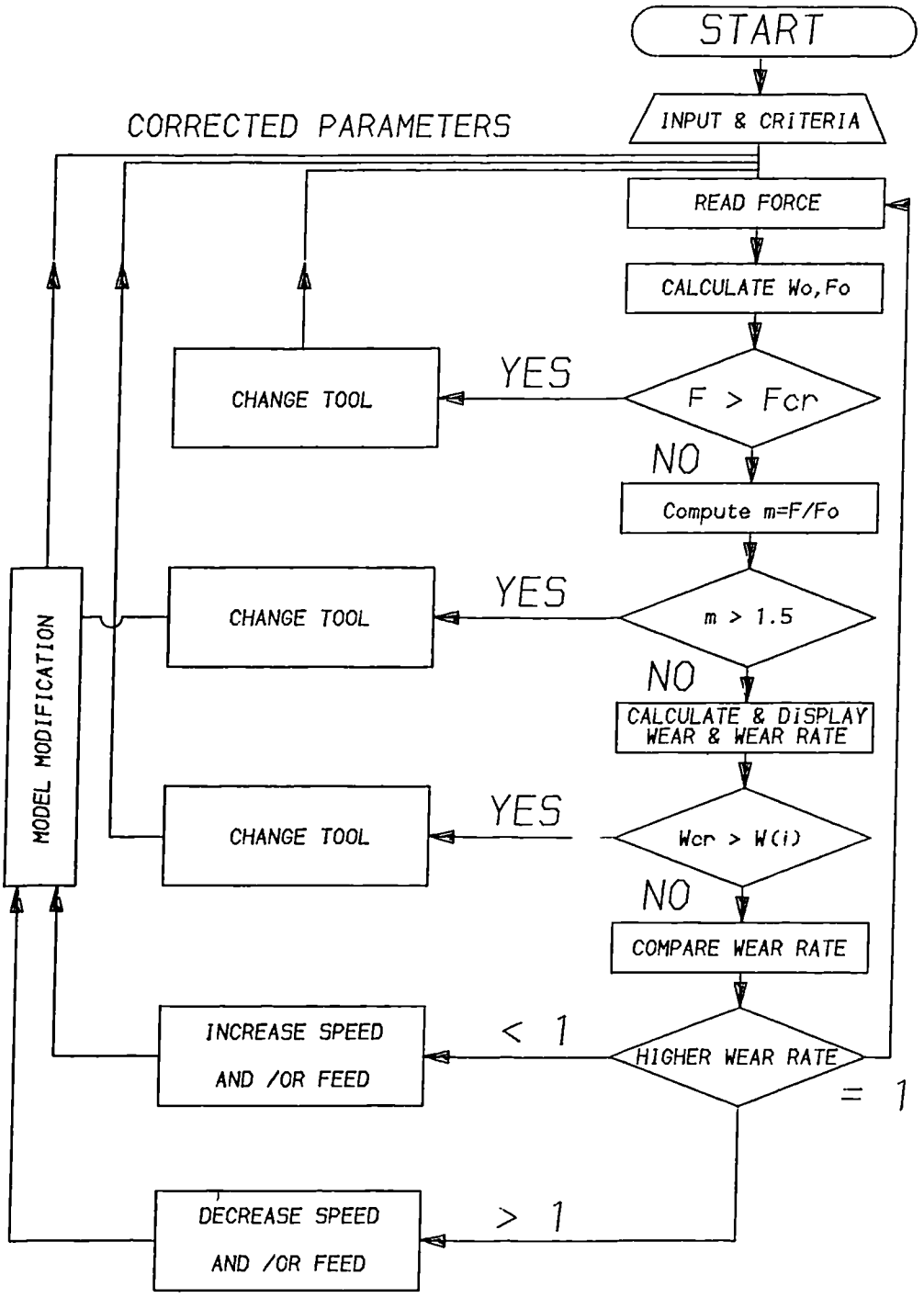

Fig. 7.10 Wear Monitoring Strategy for AC System

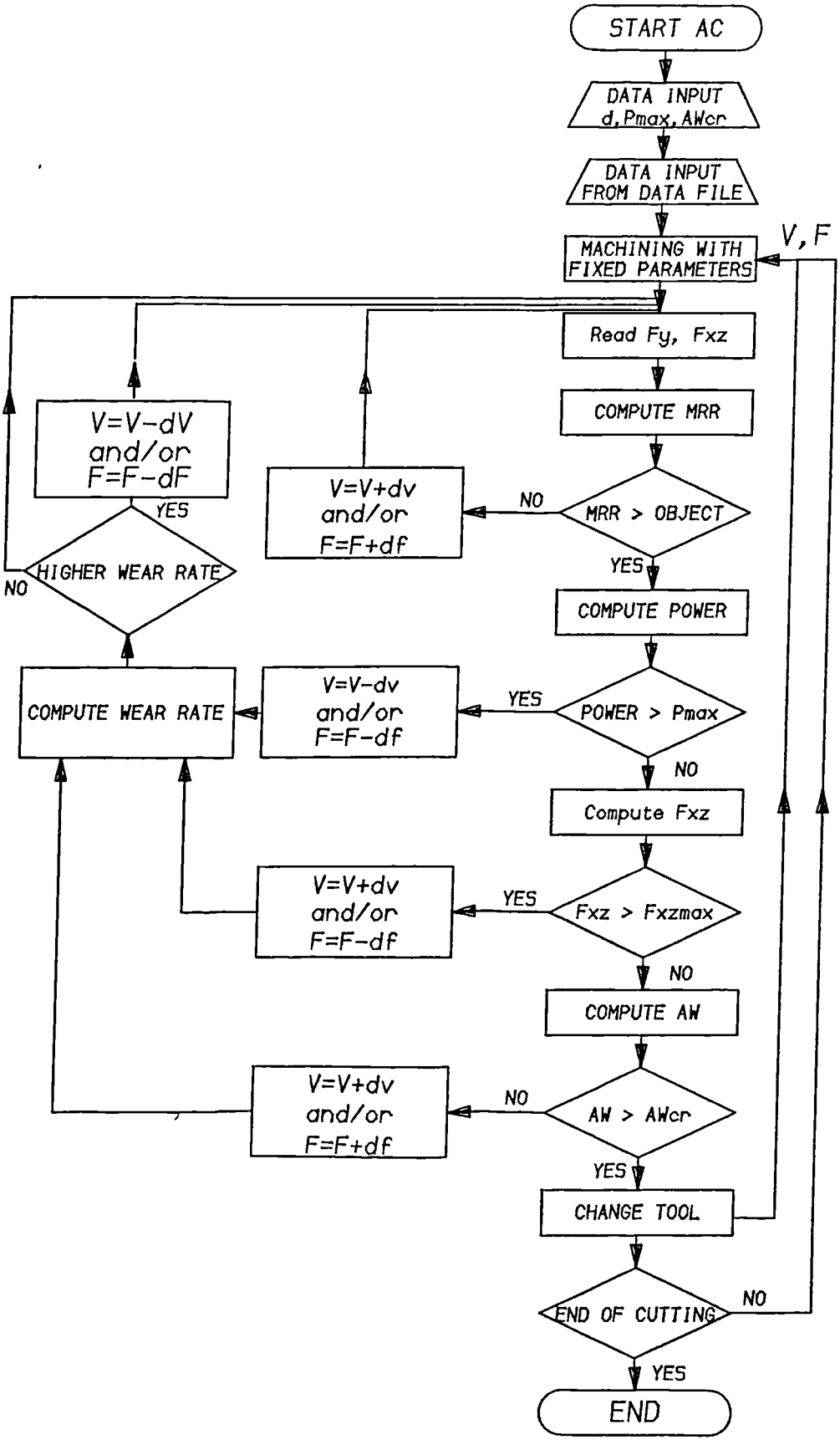

Fig. 7.11 AC System for MRR and Minimum Wear Rate

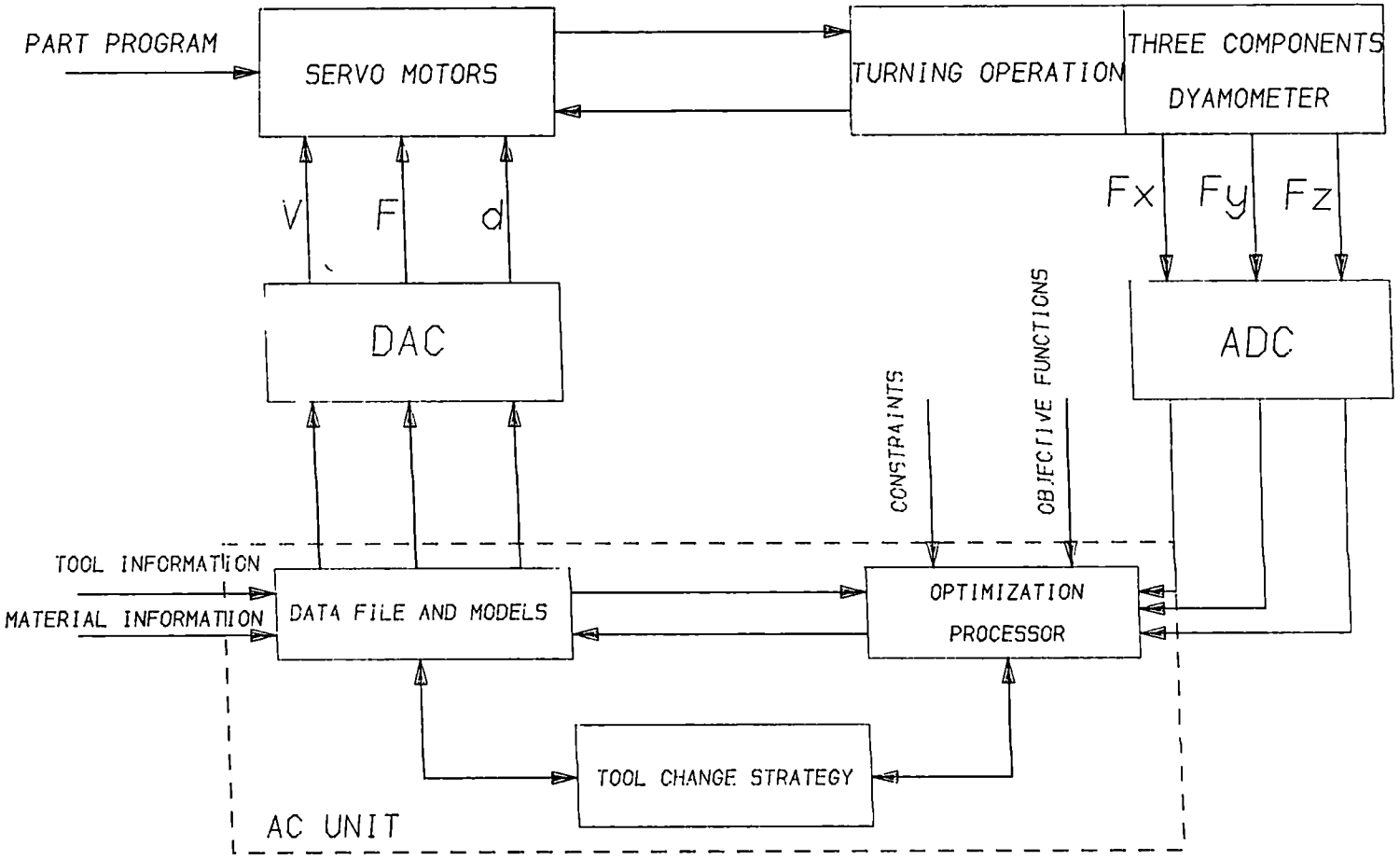

Fig. 7.12 Adaptive Control System Structure

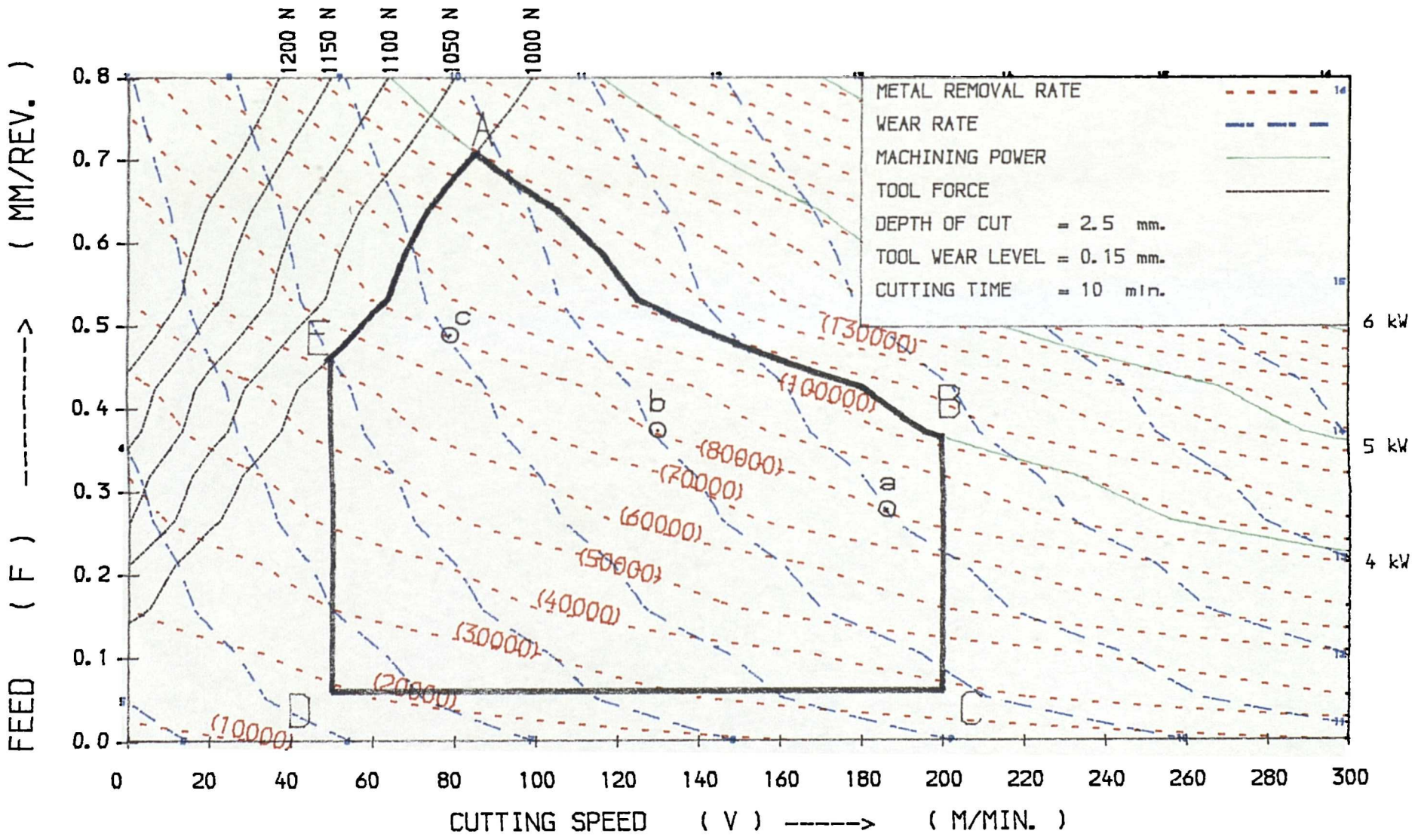

Fig. 7.13 ADAPTIVE CONTROL STRATEGY FOR METAL REMOVAL RATE (MRR)

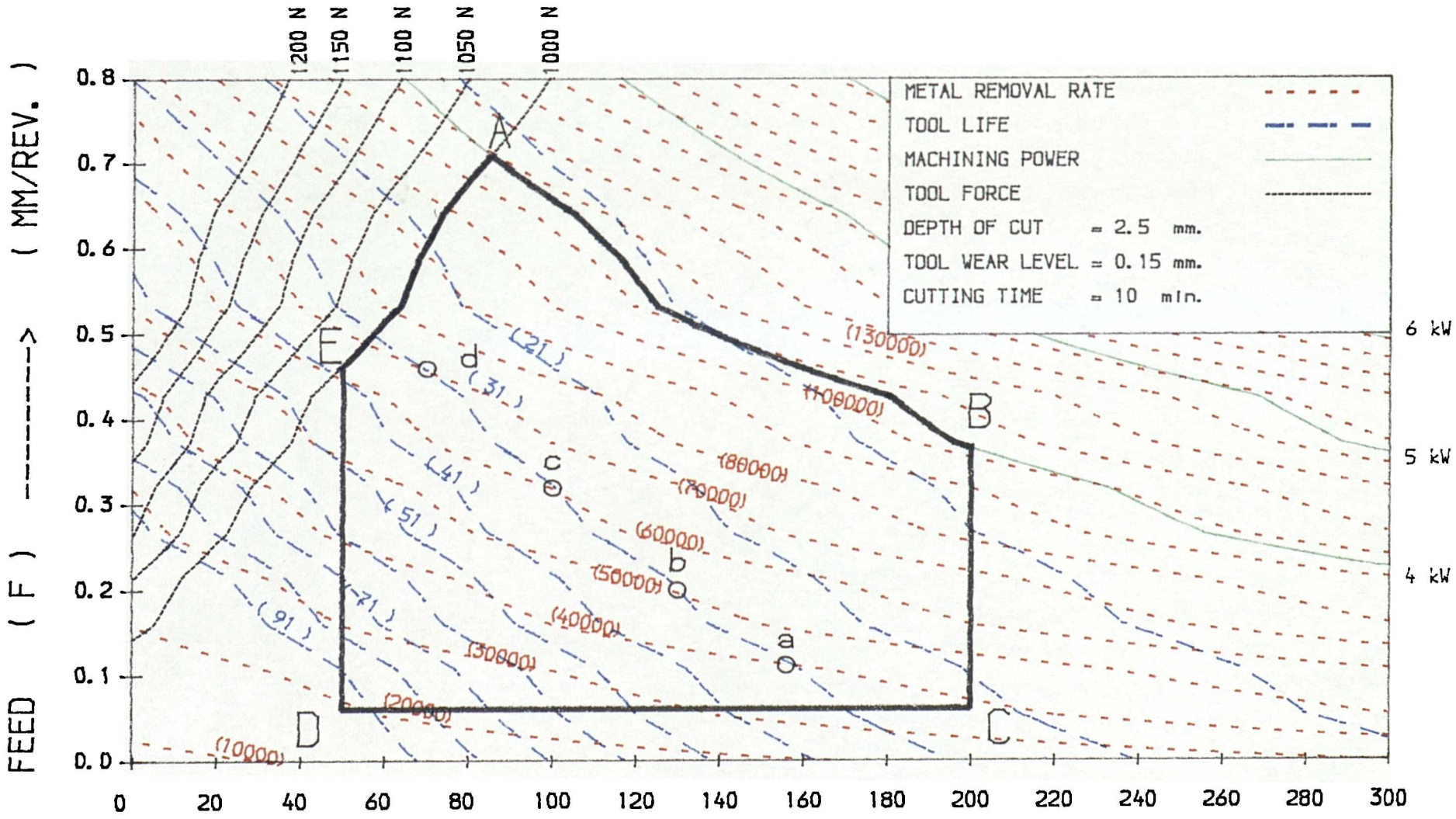

Fig. 7.14 ADAPTIVE CONTROL STRATEGY FOR TOOL LIFE

7.3 Using the models in Machinability Data Bank Systems

A machinability data bank system *MDB* is a computerized system used for rapidly selecting the most economical and reliable machining parameters, speeds, feeds, and depth of cut values. Such machining parameters are always required in computer aided manufacturing as well as other machining systems. To a large extent, machinability data resides in the personal experience of machine operators and process planners. Following the introduction of numerical control machine tools, the responsibility for selection of speeds and feeds has shifted from machine operator to part programmer who, in most cases, has insufficient experience in metal cutting technology. The introduction of super-hard materials, such as titanium, and complicated part configuration has made the problem even worse. Dependence on experience, or even data from machinability handbook, such as *Machining Data Handbook [101]*, could lead to disastrous consequences. To avoid such situations, operators and programmers tend to select very conservative parameters which adds to the total machining cost. An approach using a machinability data bank system could lead to the optimal selection of the operating parameters.

The Computerized Machinability Data Base systems *CMDB* may be classified into three general types:;

1. Data Storage and Retrieval Systems.
2. Generalized Empirical Equation Systems.
3. Mathematical Model systems.

In data storage and retrieval systems, the storage data have been collected from many sources such as shop floor experience, laboratory experiments, or handbooks. Such information are stored in the computer data base for use when necessary. This is

a simple procedure which is often characterized by the lack of adequate maintenance, and by difficulties in updating current machining recommendations; it also requires a huge permanent storage capability.

In the generalized empirical equation systems, the data for a particular machining operation is reduced to a suitable empirical form which could take the form of charts, monographs, or graphs.

The current study deals with the third type of systems which is the mathematical model machinability data bank system. The difference between the mathematical model type and the empirical systems is that in the latter the developed equation is very general, whereas in the mathematical model system the equation is obtained from experimental data which closely match a particular machining situation. For instance, using the mathematical model type, the extended Taylor's equation for tool life T takes the form (4.2):

$$TL \quad = ao \quad V^{a1} \quad F^{a2} \quad d^{a3}.$$

The constants ao, $a1$, $a2$, $a3$ depend solely on the machine- tool-workpiece MTW combination under which the experimental data are collected. For the empirical equation, these constants are further divided into many other constants of tool material difference, workpiece material difference, coolant difference, etc.

The empirical equation could be used to retrieve approximate parameters but if precise values are required, then the mathematical models are recommended. Regardless the long experimental procedures necessary for the generalization of the empirical equation; maintenance of the equation and updating is very difficult. The maintenance of the mathematical model is simple since the recommended cutting conditions are only indirectly related to the data through the coefficient values. Therefore, maintenance and updating need not be performed by experienced engineer and a suitable software could be used instead. *Fig. 7.15* shows a mathematical model type machinability data base system proposed by *Balakrishnon [113]*. A data storage and retrieval system is normally used along with the mathematical model system for storage of experimental data. Once the new model is developed, it is interpreted in the optimization algorithm

which is designed to obtain an optimum set of cutting conditions. Some of these problems which still inhibit their general acceptance are in the following discussed.
The first problem: the extent of model applicability, concerns the validity of the model for use during the whole period of tool working life. In other words, what will the time effect be when the tool is no longer very sharp. So far, investigators concentrated on establishing models to be used in the first few second of cut. Such models represent the initial value of the response rather than the time-varying instantaneous value. For optimum selection of cutting conditions in practical situation, the cutting tool is not always absolutely sharp and as discussed before, the same tool could be used for several operations with different cutting conditions. The selection of certain parameters to give constant forces on tool is impossible using such models since the force is in itself wear dependent. The developed model should have the capability of detecting any variations within the whole tool working life, otherwise, as discussed in **Chapter2,** it represents only the initial value of the response.

For the first time, cutting responses mathematical models with a time-varying and/or wear-varying techniques have been developed in this study. As indicated in previous chapters these included :

1. Individual and resultant cutting force components as a function of cutting conditions, cutting time, and tool wear (see **Chapter 5**).
2. Individual and average tool wear land elements as a function of cutting conditions, cutting time, and one or more of force components (see **Chapter 5**).
3. Tool vibrations as a function of time and wear (see **Chapter 6**).
4. Tool life equations based on extended Taylor's equation, or second-order model. Both linear and non- linear models are developed and the best environments for each one is specified (see **Chapters 4 & 5**).

This group of models covers every aspect relevant to the process and the possible in-process variations. The difference between the old technique of modelling only the

initial response value and the new one used in this study can be explained by plotting the force estimation error along the tool working life. Suppose that a tool is working under the conditions $(100, 0.2, 2.25)$. Substitution of these fixed conditions in the wear model given by Eq. *(7.3)* yields the average wear

$$AW = 9.8 \times 10^{-2} \quad t^{0.246}. \tag{7.15}$$

Also, substitution of these fixed conditions in each of models *(5.21)* and *(5.32)* gives the initial tool wear force $F_{xzo} = 598.55$, and the tool force

$$F_{xz} = 7266.4 \quad t^{-0.173} \quad AW^{1.01}. \tag{7.16}$$

On Substitution of Eq. *(7.16)* into *(7.17)* one obtains the following expression of too force error ΔF_{xz}

$$\begin{aligned} \Delta F_{xz} &= F_{xz} - F_{xzo} \\ &= 693.8 \quad t^{0.076} - 598.6. \end{aligned} \tag{7.17}$$

where t is the cutting time starts when the tool is new and ends by the end of the tool life. For such conditions, the tool life given by Eq. *(4.33)*, is 44 minutes. *Fig. 7.16* shows a plot of the computation error over the entire tool life period as a result of using the initial value model technique instead of the time-varying value. This figure indicates that a deviation up to $325N$, which is about 54% of the initial value, does exists at the end of working tool life. However, in some diverse situations where higher parameters and/or higher tool life level criteria are used, such deviation could be much higher than the initial value itself. By using the time-varying models a reliable mathematical model machinability data base system can be facilitated.

Another problem involved with the existing *MDBS* systems, which is common in all systems, is how the system can be maintained and updated. The problem size depends on the nature of the production system. For a fixed type mass production process, the models are likely to be sufficient for long periods. Any changes of the cost elements can be included in the optimization algorithm without the need of modifying

the model itself. For low or medium-sized production processes and for unique component production, the models should have the capability to deal with the new variations. The factor of different tool materials and/or workpiece materials should be accounted for. The difficulties in using least-squares linear regression, which was used in all previous techniques, requires certain design of experiments, model building techniques, and certain statistical criteria. Using non- linear least-squares regression, used in this study, added flexibility is provided to the estimation procedures. Providing approximate prior knowledge about the model is available, using the ordinary least-squares procedures, minimal amount of new data information are required for the model adaptation. This information could be retrieved from data storage files. Another suggestion to overcome such problem is the use of the models with a correction factor taking into consideration the workpiece hardness difference.

In summary, the developed mathematical models might help in building a robust computerized machinability information system. The models are used to generate great deal of technical information and cutting parameters which are suitable for certain environments to meet the production requirements. The new modelling technique used in this study may enhance the system prediction capability, and may lead to a universal information system.

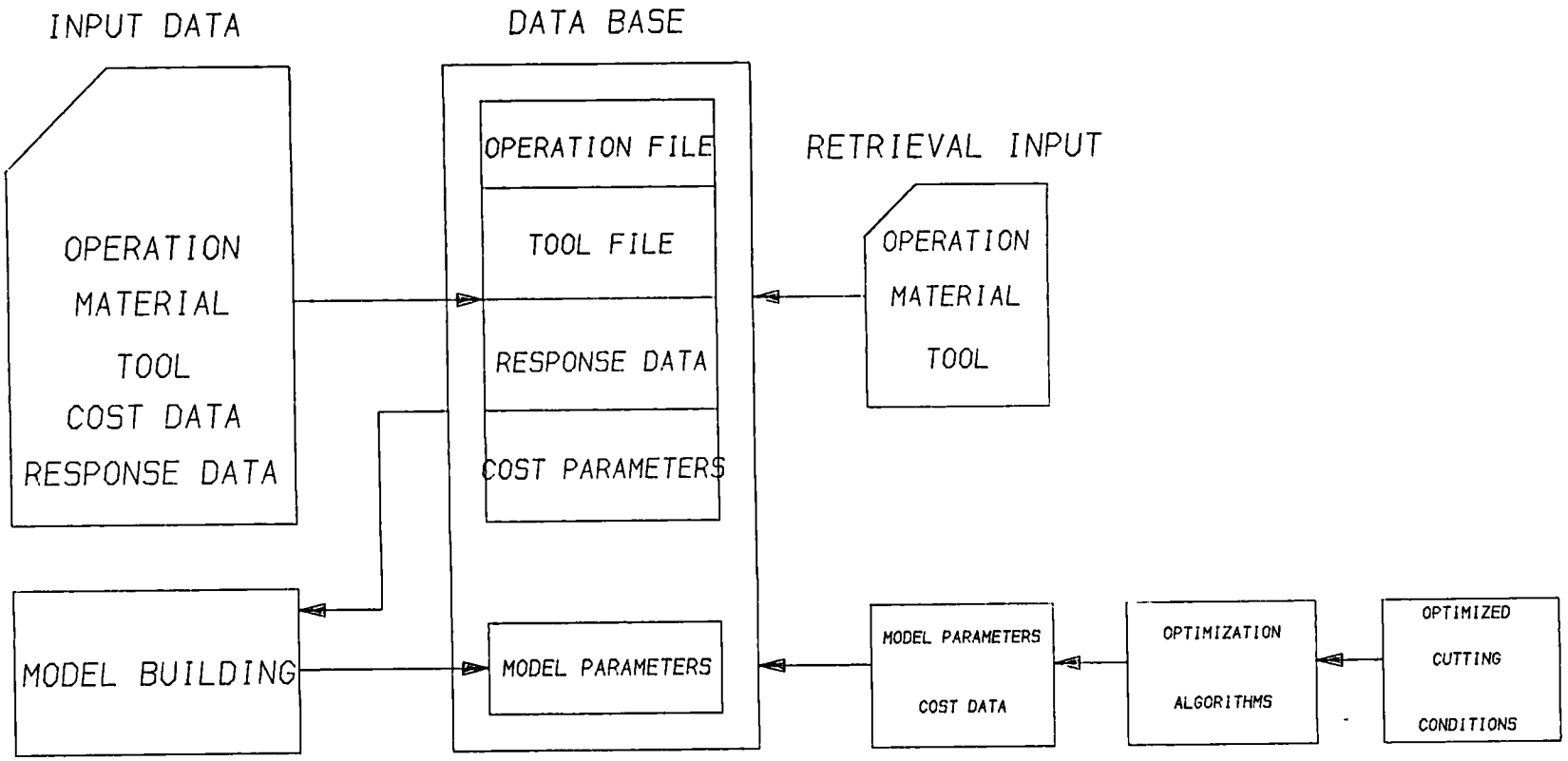

Fig. 7.15 Mathematical Model Type Machinability Data Base System

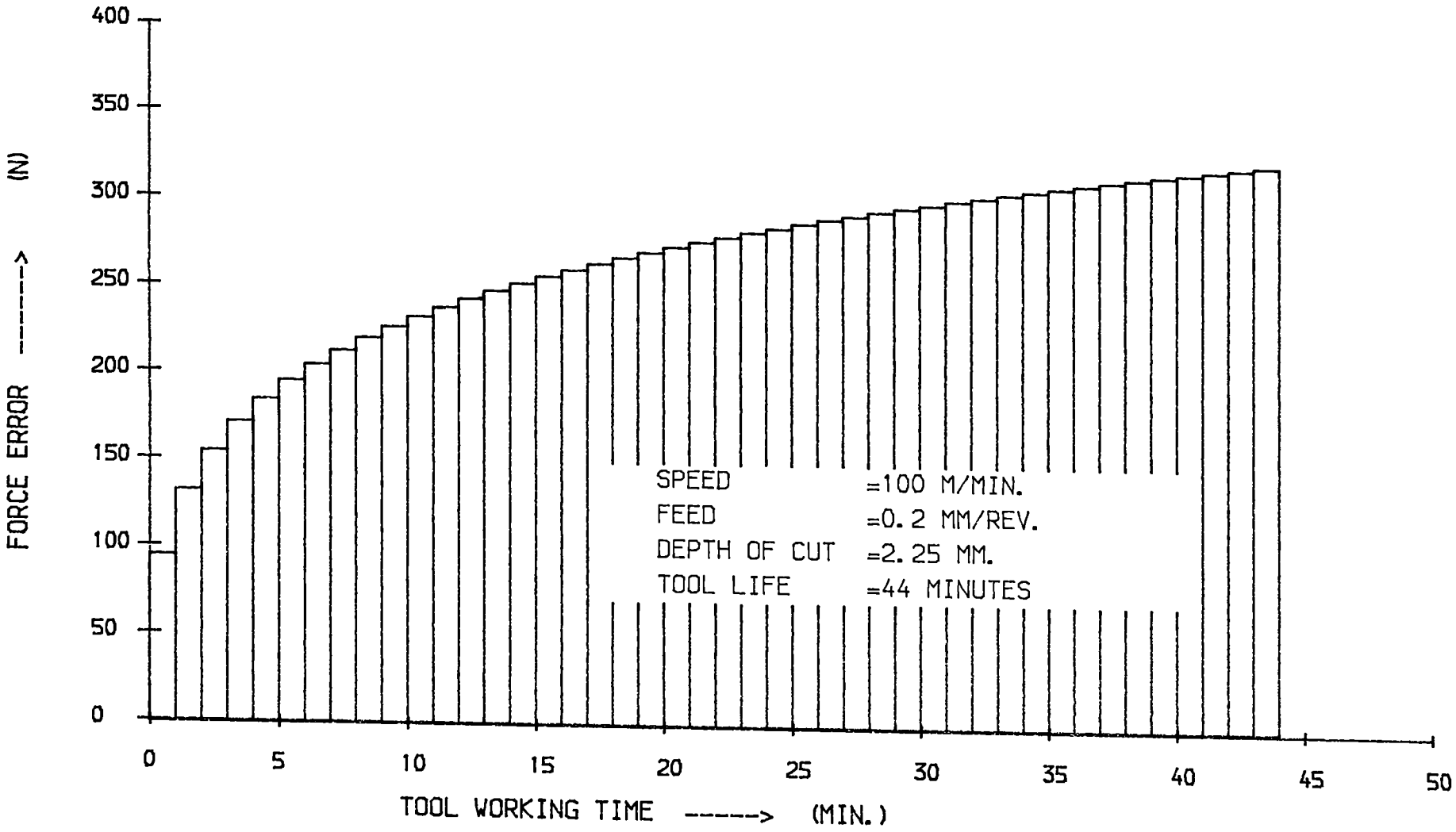

Fig. 7.16 Error Between Using Fixed And Time-Varing Cutting Force Model

7.4 Qualitative and Quantitative Understanding of the Machining Process

Along with the technological applications purposes which have already discussed, the mathematical models may provide a better understanding of the entire machining process. The tool behaviour under different cutting conditions and machining responses is better explained by the mathematical formulation of the relevant parameters. This is further explored by the graphical representation within the boundary of the operational region. This includes the three-dimensional representation, or the the response surface methodology as explained by *Figs. 5.5 & 6.16.* Also, this strategy is achieved by determining the surface contours as explained by *Figs. 5.6, 7.13, and 7.14.* Another way to obtain quantitative information of the machining process within the prespecified operational region is by establishing a computer software which include mathematical models and machining conditions. This is to provide a prior information of what level of the operation responses will be.

Table 7.3 shows a sheet output which might be obtained from such an software. Information of the process is required by the system, and could be in a menu style, or any other input means. The levels of the various responses are determined using the mathematical models which have been developed in **Chapters 4,5, and 6.**

This procedure may be generalized by adding information of new tool and workpiece materials, and this is discussed in the following chapter when recommendations for the possible future work are proposed.

INPUT DATA	
Tool Material	GC435-SPUN 12 13 12 - Multi-Coated Carbide
Tool Angles	$6^o, 5^o, 0^o, 60^o, 30^o$
Workpiece Material	EN 19
Cutting Parameters:	
a) Speed	120 m/min.
b) Feed	0.25 mm/rev.
c) Depth of Cut	3.0 mm.
d) Workpiece Diameter	100 mm.
e) Cutting Time	8 minutes.

OUTPUT DATA	
(1) Expected Tool Wear Levels	
a) Initial Wear	0.12 mm.
b) Nose Wear	0.205 mm.
c) Flank Wear	0.186 mm.
d) Notch Wear	0.189 mm.
e) Average Wear	0.209 mm.
(2) Expected Tool Life	
a) Based on 0.25 mm Average Wear	13.5 minutes.
b) Based on 0.25 mm Nose Wear	14.3 minutes.
(3) Expected Cutting forces	
a) Initial Force Value	Instantaneous Force Values
F_x 648 N	822 N.
F_y 1870 N	2071 N.
F_z 555 N	1077 N.
(4) Expected Tool Vibration amplitude	
a) Initial Tool Vibration	3.69 m/sec^2.
b) Critical Vibration Amplitudes	1.92×10^{-5} m/sec^2.

Table 7.3 An Output Sheet from the proposed Computerized Data Bank Using the Mathematical Models Developed in this Study

7.5 Conclusions

Some of the implementation and the interpretation of the developed mathematical models have been discussed throughout this chapter. As a result, some conclusions and concluded remarks have arose and can be summarized as follows:

1. The developed time-varying, or wear-varying, mathematical models have proved to have the prediction capability for most of turning responses. In contrast to the fixed value response approach, the current one enables of the detecting of the instantaneous state of machining process throughout the entire tool working life.

2. The validity of using such models, in situations where cutting conditions are subject to change for the same tool during the same cut is verified. It has been concluded that the models, which are based on fixed cutting conditions tests, to great extent, can be used in such situations. Group of relationships are produced for the computation of the resultant wear level developed in such situations.

3. Three cases are discussed in which the mathematical models can be used for building adaptive control systems. The advantages of on-line tool wear monitoring; maximization of metal removal rate; and, attaining tool life have been achieved. The advantage of optimizing secondary objective function, along with the primary one, has found to give much extra system output improvement. Such idea is graphically explained so that it can be used for parameters selection as a reference information source.

4. It has been discussed how the current approach of time-varying mathematical models can enhance the existing machinability data bank systems, and lead to permanent solution to its two main problems. This helps in making the machinability data bank systems more universally applicable.

5. It should emphasize here that the utilization of the developed mathematical models can be extended to include several other application fields such as updating the existing machinability data handbooks as a consequences of introducing new

tool and workpiece materials, and to help for better understanding of the nature of the machining process.

Chapter 8

GENERAL DISCUSSIONS AND RECOMMENDATIONS FOR FUTURE WORK

8.1 General Discussions

The mathematical modelling approach followed in this study has shown that it has potential to characterize the machining process; and to be utilized in modern machining systems. The general strategy which is followed to accomplish such an approach is now assessed.

First, it should be emphasized that critical examination of the resulting model is of vital importance to their successful use. In regression analysis, either linear or non-linear, the procedure usually leads to a solution. Acceptance of this without verification may lead to serious mistakes and to misleading results. Also, the use of a single criterion to assess the final model is unwise, since important statistical criteria may be neglected.

A great deal of significant information is obtained by conducting a minimal testing procedure of *24* trials carried out in appropriately-designed experiments. The advantage of designing the experiments may be illustrated by comparing the number of tests required to establish a tool life prediction equation with the number required in a conventional technique. The use of *Taylor's* conventional approach of one-variable-at-a time for five levels of each of the three operating parameters requires a total of *125* individual tests while, in this study, this has been achieved by only 24 tests without affecting the quality.

The experimental data for the cutting forces indicates that the variation in the value of the radial component F_z is most sensitive to wear progress, especially the nose wear. This signifies the importance of measuring all three force components. Measuring only one or two components leads to inadequate interpretation of the machining operation. *Taraman [82]* claimed that the vertical component F_y was the only force component sensitive to tool wear. In fact, this conclusion was due to the insufficient knowledge of the system characteristics. *Taraman* measured only the feed F_x and the vertical F_y components during his work on a finish turning. In finish turning, the cutting is almost entirely executed on the tool nose and, therefore, a measure of the radial

component F_z is necessary to detect wear progress.

The development of mathematical models to represent the various stages of tool life is necessary to achieve machining optimization. The models for the initial response, when a tool is perfectly sharp, might help only in the selection of starting parameters. As experienced in this investigation, a particular response may change several times throughout a tool's working life and therefore, the developed model should have the capability of detecting any variation which, in most cases, reflect the tool state. *Micheltti et al [84]* concluded that the variation in cutting force with time was too small to be useful in the monitoring of tool wear. This was due to the fact that they used a low to moderate cutting parameters which tended to induce low wear rates. This requires a longer testing time before it becomes noticeable.

Similarly, investigation of an individual case rather than the study of the global effect may lead to a disappointing and scientifically insignificant outcome. Also, an investigation of the tool's dynamic characteristics in isolation from the other responses is not always a wise strategy since any tiny disturbances may predominate and reduce the probability of observing the existing trend.

If the models proposed in this research are to be used with accuracy to monitor and to control the use of cutters in a production environment, then the models must be capable of predicting the times to achive given levels of wear for commercially available toolholders. To assess capability of the dynamometer to give results similar to what would be obtained by the satandard Sandvik toolholder, results for the time to achieve 0.25 mm wear level are presented in Table 8.1. The test number, (c.f column 1), refers to the trial location in CCD with corresponding tool life values as in Table 4.2. The tests# 3, 4, and 5, (c.f column 2), were conducted with workpiece material taken from the same batch used for the dynamometer tests. It can be seen from column 3 that the cutting times for the dynamometer are in the case of tests# 3 and 4 slightly reduced and in the case of test#5 increased. This indicates that the dynamometer is not producing a significant reduction in the cutting times. Hence the models are applicable for use

Test#	Time to accumulate 0.25mm wear level Sandvik Toolholder	Time to accumulate 0.25mm wear level Dynamometer
3	23.5 min.	20.0 min.
4	32.0 min.	30.0 min.
5	30.0 min.	36.0 min.

Table 8.1 Coparison of Cutting Times to Achieve a Wear Level of 0.25mm determined experimentally for Sandvik and for the Dynamometer

with the standard toolholder.

What follows is a discussion of how the mathematical approach followed in this study can be extended.

8.2 Recommendations for Future Work

8.2.1 Generalization of the Developed Models

The mathematical models developed in this study can be made more universal by adding information of new tool and workpiece materials. As far as the workpiece material is concerned, this could be achieved by taking account of the hardness variation among the different materials. The material used in this study, *EN 19*, can be considered as a reference and an index taken as the ratio between its hardness and the one for the new material.

8.2.2 Computer Simulation of Adaptive Control Strategies

In **Chapter 7**, it was discussed how the developed models may be implemented in adaptive control strategies with different objective functions and system constraints. The experimental development and verification of such strategies in practical situations

represent a very important topic of research.

8.2.3 Tool Wear Monitoring via Spindle Speed Variation

During the experimental work it was noticed that the spindle speed was affected by the level of wear developed on the tool clearance face. Although it was a small fraction, accurate instrumentation could be used to detect such a variation. Instead of using continuous machining tests in which the wear scars are often irregularly distributed, a set of artificial pre-worn tools, possibly by grinding the tool edge, may be used. Also, it is recommended that a constant workpiece diameter be employed throughout the testing procedures; since the variation in diameters may affect the spindle rotation.

8.2.4 Tool Wear Monitoring via Dynamic Force-Vibration Signals

One disadvantage of the use of the *BBC* microcomputer to capture and process force signals resides in its limiting storage. Even though it was sufficient enough for the purpose of the current research, it would be very interesting to obtain wider force frequency responses through the simultaneous recording of force-vibration signals on magnetic tapes. These signals may be analyzed and compared with each other for a possible correlation with wear progress using the frequency analyzer and the power spectral technique.

Chapter 9

GENERAL CONCLUSIONS

In this study a new approach is followed to investigate and characterize the cutting action and to look for new and more reliable techniques for use in in-process tool wear monitoring. Although each chapter is followed by its own detailed conclusions and concluding remarks, it is convenient to summarize the general conclusions as follows:

1. •• **A very efficient** and compact three-component cutting force dynamometer has been designed and manufactured using a new technique of non-central circular-hole as sensing element. Cross-sensitivity among the components has been reduced to its lowest level by accurately locating the true cutting application point and by mathematically modelling the dynamometer performance.

2. •• **The wear** resistance of the multi-coated carbide tips has been found to be strongly dependent upon how long the coatings remain on the substrate. Tools exhibit a very high wear resistance for relatively long periods at low to moderate feeds and speeds. Once a certain band of coatings has been rubbed out, the wear rate is rapidly accelerated which terminates in most cases in a catastrophic failure and breakage of the tool. In general, the rate at which coatings are removed is strongly dependent on the cutting conditions employed. A speed higher than *150 m/min* tends to significantly reduce the tool life. The best feed range was found between *(0.12-0.3) mm/rev.*

3. •• **The experimental** wear-time relationships exhibit the general three wear region pattern. However, random disturbances, such as chipping, fracture, and flaking, frequently occurred, especially in the nose area and in particular, when feeds lower than *0.12 mm/rev* were employed.

4. •• **Generally,** symptoms of tool failure always originate in the nose area and then failure in the other locations on the clearance face is triggered accordingly.

5. •• **The mathematical** models developed using the linear regression techniques to relate wear level to the cutting parameters and cutting time have been found to be more appropriate in predicting wear levels only within the region of constant wear rate.

6. •• **The mathematical** models for the initial wear level during the first few moments of cutting indicated that the initial wear was dependent on cutting conditions and on the workpiece hardness.

7. •• **Mathematical models** have been developed to relate the tool life to the cutting conditions: speed, feed, and depth of cut. Average wear has been found to be a better criterion for tool life modelling than the nose wear. A first-order model has been found to be inadequate to fit the experimental tool life data. A second-order model has been found to give better statistical and technological criteria and to improve the model predictability. However, the resulting models are found to be affected by some outlier and influential cases. This increases the standard error of estimates, and affects the homogeneity of the residuals. Consequently, a robust regression technique, via iteratively re-weighting data points, was used to reduce the high impact of the outlier and the influential cases on the rest of data points. A considerable improvement has been achieved in the predictability of the models and in their statistical significance.

8. •• **The tool life** behaviour within the operational region of speed and feed is examined through the response surface methodology and the surface contours. The strong dependence of tool life on both speed and feed is confirmed. Depth of cut has the least effect and is not significant enough to be included in the average wear tool life model. The tool life surfaces exhibit a non-linear trends, especially at low to moderate ranges of cutting conditions. It has been found that, for a low-to-moderate range of cutting speed, there is a certain feed value of *0.12 mm/rev*, below which the tool life is reduced.

9. •• **The force variation** during cutting has been found very sensitive to wear progress; tool chipping; and, machining instability. Mathematical models of the various force components indicate that each of the feed F_x and the radial F_z components are very sensitive to wear progress. The nose wear has the strongest influence on all force components with its highest effect on the radial component F_z.

10. •• **An approach** has been proposed of the in-process detection and prediction of tool wear and breakage using the force variation. This approach depends on the determination of the force variation of the force ratio (F_z/F_y) which is found to correlate most closely with the tool wear progress; failure, and breakage. Moreover, the use of this force ratio will eliminate the effect of hardness variation either from one cut to another or from one workpiece to another.

11. •• **Tool vibration** signals in both the feed X and the vertical Y directions are collected simultaneously with values of the cutting forces using vibration accelerometers which are located at the back of the dynamometer body. These vibration signals are later analyzed using a Fast Fourier Transform analyzer and spectral analysis. Among the vibration signatures which appeared in the power spectrum envelope, the component at a frequency corresponding to the first fundamental natural frequency of the toolholder in the X-direction has been found to be the most affected by tool wear progress.

12. •• **The power amplitude** of such a mode of tool vibration continued to decrease as wear increased until it reached a limit, after which it tended to reverse its direction and to promptly increase. The point at which the power amplitude reached its minimum value was found to be in a very good agreement with the moment at which higher rates of both wear and force were obtained.

13. •• **Based on this fact,** an in-process tool wear monitoring approach has been proposed which uses the mathematical models to quantitatively characterize the vibration response. A non-linear model has been developed to relate the variation of the power amplitude to the corresponding wear value. A critical wear is determined which can be used as an in-process tool life measure. Also, a non-linear model has been developed using force-vibration combination to predict the values of the nose wear during cutting.

14. •• **The validity** is verified of using the mathematical models developed in this study in an adaptive control situations where cutting conditions are subject to change for the same tool during the same cut when the need arises. It has

been found that the developed models are capable of accurately predicting and monitoring the tool-state during such situations.

15. •• **A critical discussion** is presented of how the mathematical models developed in this study can be interpreted and utilized in practical industrial situations. Three adaptive control strategies are proposed: on-line tool wear monitoring; maximization of metal removal rate; and attaining tool life under system constraints of tool forces, machine power, and limiting cutting conditions.

16. •• **A machinability** data bank has been proposed in a form of computer output using the developed models. This is to provide a more practical way to understand the machining process; to provide accurate starting cutting conditions; and to predict in advance the simultaneous levels of system responses at any moment within the entire operational region.

REFERENCES

1. • **Bhattacharya, D.,** *"Development in Machinability of Steel"*, The Inst. of Metals, Paper No. 10, Proc., 1 st Int. Conf. on Behaviour of Material in Machining, Stratford-upon-Avon, England, Nov. 1988.

2. • **Pickett, M., L., and Naylor, D., J.,** *"Effect of Bright Drawing on the machinability of Free Cutting steels"*, The Inst. of Metals, Paper No. 11, Proc., 1 st Int. Conf. on Behaviour of Material in Machining, Stratford-upon-Avon, England, Nov. 1988.

3. • **Mori, T., Tanase, M., Ebihara, T., Yoshida, M., and Niwa, S.,** *"Qualities of Free Cutting Steels for Machine Structural Use, Containing Calcium, Sulphur and Lead, Produced by Continuous Casting Process"*, The Inst. of Metals, Proc., 1 st Int. Conf. on Behaviour of Material in Machining, Stratford-upon-Avon, England, Nov. 1988.

4. • **Joseph, R., A., Yogauchi, H., and Bhattacharya, D.,** *"The Development and Characterization of Bloom Cast, Low Carbon, Resulphurized, Free Machining Steel"*, Inst. of Metals, Paper No. 10, Proc., 1 st Int. Conf. on Behaviour of Material in Machining, Stratford-upon-Avon, England, Nov. 1988.

5. • **Engineer, S., Huchtemann, B., and Schuler,** *"An Investigation of the Effect of Sulfur, Tellurium and Calcium on the Machinability and the Technological Properties of Engineering Steels "*, The Inst. of Metals, Paper No. 14, Proc., 1 st Int. Conf. on Behaviour of Material in Machining, Stratford-upon-Avon, England, Nov. 1988.

6. • **Davies, I., G., Finch, N., A., and Pickett, M., L.,** *"Development and Applications of Alloy and Stainless Stress with Improved Machinability"*, The Inst. of Metals, Paper No. 15, Proc., 1 st Int. Conf. on Behaviour of Material in Machining, Stratford-upon-Avon, England, Nov. 1988.

7. • **Pöntinen, H., Paju, M., and Holistö, P.,** *"Machinability of the Calcium Treated M Steel using Ceramic Tools and Titanium Nitride Coated HSS Tools"*, The Inst. of Metals, Paper No. 16, Proc., 1 st Int. Conf. on Behaviour of Material in Machining, Stratford-upon-Avon, England, Nov. 1988.

8. • **Bleton, O., Duet, R., and Pedarre, P.,** *"Influence of Oxide Nature on the Machinability of 316L Stainless Steels"*, The Inst. of Metals, Paper No. 17, Proc., 1 st Int. Conf. on Behaviour of Material in Machining, Stratford-upon-Avon, England, Nov. 1988.

9. • **Kronenberg, M.,** *Machining Science & Application*, Pergamon Press, 1966.

10. • **Taylor, F., W.,** *"On the Art of Cutting Metals"*, Trans ASME, Vol. 28, 1907, p.31.

11. • **Tipnis, V., A., and Garrison, R., C.,** *"Mathematically Modelled Machining Data for Adaptive Control of End Milling Operations "*, proc. NAMRC-VI, 1976, pp. 279-286.

12. • Bhattacharyya, A., and Ham, I., *"Analysis of Tool Wear - Part I: Theoretical Models of Flank Wear"*, Trans ASME, J. Eng. Ind., Series B, Vol. 91, 1969, p. 790.

13. • Etheridge, R., A., and Hsü, T., C., *"The Specific Wear rate and its Application to the Assessment of Machinability"*, Annals CIRP, Vol. 18, 1970, p. 10.

14. • Wager, J., G.,and Brash, M., M., *"Study of the Distribution of the Life of HSS Tools"*, Trans ASME, J. Eng. Ind., Series B, Nov. 1972, pp. 1044-1050.

15. • Friedman, M., Y., and Zlatin, N., *"Variability of Tool Life as a Function of its Mean Value"*, Proc. NAMRC-II, Madison, May 1974, pp. 128-138.

16. • Ermer, D., S., and Wu., S., M., *"The Effect of Experimental Error on the Determination of the Optimum Metal Cutting Conditions"*, Trans ASME, J. Eng. Ind., Series B, Vol. 89, No. 2, May 1966, pp. 315-322.

17. • DeVor, R., E., Anderson, D., l., and Zdeblick, W., J., *"Tool Life Variation and its effects on the development of Tool Life Models"*, Trans ASME, J. Eng. Ind., Series B, Vol. 99, No. 3, August 1977, pp. 578-584.

18. • Colding, B., N., *"A Three-Dimensional Tool Life Equation - Machining Economics"*, Trans ASME, J. Eng. Ind., Series B, Vol. 81, 1959, pp. 239-250.

19. • Wu, S., M., *"Tool Life Testing by Response Surface Methodology - Part 1 & 2 "*, Trans. ASME, J. Eng. Ind., May 1964, pp. 105-116.

20. • Wu, S., M., Ermer, D., S., and Hill, H., J., *"An Exploratory Study of Taylor's Tool Life Equation by Power Transformations"*, Trans ASME, J. Eng. Ind., Series B, Vol. 88, No. 1, Feb. 1966, pp. 81-92.

21. • Colding, B., N., and König, W., *"Validity of the Taylor Equation in Metal Cutting"*, Annals CIRP, Vol. 19, No. 4, 1971, p. 793.

22. • Kronenberg, M., *"Replacing the Taylor Formula by a New Tool life Equation"*, Int. J. MTDR, Vol. 10, 1970, p. 193.

23. • Shaw, M., C., *Metal Cutting Principles*, Clarendon Press, Oxford, 1984.

24. • Shaw, M., C., and Smith, P., A., *"Tool Wear Results from Several Causes"*, American Machinist, New York, Vol. 95, No. 22, Oct. 1951, pp. 100-103.

25. • Takeyama, H., and Murata, R., *"Basic Investigation of Tool Wear"*, Trans ASME, J. Eng. Ind., Series B, 1963, pp. 33-38.

26. • Boothroyd, G., Eagle, J., M., and Chisholm, A., W., J., *"Effect to Flank Wear Cutter Temperature Generated During Metal Cutting"*, Proc. 8 th Int. MTDR Conf., Manchester, England, 1967.

27. • Chao, B., T., and Trigger, K., J., *"Temperature Distribution at the Tool-Chip Interface in Metal Cutting"*, Trans ASME, Oct. 1955, pp. 1107-1121.

28. • Ber, A., *"Relationship Between Thermal Properties and Flank Wear of Cemented Carbide Tools"*, Annals CIRP, Vol. 21, No. 1, 1972.

29. • **Colding, B., N.,** *"Coated Cutting Tools"*, SMS's Cutting Tools Clinic, March 1980.

30. • **Shabaik, A., H.,** *"Wear of Cutting Tools"*, Proc. 21 th Int. MTDR Conf., 1980, pp. 421-430.

31. • **Ekemer, S.,** *"Coated Indexable Cemented Carbide Inserts - A Development in Progress"*, Presented at SME's Westec'77 Conference.

32. • **Smith, A., B., Abbas, F., M., H., and Williams, R.,** *"Improved Cutting Performance of High Speed Steel Tools Coated with Titanium Nitride by C.V.D"*, The Inst. of Metals, Proc., 1 st Int. Conf. on Behaviour of Material in Machining, Stratford-upon-Avon, England, Nov. 1988.

33. • **Ber, A., and Kalder, S.,** *"The First Seconds of Cutting, Wear Behaviour"*, Annals CIRP, Vol. 22, No. 1, 1973.

34. • **Gates, A., S., and Peters, R., L.,** *"Structure and Wear of Coated Cemented Carbides: TiC, TiN, and Al_2O_3"*, Modern Trends in Cutting Tools, SME, 1 st Edition, Dearborn, Michigan, 1982.

35. • **Shanshal, D., and Dugdale, D., S.,** *"Effectiveness of Hard Coatings in Reducing Tool Tip Wear"*, Proc. 24 th Int. MTDR Conf., 1984, pp. 163-166.

36. • **Wood, G., A.,** *"Cemented Carbides - Their Present Status as Tool and Die Materials"*, Proc. 25 th Int. MTDR Conf., 1985, pp. 253-259.

37. • **Suh, N., P.,** *"Coated Carbides - Past, Present and Future"*, Int. Conf. on Hard Materials of Tool Technology, Carnegie-Melton University, Pittsburgh, Penna., June, 1976.

38. • **Schintlmeister, W., Pacher, O., Krall, T., Wallagram, W., and Raine, T.,** *"Wear Characteristics of CVD-Coated Hard Metal Cutting Tools"*, Powder Metallurgy International, Vol. 13, No. 1, Feb. 1981, pp. 26-30.

39. • **Chubb, J., P., and Billingham, J.,** *"Coated Cutting Tools - A Study of Wear Mechanisms in High Speed Machining"*, Wear, Vol. 61, 1980, pp. 283-293.

40. • **Hale, T., and Graham, D.,** *"How Effective are the Carbide Coatings?"*, Modern Machine Shop, April 1981.

41. • *Machining Times Cut by 90% with CBN,* Report by De Beers, Production Engineer, Feb. 1985, p. 55.

42. • **Kalish, H., S.,** *Status Report: Cutting Tool Materials,* Metal Progress, Nov. 1983, pp. 21-23 & 25-27.

43. • **Hiroshieda, K., K., and Hashimoto,** *"The Newly Developed CBN Cutting Tool"*, Proc. 21 st Int. MTDR Conf., 1980, pp. 253-258.

44. • **Aspinwall, D., K., Tunstall, M., and Hammerton, R.,** *"Cutting Tool Life Comparisons"*, Proc. 25 th Int. MTDR Conf., 1985, pp. 269-277.

45. • **Cother, N., E., and Hodgson, P.,** *"Review Paper - The Development of Syalon Ceramics and their Engineering Applications"*, Trans Bull. J. Br. Ceram. Soc., Vol. 81, 1982, pp. 141-144.

46. • *Sialon Ceramics will Cut Nickel Steels at Speed,* The Production Engineer, Feb. 1984, p. 18.

47. • **Chandrupatta, T., R.,** *"An Alternative Method for the Determination of Tool Life Equations"*, Proc. 26 th Int. MTDR Conf., 1986, pp. 359-361.

48. • **Taylor, J.,** *"Tool Wear-Time Relationship in Metal Cutting"*, Int. J. MTDR, Vol. 2, 1962, pp. 119-148.

49. • **Mills, b., and Redford, A., H.,** *Machinability of Engineering Materials,* Applied Science Publishers, London and New York, 1983.

50. • **Groover, M., P.,** *"Monte Carlo Simulation of the Machining Economics Problems"* Trans ASME, August 1975, pp. 931-938.

51. • **Koren, Y.,** *"Flank Wear Model of Cutting Tools using Control Theory"*, Trans ASME, J. Eng. Ind., Vol. 100, Feb. 1978, pp. 103-109.

52. • **Taraman, K., S.,** *"Development and Utilization of Mathematical Models for Metal Cutting Responses "*, Ph.D. Thesis, Texas Tech. University, USA, 1971.

53. • **French, H., J., Bayonne, N., J., and Digges, T., G.,** *"Turning with Shallow Cuts at High Speed"*, Trans ASME, Vol. 52, 1930, pp. 35-86.

54. • **Becker, W., R., and Krabacher, E., J.,** *"New Techniques in Metal Cutting Research "*, Trans. ASME, Oct. 1958, pp. 1497-1505.

55. • **Merchant, M., E., Ernst, H., and Krabacher, E., J.,** *"Radioactive Cutting Tools for Rapid Tool Life Testing"*, Trans ASME, Vol. 75, 1953, pp. 549-559.

56. • **Sata, T.,** *"Rapid Tool Life Tests by Means of Irradiated Carbide Cutting Tools"*, J. Jap. Soc. Prec. Eng., No. 24, 1985, p. 453.

57. • **Uehara, K.,** *"Study on the Tool Wear in Metal Cutting"*, (1 st & 2 nd Report), J. Jap. Soc. of Prec. Eng., No. 38, 1972, p. 167 & p. 261.

58. • **Uehara, K.,** *"New Attempts for Short Time Tool Life Testing"*, Annals CIRP, Vol. 22, No. 1, 1973.

59. • *Specification for Tool-Life Testing with Single-Point Turning Tools,* BSI [BS 5623; 1979 (ISO 3685-1979)].

60. • **Maekawa, K.,** *"Scattering in Flank Wear of Carbide Cutting Tools "*, Bull. Jap. Soc. Prec. Eng., Vol. 18, No. 3, Sep. 1984.

61. • **Hsü, T., C.,** *"A Study of Wear on Cemented Carbide Cutting Tools"*, Trans ASME, J. Eng. Ind., August 1969, pp. 652-658.

62. • **Smith, A., B., and Whittle, N., C.,** *"Effect of A CVD Titanium Nitride on the Cutting Properties of High Speed Steel Tools"*, Proc. 25 th Int. MTDR Conf., 1985, pp. 261-268.

63. • **Jemielniak, K., Szafarczyk, M., and Zawistowski, J.,** *"Difficulties in Tool Life Predicting When Turning with Variable Cutting Parameters "*, Annals CIRP, Vol. 34, No.1, 1985, pp. 113-116.

64. • **Nagasaka, K., Hashimoto, F.** *"Tool Wear Prediction and Economics in Machining Stepped Parts"*, Int. J. Mac. Tools Manuf., Vol. 28, No. 4, 1988, pp. 569-576.

65. • **Koren, Y.,** *"A Variable Cutting Speed Method for Tool Life Evaluation"*, Proc. 4 th Int. Conf. Prod. Eng., Tokyo, 1980, pp. 530-534.

66. • **Chen, W.,** *"A New Rapid Wear Test for Cutting Tools"*, Proc. 27 th Int. MTDR Conf., 1988, pp. 261-265.

67. • **Zdeblick, W., J., and DeVor, R., E.,** *"An Experimental Strategy for Designing Tool Life Experiments"*, Trans ASME, J. Eng. Ind., Series B, 1977.

68. • **Novak, A., and Ossbahr, G.,** *"Reliability of the Cutting Force Monitoring in FMS Installations"*, Proc. 26 th Int. MTDR Conf., 1986, pp. 325-329.

69. • **Liao, Y., S.,** *"Development of A Monitoring Techniques for Tool Change Purpose in Turning"*, Proc. 26 th Int. MTDR Conf., 1986, pp. 331-337.

70. • **Constantinides, N., and Benneti, S.,** *"An Investigation of Methods for the On-Line Estimation of Tool Wear"*, Int. J. Mach. Tools Manuf., Vol. 27., No. 2, 1987, pp. 225-237.

71. • **Martin, K., F., Brandon, J., A., Grosvener, R., I., and Owen, A.,** *"A Comparison of In-Process Tool Wear Measurement Methods in Turning"*, Proc. 26 th Int. MTDR Conf., 1986.

72. • **Lister, P., M., and Barrow, G.,** *"Tool Condition Monitoring Systems "*, Proc. 26 th Int. MTDR Conf., 1985, pp. 271-288.

73. • **Barrow, G.,** *"A Review of Experimental and Theoretical Techniques for Assessing Cutting Temperature"*, Annals CIRP, Vol. 22, No. 2, 1973, pp. 203-211.

74. • **Moriwaki, T.,** *"Detection of Cutting Tool Fracture by Acoustic Emission Measurement"*, Annal CIRP, Vol. 29, No. 1, 1980, pp. 35-40.

75. • **Moriwaki, T.,** *"Application of Acoustic Emission Measurement to Sensing of Wear and Breakage of Cutting Tool"*, Bull. Jap. Soc. Prec. Eng., Vol. 17, No. 3, 1983.

76. • **Lee, M., Thomas, C., E., Wildes, and D., G.,** *"Prospects for In-Process Diagnosis of Metal Cutting by Monitoring Vibration Signals"*, General Electric Company, Corporate Research and Development, Schenetady, NY.

77. • **Kinnander, A.,** *"Choice of Wear Criteria in Fully Automated Turning"*, Proc. 22 nd MTDR Conf., 1981.

78. • **Moriwaki, T.,** *"Sensing and Prediction of Cutting Tool Failure"*, Bull. Jap. Soc. Prec. Eng., Vol. 18, No. 2, June 1984.

79. • **Uehara, K., Kiyosawa, F., and Takeshita, A.,** *"Automatic Tool Wear Monitoring in NC Turning"*, Annals CIRP, Vol. 28, 1979, pp. 39-42.

80. • **Colwell, L., V.,** *"Cutting Temperature Versus Tool Wear"*, Annals CIRP, Vol. 24, No. 1, 1975, pp. 73-76.

81. • **Colwell, L., V.,** *"Methods for Sensing the Rate of Tool Wear"*, Annals CIRP, Vol. 19, No. 4, 1971, pp. 647-651.

82. • **Taraman, K., S., Swando, R., and Yumauchi, W.,** *"Relationship Between Tool Forces and Flank Wear"*, SME Tech. Paper No. MR 74.

83. • **Wolf, W., and Magadanz, P.,** *"Feed Force Monitoring for Operation Security and Reliability"*, SME Tech. Paper No. nIQ 81-161,1974.

84. • **Micheletti, G., F., De Filippi, and Ippolito, R.,** *"Tool wear and Cutting Forces in Steel Turning"*, Annals CIRP, Vol. 16, No. 4, 1968, pp. 353-360.

85. • **Kōning, W.,** *"Correlation between Cutting Force Components and Tool Wear"*,Annals CIRP, Vol. 21, No. 1, 1972.

86. • **Mackinnon, R., Wilson, G., E., and Wilkinson, A., J.,** *"Tool Condition Monitoring using Multi-Component Force Measurements"*, Proc. 26 th Int. MTDR Conf., 1986, pp. 317-324.

87. • **Hsü, T., C., and Chaoi, C., Y.,** *"Measurement and Representation of Cutting Force Due to Oblique Machining"*, Int. J. MTDR, Vol. 10, 1970, pp. 40-64.

88. • **Zhe-Jun, Y., Li-Jun, C., and Pan, Z.,** *"A New Type of Three-Component Dynamometer with High Stiffness and High Natural Frequency "*, Proc. 26 th Int. MTDR Conf., 1986, pp. 313-316.

89. • **Levi, R.,** *"Multicomponent Calibration of MachineTool Dynamometers"*, Trans. ASME, J. Eng. Ind., Nov. 1972, pp. 1067-1071.

90. • **Hallam, R., A., and Allsopp, R., S.,** *"The Design, Development and Testing of A Prototype Boring Dynamometer ,"* Int. J. MTDR, Vol. 2, 1962, pp. 241-266.

91. • **Sun, P., Y., Chang, Y., K., Wang, T., C., Liu, P., T.,** *"A Simple and Practical Piezo-Electric Shank Type Three-Component Dynamometer "*, Int. J. MTDR, Vol. 22, No. 2, 1982, pp. 111-124.

92. • **Shanshal, D.,** *Effect of A Nitride Coating on The Life of Cutting Tools,* Ph.D. Thesis, University of Sheffield, 1983.

93. • **Tani, Y., Hatamura, Y., and Nagoa, T.,** *"Development of Small Three-Component Dynamometer for Cutting Force Measurement ,"* Bull. JSME, Vol. 26, No. 214, April 1983, pp. 650-658.

94. • **Andrew, C.,** *"Chatter in Horizontal Milling"*, Proc. Instn. Mech. Engrs., Vol. 179, Part 1, No. 28, 1964-65, pp. 877-906.

95. • **Kegg, R., L.,** Communication on Ref. 94.

96. • **Andrew, C.,** Reply to Dr. Kegg's Contribution to Ref. 94.

97. • **Broch, J., T.,** *Technical literature booklet issued by Bruel & Kjaer on the Mechanical Vibration and Shock Measurements,* 1976.

98. • **Walshaw, A., C.,** *Mechanical Vibration with Application,* Jhon Wiley & Sons, 1984.

99. • *Optimizing Strain Gauge Excitation Levels,* WSM Technical Note TN 502, June 1882.

100. • **Newland, D., E.,** *An Introduction to Random Vibrations and Spectral Analysis,* Second Edition, Longman Group Limited, 1984.

101. • *Machining Data Handbook,* 3rd Edition, Metcut Research Associates, 1980.

102. • **Wu, S., M., and Meyer, R., N.,** *"Mathematical Models of Carbide Tool Crater Surfaces"*, Int. J. MTDR, Vol. 7, 1967, pp. 445-463.

103. • **Wu, S., M., and Meyer, R., N.,** *"An Analysis of the Development of Carbide Tool Crater Wear"*, Int. J. MTDR, Vol. 7, 1967, pp. 123-153.

104. • **Claycombe, W., W., and Sullivon, W., G.,** *"Use of Response Surface Methodology to Select a Cutting Tool to Maximize Profit "*, Trans. ASME, J. Eng. Ind., Feb. 1976, pp. 63-65.

105. • **DeVor, R., E., and Tipnis, V., A.,** *"Development of Mathematical Models For Process Planning of Machining Operations "*, Proc. NAMRC-XI, 1978, pp. 395-401.

106. • **Balakrishnan, and DeVries, M., F,** *"Sequential Estimation of Machinability Parameters for Adaptive Optimization of Machinability Data Base Systems"*, Trans ASME, J. Eng. Ind., Vol. 107, May 1985, pp. 159-166.

107. • **Vilenchich, R., Stroele, K., and Venter, R.,** *"Tool-Life Testing By Response Surface Methodology Coupled with A Random Strategy Approach "*, Proc. 13 th Int. MTDR Conf., 1972.

108. • **Taraman, K., S.,** *"Multi-Machining Output Multi-Independent Variables Turning Research by Response Surface Methodology "*, Int. J. Prod. Res., 1974, Vol. 112, No.2, pp. 233-245.

109. • **Friedman, M., Y., and Field, M.,** *"Building of Tool Life Models for Use in A Computerized Numerical Machining Data Bank* , Proc. Int. Conf. Prod. Engng., Tokyo, 1974, part 1.

110. • **Tipnis, V., A.,** *"Development of Mathematical Models for adaptive control Systems "*, Proc. 13 th Annual Meeting, Numerical Control Society, 1976, pp. 149-156.

111. • **Mukherjee, S., N., and Basu, S., K.,** *"Multiple Regression in Evaluation of Tool Wear"*, Int. J. MTDR, Vol. 7, No. 1, 1967, pp. 15-21.

112. • **Wu, S., M., and Meyer, R., N.,** *"Cutting Tool Temperature Predicting Equation by Response Surface Methodology"*, Trans ASME, J. Eng. Ind., May 1964, pp. 150-156.

113. • **Balakrishnan, P., and DeVries, M., F.,** *"Analysis of Mathematical Model Building Techniques Adaptable to Machinability Data Base Systems "*, Proc. NAMRC-XI, May 1983, pp. 466-475.

114. • **Fisher, R., A.,** *The Design of Experiments,* Oliver and Boyd Ltd., 6 th Edition, 1951.

115. • **Box, G., E., P.,** *Statistics for Experimenters,* Jhon Wiley & Sons, 1978.

116. • **Robinson, E., A.,** *Least Squares Regression Analysis in Terms of Linear Algebra,* Goose Pond Press, 1981.

117. • *SPSSX Statistical Computer Package,* SPSS Inc., 444 N.Michigan Av., Chicago, Illinois, USA.

118. • **Draper, N., R., and Smith, H.,** *Applied Regression Analysis,* Wiley, New York, 1967.

119. • **Daniel, C., and Wood, F., S.,** *Fitting Equations to Data,* Jhon Wiley & Sons, 1971.

120. • **Hines, W., W., and Montgomery, D., C.,** *Probability and Statistics in Engineering and Management Science,* Jhon Wily & Sons, 2 nd Edition, 1982.

121. • **Hoaglin, Mosteller, and Tukey,** *Understanding Robust and Exploratory Data Analysis,* 1983.

122. • **Ermer, D., S.,** *"A Bayesian Model of Machining Economics for Optimization Adaptive Control"*, Trans ASME, J. Eng. Ind., August 1970, pp. 628-632.

123. • **Rao, S., B.,** *"Tool Wear monitoring Through the Dynamics of Stable Turning"*, Trans. ASME, J. Eng. Ind., Vol. 108, August 1986, pp. 183-190.

124. • **Akhtar, S., Redford, A., H., and Mills, B.,** *"Short-Time Method for the Assessment of the Machinability of Low Carbon Free-Machining Steels"*, Int. J. MTDR, Vol. 16, 1976, pp. 71-75.

125. • **Arnold, R., N.,** *"The Mechanism Of Tool Vibration In Cutting Of Steel"*, Proc. Inst. Mech. Engrs., Vol. 27, 1946, pp 261-276.

126. • **Tourret, R.,** *Performance of Metal Cutting tools,* Butterworth Scientific Publications, London, 1963.

127. • *Vibration Monitoring Signals Tool Failure,* Report By PERA, Machinery and Production Engineering, November 1986, p.19.

128. • **Weller, E., J., Schrier, H., M., and Weichbrodt, B.,** *"What Sound Can Be Expected from a Worn Tool?"*, Trans. ASME, J Eng. Ind., August 1969, pp 525-534.

129. • **Andrew, C., and Tobias, S., A.,** *"Vibration in Horizontal Milling"*, Int. J. MTDR, Vol. 2, 1962, pp. 369-378.

130. • **Andrew, C., and Tobias, S., A.,** *" A Critical Comparison of Two Current Theories of Machine Tool Chatter"*, Int. J. MTDR, Vol. 1, 1961, pp. 325-335.

131. • **Tobias, S., A., and Fishwick, W.,** *" The Chatter of Lathe Tools Under Orthogonal Cutting Conditions"*, Trans. ASME, July 1958, pp. 1079-1088.

132. • **Jemielniak, K., and Widota, A.,** *"Suppression of Self-Excited Vibrations by the Spindle Speed Variation Method"*, Int. J. MTDR, Vol. 24, No.3, pp. 1984, 207-214.

133. • **Mauri, E., Ema, S., and Kato, S.,** *"Chatter Vibration of Lathe Tools:- Part 1: General Characteristics of Chatter Vibrations. Part 2: On the Mechanism of Exciting Energy Supply."*, Trans. ASME, J. Eng. Ind., Vol. 105, May 1983, pp. 106-113.

134. • **Tobias, S., A.,** *Machine-Tool Vibrations,* Blakie & Son Ltd., 1965.

135. • **Doi, S., and kato, S.,** *"Chatter Vibration of Lathe Tools"*, Trans ASME, July 1956, pp. 1127-1134.

136. • **Mauri, E., Kato, S., Hashimoto, M., and Yamanda, T.** *", The Mechanism Of Chatter Vibrations in a Spindle-Workpiece System:- Part 1: Properties of Self-excited Chatter Vibration in Spindle-Workpiece System. Part 2: Characteristics of Dynamic Cutting Force and Vibrations Energy. part 3: Analytical Considerations."*, Trans. ASME, J. Eng. Ind., Vol. 104., August 1988, pp. 236-253.

137. • *Monitoring for Tool Breakage and Workpiece Probing* , Report by General Electric, Machinery and Production Engineering, November 1986, p.20.

138. • **Pandit, S., M., and Kashou, S.,** *"A Data Dependent Systems Strategy of On-line Tool Wear Sensing"*, Trans. ASME, J. Eng. Ind., Vol. 104, August 1982, pp. 217-223.

139. • **Taglia, A., Portundo, S., and Tani, P.,** *", An Approach to On-line Measurement of Tool Wear by Spectrum Analysis"*, Proc. 17th. Int. MTDR Conf., 1976, Vol. 1, pp. 141-148.

140. • **Lindstrom, B., and Lindberg,** *"Measurement of Dynamic Cutting Forces in the Cutting Process, a New Sensor for In-Process Measurements"*, Proc. 24th Int. MTDR Conf., 1984, pp. 137-142.

141. • **Micheletti, G., F., Rossetto, S., and Ponti, M.,** *"Tool Vibration Pattern and Tool Life on Automatic Screw Machine"*, Proc. 11th. Int MTDR Conf., 1970, pp. 145-158.

142. • **Martin, P., Mutels, B., and Draiper, J., P.,** *"Influence of Lathe Tool Wear on the Vibrations Sustained in Cutting"*, Proc. 15th. MTDR Conf., 1975, p.339.

143. • **Pandit, S., M., and Kashou, S.,** *"Variation in Friction Coefficient with Tool Wear"*, Wear, VOL. 84, No.1, 1983 , pp. 65-79.

144. • **Shiraishi, M.,** *"Geometrical Adaptive Control in NC Turning Operation "* Trans. ASME, J. Eng. Ind., Feb. 1984, Vol. 106, pp. 75-80.

145. • **Szafarczyk, M., Misiewicz, M., and Dagil, S.,** *"Adaptive Control Improving Size Accuracy of Centre Turning"*, Proc. 25 th Int. MTDR Conf., 1985, pp. 187-191.

146. • **Bedini, R., Lisini, G., G., and Pinoti, P., C.,** *"Experiments on Adaptive Control of a Milling Machine "*, Trans. ASME, J. Eng. Ind., Feb. 1976, pp. 239-245.

147. • **Davis, R., P., Wysk, R., A., Agee, M., H., and Kimbler, D.,L.,** *"Optimizing Machining Parameters in a Frame Work for Adaptive Computer Control* ", Compu. & Indust. Engng, Vol. 4, 1980, pp 143-151.

148. • **Bedini, R., Pinotti, P., C., and Presciuttini, G.,** *"Adaptive Control in Drilling* ", Int. J. MTDR, Vol. 17, 1977, pp. 91-102.

149. • **Bedini, R., and Pinotti, P., C.,** *"A Hardwired Logic for the Adaptive Control of a Milling Machine* ", Int. J. MTDR, Vol. 16, 1976, pp. 193-207.

150. • **Bedini, R., and Pinotti, P., C.,** *"Experiments on Adaptive Constrained Control of A CNC Lathe* ", Trans. ASME, J. Eng. Ind., Vol. 104, May 1982, pp. 139-149.

151. • **Mathias, A.,** *"Adaptive Control for the Eighties* ", SME Technical Paper No. MS80-242, 1980.

152. • **Wilson, G., E., and Wilkinson, A., J.,** *"Adaptive Control for a CNC Lathe* ", Proc. 22 nd Int. MTDR Conf., 1980, pp. 205-214.

153. • **Mackinnon, R., Wilson, G., E., and Wilkinson, A., J.,** *"Constraints on Adaptive Control in Unmanned Machining* ", Proc. 25 th Int. MTDR Conf., 1985, pp. 177-186.

154. • **Klein, B., Kuchta, M., Szafraczyk, M., and Winiarski, A.,** *"Feed Rate and Cutting Speed Adaptive Control System for Turning Process* ", Proc. 26 th Int. MTDR Conf., 1985, pp. 95-102.

155. • **Giusti, F., Santochi, M., and Tantussi, G.,** *"A Constant Cutting Power Adaptive Control for Rough and Fine Turning* ", Proc. 24 th Int. MTDR Conf., 1984, pp. 187-193.

156. • **Chang, Y., and Chen, B., S.,** *"The VSS Controller Design and Implementation for the Constant Turning Force Adaptive Control System* ", Int. J. MTDR, Vol. 28, No.4, 1988, pp. 373-387.

157. • **Porter, B., and Summers, R., D., M., J.,** *"The Performance of the Self-Optimizing Strategies in the Adaptive Control of the Metal Cutting Process* ", Int. J. MTDR, Vol. 8, No. 4, 1968, pp. 217-237.

158. • **Yen, D., W., and Wright, P., K.,** *"Adaptive Control in Machining - A New Approach Based on the Physical Constraints of Tool Wear Mechanisms* ", Trans. ASME, J. Eng. Ind. , Vol. 105, Feb. 1983, pp. 31-38.

159. • **Milner, D., A.,** *"Adaptive Control of Feedrate in the Milling Process* ", Int. J. MTDR, Vol. 14, 1974, pp. 187-197.

Appendix A

EXPERIMENTAL DATA FOR WEAR AND FORCE

A.1 Foreword

In this section, the collected tool wear and cutting forces experimental data are listed. These data represent the entire composite central design *CCD* experimental design explained in **Chapter 4, section 4.3** (see also *Tables 4.1 & 4.2).* Each test, which is referred here to as *Ti* where i takes the values 1 to 24, consists of sub-tests in column 2. These sub-tests were carried out randomly as indicated by the No. in the first column. The third column represents the accumulated cutting time at the end of the corresponding sub-test.

Tool wear scars were measured on three different locations on the tool's clearance face as previously explained in **Chapter 3, Fig. 3.37.** These are the nose wear *NW,* the flank wear *FW,* and the notch wear *NCW.* These values are listed in the fourth, fifth, and sixth columns respectively.

Columns 7-9 list the values of the static cutting force components: the feed component F_x, the vertical component F_y, and the radial component F_z.

No.	Sub-Test	Time min.	NW mm.	FW mm.	NCW mm.	F_x [N]	F_y [N]	F_z [N]
1	T14-1	2.000	.09150	.06908	.08674	520	1310	457
2	T14-2	4.000	.09702	.09702	.07640	515	1326	488
3	T14-3	6.000	.10198	.08229	.08674	519	1303	475
4	T14-4	8.000	.10985	.08763	.08674	530	1320	500
5	T14-5	10.00	.11379	.08813	.08674	547	1331	510
6	T14-6	12.00	.11379	.10121	.10121	556	1333	509
7	T14-7	14.00	.11379	.10718	.10718	577	1346	534
8	T14-8	16.00	.11709	.11264	.11709	560	1345	534
9	T14-9	18.00	.12915	.11264	.11709	558	1345	514
10	T14-10	20.00	.12915	.11264	.12217	577	1355	534
11	T14-11	22.00	.13004	.11811	.12217	591	1365	538
12	T14-12	24.00	.13004	.12496	.12496	594	1365	546
13	T14-13	26.00	.13817	.12496	.13093	600	1370	550
14	T14-14	28.00	.14345	.12496	.13944	602	1374	554
15	T14-15	30.00	.14655	.12496	.14655	589	1359	560
16	T14-16	32.00	.14757	.12496	.14846	583	1414	552
17	T14-17	34.25	.14935	.12496	.15024	582	1340	519
18	T13-1	2.00	.19253	.19253	.19253	492	1217	511
19	T13-2	4.00	.25603	.25603	.25603	585	1271	565
20	T13-3	6.00	1.5000	1.0000	1.0000	4853	2339	5171
21	T19-1	2.25	.28003	.19088	.19088	512	1217	549
22	T2-1	2.00	.1767	.14363	.10845	483	1490	487
23	T2-2	4.00	.1971	.16764	.13995	495	1510	500
24	T2-3	6.00	.2161	.18542	.14401	501	1537	537
25	T2-4	7.00	.2195	.19558	.15836	528	1579	547
26	T5-1	2.00	.13182	.11887	.11506	467	1244	503
27	T5-2	4.00	.13790	.12954	.12954	496	1226	471
28	T5-3	6.00	.14630	.13817	.13817	500	1235	495
29	T5-4	8.00	.16141	.15246	.16421	499	1237	472
30	T5-5	10.00	.19443	.17532	.16421	477	1238	467
31	T5-6	12.00	.20332	.17532	.16421	488	1242	455
32	T5-7	14.33	.21602	.17532	.18427	500	1236	467
33	T5-8	16.33	.22491	.17532	.18427	498	1205	455
34	T5-9	18.45	.22491	.17532	.18427	519	1229	449
34	T14-18	36.25	.15519	.12496	.16123	444	1358	440
36	T14-19	38.25	.15519	.14173	.17018	492	1226	421
37	T14-20	41.25	.15621	.14960	.17018	502	1220	427
38	T14-21	43.25	.15621	.14960	.17018	503	1254	432
39	T14-22	45.25	.15621	.14960	.17018	509	1229	416
40	T14-23	47.25	.15748	.14960	.17018	503	1234	418
41	T14-24	49.25	.15748	.14960	.17018	505	1228	419
42	T14-25	51.25	.16256	.14960	.17018	513	1246	436
43	T14-26	53.25	.16256	.14960	.17018	528	1249	422
44	T14-27	55.25	.16256	.15621	.17018	529	1268	431
45	T14-28	57.25	.16256	.15621	.17018	527	1267	431
46	T14-29	59.92	.16256	.15621	.17018	519	1261	433
47	T5-10	20.45	.23584	.17532	.18427	577	1255	477
48	T19-2	4.25	.29006	.20193	.20193	744	1220	661
49	T19-3	6.25	.97155	.24003	.24003	2920	1509	2576
50	T2-5	9.00	.2242	.22428	.22428	551	1530	502
No.	Sub-Test	Time	NW	FW	NCW	F_x	F_y	F_z

No.	Sub-Test	Time min.	NW mm.	FW mm.	NCW mm.	F_x [N]	F_y [N]	F_z [N]
51	T7-1	2.00	.15316	.14427	.1379	396	745	330
52	T7-2	4.00	.16459	.15951	.1506	371	734	331
53	T7-3	6.00	.17348	.16459	.1518	380	737	326
54	T7-4	7.08	.17957	.16586	.1658	374	744	320
55	T6-1	2.00	.13576	.12522	.12522	480	1203	455
56	T6-2	4.00	.15468	.12877	.13284	490	1184	419
57	T6-3	6.33	.15773	.13665	.13817	450	1145	400
58	T5-11	22.45	.24533	.17532	.18427	567	1288	471
59	T18-1	2.00	.12446	.14097	.11518	277	792	296
60	T18-2	4.00	.12725	.15519	.11684	283	798	287
61	T18-3	6.00	.15875	.15519	.11684	276	784	281
62	T18-4	8.00	.15875	.15519	.11684	279	787	295
63	T18-5	10.25	.15875	.15519	.13843	299	805	299
64	T5-12	25.78	.24533	.19024	.18427	606	1323	546
65	T5-13	27.95	.26060	.19304	.18427	597	1329	532
66	T5-14	30.12	.31470	.20675	.18427	605	1363	564
67	T7-5	9.08	.18046	.17716	.1700	360	743	314
68	T7-6	11.08	.18288	.17716	.1740	360	714	311
69	T7-7	13.08	.18388	.17716	.1757	331	709	296
70	T7-8	15.66	.18400	.17716	.1771	325	701	295
71	T6-4	8.33	.15773	.13944	.13944	434	1150	393
72	T6-5	10.33	.16891	.15062	.15062	443	1144	389
73	T6-6	12.33	.17754	.16002	.16002	467	1197	407
74	T6-7	13.75	.17754	.16002	.16002	470	1207	418
75	T4-1	2.00	.12827	.10998	.10998	621	1853	545
76	T4-2	4.00	.13589	.11684	.11684	622	1853	540
77	T4-3	6.00	.13781	.12273	.12273	628	1851	536
78	T7-9	17.66	.18415	.17716	.1771	334	722	298
79	T7-10	19.66	.18623	.17716	.1771	345	712	299
80	T7-11	22.16	.18824	.17716	.1771	325	726	325
81	T6-8	15.75	.18923	.16637	.16637	460	1200	400
82	T6-9	17.08	.19583	.16891	.16891	463	1165	386
83	T4-4	8.66	.13881	.12273	.12611	639	1860	535
84	T4-5	11.23	.15634	.12839	.12839	617	1842	530
85	T4-6	13.23	.16633	.13131	.13131	647	1890	622
86	T4-7	15.23	.16733	.13282	.13282	674	1917	644
87	T4-8	17.23	.16833	.13436	.13436	706	1891	623
88	T18-6	12.25	.15875	.15519	.13843	280	815	256
89	T18-7	14.25	.15875	.15519	.14351	287	818	277
90	T4-9	19.23	.16954	.15582	.15582	735	1860	675
91	T9-1	2.00	.13576	.11557	.11557	480	1015	437
92	T9-2	4.00	.14147	.13004	.16141	481	1050	450
93	T9-3	6.00	.14401	.13004	.16141	488	1054	463
94	T9-4	8.00	.15059	.13119	.16141	494	1057	464
95	T9-5	10.00	.15290	.13893	.18222	490	1055	473
96	T9-6	12.00	.15659	.14058	.18537	499	1068	472
97	T9-7	13.41	.15722	.14236	.19023	518	1058	456
98	T14-30	61.92	.16687	.15621	.17101	549	1310	516
99	T14-31	63.92	.16687	.15621	.17101	527	1280	486
100	T14-32	65.92	.16687	.15621	.17101	521	1250	478
No.	Sub-Test	Time	NW	FW	NCW	F_x	F_y	F_z

No.	Sub-Test	Time min.	NW mm.	FW mm.	NCW mm.	F_x [N]	F_y [N]	F_z [N]
101	T14-33	67.92	.17043	.15621	.17101	515	1286	488
102	T14-34	69.92	.17881	.15875	.17101	529	1278	490
103	T14-35	71.92	.17881	.15875	.17101	524	1272	501
104	T14-36	73.92	.17881	.15875	.17101	519	1272	480
105	T14-37	75.92	.17881	.15875	.17101	524	1270	485
106	T14-38	77.92	.17881	.16002	.17101	535	1335	500
107	T14-39	79.92	.19380	.16002	.17101	523	1292	488
108	T14-40	81.92	.19380	.16002	.17101	534	1296	511
109	T14-41	83.92	.21107	.16002	.17101	530	1298	501
110	T14-42	86.09	.21107	.16002	.17101	522	1281	500
111	T14-43	88.09	.21107	.16002	.17101	522	1281	506
112	T7-12	24.16	.18999	.17729	.1771	357	782	342
113	T7-13	26.41	.19634	.18313	.1831	390	775	369
114	T7-14	28.41	.20000	.18400	.1844	363	771	349
115	T7-15	30.41	.20100	.28422	.1940	419	805	381
116	T7-16	32.58	.20150	.34925	.1960	455	794	392
117	T7-17	35.08	.20200	.34933	.1980	465	798	398
118	T6-10	19.08	.21228	.16891	.16891	466	1165	426
119	T6-11	21.08	.22910	.17122	.17122	444	1156	407
120	T6-12	23.08	.23698	.17360	.17360	433	1166	417
121	T6-13	25.33	.24942	.17360	.17360	437	1161	425
122	T6-14	27.83	.25031	.17360	.17360	432	1182	418
123	T9-8	15.41	.15794	.15209	.19304	482	1028	426
124	T9-9	17.41	.16023	.15222	.19481	478	1010	420
125	T9-10	19.41	.16552	.15322	.20000	481	1011	411
126	T9-11	21.41	.17018	.15422	.20500	478	1013	425
127	T9-12	23.41	.17118	.15522	.20640	479	1013	420
128	T9-13	25.41	.17218	.15622	.20750	481	1013	430
129	T9-14	27.66	.17318	.15722	.20999	480	1016	428
130	T9-15	29.66	.17318	.15822	.21031	496	1015	434
131	T9-16	31.66	.17518	.15922	.21533	492	1016	430
312	T9-17	33.66	.17618	.16022	.21666	493	1014	432
133	T9-18	35.66	.17754	.16154	.22200	499	1025	427
134	T9-19	36.49	.17754	.16160	.22250	505	1032	428
135	T14-44	90.09	.22428	.16078	.17106	473	1232	407
136	T14-45	92.09	.22428	.16078	.17106	470	1213	406
137	T14-46	94.09	.22428	.16078	.17106	461	1200	400
138	T14-47	96.09	.22628	.16078	.17106	461	1200	403
139	T14-48	98.09	.22828	.16129	.17106	460	1211	413
140	T14-49	100.0	.23001	.16129	.17106	481	1218	420
141	T14-50	102.0	.23333	.16129	.17211	476	1211	411
142	T14-51	104.0	.23633	.16129	.17246	493	1236	427
143	T14-52	106.0	.23924	.16129	.17524	490	1215	417
144	T14-53	107.6	.24180	.16129	.17717	500	1224	421
145	T3-1	2.00	.1656	.11480	.11480	445	919	386
146	T3-2	4.00	.1708	.14033	.25552	467	970	440
147	T3-3	6.00	.1717	.16459	.26695	516	976	453
148	T3-4	8.00	.1803	.18503	.28613	535	983	457
149	T3-5	9.00	.1890	.18503	.28613	535	989	450
150	T11-1	2.00	.12306	.10972	.10972	443	1184	434

No.	Sub-Test	Time	NW	FW	NCW	F_x	F_y	F_z

No.	Sub-Test	Time min.	NW mm.	FW mm.	NCW mm.	F_x [N]	F_y [N]	F_z [N]
151	T11-2	4.00	.13182	.12560	.12560	450	1151	418
152	T11-3	6.00	.15494	.14096	.15875	453	1172	423
153	T11-4	7.67	.16383	.15036	.17449	467	1163	430
154	T18-8	16.25	.16383	.16637	.14351	277	801	299
155	T18-9	18.25	.20066	.16916	.14351	283	798	267
156	T18-10	19.50	.20599	.16916	.14351	279	802	300
157	T9-20	38.49	.17754	.16165	.22275	500	1000	480
158	T9-21	42.49	.17754	.16185	.22350	465	999.	487
159	T9-22	44.61	.17805	.16186	.22428	507	1068	473
160	T9-23	47.61	.17940	.16195	.22758	524	1061	465
161	T14-54	109.6	.24485	.16357	.17856	485	1233	410
162	T14-55	112.6	.24688	.16924	.18111	496	1227	421
163	T14-56	117.0	.24688	.17422	.18333	504	1248	499
164	T18-1	21.50	.21599	.16916	.15341	291	808	332
165	T18-12	23.3	.32918	.17170	.17170	330	835	409
166	T9-24	49.61	.18232	.16200	.23009	498	996	399
167	T9-25	51.61	.18249	.16205	.24236	499	997	410
168	T9-26	55.33	.18542	.16383	.25019	481	1005	452
169	T11-5	9.67	.16637	.16192	.17449	475	1181	406
170	T11-6	10.59	.16697	.16192	.17678	491	1209	438
171	T11-7	12.59	.17932	.16192	.18186	538	1285	555
172	T11-8	14.59	.19304	.16179	.18796	544	1260	523
173	T11-9	16.59	.20192	.16383	.19812	548	1269	520
174	T11-10	18.59	.20192	.16916	.19812	545	1264	509
175	T11-11	20.59	.20370	.17932	.21145	525	1264	502
176	T11-12	22.59	.22123	.18415	.22631	533	1263	497
177	T11-13	24.59	.22428	.21615	.22631	511	1218	478
178	T11-14	26.37	.22428	.21615	.22631	505	1199	470
179	T20-1	2.00	.09921	.09677	.09677	547	1306	507
180	T20-2	4.00	.10922	.09677	.12065	521	1257	469
181	T20-3	6.00	.12331	.11963	.12065	540	1282	487
182	T20-4	8.00	.12331	.11963	.12065	536	1282	511
183	T20-5	10.0	.12331	.11963	.12065	536	1287	490
184	T20-6	12.0	.13335	.12065	.12065	552	1298	507
185	T20-7	14.25	.13335	.12065	.12065	537	1286	509
186	T20-8	16.25	.14287	.12534	.12534	560	1296	509
187	T20-9	18.25	.14287	.12534	.12534	560	1296	509
188	T20-10	20.25	.14287	.12534	.12534	553	1339	534
189	T20-11	22.25	.14287	.12534	.12534	564	1315	508
190	T20-12	24.25	.14376	.12687	.12598	578	1333	522
191	T20-13	26.25	.14376	.12687	.12598	572	1345	536
192	T20-14	28.25	.15062	.13081	.12598	587	1355	538
193	T3-6	11.00	.1925	.18719	.28613	535	981	453
194	T3-7	13.00	.1955	.19326	.28613	532	986	466
195	T10-1	1.00	.13589	.12865	.12865	618	1862	563
196	T10-2	2.00	.16129	.16256	.13296	624	1862	577
197	T10-3	3.67	.18034	.22199	.13296	672	1905	627
198	T12-1	2.00	.13258	.11480	.11480	464	1201	443
199	T12-2	4.00	.13970	.11633	.11632	464	1213	453
200	T12-3	6.00	.14338	.12395	.12395	486	1192	429

No.	Sub-Test	Time	NW	FW	NCW	F_x	F_y	F_z

No.	Sub-Test	Time min.	NW mm.	FW mm.	NCW mm.	F_x [N]	F_y [N]	F_z [N]
201	T12-4	8.25	.15227	.12763	.12763	548	1248	521
202	T12-5	10.75	.17348	.15341	.2413	573	1291	523
203	T12-6	12.75	.20370	.15328	.2413	578	1236	536
204	T12-7	14.75	.20421	.15328	.24257	563	1255	545
205	T12-8	16.75	.20840	.16002	.25146	551	1263	541
206	T12-9	19.00	.21729	.16383	.25488	569	1264	542
207	T12-10	21.50	.21958	.16386	.25488	533	1263	532
208	T20-15	30.25	.15062	.13081	.12598	537	1285	477
209	T20-16	32.25	.15062	.13817	.12598	542	1297	483
210	T20-17	34.25	.15062	.13817	.12598	558	1320	485
211	T20-18	36.25	.15417	.13817	.12598	584	1337	491
212	T20-19	38.25	.15417	.13817	.12598	573	1308	483
213	T20-20	40.25	.15417	.13817	.12598	559	1300	481
214	T9-27	57.33	.18923	.17145	.25527	559	1034	462
215	T9-28	59.33	.18923	.17576	.26400	527	1033	449
216	T9-29	61.33	.19024	.17576	.27940	559	1025	457
217	T9-30	63.33	.19215	.17818	.28425	567	1043	462
218	T9-31	65.33	.20301	.18288	.28803	561	1030	456
219	T9-32	67.33	.21310	.18542	.28927	554	1011	445
220	T9-33	69.33	.21310	.18999	.29002	557	1027	450
221	T9-34	71.33	.21361	.18999	.29035	560	1018	454
222	T8-1	2.83	.12420	.11531	.10922	477	1520	490
223	T20-21	42.25	.15417	.13817	.12598	552	1319	494
224	T20-22	44.25	.15544	.13817	.13766	554	1322	482
225	T20-23	46.25	.15544	.13817	.13766	550	1288	472
226	T20-24	47.75	.17195	.14909	.14579	551	1293	462
227	T10-4	5.67	.24003	.24000	.13296	681	1843	687
228	T10-5	7.42	.47205	.25019	.13296	915	1952	1196
229	T24-1	2.00	.13423	.11417	.11417	301	793	333
230	T24-2	4.00	.14198	.12801	.12801	273	779	305
231	T24-3	6.00	.14909	.13131	.13131	288	810	330
232	T24-4	7.83	.15087	.14884	.14884	302	831	332
233	T24-5	9.83	.15671	.15671	.15671	313	849	346
234	T24-6	11.8	.15748	.15671	.15748	307	821	329
235	T24-7	13.8	.16052	.16052	.16052	324	855	358
236	T24-8	15.5	.16789	.16205	.16205	343	882	350
237	T8-2	4.83	.14325	.12852	.11850	499	1537	485
238	T8-3	6.83	.14579	.13131	.11982	505	1517	470
239	T8-4	8.83	.14579	.13332	.12000	495	1512	462
240	T20-25	49.75	.17195	.14909	.14579	571	1275	461
241	T20-26	51.75	.17195	.14909	.14579	527	1246	447
242	T20-27	53.75	.17195	.14909	.14579	520	1248	444
243	T20-28	55 75	.17195	.14909	.14596	527	1263	452
244	T20-29	57.75	.17195	.14909	.14596	520	1239	449
245	T20-30	59.75	.17195	.14909	.14596	522	1247	449
246	T20-31	61.58	.17297	.15481	.14596	538	1259	472
247	T24-9	17.5	.18554	.17856	.17856	328	835	352
248	T24-10	19.5	.18796	.18542	18542	316	840	350
249	T24-11	21.5	.18923	.19304	.19304	314	823	330
250	T8-5	10.83	.14671	.13524	.12827	483	1507	456

No	Sub-Test	Time	NW	PW	NCW	F_x	F_y	F_z

No.	Sub-Test	Time min.	NW mm.	FW mm.	NCW mm.	F_x [N]	F_y [N]	F_z [N]
251	T8-6	13.58	.14701	.13722	.13462	485	1519	455
252	T24-12	23.5	.20167	.19523	.19304	307	812	342
253	T24-13	25.33	.2047	.2021	.2021	320	830	355
254	T24-14	27.58	.2047	.2021	.2021	340	850	370
255	T8-7	15.58	.14897	.13843	.13843	505	1504	452
256	T8-8	16.96	.15443	.14173	.14173	484	1552	461
257	T20-32	63.58	.17297	.15481	.14596	540	1270	480
258	T20-33	65.83	.18059	.15481	.14579	540	1270	480
259	T20-34	68.41	.19354	.16687	.14579	538	1259	472
260	T15-1	2.00	.15544	.10248	.10922	645	2880	649
261	T15-2	4.00	.17678	.13462	.13462	651	2951	679
262	T15-3	5.17	.18897	.15748	.15748	700	2989	724
263	T8-9	18.96	.15938	.14922	.15000	562	1599	561
264	T8-10	20.96	.17018	.15570	.16000	563	1583	562
265	T8-11	22.96	.17653	.15836	.17222	569	1590	575
266	T8-12	24.96	.18224	.16000	.18529	566	1575	567
267	T8-13	26.96	.18491	.16256	.18882	559	1580	598
268	T8-14	28.96	.19024	.16356	.19100	559	1567	570
269	T8-15	30.66	.19224	.16456	.19200	565	1559	555
270	T20-35	70.41	.19354	.16687	.14579	607	1325	530
271	T20-36	72.41	.21945	.17754	.14579	616	1319	511
272	T20-37	74.41	.21945	.17754	.14579	589	1316	524
273	T20-38	76.41	.22783	.17754	.14579	609	1320	525
274	T20-39	78.41	.22783	.17754	.14579	609	1324	525
275	T20-40	80.41	.22783	.18313	.14579	628	1333	527
276	T20-41	82.41	.22783	.18313	.14579	613	1326	528
277	T20-42	84.41	.22783	.18592	.15595	638	1342	550
278	T20-43	86.41	.22783	.18592	.15595	619	1322	537
279	T20-44	88.41	.22885	.19024	.16637	625	1295	514
280	T20-45	90.41	.22885	.19024	.16637	625	1326	535
281	T20-46	92.41	.22885	.19710	.17475	630	1318	531
282	T20-47	94.41	.22885	.19710	.17475	646	1341	544
283	T20-48	97.05	.22885	.20116	.17475	652	1353	554
284	T15-4	7.17	.24333	.18975	.15748	727	3008	769
285	T15-5	8.84	.27736	.21629	.17748	838	3150	864
286	T16-1	2.000	.13081	.10049	.10049	299	546	265
287	T16-2	4.000	.13081	.11849	.11849	299	546	265
288	T16-3	6.000	.14160	.12573	.13462	314	568	275
289	T16-4	8.000	.14376	.12979	.13106	332	581	290
290	T16-5	10.00	.14757	.13766	.13766	331	561	277
291	T16-6	12.00	.14833	.13893	.13893	316	534	259
292	T16-7	14.00	.15049	.14046	.14046	286	527	244
293	T16-8	16.00	.15290	.14478	.14478	269	525	228
294	T16-9	18.00	.15360	.14732	.14732	305	527	260
295	T16-10	20.00	.15476	.15265	.15265	286	540	243
296	T16-11	22.00	.15582	.15595	.15595	299	538	248
297	T16-12	24.00	.15532	.15588	.15595	290	536	242
298	T16-13	26.00	.15697	.15703	.15595	284	546	239
299	T16-14	28.00	.17805	.15824	.15824	314	552	273
300	T16-15	30.00	.19050	.16205	.15976	324	548	273

No.	Sub-Test	Time	NW	FW	NCW	F_x	F_y	F_z

No.	Sub-Test	Time min.	NW mm.	FW mm.	NCW mm.	F_x [N]	F_y [N]	F_z [N]
301	T16-16	32.00	.19685	.16989	.15976	292	548	279
302	T16-17	33.83	.20320	.17881	.17881	301	560	280
303	T8-16	32.66	.19324	.16556	.19422	496	1545	470
304	T8-17	34.86	.19424	.16655	.19622	487	1559	492
305	T8-18	37.11	.19524	.16766	.19755	487	1558	489
306	T8-19	39.53	.19624	.16888	.19964	496	1565	489
307	T20-49	99.05	.23431	.20193	.17475	612	1323	586
308	T20-50	101.0	.23545	.20193	.17475	629	1326	531
309	T20-51	103.0	.23545	.20193	.17475	623	1316	525
310	T20-52	105.0	.24053	.20980	.17475	637	1341	545
311	T20-53	107.0	.24053	.20980	.17475	626	1314	529
312	T20-54	109.0	.24053	.21082	.17475	630	1334	531
313	T20-55	111.0	.24053	.21082	.17475	634	1351	538
314	T20-56	113.0	.24053	.21082	.17475	643	1366	554
315	T20-57	115.0	.24053	.21082	.17475	639	1358	548
316	T20-58	116.9	.24231	.21539	.17475	652	1374	550
317	T16-18	35.83	.20396	.17881	.17881	308	563	290
318	T16-19	37.83	.21005	.17881	.17881	301	536	286
319	T16-20	39.83	.20955	.17881	.17881	286	529	262
320	T16-21	41.83	.21463	.17881	.17881	298	536	274
321	T16-22	43.83	.21615	.17881	.17881	287	531	260
322	T16-23	46.08	.21615	.17881	.17881	293	539	268
323	T16-24	48.33	.21615	.17881	.17881	295	535	270
324	T16-25	50.58	.21704	.17881	.17881	297	539	274
325	T16-26	52.58	.21780	.17881	.17881	307	566	297
326	T16-27	57.58	.21863	.17881	.17881	340	558	318
327	T16-28	60.03	.21934	.17881	.17881	320	557	301
328	T16-29	61.33	.22234	.17891	.17881	309	566	290
329	T8-20	41.53	.19710	.16922	.20472	437	1491	534
330	T8-21	43.53	.19810	.17023	.20815	454	1494	476
331	T8-22	46.11	.19910	.17222	.21463	499	1582	510
332	T14-57	119.0	.24888	.17888	.18592	501	1236	418
333	T14-58	121.0	.25111	.18000	.18821	493	1214	414
334	T14-59	123.0	.25911	.18694	.19177	491	1208	410
335	T14-60	125.0	.25552	.19685	.19177	497	1218	419
336	T14-61	127.0	.25552	.19837	.19523	507	1253	438
337	T14-62	129.1	.25552	.20408	.19788	516	1262	440
338	T14-63	131.1	.25552	.21297	.19888	512	1257	445
339	T16-30	63.33	.22334	.17901	.17881	328	603	334
340	T16-31	65.33	.22434	.17921	.17881	364	604	356
341	T16-32	67.33	.22634	.17941	.17881	392	609	388
342	T16-33	69.33	.22898	.18221	.17881	367	589	349
343	T16-34	71.33	.23114	.18415	.17881	398	613	393
344	T16-35	73.33	.23749	.18415	.17881	358	579	347
345	T16-36	76.33	.24358	.18415	.17881	359	584	350
346	T16-37	78.50	.25488	.19431	.17881	355	590	345
347	T8-23	48.78	.20447	.17398	.21663	488	1497	478
348	T8-24	50.90	.22714	.17455	.22402	519	1555	489
349	T17-1	2.00	.13512	.11480	.11480	532	1472	503
350	T17-2	3.00	.16675	.13919	.13919	551	1473	477

No.	Sub-Test	Time	NW	FW	NCW	F_x	F_y	F_z

No.	Sub-Test	Time min.	NW mm.	FW mm.	NCW mm.	F_x [N]	F_y [N]	F_z [N]
351	T14-64	133.6	.28473	.21582	.19964	526	1259	493
352	T14-65	136.1	.29476	.21920	.20000	539	1267	504
353	T14-66	138.4	.29972	.22000	.20243	552	1261	501
354	T17-3	5.00	.17030	.16205	.16205	559	1478	485
355	T1-1	2.00	.1295	.11785	.11785	353	821	372
356	T1-2	4.00	.1320	.12280	.12280	344	820	361
357	T1-3	6.00	.1373	.13449	.13449	374	848	378
358	T1-4	8.00	.1383	.14675	.13284	386	854	388
359	T1-5	10.00	.1406	.14675	.13271	395	856	394
360	T1-6	12.00	.1584	.14879	.14223	402	862	397
361	T1-7	14.00	.1584	.16487	.14223	408	866	398
362	T1-8	16.00	.1590	.16487	.14223	411	875	403
363	T1-9	18.00	.1675	.17805	.14803	425	877	409
364	T1-10	20.00	.1658	.17805	.14803	420	874	406
365	T1-11	22.00	.1684	.18197	.14981	424	878	408
366	T1-12	24.00	.1689	.18197	.14981	427	876	410
367	T1-13	26.00	.1695	.18197	.14981	428	883	407
368	T1-14	28.00	.1707	.18197	.15443	422	873	401
369	T1-15	30.00	.1717	.18197	.15951	423	892	410
370	T1-16	31.75	.1717	.18333	.15951	425	863	393
371	T1-17	33.75	.1729	.18542	.15951	412	864	387
372	T1-18	35.75	.1738	.18912	.16079	417	885	397
373	T1-19	37.75	.1749	.19065	.16283	399	850	379
374	T1-20	39.75	.1752	.19065	.16283	387	866	392
375	T1-21	41.75	.1769	.19278	.16334	394	854	377
376	T1-22	44.00	.1772	.19278	.16334	391	855	376
377	T1-23	46.00	.1764	.19278	.16589	376	843	372
378	T1-24	48.00	.1764	.19278	.16589	382	842	365
379	T1-25	50.00	.1764	.19278	.16589	390	865	377
380	T1-26	52.00	.1778	.19278	.16666	390	865	377
381	T1-27	54.00	.1778	.19278	.16666	386	844	362
382	T1-28	56.00	.1769	.19278	.16666	407	874	382
383	T1-29	58.00	.1769	.19371	.16666	388	848	380
384	T1-30	60.17	.1769	.19601	.16462	400	875	391
385	T1-31	63.17	.1878	.19601	.16768	400	876	395
386	T1-32	66.17	.1929	.20239	.16947	402	869	385
387	T17-4	7.00	.17272	.18034	.16205	590	1479	485
388	T17-5	9.00	.17373	.18542	.16205	660	1544	574
389	T17-6	11.00	.18135	.18897	.16205	658	1533	571
390	T17-7	13.00	.18135	.19062	.16205	702	1589	630
391	T17-8	16.00	.22098	.19062	.16205	726	1639	625
392	T22-1	2.00	.14020	.12446	.12446	319	551	288
393	T22-2	4.00	.14859	.13030	.12446	304	581	309
394	T22-3	6.00	.16713	.14262	.13106	317	612	310
395	T22-4	8.00	.16967	.14490	.13106	327	608	310
396	T22-5	10.0	.16967	.14490	.13106	340	613	315
397	T22-6	12.0	.16967	.14490	.13106	340	603	308
398	T22-7	14.0	.16967	.15090	.13106	319	589	293
399	T22-8	16.0	.16967	.15367	.13106	304	582	279
400	T22-9	18.0	.17106	.15836	.13128	281	566	271

No.	Sub-Test	Time	NW	FW	NCW	F_x	F_y	F_z

No.	Sub-Test	Time min.	NW mm.	FW mm.	NCW mm.	F_x [N]	F_y [N]	F_z [N]
401	T22-10	20.0	.17106	.15925	.13229	266	556	276
402	T22-11	22.0	.17106	.15925	.13678	270	557	267
403	T22-12	24.0	.17106	.15925	.13821	275	567	275
404	T22-13	26.0	.17106	.16281	.14123	351	576	327
405	T22-14	28.0	.23672	.16408	.14123	350	603	345
406	T22-15	29.8	.23672	.17081	.14123	408	619	345
407	T1-33	68.17	.1929	.20239	.16947	397	852	382
408	T1-34	70.17	.1929	.20239	.16947	381	852	380
409	T1-35	72.17	.1929	.20239	.16947	408	866	399
410	T1-36	74.17	.1929	.20239	.16947	413	869	399
411	T1-37	76.17	.1992	.20239	.16947	433	879	412
412	T1-38	78.17	.2080	.20239	.16947	433	885	408
413	T1-39	80.17	.2080	.20239	.16947	428	875	402
414	T1-40	82.17	.2123	.20239	.16947	402	857	381
415	T1-41	84.42	.2123	.20239	.17526	388	837	390
416	T1-42	86.92	.2172	.20239	.18211	392	850	400
417	T1-43	89.42	.2172	.20239	.18211	393	840	402
418	T2-6	11.0	.2381	.23812	.23812	548	1589	536
419	T2-7	12.8	.2498	.24980	.24980	626	1645	636
420	T22-16	31.8	.25488	.17500	.14123	419	620	359
421	T22-17	33.8	.26746	.17500	.14123	423	636	372
422	T22-18	35.8	.27432	.17500	.14123	433	636	373
423	T22-19	37.8	.27990	.17500	.14124	403	646	392
424	T22-20	39.8	.28155	.17500	.14134	408	639	371
425	T22-21	42.0	.28255	.17500	.14144	407	632	353
426	T22-22	44.0	.28261	.17500	.14154	419	650	389
427	T22-23	46.0	.28271	.17500	.14164	431	645	369
428	T22-24	48.0	.28360	.17500	.14264	433	654	401
429	T22-25	50.3	.28460	.17500	.14464	425	652	393
430	T22-26	52.1	.28662	.17500	.14764	442	661	403
431	T22-27	54.0	.28760	.17500	.15022	443	661	409
432	T23-1	2.083	.13081	.11836	.11836	610	1589	557
433	T23-2	4.083	.14046	.12446	.12446	618	1585	510
434	T23-3	5.583	.14452	.13716	.13716	592	1625	511
435	T23-4	7.583	.17183	.13665	.14503	589	1534	509
436	T23-5	9.583	.1778	.22098	.14605	603	1509	513
437	T23-6	11.58	.20000	.24098	.16002	710	1632	602
438	T4-10	21.23	.16955	.16230	.16230	763	2029	728
439	T4-11	23.23	.17170	.17602	.17602	805	2041	702
440	T4-12	25.23	.17399	.18000	.18000	817	2066	714
441	T4-13	27.23	.18034	.18300	.18300	828	2091	711
442	T4-14	29.23	.1905	.19000	.19000	808	2043	750
443	T4-15	31.23	.40982	.19192	.19192	887	2140 1	171
444	T4-16	33.1	.70040	.19392	.19392	1424	2353	2221
445	T14-67	140.4	.29972	.22225	.21691	701	1484	702
446	T14-68	142.4	.31043	.22450	.21891	682	1481	667
447	T14-69	144.4	.31242	.22650	.21907	685	1489	679
448	T14-70	146.4	.31496	.22750	.22352	671	1434	647
449	T14-71	148.4	.31572	.22950	.22352	715	1519	672
450	T14-72	150.4	.32575	.23010	.22752	683	1423	644

No.	Sub-Test	Time	NW	FW	NCW	F_x	F_y	F_z

No.	Sub-Test	Time min.	NW mm.	FW mm.	NCW mm.	F_x [N]	F_y [N]	F_z [N]
451	T14-73	152.4	.32600	.23110	.22952	679	1424	656
452	T14-74	154.4	.32639	.23190	.23152	672	1417	640
453	T14-75	156.4	.32839	.23210	.23558	685	1446	644
454	T14-76	158.4	.33000	.23290	.23558	700	1450	660
455	T14-77	160.4	.33312	.23310	.23558	720	1459	689
456	T14-78	162.4	.33558	.23393	.23558	788	1503	739
457	T14-79	164.4	.62000	.33965	.23558	1044	1844	1404
458	T20-59	119.1	.27774	.24345	.17475	636	1386	656
459	T20-60	120.3	.45262	.32067	.17475	757	1439	894
460	T21-1	2.00	.19608	.14122	.14122	685	3035	750
461	T21-2	3.67	.22440	.16129	.14122	731	3176	832
462	T6-15	29.83	.25196	.17360	.17360	417	1186	420
463	T6-16	31.83	.25196	.17360	.17360	451	1206	427
464	T6-17	33.83	.25196	.17360	.17360	456	1204	427
465	T6-18	35.83	.27749	.17360	.17360	460	1229	471
466	T6-19	38.08	.27749	.17462	.18884	470	1220	480
467	T8-25	52.90	.2307	.17622	.22661	556	1625	554
468	T8-26	54.90	.2383	.17700	.22720	531	1631	531
469	T8-27	56.90	.2467	.17750	.22755	538	1650	533
470	T8-28	58.90	.2499	.17780	.22771	530	1605	540
471	T8-29	60.57	.24999	.18415	.23241	513	1588	527
472	T11-15	28.37	.22631	.21654	.22631	498	1205	445
473	T11-16	30.37	.22631	.22631	.22613	490	1210	454
474	T11-17	32.37	.22707	.22707	.22707	501	1254	467
475	T11-18	34.37	.22733	.22733	.22733	502	1256	484
476	T23-7	13.58	.20116	.25171	.16052	764	1580	663
477	T23-8	15.58	.21615	.26301	.18186	776	1632	686
478	T23-9	17.78	.21615	.26492	.18186	790	1677	691
479	T23-10	19.58	.22275	.26797	.19202	775	1653	685
480	T1-44	91.42	.2172	.20239	.18211	394	839	403
481	T1-45	93.42	.2410	.20239	.18211	389	827	398
482	T1-46	95.42	.2410	.20320	.18643	387	824	397
483	T1-47	97.42	.2410	.20320	.18643	392	824	405
484	T1-48	100.4	.2437	.20320	.18643	395	826	406
485	T1-49	103.4	.2437	.20574	.18732	396	833	408
486	T1-50	105.8	.2500	.20574	.18999	395	831	399
487	T9-35	73.33	.22361	.19888	.29349	579	1039	513
488	T9-36	75.33	.23362	.20066	.29623	588	1069	525
489	T9-37	77.33	.23862	.20154	.29921	588	1053	525
490	T9-38	79.33	.24222	.20955	.30124	597	1084	510
491	T9-39	81.33	.24911	.21412	.30657	582	1070	501
492	T9-40	83.66	.25000	.21564	.30678	576	1051	491
493	T9-41	85.66	.25312	.22504	.30700	571	1049	488
494	T24-15	29.58	.2047	.2021	.2021	356	871	388
495	T24-16	31.58	.2047	.2021	.2021	349	873	370
496	T24-17	33.28	.2047	.2138	.2021	337	878	370
497	T12-11	23.50	.22021	.16386	.26746	566	1231	515
498	T12-12	25.50	.22021	.16386	.27228	552	1246	538
499	T12-13	27.00	.22021	.16386	.27254	565	1272	544
500	T21-3	6.34	.30010	.16129	.14122	793	3089	914

No.	Sub-Test	Time	NW	FW	NCW	F_x	F_y	F_z

No.	Sub-Test	Time min.	NW mm.	FW mm.	NCW mm.	F_x [N]	F_y [N]	F_z [N]
501	T1-51	107.8	.2872	.20574	.19049	384	832	404
502	T1-52	109.8	.2872	.21005	.19735	412	838	411
503	T1-53	111.8	.2959	.21005	.19837	449	879	491
504	T1-54	113.8	.3085	.21005	.20878	479	911	524
505	T1-55	115.8	.3095	.21005	.21488	475	904	520
506	T1-56	117.8	.3102	.21005	.21894	481	934	539
507	T3-8	15.50	.2016	.19526	.28625	480	952	436
508	T3-9	17.75	.2016	.19626	.28625	520	979	473
509	T24-18	35.28	.2047	.2138	.2021	304	846	369
510	T24-19	37.38	.2047	.2138	.2021	317	840	368
511	T9-42	87.66	.25324	.22564	.30751	575	1060	495
512	T9-43	89.66	.25347	.22564	.30870	581	1070	508
513	T9-44	91.66	.25523	.22907	.30951	586	1050	530
514	T9-45	93.74	.26000	.24790	.30999	577	1036	519
515	T24-20	39.38	.2051	.2138	.2021	326	861	368
516	T24-21	40.5	.20510	.21767	.20218	399	903	403
517	T8-30	63.07	.25000	.18707	.23441	499	1513	494
518	T24-22	42.5	.21348	.23761	.23761	471	969	507
519	T24-23	44.5	.21564	.24523	.24523	457	981	471
520	T24-22	46.5	.21564	.25400	.25400	436	972	463
521	T24-25	48.5	.22098	.26822	.26822	438	985	465
522	T24-26	50.5	.22529	.27787	.27787	435	984	470
523	T24-27	52.5	.66700	.29286	.29286	670	1100	1500
524	T24-28	54.5	.68376	.38836	.29286	809	1109	1542
255	T24-29	56.0	.74066	.39827	.29286	878	1143	1690
526	T1-57	119.8	.3113	.21894	.22301	530	1016	600
527	T1-58	121.8	.3132	.22161	.23063	500	994	607
528	T1-59	123.8	.3142	.22199	.24079	526	973	585
529	T2-8	14.8	.2722	.27228	.27228	744	1813	783
530	T2-9	16.5	.3253	.32537	.32537	850	1823	861
531	T3-10	19.5	.3044	.19888	.29540	649	1097	572
532	T3-11	21.5	.4196	.21742	.29540	946	1175	826
533	T6-20	40.8	.27749	.17627	.19177	488	1217	496
534	T6-21	42.8	.27749	.17627	.19177	482	1257	485
535	T6-22	44.8	.27749	.17627	.19177	494	1274	496
536	T6-23	46.8	.28448	.18389	.20447	500	1297	503
537	T6-24	48.8	.28448	.18389	.21259	503	1284	492
538	T6-25	48.3	.28448	.18389	.21259	492	1285	488
539	T23-11	21.8	.23155	.28155	.19202	766	1661	704
540	T23-12	23.8	.23926	.28270	.19380	770	1702	700
541	T23-13	25.8	.24263	.2886	.1976	776	1722	692
542	T23-14	27.5	.24263	.2943	.1976	764	1697	675
543	T23-15	30.3	.24263	.2959	.2000	767	1731	706
544	T1-60	125.8	.3152	.22529	.26670	479	942	531
545	T1-61	127.8	.3162	.23850	.26670	475	922	529
546	T1-62	129.8	.3172	.23850	.26670	474	927	528
547	T1-63	131.8	.3182	.23850	.26670	475	940	530
548	T1-64	133.8	.3192	.24193	.26670	475	945	526
549	T1-65	135.8	.3198	.24193	.27114	474	932	526
550	T1-66	137.8	.3198	.24434	.27114	469	930	521

No.	Sub-Test	Time	NW	FW	NCW	F_x	F_y	F_z

No.	Sub-Test	Time min.	NW mm.	FW mm.	NCW mm.	F_x [N]	F_y [N]	F_z [N]
551	T1-67	139.8	.3199	.24993	.27114	468	925	517
552	T1-68	141.8	.3199	.25044	.27114	498	949	541
553	T1-69	144.8	.3199	.25044	.27114	485	942	539
554	T1-70	146.5	.3200	.25400	.27114	527	1040	614
555	T17-9	18.00	.23964	.19177	.1778	700	1613	618
556	T17-10	20.00	.24180	.19583	.20167	721	1624	661
557	T17-11	22.00	.24460	.20104	.21056	761	1687	681
558	T17-12	23.75	.25196	.20967	.21869	757	1699	671
559	T8-31	65.07	.25171	.19000	.23622	542	1623	557
560	T8-32	67.15	.25227	.19494	.24155	567	1668	563
560	T8-33	69.57	.25361	.19494	.25102	561	1665	585
562	T9-46	95.74	.27432	.25552	.30999	611	1093	557
563	T9-47	97.99	.27495	.25781	.31001	581	1061	539
564	T9-48	99.99	.28765	.26060	.31002	628	1124	592
565	T9-49	102.0	.32092	.26111	.31019	661	1144	595
566	T9-50	104.0	.33216	.26556	.31024	675	1170	657
567	T9-51	106.0	.33216	.26885	.31242	704	1196	673
568	T9-52	108.0	.33244	.27686	.31419	704	1181	682
569	T9-53	109.5	.33244	.28041	.31800	706	1173	680
570	T15-6	10.59	.36512	.28473	.18059	876	3240	1035
571	T16-38	80.50	.26263	.19431	.19431	341	604	361
572	T16-39	82.50	.26784	.19431	.19431	343	601	360
573	T16-40	84.50	.26784	.19431	.19431	340	595	355
574	T16-41	86.50	.26784	.19431	.19596	344	602	360
575	T16-42	88.50	.26784	.19431	.19596	355	607	365
576	T16-43	90.50	.27139	.19431	.19646	379	640	365
577	T16-44	93.00	.27139	.20281	.19646	399	673	408
578	T16-45	95.33	.27139	.20472	.23863	396	648	418
579	T7-18	37.33	.20323	.34944	.1999	492	847	413
580	T7-19	39.83	.20383	.34955	.2099	499	853	503
581	T22-28	56.0	.28803	.17678	.16560	435	650	389
582	T22-29	58.0	.28803	.17678	.17983	446	660	409
583	T22-30	59.9	.28803	.17678	.17678	441	659	402
584	T22-31	61.9	.28803	.19532	.17564	443	652	408
585	T22-32	64.1	.29718	.20599	.18542	453	666	425
586	T22-33	66.4	.31318	.26263	.18465	492	670	432
587	T22-34	71.57	.25361	.19494	.25933	527	1588	506
588	T22-35	72.90	.25361	.19494	.25933	538	1632	523
589	T22-36	75.27	.25628	.19494	.25933	668	1723	747
590	T21-4	7.16	.31216	.22580	.14122	860	3150	1150
591	T21-5	7.98	.33528	.23749	.14782	1036	3357	1210
592	T21-6	8.83	.35483	.24942	.17018	1031	3160	1212
593	T21-7	9.69	.37058	.24942	.17018	1065	3270	1291
594	T8-37	77.67	.27216	.21145	.25933	801	1768	950
595	T8-38	80.12	.28536	.22694	.25996	770	1770	953
596	T7-20	42.55	.21945	.34965	.2099	506	909	459
597	T12-14	29.42	.25400	.1905	.27597	581	1342	578
598	T12-15	31.92	.25527	.19177	.28359	585	1362	581
599	T8-39	81.62	.30937	.23063	.25996	750	1750	900
600	T7-21	44.83	.21945	.34978	.2099	478	856	454

No.	Sub-Test	Time	NW	FW	NCW	F_x	F_y	F_z

No.	Sub-Test	Time min.	NW mm.	FW mm.	NCW mm.	F_x [N]	F_y [N]	F_z [N]
601	T12-16	33.92	.25654	.19392	.28498	606	1326	585
602	T8-40	83.40	.31597	.23063	.25996	745	1738	883
603	T7-22	46.76	.25527	.34999	.2099	499	889	527
604	T12-17	35.47	.28448	.19393	.28493	616	1383	599
605	T8-41	84.82	.32017	.23063	.26238	736	1738	883
606	T7-23	48.76	.28092	.35534	.2099	487	891	503
607	T8-42	87.74	.32222	.25196	.26238	822	1753	991
608	T7-24	51.59	.28194	.36000	.2100	535	900	530
609	T11-19	34.37	.22733	.22733	.26377	501	1274	491
610	T11-20	39.37	.22961	.22733	.27101	503	1200	460
611	T7-25	54.36	.28448	.36136	.2110	534	900	556
612	T11-21	41.87	.22961	.22733	.27101	505	1270	467
613	T8-43	89.94	.32385	.25563	.26238	783	1800	974
614	T11-22	44.35	.22961	.23495	.27101	504	1233	478
615	T11-23	46.65	.23901	.23495	.27101	495	1234	462
616	T8-44	91.94	.33883	.25882	.27686	717	1850	942
617	T7-26	56.69	.28448	.36146	.2110	534	920	538
618	T11-24	48.65	.23901	.23495	.27101	498	1234	465
619	T8-45	93.76	.34000	.25882	.27686	758	2000	903
620	T7-27	58.69	.28829	.36158	.2265	542	925	532
621	T11-25	50.32	.23901	.23901	.27101	499	1234	463
622	T8-46	95.26	.34290	.25882	.27686	780	2150	980
623	T8-47	96.77	.34340	.25882	.27686	810	2224	1044
624	T1-71	149.0	.3204	.25971	.27114	506	945	570
625	T7-28	60.36	.28829	.36160	.2265	577	930	579
626	T7-29	61.86	.29489	.36176	.2265	576	912	580
627	T7-30	64.66	.29489	.36184	.2265	550	911	583
628	T1-72	151.5	.3204	.25971	.27114	485	923	533
629	T1-73	153.8	.3204	.26670	.27114	475	896	528
630	T7-31	66.99	.30124	.36184	.2265	552	929	592
631	T1-74	156.3	.3380	.27127	.27114	488	939	538
632	T1-75	158.1	.3380	.27127	.27114	492	913	539
633	T7-32	68.99	.30124	.36223	.2265	555	890	579
634	T1-76	160.6	.3517	.28193	.27114	573	1004	638
635	T1-77	162.9	.3538	.28193	.28244	522	940	586
636	T-78	164.4	.3538	.28193	.28244	537	954	585
637	T7-33	71.99	.30759	.38379	.2458	742	1086	779
638	T5-15	33.00	.32613	.22809	.18237	614	1390	578
639	T5-16	35.90	.32613	.23749	.18542	651	1446	634
640	T1-79	167.0	.3566	.28193	.28244	575	1109	610
641	T1-80	169.5	.3591	.32359	.32003	600	1170	655
642	T17-13	26.18	.33000	.17222	.17170	344	821	427
643	T17-14	29.13	.33000	.17322	.17170	365	809	440
644	T17-15	32.13	.33000	.17422	.17170	377	853	459
645	T17-16	34.75	.33000	.17522	.17170	388	839	436
646	T17-17	37.42	.33000	.17622	.17520	383	912	449
647	T17-18	39.62	.33000	.17722	.17520	387	913	555
648	T17-19	41.32	.33000	.18059	.17520	397	899	439
649	T17-20	42.74	.33000	.18059	.17520	397	974	488
650	T17-21	45.07	.33000	.19558	.17520	410	991	474
No.	Sub-Test	Time	NW	FW	NCW	F_x	F_y	F_z

No.	Sub-Test	Time min.	NW mm.	FW mm.	NCW mm.	F_x [N]	F_y [N]	F_z [N]
651	T17-22	47.32	.33121	.19634	.17520	427	993	486
652	T17-23	48.99	.33502	.19634	.17520	431	1041	503
653	T17-24	51.59	.34467	.19659	.17520	461	1117	509
654	T18-13	26.35	.30251	.24434	.25933	789	1717	722
655	T16-46	97.83	.28397	.23901	.23901	403	696	420
656	T16-47	100.3	.28397	.24930	.24930	423	700	423
657	T16-48	103.3	.28448	.25552	.25552	462	701	461
658	T11-26	52.98	.24993	.24993	.28202	516	1256	482
659	T11-27	55.23	.25012	.25012	.29002	531	1242	496
660	T11-28	57.03	.26339	.26339	.30125	503	1212	495
661	T11-29	58.03	.28803	.27660	.34429	556	1251	542
662	T6-26	51.56	.28448	.19215	.21259	533	1331	554
663	T6-27	54.39	.28575	.20193	.22301	522	1328	532
664	T6-28	57.27	.28575	.20193	.22898	506	1299	616
665	T6-29	59.74	.28575	.20624	.22898	503	1278	570
666	T6-30	62.24	.28626	.20624	.22898	517	1293	565
667	T6-31	64.24	.29007	.20624	.22898	519	1260	555
668	T6-32	65.91	.29693	.20701	.22898	562	1292	561
669	T6-33	68.66	.34165	.22098	.33197	598	1295	638
No.	Sub-Test	Time	NW	FW	NCW	F_x	F_y	F_z

Appendix B

EXPERIMENTAL DATA FOR TOOL VIBRATION

B.1 Foreword

The collected vibration signals are listed in this section. As previously defined in **Appendix A,** the first, the second, and the third columns represent the test sequence, the sub-test number, and the accumulated cutting time respectively. The test sequence here does not represent the performance order. However, this could be obtained by referring back to the corresponding sub-test in **Appendix A.**

The third column represent the vibration power amplitude in millivolts for the tool's first fundamental natural frequency in the feed direction A_x. Absolute value of the power amplitude can be obtained by converting its value to engineering units using the calibration factor of (5 mv/g), where g is the gravity (9.81 m/sec^2).

No.	Sub-Test	Time min.	Amplitude ×0.2g	No.	Sub-Test	Time min.	Amplitude ×0.2g
1	T2-2	4.00	18.9	51	T6-5	10.33	2.32
2	T2-3	6.00	19.7	52	T6-6	12.33	2.30
3	T2-4	7.00	11.3	53	T6-7	13.75	2.86
4	T2-5	9.00	7.74	54	T6-8	15.75	2.73
5	T2-6	11.00	3.55	55	T6-9	17.08	2.70
6	T2-7	12.80	4.45	56	T6-10	19.08	1.31
7	T3-1	2.00	3.71	57	T6-11	21.08	1.10
8	T3-2	4.00	3.82	58	T6-12	23.08	1.20
9	T3-3	6.00	4.84	59	T6-13	25.33	1.35
10	T3-4	8.00	5.42	60	T6-14	27.83	1.65
11	T3-5	9.00	5.80	61	T6-15	29.83	0.77
12	T3-6	11.00	2.65	62	T6-16	31.83	1.09
13	T3-7	13.00	2.70	63	T6-17	33.83	1.16
14	T3-8	15.50	3.26	64	T6-18	35.83	1.18
15	T3-9	17.75	3.85	65	T6-19	38.08	1.01
16	T4-1	2.00	9.60	66	T6-20	40.08	1.18
17	T4-2	4.00	8.98	67	T6-21	42.08	1.28
18	T4-3	6.00	6.18	68	T7-1	2.00	4.00
19	T4-4	8.66	5.69	69	T7-2	4.00	3.14
20	T4-5	11.23	5.13	70	T7-3	6.00	2.80
21	T4-6	13.23	3.48	71	T7-4	7.08	3.45
22	T4-7	15.23	3.53	72	T7-5	9.08	3.85
23	T4-8	17.23	3.53	73	T7-6	11.08	2.07
24	T4-10	21.23	2.37	74	T7-7	13.08	2.41
25	T4-11	23.23	2.37	75	T7-8	15.66	2.81
26	T4-12	25.23	2.67	76	T7-9	17.66	3.81
27	T4-13	27.23	1.96	77	T7-10	19.66	2.90
28	T4-14	29.23	2.37	78	T7-11	22.16	3.47
29	T4-15	31.23	4.45	79	T7-12	24.16	1.94
30	T4-16	33.10	4.70	80	T7-13	26.41	4.60
31	T5-1	2.00	5.75	81	T7-14	28.41	6.61
32	T5-2	4.00	7.99	82	T7-15	30.41	2.23
33	T5-3	6.00	7.79	83	T7-16	32.58	2.13
34	T5-4	8.00	6.07	84	T7-17	35.08	3.21
35	T5-5	10.00	10.9	85	T9-1	2.00	1.88
36	T5-6	12.00	14.7	86	T9-2	4.00	0.97
37	T5-7	14.33	5.97	87	T9-3	6.00	1.16
38	T5-8	16.33	3.59	88	T9-4	8.00	1.11
39	T5-9	18.45	2.81	89	T9-5	10.00	1.39
40	T5-10	20.45	3.79	90	T9-6	12.00	1.55
41	T5-11	22.45	4.05	91	T9-7	13.41	1.78
42	T5-12	25.78	1.17	92	T9-8	15.41	1.56
43	T5-13	27.95	0.939	93	T9-9	17.41	1.33
44	T5-14	30.12	0.860	94	T9-10	19.41	1.21
45	T5-15	33.00	1.05	95	T9-11	21.41	1.50
46	T5-16	35.90	1.09	96	T9-12	23.41	1.12
47	T6-1	2.00	2.36	97	T9-13	25.41	1.08
48	T6-2	4.00	2.31	98	T9-14	27.66	1.11
49	T6-3	6.33	2.45	99	T9-15	29.66	0.98
50	T6-4	8.33	2.35	100	T9-16	31.66	1.36

No.	Sub-Test	Time	Amplitude	No.	Sub-Test	Time	Amplitude

No.	Sub-Test	Time min.	Amplitude ×0.2g	No.	Sub-Test	Time min.	Amplitude ×0.2g
101	T9-17	33.66	1.26	151	T11-14	26.37	1.56
102	T9-18	35.66	1.28	152	T11-15	28.37	0.865
103	T9-19	36.49	1.70	153	T11-16	30.37	1.09
104	T9-24	49.61	1.20	154	T11-17	32.37	1.54
105	T9-25	51.61	0.77	155	T11-18	34.37	1.57
106	T9-26	55.33	0.62	156	T11-19	37.37	1.55
107	T9-27	57.33	1.10	157	T11-20	39.37	1.78
108	T9-28	59.33	0.92	158	T11-21	41.87	1.38
109	T9-29	61.33	0.99	159	T11-22	44.35	1.67
110	T9-30	63.33	0.94	160	T11-23	46.65	1.64
111	T9-31	65.33	0.94	161	T11-26	42.98	1.46
112	T9-32	67.33	0.91	162	T11-27	45.23	1.14
113	T9-33	69.33	1.15	163	T11-28	47.03	1.13
114	T9-34	71.33	1.32	164	T11-29	48.03	1.39
115	T9-35	73.33	1.08	165	T12-1	2.00	1.27
116	T9-36	75.33	1.14	166	T12-2	4.00	1.14
117	T9-37	77.33	1.03	167	T12-3	6.00	1.08
118	T9-38	79.33	1.20	168	T12-4	8.25	1.18
119	T9-39	81.33	1.16	169	T12-5	10.75	1.40
120	T9-40	83.66	1.17	170	T12-6	12.75	1.10
121	T9-41	85.66	1.01	171	T12-7	14.75	1.16
122	T9-42	87.66	0.87	172	T12-8	16.75	1.11
123	T9-43	89.66	0.91	173	T12-9	19.00	1.29
124	T9-44	91.66	1.18	174	T12-10	21.50	1.42
125	T9-45	93.74	1.33	175	T12-11	23.50	1.12
126	T9-46	95.74	0.83	176	T12-12	25.50	1.49
127	T9-47	97.99	1.18	177	T12-13	27.00	1.82
128	T9-48	99.99	1.68	178	T12-14	29.42	2.91
129	T9-49	101.99	1.56	179	T12-15	31.92	3.35
130	T9-50	103.99	1.61	180	T12-16	33.92	2.01
131	T9-51	105.99	1.84	181	T12-17	35.47	2.24
132	T9-52	107.99	1.98	182	T13-1	2.00	4.44
133	T10-1	1.00	4.02	183	T13-2	4.00	3.26
134	T10-2	2.00	3.19	184	T13-3	6.00	4.69
135	T10-3	3.67	3.82	185	T14-2	4.000	1.00
136	T10-4	5.67	2.77	186	T14-3	6.000	0.984
137	T10-5	7.42	2.68	187	T14-4	8.000	1.70
138	T11-1	2.00	2.76	188	T14-5	10.00	1.73
139	T11-2	4.00	3.62	189	T14-6	12.00	1.55
140	T11-3	6.00	3.16	190	T14-7	14.00	1.18
141	T11-4	7.67	2.91	191	T14-8	16.00	0.725
142	T11-5	9.67	2.58	192	T14-9	18.00	0.640
143	T11-6	10.59	1.73	193	T14-10	20.00	0.801
144	T11-7	12.59	1.64	194	T14-11	22.00	0.781
145	T11-8	14.59	1.25	195	T14-12	24.00	0.763
146	T11-9	16.59	1.55	196	T14-13	26.00	0.881
147	T11-10	18.59	1.02	197	T14-14	28.00	0.678
148	T11-11	20.59	1.07	198	T14-15	30.00	0.756
149	T11-12	22.59	1.04	199	T14-16	32.00	0.942
150	T11-13	24.59	1.22	200	T14-17	34.25	0.971
No.	Sub-Test	Time	Amplitude	No.	Sub-Test	Time	Amplitude

No.	Sub-Test	Time min.	Amplitude ×0.2g	No.	Sub-Test	Time min.	Amplitude ×0.2g
201	T14-18	36.25	5.13	251	T18-14	29.13	1.27
202	T14-19	38.25	5.96	252	T18-15	32.13	1.04
203	T14-20	41.25	5.31	253	T18-16	34.75	1.32
204	T14-21	43.25	6.00	254	T18-17	37.42	1.15
205	T14-22	45.25	5.79	255	T18-18	39.62	1.00
206	T14-23	47.25	5.60	256	T18-19	41.32	1.44
207	T14-24	49.25	5.92	257	T18-20	42.74	1.12
208	T14-25	51.25	5.53	258	T18-21	45.07	1.41
209	T14-26	53.25	5.46	259	T18-22	47.32	1.05
210	T14-27	55.25	6.38	260	T18-23	48.99	1.56
211	T14-28	57.25	7.95	261	T18-24	51.59	1.20
212	T14-29	59.92	7.71	262	T19-1	2.25	3.91
213	T14-30	61.92	1.07	263	T19-2	4.25	8.15
214	T14-31	63.92	1.26	264	T19-3	6.25	8.03
215	T14-32	65.92	.925	265	T23-1	2.083	1.4
216	T14-33	67.92	1.00	266	T23-2	4.083	1.1
217	T14-34	69.92	1.11	267	T23-3	5.583	1.0
218	T14-35	71.92	1.08	268	T23-4	7.583	1.4
219	T14-36	73.92	1.53	269	T23-5	9.583	1.0
220	T14-37	75.92	1.79	270	T23-6	11.58	1.3
221	T14-38	77.92	1.60	271	T23-7	13.58	1.4
222	T14-39	79.92	1.67	272	T23-8	15.58	2.1
223	T14-40	81.92	1.17	273	T23-9	17.78	2.9
224	T14-41	83.92	1.12	274	T23-10	19.58	2.5
225	T14-42	86.09	.965				
226	T14-43	88.09	1.59				
227	T14-44	90.09	1.47				
228	T14-45	92.09	1.56				
229	T14-46	94.09	1.53				
230	T14-47	96.09	1.35				
231	T14-48	98.09	1.34				
232	T14-49	100.0	1.52				
233	T14-50	102.0	1.40				
234	T14-51	104.0	1.13				
235	T14-52	106.0	1.35				
236	T14-53	107.6	.563				
237	T14-54	109.6	2.10				
238	T14-55	112.6	2.36				
239	T14-56	117.0	1.45				
240	T18-1	2.00	1.17				
241	T18-2	4.00	1.00				
242	T18-3	6.00	1.07				
242	T18-4	8.00	0.90				
245	T18-5	10.25	1.12				
246	T18-6	12.25	0.81				
247	T18-7	14.25	0.92				
248	T18-11	21.50	1.36				
249	T18-12	23.30	0.64				
250	T18-13	26.18	1.13				
No.	Sub-Test	Time	Amplitude	No.	Sub-Test	Time	Amplitude